# THE ENVIRONMENTAL HAZARDS OF TOXIC METALS POLLUTION

EDITED BY: Dragana S. Đorđević, Bernardo Duarte and Senthil Kumar Ponnusamy
PUBLISHED IN: Frontiers in Environmental Science and Frontiers in Marine Science

frontiers Research Topics

# frontiers



ISSN 1664-8714
ISBN 978-2-88971-343-1
DOI 10.3389/978-2-88971-343-1

## About Frontiers

Frontiers is more than just an open-access publisher of scholarly articles: it is a pioneering approach to the world of academia, radically improving the way scholarly research is managed. The grand vision of Frontiers is a world where all people have an equal opportunity to seek, share and generate knowledge. Frontiers provides immediate and permanent online open access to all its publications, but this alone is not enough to realize our grand goals.

## Frontiers Journal Series

The Frontiers Journal Series is a multi-tier and interdisciplinary set of open-access, online journals, promising a paradigm shift from the current review, selection and dissemination processes in academic publishing. All Frontiers journals are driven by researchers for researchers; therefore, they constitute a service to the scholarly community. At the same time, the Frontiers Journal Series operates on a revolutionary invention, the tiered publishing system, initially addressing specific communities of scholars, and gradually climbing up to broader public understanding, thus serving the interests of the lay society, too.

## Dedication to Quality

Each Frontiers article is a landmark of the highest quality, thanks to genuinely collaborative interactions between authors and review editors, who include some of the world's best academicians. Research must be certified by peers before entering a stream of knowledge that may eventually reach the public - and shape society; therefore, Frontiers only applies the most rigorous and unbiased reviews.
Frontiers revolutionizes research publishing by freely delivering the most outstanding research, evaluated with no bias from both the academic and social point of view. By applying the most advanced information technologies, Frontiers is catapulting scholarly publishing into a new generation.

## What are Frontiers Research Topics?

Frontiers Research Topics are very popular trademarks of the Frontiers Journals Series: they are collections of at least ten articles, all centered on a particular subject. With their unique mix of varied contributions from Original Research to Review Articles, Frontiers Research Topics unify the most influential researchers, the latest key findings and historical advances in a hot research area! Find out more on how to host your own Frontiers Research Topic or contribute to one as an author by contacting the Frontiers Editorial Office: frontiersin.org/about/contact

# THE ENVIRONMENTAL HAZARDS OF TOXIC METALS POLLUTION

Topic Editors:
**Dragana S. Đorđević,** University of Belgrade, Serbia
**Bernardo Duarte,** Center for Marine and Environmental Sciences (MARE), Portugal
**Senthil Kumar Ponnusamy,** SSN College of Engineering, India

**Citation:** Đorđević, D. S., Duarte, B., Ponnusamy, S. K., eds. (2021). The Environmental Hazards of Toxic Metals Pollution. Lausanne: Frontiers Media SA.
doi: 10.3389/978-2-88971-343-1

# Table of Contents

frontiers in Environmental Science

ORIGINAL RESEARCH
published: 17 July 2020
doi: 10.3389/fenvs.2020.00107

# Multi-Year Concentrations, Health Risk, and Source Identification, of Air Toxics in the Venice Lagoon

*Elisa Morabito[1]*, Elena Gregoris[2], Franco Belosi[3], Daniele Contini[4], Daniela Cesari[4] and Andrea Gambaro[1]*

*[1] Department of Environmental Sciences, Informatics and Statistics, Ca' Foscari University of Venice, Venice-Mestre, Italy, [2] Institute of Polar Sciences, National Research Council of Italy, ISP-CNR, Venice-Mestre, Italy, [3] Institute of Atmospheric Sciences and Climate, National Research Council of Italy, ISAC-CNR, Bologna, Italy, [4] Institute of Atmospheric Sciences and Climate, National Research Council of Italy, ISAC-CNR, Lecce, Italy*

This work presents and discusses the results of multi-year measurements of air toxics concentrations from different sites of Venice Lagoon. The aim of the study is the characterization of the air quality of the area, in terms of $PM_{10}$, $PM_{10}$-bound metals, and polycyclic aromatic hydrocarbons (PAHs) concentrations, even with the individuation of the related inhalation risk and the identification of the main contaminants' sources. The study moreover provides an important multi-years trend of chemical characterization of the Venice Lagoon. Sampling for $PM_{10}$ and its metal content was carried out between 2010 and 2015, using low volume sequential aerosol samplers; V, Cr, Fe, Co, Ni, Cu, Zn, As, Mo, Cd, Sb, Tl, and Pb were measured by ICP-MS. Samples for PAHs concentration in gas and particle phases were collected from 2010 to 2014, using a high-volume air sampler that allows to sample both phases simultaneously. Samples for PAHs determinations were analyzed by GC-HRMS. Concentrations of air toxics have been studied with the use of enrichment factor, the coefficient of divergence, and the Mann-Kendal test, to individuate eventual local divergences, seasonal and other temporal trends. The inhalation risk assessment has been achieved by the calculation of the cumulative incremental carcinogenic risk for all the air toxics analyzed. The sources' identification and impact evaluation have been carried out using the atmospheric vanadium concentration, to calculate the primary contribution of ship traffic to $PM_{10}$, the Positive Matrix Factorization, and the Diagnostic Ratios, with the aim of evaluating the impact of construction activities of M.o.S.E, (Modulo Sperimentale Elettromeccanico-Electromechanical Experimental Module) as well as of ship traffic and other possible air toxics' sources. Temporal trends indicate a slight decrease of PAHs and $PM_{10}$ and of its content of Pb, Zn, Sb. Sharp increases of As and Cd during 2014 and 2015 may be due to local sources like emissions from the construction yard, ship, and road traffic. The cumulative incremental carcinogenic risk was below the unconditionally acceptable risk; Co and As are the most important contributors among metals, followed by Cd and Ni while the PAH congeners that most contribute to the carcinogenic risk were benzo(a)pyrene and dibenzo(A,H)anthracene.

**Keywords: metals, $PM_{10}$, aerosol, PAHs, Venice Lagoon**

OPEN ACCESS

***Edited by:***
*Dragana S. Đorđević, University of Belgrade, Serbia*

***Reviewed by:***
*Michael Edward Deary, Northumbria University, United Kingdom*
*Joanna Wragg, British Geological Survey (BGS), United Kingdom*

****Correspondence:***
*Elisa Morabito*
*elisamora@unive.it*

***Specialty section:***
*This article was submitted to Toxicology, Pollution and the Environment, a section of the journal Frontiers in Environmental Science*

***Received:*** *04 May 2020*
***Accepted:*** *23 June 2020*
***Published:*** *17 July 2020*

***Citation:***
*Morabito E, Gregoris E, Belosi F, Contini D, Cesari D and Gambaro A (2020) Multi-Year Concentrations, Health Risk, and Source Identification, of Air Toxics in the Venice Lagoon. Front. Environ. Sci. 8:107. doi: 10.3389/fenvs.2020.00107*

## INTRODUCTION

Air pollution may cause effects on visibility and climate, effects on materials, direct and indirect effects on vegetation (Harrison et al., 2014), and nevertheless, particulate air pollution is an important risk factor for cardiopulmonary disease and mortality, both as a result of acute and chronic exposure (Arden Pope and Dockery, 1999). This has shown an association between exposure to particulate matter air pollution and the incidence of lung cancer (Raaschou-Nielsen et al., 2013). Between toxic air pollutants, known or suspected to cause serious health effects, a great deal of interest from scientific community, is addressed to heavy metals and polycyclic aromatic hydrocarbons.

Inorganic elements are present in atmosphere associated with particulate matter, although their origin can be from natural (e.g., Na, Mg, K, Ca, Si, and Al), or anthropogenic (e.g., V, Cr, Mn, Ni, Cu, Zn, Cd, and Pb) emissions. Natural sources of metals and semi-metals are rocks and soils, volcanic emissions, forest fires, sea sprays, and biogenic emissions. Anthropogenic emissions include instead a wide variety of sources, such as agriculture, mining, coal and oil combustion, ceramic and glass production, road traffic, waste incineration, a variety of industrial activities, and human activities. Elements like As, Cd, Pb, Sb, Se, Cr, Co, Cu, Ga, Hg, and Mo are emitted by coal combustion (Bool et al., 1996), while V, Ni, and Pb are emitted mostly by oil combustion (United States Environmental Protection Agency, 1998); V and Ni may also be tracers of ship traffic emissions (Zhao et al., 2013; Viana et al., 2014); Cu, Zn, Pb, and Sb are often associated with traffic emissions and road dust (Han et al., 2011; Contini et al., 2012). Heavy metal associated with atmospheric particles may accumulate in human being via inhalation and may cause dangerous effects on human health: effects on the respiratory system, effects via the cardiovascular system, and carcinogenesis (Harrison et al., 2014).

Another class of very widespread toxic air pollutants is that of polycyclic aromatic hydrocarbons (PAHs). These compounds are produced by incomplete combustion of organic material emitted by a multiplicity of sources, such as industrial activities, motor vehicles, residential heating, forest fires, biomass burning, and shipping activities (Mastral and Callén, 2000; Ravindra et al., 2008; Riva et al., 2011). It has been estimated that emission of PAHs from natural sources, such as non-anthropogenic burning of forests or volcanic eruptions, may be negligible (Wild and Jones, 1995). PAHs are persistent in the environment and ubiquitous, and moreover may bioaccumulate through the food web. For these reasons they constitute a risk for both environment, animal, and human health. PAHs were one of the first atmospheric pollutants identified as suspected carcinogen: the carcinogenic, mutagenic and teratogenic potential of PAHs increases with their molecular weight (ATSDR, 2002; Ravindra et al., 2008). Moreover the vapor/particle phase partitioning of PAHs indeed influences their transport, deposition, and chemical transformation and, as a result, is crucial in terms of reactivity and effects on human health.

For these reasons, a specific issue of interest, as recognized also by EPA, is to identify specific chemicals as well as specific sources that can impact air quality and consequently responsible for health risks.

The studied area in this work is the Venice Lagoon, a fragile highly urbanized costal environment. Due to its position, the Venice Lagoon is subjected to anthropogenic inputs of organic and inorganic pollutants, regarding the whole environment: atmosphere, lagoon water, and sediments. As far as the atmosphere is concerned, the lagoon is subjected to long-range transport of both organic and inorganic contaminants, coming from the Po Valley, one of the most polluted area of Europe, via aerosol. Moreover, it is affected by local anthropogenic emissions produced by different sources such as industrial activities, thermoelectric power plants, petrochemical plants, incinerator plants, domestic heating, ship traffic, glass factories, and vehicular emissions transported from the mainland (Prodi et al., 2009; Stortini et al., 2009; Contini et al., 2012; Valotto et al., 2014; Squizzato and Masiol, 2015; Squizzato et al., 2016). Additionally, since 2005, the Venice Lagoon has been affected by the emissions related to the construction yards of the M.o.S.E. (Modulo Sperimentale Elettromeccanico – Electromechanical Experimental Module), a system of mobile dams, located one for each lagoon inlet (Chioggia, Malamocco, and Lido; Morabito et al., 2014).

The aim of this study is to characterize the air quality of the Venice Lagoon, related to the presence of $PM_{10}$- bound potentially toxic elements and PAHs. A study of the inhalation risk due to the contaminant analyzed and an evaluation of their possible sources in the Venice air environment, has also been carried out. Sampling was carried out from 2010 to 2015 (for $PM_{10}$ and its metal content) and from 2010 to 2014 (for the PAHs concentration, in gas and particle phase) in three sites of the lagoon area. Concentrations of pollutants have been studied with the use of enrichment factor, the coefficient of divergence (COD), and the Mann-Kendal test, to individuate eventual local divergences, seasonal, and other temporal trends. The inhalation risk assessment has been achieved by the calculation of the cumulative incremental carcinogenic risk both for potentially toxic elements in $PM_{10}$ and for PAH in gas and particulate phase. Moreover a deep study to investigate the source identification and apportionment has been carried out, to enhance the principal sources of contamination in the three sites, and to evaluate the impact of construction activities of M.o.S.E, as well as of ship traffic and other possible sources. The sources' identification and sources' impact evaluation have been carried out by the use of the atmospheric vanadium concentration, to calculate the primary contribution of ship traffic to $PM_{10}$, the Positive Matrix Factorization (PMF), and the Diagnostic Ratios (DR). Moreover, by integrating our data with those obtained in other previous studies (Contini et al., 2012; Gregoris et al., 2016), this study provides a significant temporal trend of the characterization of aerosol in the Venice Lagoon in terms of $PM_{10}$ concentration and its elemental characterization.

# MATERIALS AND METHODS

## Sampling

The sampling covers a temporal range of about 5 years, from January 2010 to September 2015. Sampling sites were placed in the vicinity of the three lagoon inlets and next to the M.o.S.E. construction yards: Punta Sabbioni (PS) at the northern lagoon inlet, Malamocco (MM) next to the central lagoon inlet, and Chioggia (CH) at the southern inlet (**Figure 1**).

### Inorganic Pollutants

Sampling of $PM_{10}$ for the metal content analysis were carried out from January 2010 to September 2015. The sampling was not a continuous activity: each campaign lasted 14 days, with frequency from 2 to 4 campaigns/year. In detail, 16 sampling campaigns were carried out in PS from January 2010 to September 2015, 13 in MM from January 2010 to March 2015, and 11 in CH site from March 2010 to March 2015, with a total of 209, 181, and 144 daily samples in the three sites, respectively. The periods of sampling include different seasons, both holidays and working days. The $PM_{10}$ samples were collected using low volume sequential aerosol samplers (Skypost PM-TCR Tecora) with an electronically adjustable flow (2.3 $m^3$ $h^{-1}$), 16 filters capacity, and a sampling module for automatic filter changing after 24 h. Two of the 16 filters were used as field blank, one before and one after the campaign, to control the uncertainties. The filters, in quartz (Sartorius, diameter 47 mm) were weighed three times (%RSD 5–10%) over 24 h, before and after the sampling, using a Sartorius Competence CP64-0CE balance (precision of 0.01 mg) in a nitrogen box glove with controlled humidity (50 ± 5%), and temperature (20 ± 5%).

### Organic Pollutants

Sampling of PAHs was carried out from February 2010 to February 2014 in PS and from March 2010 to October 2014 in MM, with a total of 10 sampling campaigns in PS and 13 in MM. Each campaign lasted 14 days and during each campaign, 8 samples, and 8 blanks were collected. The dates of the sampling, together with relative meteorological information (wind direction, wind speed, precipitations, and temperature) are reported in the **Supplementary Information** (**Supplementary Tables SI 1, SI 2**). The sampling was conducted using a high volume sampler (AirFlowPUF, Tish Environmental Inc., Village of Cleves, OH, United States), which allows to separate the gas from the particulate phase (TSP, Total Suspended Particles). The latter was collected on quartz fiber filters (QFF, porosity 1 μm, diameter 102 mm, and SKC Inc., United States), while the gas

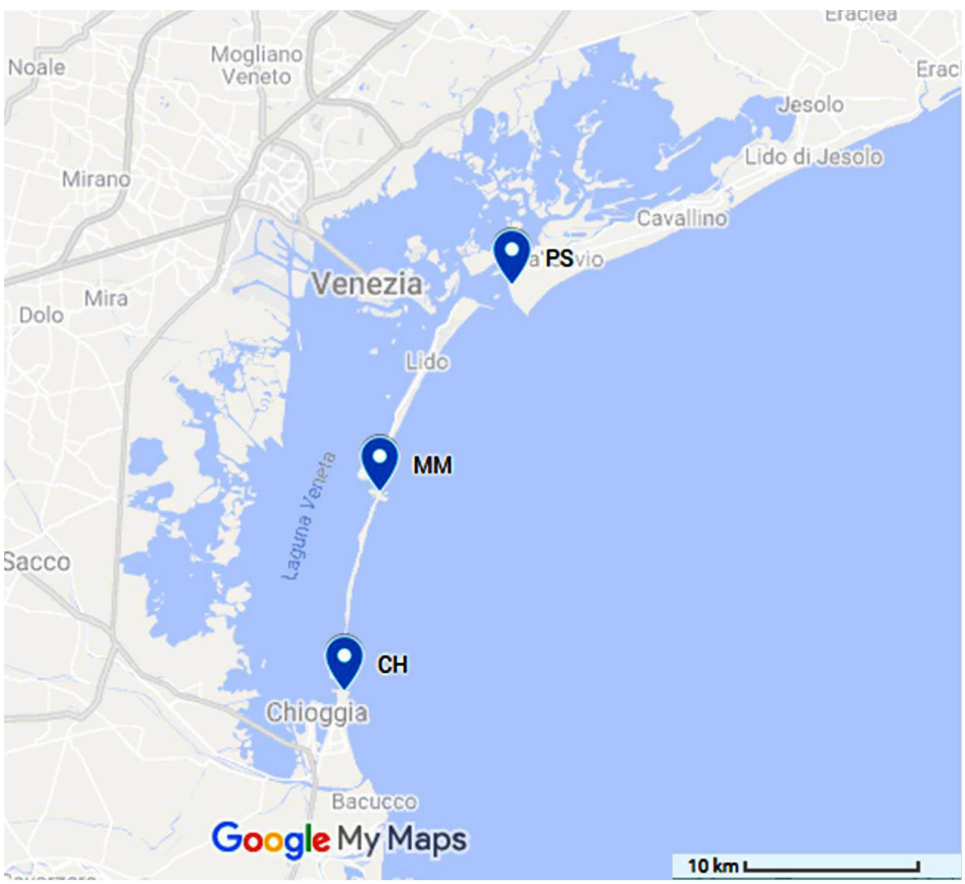


**FIGURE 1 |** Location of the sampling sites.

phase was collected on polyurethane foams (PUF, height 75 mm, diameter 65 mm, and SKC Inc., United States). The sampling system maintained a constant flow rate of 0.3 $m^3$ $min^{-1}$. PUFs and QQFs were replaced every 24–96 h. Before sampling, QFFs were furnace-treated at 400°C for 4 h and PUFs were pre-cleaned by extraction using the Pressurized Liquid Extractor (PLE, Fluid Management Systems Inc., United States) under the following working conditions: 100°C temperature, 1000 psi pressure, 7 min static duration, using toluene (two cycles), and an n-hexane and dichloromethane mixture (1:1; one cycle)2 cycles. Pesticide-grade dichloromethane, n-hexane and toluene (Romil Ltd., Cambridge, United Kingdom) were used. Cleaned QFFs and PUFs were individually wrapped in double aluminum foil until the time of sampling. After the sampling, QFFs and PUFs were individually wrapped again in double aluminum foil and stored at −20°C until preparation for analysis.

## Procedures, Analytical Methods, and Materials

### Inorganic Pollutants

Each filter was digested by microwave (Ethos1-Milestone) inside a Teflon vessel (100 mL) held in a 10-place high-pressure carousel (Milestone HPR-1000/10S High Pressure), with 6 mL $HNO_3$, 3 mL $H_2O_2$, and 1 mL HF (Romil ®Ultra-pure Acid, UpA). The digestion temperature program consisted of a ramp from room temperature to 100°C in 10 min, followed by a time sequence (5 min/step), allowing the maintenance and increase ($\Delta$t 20°C) of the temperature to 180°C, after which this value was maintained for 10 min. In all the digestion sessions, one or two vessels were used as a blank to check the quality of the reagent and the procedure. After each digestion program, the vessels were cleaned using a temperature-controlled program (20 min ramp from room temperature to 160°C and 10 min at 160°C) with 10 mL of $HNO_3$ (Romil Suprapur Acid, SpA), and 1 mL of HF (Romil Ultra-pure Acid, UpA). Samples solutions and blanks obtained by the digestion were then diluted to 50 mL (by weight) with ultrapure water and stored at −20°C until instrumental analysis.

Inorganic elements (V, Cr, Fe, Co, Ni, Cu, Zn, As, Mo, Cd, Sb, Tl, and Pb) in $PM_{10}$ samples were measured by Inductively Coupled Plasma- Quadrupole Mass Spectrometer (ICP-QMS, Agilent 7500). Element concentrations in samples were obtained after subtraction the relative field blank values. The accuracy of the method was controlled using the standard reference material (SRM NIST1648a, Urban Particulate Matter) and the recoveries of the analyzed elements were between 90% and 100%.

All the vessels and materials used during the preparation and the analysis of the samples were acid-cleaned and conditioned following the cleaning procedures described elsewhere (Capodaglio et al., 1994), to minimize sample contamination. For the same reason handling, treatment of the samples, and analysis were carried out in a clean chemistry laboratory (Class 100), an atmosphere-controlled laboratory, along with sample pre-treatment.

### Organic Pollutants

Analyses of organic pollutants were carried out in the CSMO (Centro Studi Microinquinanti Organici – Study Center of Organic Micropollutants) laboratory in Voltabarozzo, Padua, Italy, following the EPA 8270 D method.

We determined 16 of the United States Environmental Protection Agency (United States Environmental Protection Agency, 1981) priority PAHs: naphthalene (NAP), acenaphthylene (ACY), acenaphthene (ACE), fluorene (FL), phenanthrene (PHE), anthracene (ANT), fluoranthene (FLA), pyrene (PYR), benzo[a]anthracene (BaA), chrysene (CHR), benzo[b]fluoranthene (BbF), benzo[k]fluoranthene (BkF), benzo[a] pyrene (BaP), benzo[ghi]perylene (BghiP), indeno[1,2,3-c,d]pyrene (IcdP), and dibenzo[a,h]anthracene (DahA), both in QFFs and PUFs.

PUFs and QFFs samples were extracted separately using a Pressurized Liquid Extractor and the same operating conditions used for the cleaning procedure. Blank and samples were spiked before extraction with a known amount of 13C-labeled phenanthrene as internal standard (Cambridge Isotope Laboratories, Andover, MA, United States). The extracts were cleaned by injection onto a packed neutral silica column, previously conditioned with 50 mL of n-hexane, using the automated PowerPrep system (Fluid Management Systems Inc.).

Determination of PAHs were performed with a MAT 95XP (Thermo Finnigan, Bremen, Germany) high-resolution mass spectrometer, coupled with a Hewlett-Packard model 5890 series II gas chromatograph, equipped with a fused silica capillary column (J&W Scientific DB-5MS, 60 m × 0.25 mm O.D. 0.25 μm film thickness). Details of the gas-chromatograph operating conditions are reported in Gambaro et al., 2009. Pesticide-grade dichloromethane, n-hexane and toluene (Romil Ltd., Cambridge, United Kingdom) were used. Recoveries, laboratory and procedural blanks, and further details about the analytical method have been already reported (Gambaro et al., 2009; Contini et al., 2011; Gregoris et al., 2014; Morabito et al., 2014).

### Statistical Analysis of Data

#### *Coefficient of divergence (COD)*

Some diagnostic statistical analyses have been carried out, In order to investigate any spatial differences in $PM_{10}$ concentration, in its metals content, and further differences between holidays and working days, or other temporal variations, the COD has been calculated. This coefficient is often used when there is the necessity of investigating the discrepancy between two different datasets, which may be, for example, two sampling sites, two different events, two seasons, years of sampling, as well as variables, like chemical concentrations (Liu et al., 2019; Ramírez et al., 2019; Galindo et al., 2020).

The COD is calculated following the formula (Eq. 1):

$$COD = \sqrt{\frac{1}{n}\sum_{i=1}^{n}\left(\frac{X_{ij} - X_{ih}}{X_{ij} + X_{ih}}\right)^2} \quad (1)$$

Where $j$ and $h$ stand for two sampling sites (or event/non-event, working day/holidays, etc.) $X_{ij}$ and $X_{ih}$ are the average concentrations of the chemical element $i$, $n$ is the number of the analyzed chemical elements (Wongphatarakul et al., 1998). If the value of COD is zero, there is no divergence, if COD is near 1, there is heterogeneity in the data set. In literature is considered

that COD < 0.2 indicates similarity, 0.2 < COD < 0.5 indicates moderate heterogeneity, and COD > 0.5 indicates that the two studied cases are different (Zou et al., 2018).

For these statistical evaluations, the values under MDL were substituted with half MDL, and the variables with more than 50% of samples under MDL have been eliminated from the dataset.

### *Incremental carcinogenic inhalation risk*

The cumulative incremental carcinogenic inhalation risk was calculated for $PM_{10}$, based on metals concentrations, and for gas and particulate matter, together accounted, based on PAHs concentration. We followed the indications of the United States Environmental Protection Agency (US-EPA) summarized in the report n. EPA-540-R-070-002 (United States Environmental Protection Agency, 2009). The exposure concentration (*Ec*) of an adult in a residential scenario was calculated for each contaminant using the equation (Eq. 2) for chronic exposure:

$$Ec = \frac{Ca \cdot Et \cdot Ef \cdot Ed}{At} \quad (2)$$

where *Ca* is the air contaminant concentration; *Et* is the exposure time (24 h/day); *Ef* is the frequency of exposure (350 days/year); *Ed* is the exposure duration (30 years); and *At* is the averaging time corresponding to the lifetime (70 years × 365 days/year × 24 h/day).

The incremental carcinogenic risk was calculated multiplying the exposure concentration of each contaminant *i* for the corresponding Inhalation Unit Risk (IUR). Used IUR values were tabulated from the Regional Screening Levels (RSLs) – Residential air (United States Environmental Protection Agency, 2016) and corresponded to: $9.0 \times 10^{-3}$ $(\mu g\ m^{-3})^{-1}$ for Co; $2.6 \times 10^{-4}$ $(\mu g\ m^{-3})^{-1}$ for Ni; $4.3 \times 10^{-3}$ $(\mu g\ m^{-3})^{-1}$ for As; $1.8 \times 10^{-3}$ $(\mu g\ m^{-3})^{-1}$ for Cd; $1.1 \times 10^{-5}$ $(\mu g\ m^{-3})^{-1}$ for CHR; $1.1 \times 10^{-4}$ $(\mu g\ m^{-3})^{-1}$ for BaA, BbF, BkF, and IcdP; $1.1 \times 10^{-3}$ $(\mu g\ m^{-3})^{-1}$ for BaP, and $1.2 \times 10^{-3}$ $(\mu g\ m^{-3})^{-1}$ for DahA.

### *Positive matrix factorization (PMF)*

Positive Matrix Factorization is a multivariate factor analysis tool for investigating the contribution of sources to atmospheric contaminants. PMF was conducted using the PMF 5.0 software by US-EPA. The dataset was composed of metal concentrations measured in the three sites (CH, MM, and PS together). Data were preliminary refined in order to obtain a robust dataset. Variables with more than 50% of values under MDL were rejected. Values under MDL were substituted by half of MDL. The divergence between data collected in the periods 2010–2013 and 2014–2015, confirmed by CODs > 0.5 in all the monitoring sites (see section "Contaminant concentration"), prevented the convergence of the model: for this reason, data collected in 2014 and 2015 have been excluded from the dataset. As uncertainty, the standard deviation of the field blanks of each campaign was adopted, normalized for the average sampling volumes of each campaign. The uncertainty of values under MDL was 5/6 MDL. An additional uncertainty of 10% was included for all species. Before running the PMF model, discrimination between "strong," "weak," and "bad" variables has been made, according to the signal to noise (S/N) ratio criterion, the residual analysis and evaluating the observed/predicted scatter plots. In this dataset V, Co, As, and Cd were categories as "strong," the other variables as "weak." In order to individuate the right number of factors, different solutions were explored and the parameters IM (maximum of the average of the scaled residual), and IS (maximum of the standard deviation of the scaled residuals), together with the *Q* value (goodness of the fit) were examined, following the approach reported in Contini et al. (2012), and Gregoris et al. (2014). The validity of the selected solutions was estimated applying various tests, as suggested in the EPA PMF 5.0 user guide (US-EPA, 2014). In the Bootstrap (BS) error estimation (number of runs 100; min. correlation value 0.6), new datasets are randomly constructed from blocks of the original dataset. A number of BS datasets are then processed with PMF and the BS factors are compared to the base run factors. If each BS factor is correlated to a single base run factor, all factors are considered "mapped" and the solution can be interpreted. Rotational ambiguity was explored using the displacement (DISP) error estimation, which assesses the largest range of source profile values without an appreciable increase in the *Q*-value. The solution was considered valid only if no swaps were observed for the lowest displacement (dQmax = 4) and if the calculated decrease of *Q* was not significant (<1%). Additionally, the error estimation by BS-DISP was also conducted, for estimating the errors associated with both random, and rotational ambiguity at the same time. The solution was considered valid only if no swaps were observed for the lowest displacement (dQmax = 0.5) and if the calculated decrease of *Q* was not significant (<0.5%; US-EPA, 2014).

# RESULTS AND DISCUSSION

## Contaminant Concentration

### $PM_{10}$ and Its Metal Content

In **Table 1** samples data related to $PM_{10}$ concentration and its content in heavy metals is reported. From the gravimetric analyses emerged that $PM_{10}$ average concentrations, in the whole sampling period, (±standard deviation) in the three sites were 31.1 $\mu g\ m^{-3}$ (2.4–116.9 $\mu g\ m^{-3}$ of range) in PS, 36.5 $\mu g\ m^{-3}$ (7.5–130.9 $\mu g\ m^{-3}$) in MM, and 38.8 $\mu g\ m^{-3}$ (0.7–379.2 $\mu g\ m^{-3}$) in CH. These values are similar to those found in literature in Venice Lagoon (Masiol et al., 2010, 2012a,b; Contini et al., 2011, 2012). The concentrations of all the analyzed metals in $PM_{10}$ were consistent with those found in the mentioned previous studies in the same area, for all the sites.

Considering the average concentrations and the large range of variation, in the whole sampling period, of both $PM_{10}$ and elements, there does not appear to be any differences among the three sites (**Table 1** and **Supplementary Figure SI 1**). This has been confirmed by the CODs: 0.1 between PS and MM, which indicates similarity; 0.26 between MM and CH, and 0.24 between CH and PS, which both indicate weak difference. All CODs are reported in **Table 2**. Mo and Tl, having high percentage of samples < MDL (especially concentrated in few campaigns) were not considered in the CODs evaluation and statistical data elaborations.

**TABLE 1 |** $PM_{10}$ concentration ($\mu g\ m^{-3}$) and its metal contents ($ng\ m^{-3}$) in the three sites in the whole sampling period.

| | $PM_{10}$ | V | Cr | Fe | Co | Ni | Cu | Zn | As | Mo | Cd | Sb | Tl | Pb |
|---|---|---|---|---|---|---|---|---|---|---|---|---|---|---|
| **PS – Nr of samples: 209** | | | | | | | | | | | | | | |
| Mean | 31.1 | 4.0 | 4.0 | 307.7 | 0.6 | 4.1 | 7.6 | 32.8 | 9.7 | 3.1 | 5.5 | 2.0 | 0.9 | 7.5 |
| Median | 28.1 | 3.5 | 3.3 | 259.5 | 0.2 | 2.8 | 5.7 | 15.2 | 2.6 | 1.5 | 0.4 | 1.1 | 0.0 | 3.5 |
| SD | 18.5 | 3.2 | 3.4 | 203.7 | 1.1 | 3.9 | 5.6 | 40.1 | 16.0 | 4.7 | 13.8 | 3.0 | 2.4 | 9.9 |
| Min | 2.4 | 0.0 | 0.0 | 3.1 | 0.0 | 0.0 | 0.0 | 0.1 | 0.0 | 0.0 | 0.0 | 0.0 | 0.0 | 0.0 |
| Max | 116.9 | 17.5 | 20.1 | 963.2 | 7.4 | 19.7 | 32.4 | 232.7 | 92.8 | 27.3 | 65.5 | 26.6 | 17.9 | 43.2 |
| samples > MDL (%) | 100 | 97 | 87 | 96 | 74 | 87 | 94 | 90 | 80 | 59 | 85 | 85 | 57 | 85 |
| **MM – Nr of samples: 181** | | | | | | | | | | | | | | |
| Mean | 36.5 | 5.3 | 5.2 | 316.8 | 0.6 | 5.0 | 8.6 | 39.3 | 7.8 | 3.0 | 5.4 | 2.2 | 1.0 | 11.5 |
| Median | 30.8 | 4.3 | 3.1 | 268.1 | 0.1 | 3.3 | 6.5 | 22.4 | 2.2 | 1.5 | 0.8 | 1.1 | 0.0 | 6.0 |
| SD | 23.3 | 3.6 | 9.3 | 227.6 | 1.2 | 6.0 | 7.6 | 51.7 | 12.2 | 4.4 | 16.8 | 4.8 | 2.5 | 27.0 |
| min | 7.5 | 0.4 | 0.1 | 24.7 | 0.0 | 0.0 | 0.9 | 2.3 | 0.0 | 0.0 | 0.0 | 0.0 | 0.0 | 0.0 |
| max | 130.9 | 20.3 | 109.7 | 1746.6 | 6.3 | 52.4 | 55.8 | 471.6 | 78.5 | 35.9 | 136.2 | 58.9 | 16.4 | 325.1 |
| samples > MDL (%) | 100 | 100 | 91 | 98 | 71 | 94 | 99 | 98 | 78 | 49 | 76 | 91 | 53 | 83 |
| **CH – Nr of samples: 144** | | | | | | | | | | | | | | |
| Mean | 38.8 | 4.1 | 4.1 | 416.6 | 2.0 | 3.9 | 7.1 | 30.3 | 8.3 | 1.6 | 1.8 | 1.4 | 0.5 | 6.6 |
| Median | 29.6 | 3.0 | 2.6 | 279.9 | 0.3 | 3.1 | 4.8 | 21.8 | 1.8 | 0.8 | 0.4 | 0.8 | 0.0 | 3.0 |
| SD | 35.7 | 3.9 | 6.2 | 751.6 | 12.8 | 3.9 | 6.9 | 32.5 | 17.4 | 2.5 | 4.0 | 1.7 | 1.5 | 8.6 |
| Min | 0.7 | 0.0 | 0.0 | 9.8 | 0.0 | 0.0 | 0.1 | 0.2 | 0.0 | 0.0 | 0.0 | 0.0 | 0.0 | 0.0 |
| Max | 379.2 | 24.9 | 53.0 | 8625.7 | 153.7 | 23.4 | 40.5 | 191.2 | 118.1 | 21.6 | 25.9 | 7.4 | 9.6 | 39.4 |
| samples > MDL (%) | 100 | 98 | 81 | 96 | 83 | 85 | 92 | 92 | 77 | 47 | 81 | 81 | 53 | 78 |

**TABLE 2 |** Coefficients of divergence between the three sites.

| | | | | Working days vs holidays | | | 2010–2013 vs 2014–2015 | | |
|---|---|---|---|---|---|---|---|---|---|
| | PS vs MM | MM vs CH | PS vs CH | PS | MM | CH | PS | MM | CH |
| tot | 0,10 | 0,26 | 0,24 | 0,10 | 0,16 | 0,22 | 0,56 | 0,56 | 0,60 |
| $PM_{10}$ | 0,13 | 0,09 | 0,15 | 0,08 | 0,09 | 0,10 | | | |
| V | 0,22 | 0,20 | 0,19 | 0,08 | 0,14 | 0,17 | | | |
| Cr | 0,23 | 0,15 | 0,13 | 0,11 | 0,30 | 0,26 | | | |
| Fe | 0,15 | 0,17 | 0,22 | 0,18 | 0,22 | 0,23 | | | |
| Co | 0,30 | 0,45 | 0,49 | 0,18 | 0,50 | 0,40 | | | |
| Ni | 0,26 | 0,16 | 0,27 | 0,07 | 0,21 | 0,20 | | | |
| Cu | 0,11 | 0,13 | 0,14 | 0,17 | 0,24 | 0,21 | | | |
| Zn | 0,11 | 0,16 | 0,20 | 0,15 | 0,19 | 0,19 | | | |
| As | 0,15 | 0,34 | 0,26 | 0,15 | 0,31 | 0,15 | | | |
| Cd | 0,55 | 0,56 | 0,34 | 0,23 | 0,36 | 0,28 | | | |
| Sb | 0,26 | 0,33 | 0,24 | 0,25 | 0,41 | 0,23 | | | |
| Pb | 0,25 | 0,34 | 0,29 | 0,16 | 0,30 | 0,15 | | | |

Integrating data obtained in this study with those from previous work carried out by Contini et al. (2012) in the same three sites of the Venice Lagoon, nine-years temporal trends of elements in $PM_{10}$ are provided. The yearly average concentration of As from 2007 to 2015 highlighted a sharp increase in the last 2 years in all the three sites while, in the same years, the yearly average concentration of Pb has a sharp decrease. Cd shows a "peak" during 2014 in MM, and during 2015 in CH (**Figure 2**). The trends of yearly average concentrations of the other analyzed elements are reported in the **Supplementary Material** (**Supplementary Figures SI 2, SI 3**).

Monotonic temporal trends of $PM_{10}$ and its concentrations were evaluated using the non-parametric Mann-Kendall test, based on mean annual values. Results showed a negative monotonic trend of $PM_{10}$ in PS and CH, with a confidence of 96% and 88%, respectively. As far as elements' concentration is concerned, negative monotonic trends have emerged for Pb (confidence: 99% in PS, 92% in MM, and 88% in CH), and Sb (confidence: 100% in PS, 100% in MM, 99% in CH) in all the three sites, and for Zn only in PS (confidence: 88%). The Mann-Kendal test does not enhance the sharp increase of As and Cd in the last 2 years, because it evaluates cumulative monotonic trends. As far as Cd in PS is concerned, it should

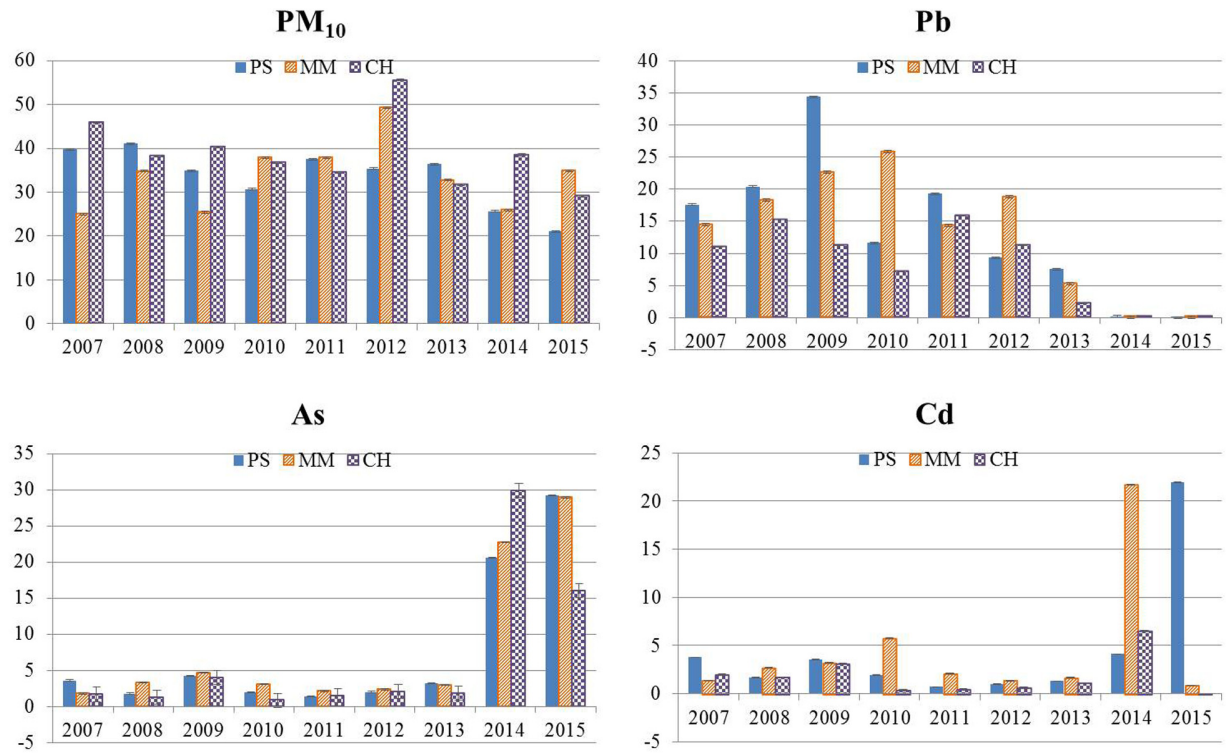


**FIGURE 2 |** Annual concentration of $PM_{10}$ ($\mu g\ m^{-3}$) and Pb, As, and Cd in $PM_{10}$ ($ng\ m^{-3}$) from 2007 to 2015.

be highlighted that the sampling area is a touristic place and that the location of the air-sampler is near the road. Considering that the sampling campaigns of 2014 and 2015 in PS have been carried out exclusively during warm season, it is likely the rise of Cd concentration in PS is due to an increase of vehicular tourist traffic.

The location of air-sampler in MM, instead, was inside the M.o.S.E. construction site so that, it is more probable that the increase of Cd in MM is due to an increase of yard activities, involving the movement of construction equipment.

The increase in arsenic during 2014 and 2015 occurs at all three sites, suggesting that the source to be long range transport rather than a local emission.

To better understand these sharp decrease (Cd and As) and increase (Pb) in metals concentrations, we compared the yearly average concentrations analyzed in this study, with data from the monitoring station located in the Venice Lagoon and organized by the Regional Environmental Protection Agency (ARPAV; **Supplementary Table SI 3**). Even if the monitoring station is located close the historical city center (Sacca Fisola), far from our sampling sites, and the methods of concentration acquisition are different, yearly average concentrations of the two data sets are comparable, for all the years, with the exception of 2014 and 2015. Altough the monitoring station detected an increase in As and Cd during these years, it is not as prominent as that analyzed in our study. For these reasons it is more likely that sharp variations highlighted in this study are due to intensity changes of local sources, like emission from the construction yard in the case of MM.

Divergences between sites during the years 2014 and 2015 have been also enhanced by the calculation of the CODs between two sampling periods: 2010–2013 and 2014–2015. The calculated CODs are: 0.56 in PS, 0.56 in MM, and 0.60 in CH (**Table 2**), indicating a great divergences between the two periods.

To enhance the contribution of construction activities in $PM_{10}$ and its metals content, CODs between holidays and working days have been calculated. Elements CODs in MM are rather higher than other sites (CODs $\geq$ 0.3 for Cr, Co, As, Cd, Sb, and Pb). These divergences in elements concentrations between working and no-working days in MM, considering the location of the site, may reflect the influence of the construction activities in the air quality of the sampling area.

The crustal enrichment factors ($EF_c$) for all analyzed elements were also calculated with the aim of assessing the impact of pollution on aerosols by the evaluation of the crustal or anthropogenic origin of the elements. $EF_c$ is calculated by the formula (Eq. 3):

$$EF_c = \left(el/Fe\right)_{air} / \left(el/Fe\right)_{crust} \quad (3)$$

comparing the ratios between the concentration of the single element and the reference element in air (samples collected in this study) and in the upper-crust (Wedepohl, 1995). We chose iron as reference element, because this element has been indicated as mainly of crustal origin in the Lagoon of Venice

(Masiol et al., 2012a, 2015), and in accordance with another study carried out in the same area (Contini et al., 2012). If $EF_c$ is below 10, a crustal origin of the element is more probable, EF < 50 indicates a slightly enriched element, while EF >> 100 indicates exceptionally enriched element. The EFs for all elements in the three sites are reported in **Figure 3**. From EFs of our data set has emerged: Co, V, (EF ≤ 10) have mainly crustal origin and are slightly enriched; Cr, Ni, Pb, Cu, and Zn (10 < EF < 100) have a predominantly anthropogenic origin, while As, Sb, and Cd are anomalously enriched. In general, except for Co, all the elements have a major enrichment in MM and PS then in CH, and it is extremely evident for Cd. These results are also rather consistent with the previous study of Contini et al. (2012) even if some differences can be noticed as a decrease of the EF of Sb (>1000 in 2012 and <1000 in this study), a slight decrease of the EF of Pb, as confirmed by the negative temporal trend (section "$PM_{10}$ and its metal content").

## Polycyclic Aromatic Hydrocarbon (PAHs)

The average concentration of PAHs, as sum of all analyzed congeners was 23.4 ng $m^{-3}$ (1.1–141.4 ng $m^{-3}$ of range) and 5.5 ng $m^{-3}$ (0.5–24.8 ng $m^{-3}$) in PS and MM, respectively. In both sites the concentration was higher than that previously observed in the summer period in Venice (Contini et al., 2011; Gregoris et al., 2014). The ΣPAHs concentration in PS was very similar to that recorded in a whole-year study in Grenoble (France, Tomaz et al., 2016). ΣPAHs concentration in PS and MM were lower than that measured in a long-term monitoring study in the United States (Liu et al., 2017) and in an 1-year study in India (Kumar et al., 2020).

The period of sampling could highly influence the concentration of PAHs (Hayakawa et al., 2020), since one of the most important anthropogenic source of PAHs is the primary emissions from residential heating, especially biomass burning, during the cold season (Tomaz et al., 2016). Moreover, the high concentration of pollutants in the cold season could also be due to the variation of the thickness of the planetary boundary layer (PBL), the volume of air where the atmospheric pollutants are dispersed. The reduction of the thickness of the PBL in the cold season, due to a reduced solar irradiance, could lead to a rise in the winter concentration of pollutants (Tositti et al., 2014). The seasonal variation of PAHs concentration could be the reason of the great difference between the measured concentration of ΣPAHs in the two sites: in PS 68% of samples have been collected in the heating season (from November to February), while in MM only 22% of them was collected in that period. Moreover, PS is characterized by a greater amount of pollution sources with respect to MM, since PS is more urbanized than MM and it is a tourist destination.

In **Figure 4** the ΣPAHs concentration (G + P: gas and particle phases) measured over the period 2010–2014 is shown. The highest average ΣPAHs concentration was observed in PS during the campaign conducted in December 2012 (83 ± 30 ng $m^{-3}$; **Figure 4A**); in MM the highest concentration values were measured during the campaign of February 2012 (16 ± 6 ng $m^{-3}$; **Figure 4B**). Monotonic trends of the chronological series were estimated using the non-parametric Mann-Kendall test, based on mean annual values, for avoiding the issue of a superimposed seasonal trend. Given the low number of values, we did not use the *Z*-statistics for the evaluation of trends, thus the *Z*-score in this case does not satisfy the normal condition, but we referred to the probability values of the *S*-statistics for number of values under 40 (ISPRA, 2017). Results showed no monotonic trend for data collected in MM and a negative monotonic trend in PS, with 77% of confidence.

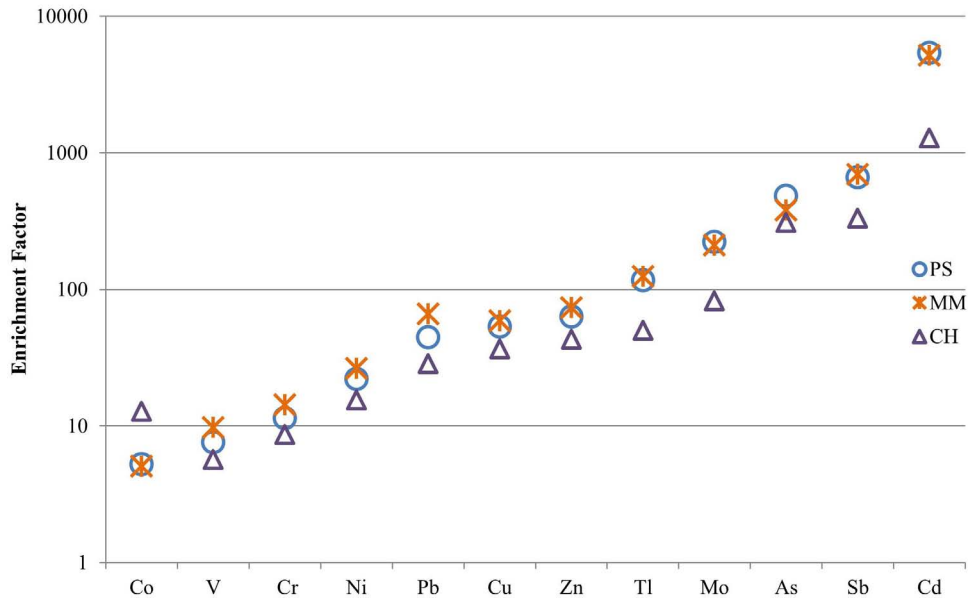


**FIGURE 3 |** EFs for all the analyzed elements in the three sites.

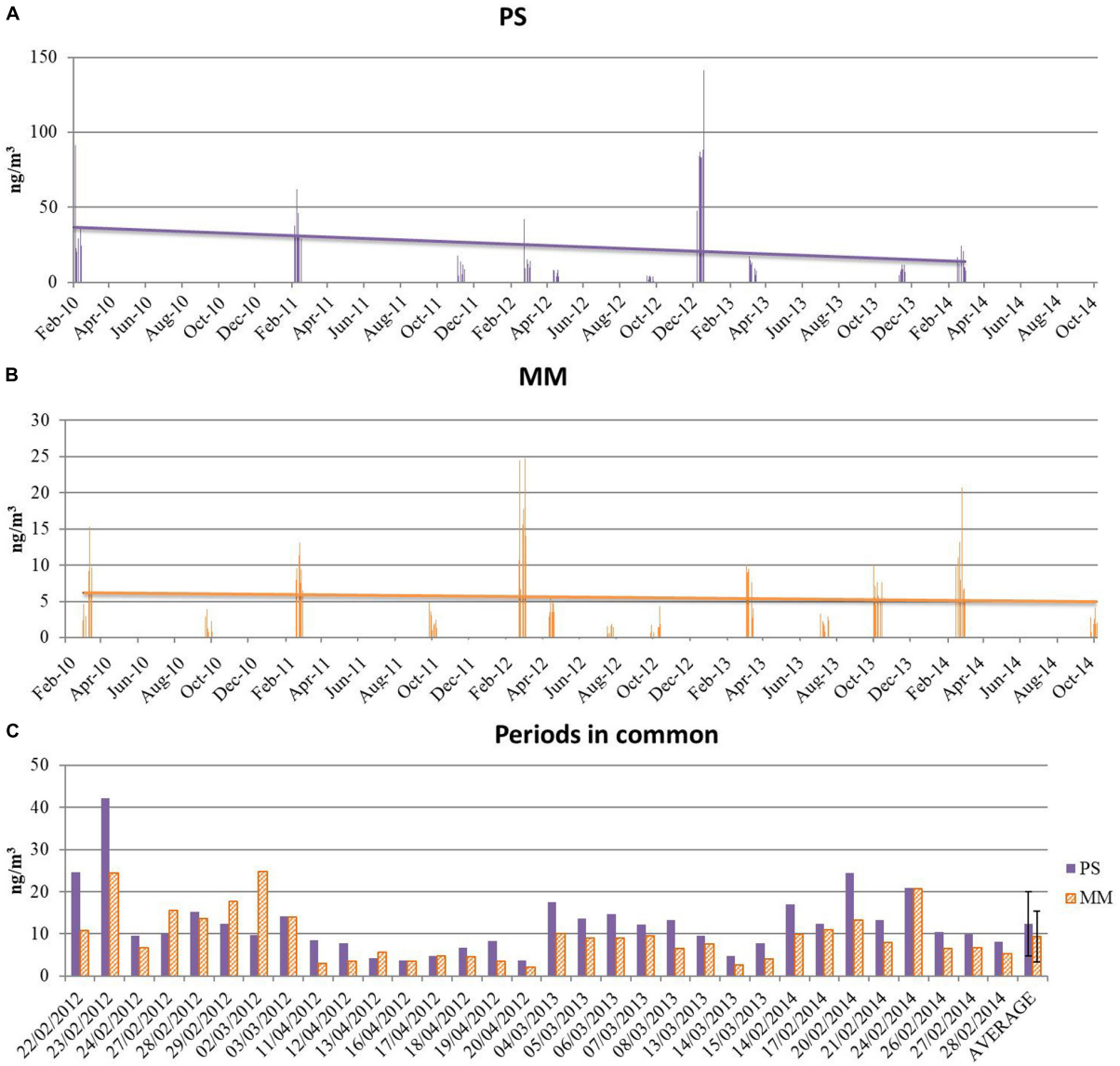


**FIGURE 4 |** Concentration of ΣPAHs (G + P): **(A)** in Punta Sabbioni; **(B)** in Malamocco; and **(C)** in both sites in the simultaneously monitored periods, with standard deviation as error bars.

Polycyclic aromatic hydrocarbons concentration was measured in the two sites in different campaigns, with only a few days in common. The comparison of ΣPAHs concentration in PS and MM was conducted selecting only the period for which the sampling was simultaneously carried out in the two sites (**Figure 4C**). The average ΣPAHs calculated in this way in the two sites was similar: 12.4 ± 7.6 ng $m^{-3}$ in PS and 9.3 ± 6.1 ng $m^{-3}$ in MM.

The average concentration of particulate PAHs, as sum of all analyzed congeners, was 7.6 ng $m^{-3}$ (0.2–47.3 ng $m^{-3}$ of range) in PS and 1.5 ng $m^{-3}$ (0.1–10.7 ng $m^{-3}$) in MM; the average ΣPAHs concentration in gas phase was 16.0 ng $m^{-3}$ (0.9–94.1 ng $m^{-3}$), and 4.0 ng $m^{-3}$ (0.02–19.6 ng $m^{-3}$). The concentration of ΣPAHs in gaseous and particulate phases of all samples is shown in **Supplementary Figure SI 4**. During the whole period, the concentration of PAHs in gas phase was higher with respect to the TSP phase, with an average contribution of about 67–68% of the gaseous PAHs to the total concentration of PAHs. The G/P ratio in PS and MM (2.1 and 2.6, respectively) was lower than that recorded in a previous work conducted in Venice with summer concentration data (Gregoris et al., 2014), and in Central Europe (Degrendele et al., 2020), and similar to that measured in the Cumalikizik region in Turkey (Gurkan Ayyildiz and Esen, 2020).

In order to have an idea of the seasonal trend of ΣPAHs, we selected the concentration measured in PS site for the year 2012, since in that year and in that site four sampling campaigns were carried out, covering various seasons. In 2012 gaseous PAHs

reached the highest total concentration (94 ng $m^{-3}$) in December and the lowest concentration (0.9 ng $m^{-3}$) in September. Particulate ΣPAHs ranged from 0.2 ng $m^{-3}$ (September) to 47 ng $m^{-3}$ (December). As reported in **Figure 5**, in both phases ΣPAHs concentration was higher in winter, decreasing moving toward the warm season, as in the classic seasonal trend of organic micropollutants. This trend draws its origin from the sources of the analyzed contaminants, that are mainly emissions from motor vehicles and domestic heating (Tomaz et al., 2016), and in the reduction of the thickness of the PBL in the cold season (Tositti et al., 2014).

The average concentration of single congeners is reported in the **Supplementary Information** (**Supplementary Figure SI 5**). It ranged from a few pg $m^{-3}$ to a few ng $m^{-3}$ for PHE in gaseous phase. The composition of samples was similar in the two sites. PHE was the main component in gaseous phase (6.3 ng $m^{-3}$ in PS, 2.0 ng $m^{-3}$ in MM, and corresponding to 39 and 48% of total congeners), followed by FL, FLA, and PYR (**Figure 6A**). PHE, FL, FLA, and PYR accounted together for 75 and 86% to total congeners in gas phase, in PS and MM, respectively. As expected, higher molecular weight PAHs were mainly present in particulate phase. In PS the main constituents of the particulate phase were BaA, CHR, BbF, BkF, and BaP, representing together about 65% of total congeners. FLA, PYR BbF, and BkF were the main present congeners in particulate matter collected in MM, with a contribution of 51% to the total PAHs. The distribution shown

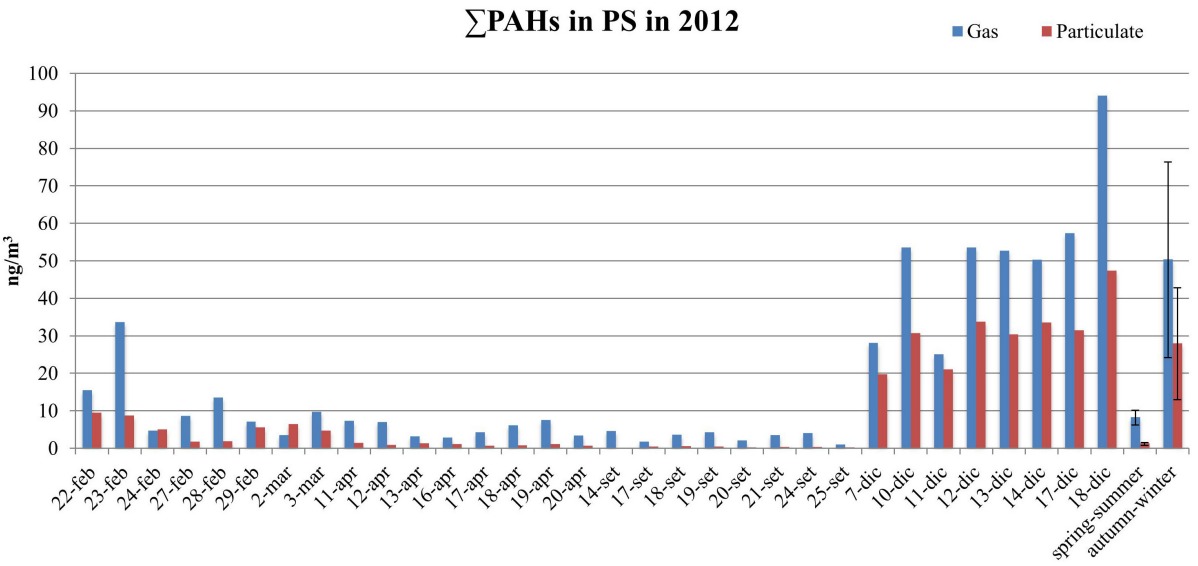


**FIGURE 5 |** Trend of ΣPAHs in particulate and gas phase, in PS site, for the year 2012, with averages and standard deviations as error bars.

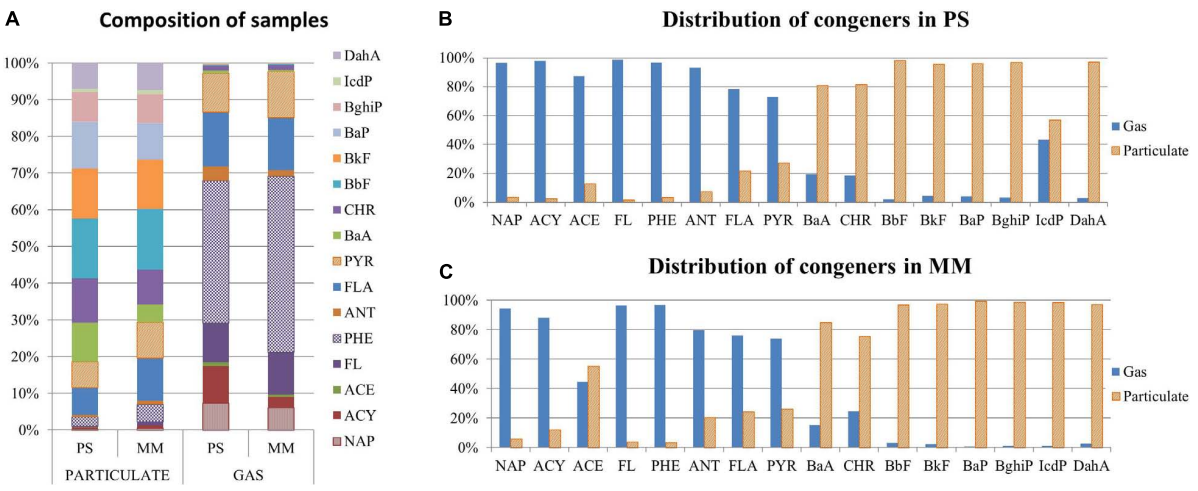


**FIGURE 6 |** Relative% of PAHs congeners. **(A)** Composition of gas and particulate samples in PS and MM; relative distribution of congeners among particulate and gas phases in **(B)** PS and **(C)** MM.

in **Figures 6B,C** is the typical congener profile in PAHs samples, with low molecular weight mainly distributed in the gaseous phase and high molecular weight compounds mainly present in the particulate phase (Gregoris et al., 2014; Tomaz et al., 2016). The distribution of chemicals between the two phases is dependent on the vapor pressure of compounds, which influences their volatilization from the particulate to the gaseous phase. Various factors, including temperature, air humidity, property of adsorption surface, and available adsorption surface, could also influence the vapor pressure and therefore the congener profile (Hassan and Khoder, 2012). The chronological trend of average concentration of PAHs is shown in **Supplementary Figures SI 6, SI 7**.

## Inhalation Risk Assessment

The cumulative incremental carcinogenic risk for $PM_{10}$ was $8.5 \times 10^{-6}$ (about one on 118,000), $1.1 \times 10^{-5}$ (about one on 92,000), and $1.2 \times 10^{-5}$ (about one on 83,000) in PS, MM, and CH, respectively. Values between $1 \times 10^{-4}$ and $1 \times 10^{-6}$ are generally considerate acceptable by the US-EPA (1999). Co and As are the most important contributors among metals, followed by Cd and Ni. The relative contribution varied among the monitoring sites: the contribution of Co increased passing from 34% in PS, to 40% in MM, and 53% in CH, while the contribution of As, on the opposite, was 47, 39, and 29% in PS, MM, and CH, respectively (**Figure 7A**).

For PAHs the cumulative incremental carcinogenic risk for G + P was $8.3 \times 10^{-7}$ (about one on 1,200,000) and $1.6 \times 10^{-7}$ (about one on 6,200,000) for the residential exposure in PS and MM, respectively. In both cases, it was below the unconditionally acceptable risk of one on one million ($1 \times 10^{-6}$), corresponding to an ample margin of safety (US-EPA, 1999). The congeners that most contribute to the carcinogenic risk were benzo(a)pyrene (51% and 45% in PS and MM) and dibenzo(A,H)anthracene (31% and 37% in PS and MM, **Figure 7B**), with percentages of contribution very similar to those obtained in previous works, using the TEF method (Gregoris et al., 2014).

## Source Identification and Apportionment

### Primary Contribution of Ship Traffic to $PM_{10}$

With the aim of evaluating the input of the source in $PM_{10}$, the primary contribution of ship traffic to $PM_{10}$ was quantified, using the atmospheric vanadium concentration, applying the equation (Eq. 4) first introduced by Agrawal et al. (2009).

$$PM_{ships} = \frac{R \cdot V_a}{F_{V,HFO}} \quad (4)$$

The constant $R$ has a suggested value of 8205.8 (Agrawal et al., 2009); $V_a$ is the ambient vanadium concentration; $F_{V,HFO}$ is a term indicating the typical V content (ppm) in heavy fuel oils (HFO) used by vessels. In this work the value of 65 ± 25 ppm was used, as previously done in the harbors of Venice (Gregoris et al., 2016), and Brindisi (Cesari et al., 2014).

The values of the primary contribution of ship traffic to $PM_{10}$ in MM and PS were published in Gregoris et al. (2016) as averages of the period 2007–2013. In this work the contribution was updated until 2015, with the additional site of CH. Annual averages from 2007 to 2015 of the primary contribution in the three sites are shown in **Figure 8**. For the calculation of the contribution in CH, vanadium concentration data previously collected in the same monitoring site was used. An increase of the primary contribution in MM during 2014 is evident, while still remaining in the average of other European cities (Viana et al., 2009, 2014), and seems indicate a change in Venice-port traffic, since MM is on the route of ships entering the lagoon.

### Source Apportionment of Metals by PMF

After the preliminary dataset refining, eleven variables were chosen as input for the model. In the final PMF run, the number of samples was 383, considering metals concentration measured from 2010 to 2013 in the three sites together. Since the total of metals represents a very small percentage of total particulate matter (about 1.2%) a source apportionment on PM was not possible. Thus, the PM mass was not included in the dataset and the apportionment was conducted to the sum of the metals analyzed, as previously done in Gregoris et al. (2016). The dataset dimension was in agreement with the suggestion by Henry et al. (1984), requiring that the minimum number of samples should be the one that yields a ratio between degrees of freedom and number of variables higher than 60. Since the number of chemically characterized ambient samples was higher than 50, the dataset agrees with the suggestion of Johnson et al. (2011). Moreover it also met the requirement of Thurston and Spengler (1985), with a number of samples exceeding the number of variables by a factor higher than three.

The solution was robust according to the test conducted using BS, DISP, and BS-DIPS error estimation. The comparison of reconstructed concentration by the PMF and the measured values showed that PMF reconstructed the observed concentrations of the coarse fraction with slope 0.89 and $R^2$ 0.64. The graphs of Q, IM, and IS trends, the results of the error estimation, and the graph of observed vs measured concentration are reported in the **Supplementary Information** (**Supplementary Figures SI 8, SI 9** and **Supplementary Tables S4, S5**). The source profile and their contribution is shown in **Figure 9**.

1. The first factor was characterized by the presence of Co, that contributes for about 98% to this source. In general, sources of environmental Co can be both natural and anthropogenic. The average EFs of Co calculated for the three sites were below or very close to 10 (see section "$PM_{10}$ and its metal content"), suggesting an average crustal origin of Co for the area of Venice (**Figure 3**). The factor was also characterized by a lesser contribution of Ni, Cr and Fe: Fe is a typical crustal element; Ni and Cr could have both natural and anthropogenic origin in the area of Venice, confirmed by the EF ranging from 7 to 15 and from 14 to 27 for Cr and Ni, respectively, and they were both not entirely contributing to the first factor. Given that Co is naturally often associated to Ni, being present and usually extracted from nickel ores (Kim et al., 2006), the first factor was assigned to have crustal origin, despite some industrial emission contamination could be present. The

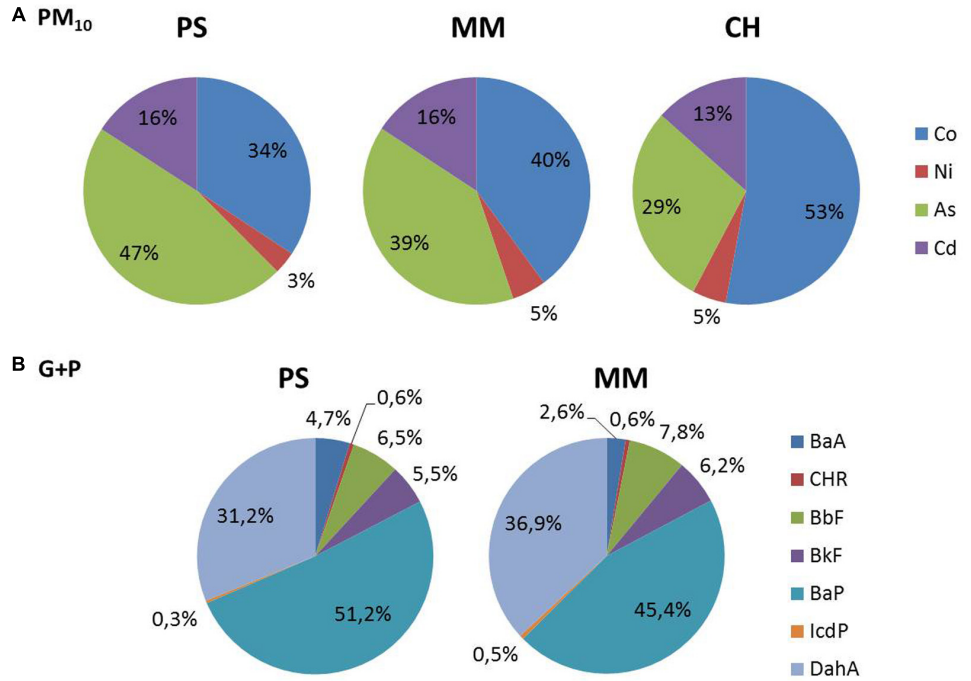


**FIGURE 7 |** Relative contribution of metals **(A)** and PAHs **(B)** pollutants in the incremental carcinogenic risk among the monitoring site.

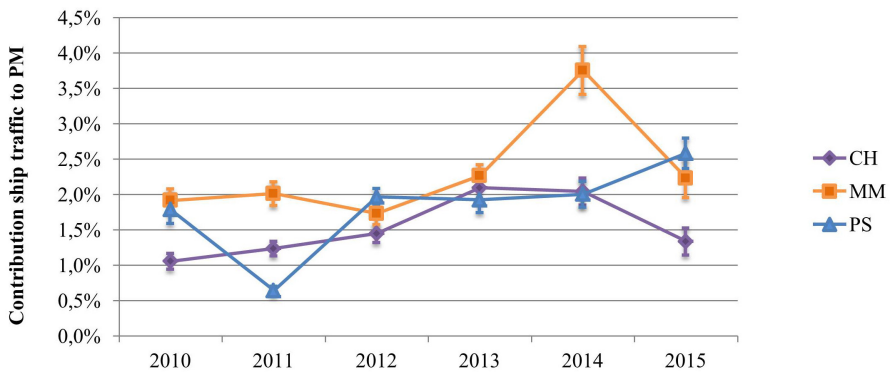


**FIGURE 8 |** Annual average of the primary contribution of ship traffic to $PM_{10}$, calculated using the Agrawal equation, in the three monitoring sites of Chioggia (CH), Malamocco (MM), and Punta Sabbioni (PS). The associated error is shown.

contribution of the factor was higher in CH (32%) with respect to MM (21%) and PS (26%).

2. The second factor was associated to the fossil fuel combustion, because of the high contribution of V and Ni. The V/Ni ratio associated to this factor was 2.4, similar to that suggested by Viana et al. (2009) as valid tracer for ship emission in the Mediterranean harbors (2.5–3.0). For this reason, even maintaining this factor associated to fossil fuel combustion in general, an important contribution of ship traffic was expected. The higher contribution of this source was calculated for MM (30%), compatible with the relative position of the three sites, given that MM lies along the path of commercial shipping to and from Porto Marghera. The correlation between the contribution of the fossil fuel combustion factor extracted by PMF and the primary contribution of ship traffic based on atmospheric vanadium [see section "Polycyclic aromatic hydrocarbon (PAHs)"] on the same samples was significant ($r = 0.69$; $p < 0.001$).
3. Various elements contributed to the third factor. Pb, Zn, and Sb, main contributors of this factor, could be associated to vehicular traffic (Contini et al., 2012). A contribution of industrial emission is not excluded, due to the presence of Cr and As, characterizing this factor. In previous works conducted in the same monitoring site (Contini et al., 2012) a similar factor was associated to a mixed

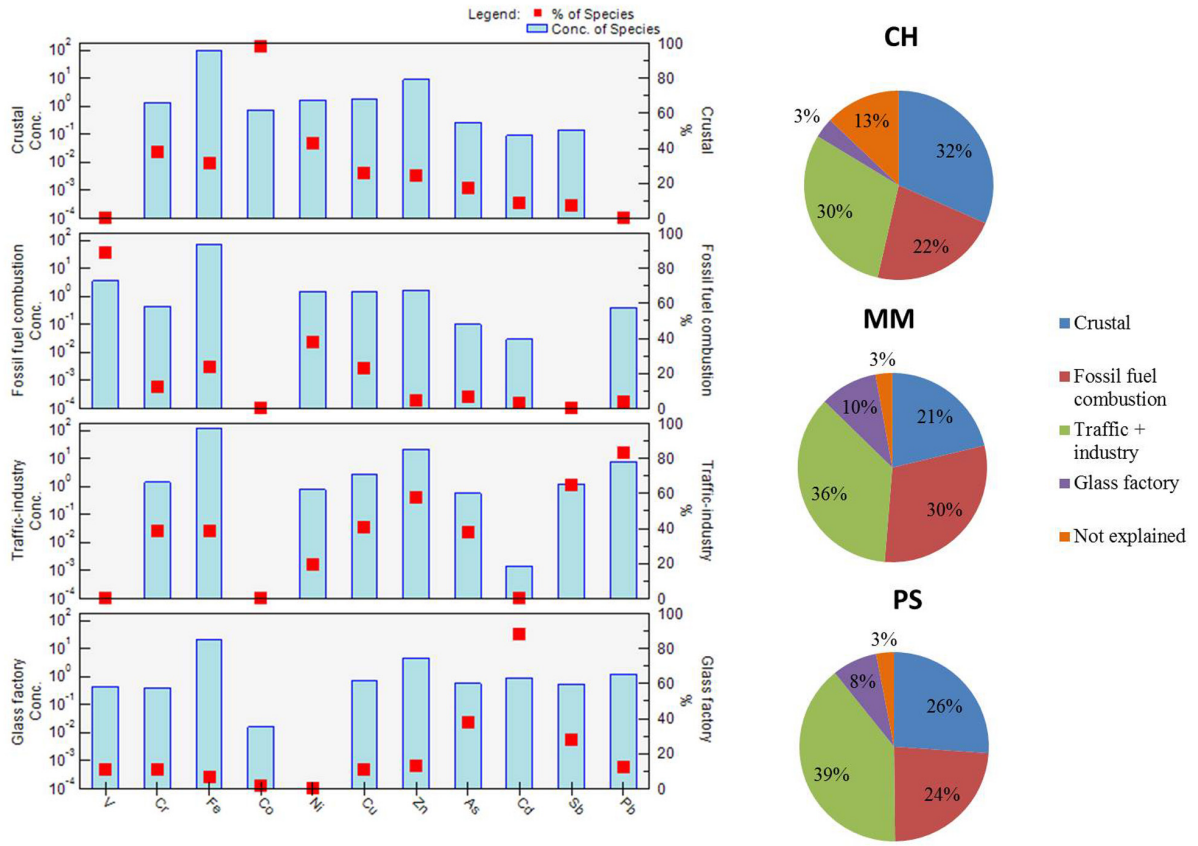


**FIGURE 9 |** On the **left**, factor source profile identified by PMF. Concentration of species are expressed both as absolute (ng/m$^3$, **left** vertical axis) and relative concentration (%, **right** vertical axis). On the **right**, contribution of the factors, including the fraction of not explained concentration, in the monitoring sites of Chioggia (CH), Malamocco (MM), and Punta Sabbioni (PS).

source including both traffic and industrial emission. The contribution of this factor was 39% in PS, 36% in MM and 30% in Chioggia. PS is a tourist destination and is characterized by an intense traffic.

4. Cd and As were associated to be originated by glass factory in the area of Venice in previous works (Rampazzo et al., 2008; Contini et al., 2012; Gregoris et al., 2016). The contribution of this factor is similar in MM and PS and higher with respect to CH, probably given to the proximity of MM and PS to the glass factories of the Murano island.

The identified sources are similar to those obtained in previous works in the same area (Contini et al., 2012; Gregoris et al., 2016), with the exception of the crustal source, identified for the first time in the area. Gregoris et al. (2016) conducted the source apportionment to metals in $PM_{10}$ from 2007 to 2013, based on the same concentration data used in this work and collected in MM and PS, but they did not include Co, and Sb variables, for homogeneity reasons. Contini et al. (2012) investigated the sources of metals in the Venice area, based on concentration data collected from 2007 to 2010 in the three monitoring sites. They observed a lower concentration of Co, with respect of the current work, since Co concentration raised in this area only in the period 2012–2013 (**Supplementary Figure SI 2**). This change in the aerosol composition could explain the different sources identified in the two works. Fe concentration showed a similar trend of Co in the period 2010–2013, with an increased concentration from 2010 to 2013. The correlation between Fe and Co concentration were significant in the three sites ($p < 0.001$; CH $r = 0.94$; MM $r = 0.47$; and PS $r = 0.39$). Annual average EFs of Co were <10 in PS and MM until 2012 and in CH until 2011, reaching average values between 25 and 30 in the following years, given to the higher increase of Co concentration with respect to Fe concentration. Given the proximity of the monitoring sites to the construction works of the M.o.S.E. mobile dams and the absence of known Co sources in the area, the increase of crustal elements could be associated to the movement of soil in the area. Despite EFs suggested a mixed origin of Co in 2012 and 2013 in the area, we associated the first factor to the crustal source, with the hypothesis of the contribution of the construction works to the factor.

## Source Estimation of PAHs

Generally, each PAHs source provides an individual profile fingerprint. Single congeners cannot be associated to a specific source, but DRs between specific congeners have been widely

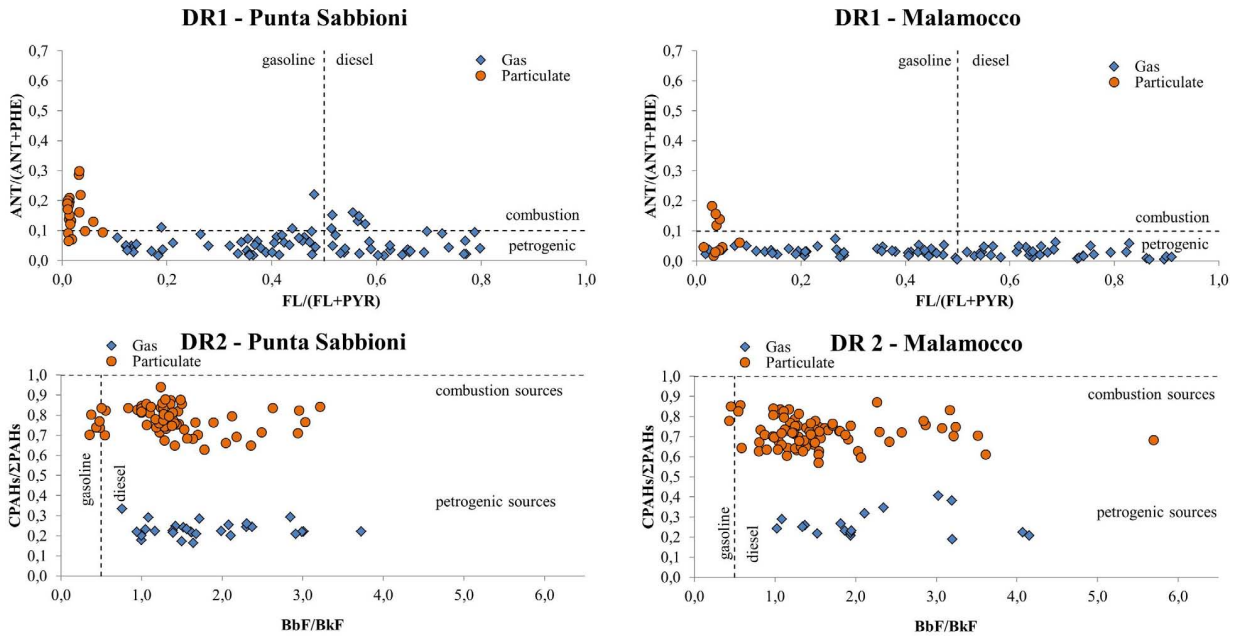


**FIGURE 10 |** PAH plots of the diagnostic ratios ANT/(ANT + PHE) versus FLA/(FLA + PYR; DR1) and CPAHs/ΣPAHs versus BbF/BkF (DR2), in Punta Sabbioni and Malamocco sites.

studied and used in order to estimate their possible sources (Ravindra et al., 2008; Lai et al., 2013; Gregoris et al., 2014; Gurkan Ayyildiz and Esen, 2020). In this work we used the congeners of molecular mass 178 to distinguish between combustion and petroleum sources: a ANT/(ANT + PHE) ratio < 0.10 is usually taken as an indicator of petroleum, while a ratio > 0.10 indicates a dominance of combustion sources (Yunker et al., 2002). Among the combustion of fossil fuels, the sources of gasoline and diesel can be separated using the FL/(FL + PYR) ratio, being a ratio < 0.50 representative of gasoline emissions and a ratio > 0.50 of diesel emissions (Ravindra et al., 2008). Since DRs only give an indication of the possible sources, without claiming to identify them in an absolute way, it is preferable investigate more indicators of the same sources, in order to improve the interpretation. For investigating the petrogenic/combustion sources we selected the additional ratio between the sum of FL, PYR, BaA, CHR, BbF, BkF, BaP, BghiP, and IcdP, typical PAHs from combustion (CPAHs), and the total concentration of PAHs: more the ratio approaches one, more important is the combustion source. Another indication for diesel emission is given by a BbF/BkF ratio higher than 0.5, while a ratio below 0.5 is an indication for gasoline emissions. The four chosen DRs were graphically represented in **Figure 10** as follows: one graph (DR1) includes the ANT/(ANT + PHE) and FL/(FL + PYR) ratios, another graph (DR2) is composed of the BaA/(BaA + CHR), and IcdP/(IcdP + BghiP) ratios, for both sites.

The plots of DR1 (**Figure 10**) referred to the PS site shows that the calculated ANT/ANT + PHE ratio was equally distributed between values above and below 0.1, indicating both combustion and petrogenic origin of measured PAHs. In MM most of the values were below 0.1, with only 22% of values above 0.1, almost exclusively constituted of samples of particulate phase. This difference was not confirmed by DR2, that shows a comparable distribution of ratios between the two sites. The average CPAHs/ΣPAHs (±standard deviation) in particulate phase was 0.70 ± 0.08 in MM and 0.77 ± 0.08 in PS; in gaseous phase was 0.26 ± 0.09 in PS and 0.24 ± 0.04 in MM. The clear distinction between the two phases in DR2 is due to the gas/particle distribution of congeners: high molecular congeners, like PAHs generated by combustion, are mainly distributed in the particulate phase due to their lower vapor pressure, while low molecular weight congeners are the main constituents of PAHs in the gaseous phase (**Figure 6**). The scarcity of data for some ratios is due to concentration values below the limit of detection for one or more compounds involved in the ratio. Regarding the distinction between gasoline and diesel emissions, DR1 suggested a mixed origin of PAHs in the area, while DR2 suggested a predominance of the diesel emissions. Globally the Venice area seems to be influenced by mixed sources of PAHs, as reported in a previous work (Gregoris et al., 2014). The average ratios and the number of values above and below the threshold are reported in the **Supplementary Information** (**Supplementary Table SI 5**).

## CONCLUSION

The comparison of the measurements taken at the different sites during the whole sampling period showed limited differences between the three sites, indicating a relatively homogeneous spatial distribution of metals in $PM_{10}$ in the Venice Lagoon

area. It has been confirmed by the coefficients of divergence which indicates similarity between PS and MM, and weak difference between MM and CH and between CH and PS. This general homogeneity was probably due to the presence of the specific meteorological circulation, which mixes air masses arriving from different directions, favoring the re-circulation and spread of pollutants in the lagoon area. Results of the non-parametric Mann-Kendall, carried out with integration of data from 2007 collected in the same three sites (Contini et al., 2012), showed a negative monotonic trend of the $PM_{10}$ in PS and CH, for Pb, and Sb in all the three sites, and for Zn in PS. However, the study of the yearly average concentrations showed sharp increase of As in the last 2 years in all the three sites while, in the same years, the yearly average concentration of Pb has a sharp decrease. Cd yearly trend shows a "peak" during 2014 in MM, and during 2015 in CH. These behavior seem most probable to be due to a change in local sources' emission. The PMF study and the indication emerged from COD between working days and holidays suggest that MM site is influenced more by the emission from construction activities and from ship traffic. From PMF other weak spatial differences have emerged between the sites which can be summarized up with a stronger contribution of emission from traffic and/or industry in PS from fossil fuel combustion in MM. The CH site is more characterized by crustal emission, which could be associated to the movement of soil in the construction area.

The evaluation of the crustal enrichment factors (EFs) indicated a specially important enrichment for Cd, Sb, and As, a significant enrichment for Pb, Zn, and Cu, while elements mainly of crustal origin were Co and V. Ni and Cr are slightly enriched but the values of EFs, in particular for Cr, are lower than the threshold of 20, so that it is not possible to exclude also a contribution of crustal nature. The EF of V is larger at Malamocco and this is compatible with a possible contribution of ship traffic emissions (characterized by V and Ni) at the Malamocco site, which is located near the path of commercial shipping.

As far as ΣPAHs is concerned, no monotonic trend have emerged for data collected in MM and a negative monotonic trend in PS, with 77% of confidence. During the whole period, the concentration of PAHs in gas phase was higher with respect to the TSP phase, with an average contribution of about 67–68% of the gaseous PAHs to the total concentration of PAHs. In both phases ΣPAHs concentration was higher in winter, decreasing moving toward the warm season, like in the classic seasonal trend due to the main sources of these contaminants, that are predominantly emissions from motor vehicles and domestic heating. Diagnostic Ratio for PAHs indicate both combustion and petrogenic origin, evidence that globally the Venice area may be influenced by mixed sources of PAHs, as enhanced by previous works carried out in the area.

The cumulative incremental carcinogenic risk for $PM_{10}$ was $8.5 \times 10^{-6}$ (about one on 118,000), $1.1 \times 10^{-5}$ (about one on 92,000), and $1.2 \times 10^{-5}$ (about one on 83,000) in PS, MM, and CH, respectively. Co and As are the most important contributors among metals, followed by Cd and Ni. The relative contribution varied among the monitoring sites: the contribution of Co increased passing from 34% in PS, to 40% in MM, and 53% in CH, while the contribution of As, on the opposite, was 47, 39, and 29% in PS, MM and CH, respectively.

As far as PAHs is concerned, the cumulative incremental carcinogenic risk for G + P was $8.3 \times 10^{-7}$ (about one on 1,200,000) and $1.6 \times 10^{-7}$ (about one on 6,200,000) for the residential exposure in PS and MM, respectively. In both cases, it was below the unconditionally acceptable risk of one on one million ($1 \times 10^{-6}$), corresponding to an ample margin of safety. The congeners that most contribute to the carcinogenic risk were benzo(a)pyrene and dibenzo(A,H)anthracene.

## DATA AVAILABILITY STATEMENT

The raw data supporting the conclusions of this article will be made available by the authors, without undue reservation.

## AUTHOR CONTRIBUTIONS

EM: sampling, metals data processing, data elaboration, and writing manuscript. EG: sampling, PAHs data processing, data elaboration, and writing manuscript. FB: coordination of sampling, review of manuscript, and of data elaboration. DCo: review of manuscript and of data elaboration. DCe: review of manuscript and of data elaboration. AG: coordination of sampling and data analysis, review of manuscript and of data elaboration. All authors contributed to the article and approved the submitted version.

## FUNDING

This work was supported by the "Ministero delle Infrastrutture e dei Trasporti – Provveditorato Interregionale per le Opere Pubbliche del Veneto – Trentino Alto adige – Friuli Venezia Giulia" (Italian Ministry of Infrastructures and Transports) through its dealer Consorzio Venezia Nuova.

## ACKNOWLEDGMENTS

The authors wish to thank the Venice Water Authority for permission to use the data and CORILA (Consortium for Managing the Research Activities Concerning the Venice Lagoon System) for the valuable assistance and logistic support during the sampling campaigns.

## SUPPLEMENTARY MATERIAL

The Supplementary Material for this article can be found online at: https://www.frontiersin.org/articles/10.3389/fenvs.2020.00107/full#supplementary-material

## REFERENCES


Agrawal, H., Eden, R., Zhang, X., Fine, P., Katzenstein, A., Miller, J., et al. (2009). Primary particulate matter from ocean-going engines in the southern california air basin. *Environ. Sci. Technol.* 43, 5398–5402. doi: 10.1021/es8035016

Arden Pope, C., and Dockery, D. W. (1999). "31 - epidemiology of particle effects," in *Air Pollution and Health*, eds T. H. Stephen, M. S. Jonathan, S. K. Hillel, J. M. S. H. S. K. Robert, L. MaynardA2 - Stephen, T. Holgate, et al. (London: Academic Press), 673–705. doi: 10.1016/b978-012352335-8/50106-x

ATSDR (2002). *Toxicological Profile for Polycyclic Aromatic Hydrocarbons (PAHS)*. Atlanta, GA: ATSDR.

Bool, L., Senior, C., Huggins, F., Huffman, G., and Shah, N. (1996). *Toxic Substances from Coal Combustion - A Comprehensive Assessment*. Reston, VA: USGS Science for changing world, 64.

Capodaglio, G., Toscano, G., Scarponi, G., and Cescon, P. (1994). Copper complexation in the surface sea water of terra nova bay (ANTARCTICA). *Int. J. Environ. Anal. Chem.* 55, 129–148. doi: 10.1080/03067319408026213

Cesari, D., Genga, A., Ielpo, P., Siciliano, M., Mascolo, G., Grasso, F. M., et al. (2014). Source apportionment of PM2.5 in the harbour–industrial area of Brindisi (Italy): identification and estimation of the contribution of in-port ship emissions. *Sci. Total Environ.* 497–498, 392–400. doi: 10.1016/J.SCITOTENV.2014.08.007

Contini, D., Belosi, F., Gambaro, A., Cesari, D., Stortini, A. M., and Bove, M. C. (2012). Comparison of PM10 concentrations and metal content in three different sites of the Venice Lagoon: an analysis of possible aerosol sources. *J. Environ. Sci.* 24, 1954–1965. doi: 10.1016/s1001-0742(11)61027-9

Contini, D., Gambaro, A., Belosi, F., De Pieri, S., Cairns, W. R. L., Donateo, A., et al. (2011). The direct influence of ship traffic on atmospheric PM 2.5, PM 10 and PAH in Venice. *J. Environ. Manag.* 92, 2119–2129. doi: 10.1016/j.jenvman.2011.01.016

Degrendele, C., Fiedler, H., Koèan, A., Kukuèka, P., Pøibylová, P., Prokeš, R., et al. (2020). Multiyear levels of PCDD/Fs, dl-PCBs and PAHs in background air in central Europe and implications for deposition. *Chemosphere* 240:124852. doi: 10.1016/J.CHEMOSPHERE.2019.124852

Galindo, N., Yubero, E., Clemente, Á, Nicolás, J. F., Varea, M., and Crespo, J. (2020). PM events and changes in the chemical composition of urban aerosols: a case study in the western Mediterranean. *Chemosphere* 244:125520. doi: 10.1016/j.chemosphere.2019.125520

Gambaro, A., Radaelli, M., Piazza, R., Stortini, A. M., Contini, D., Belosi, F., et al. (2009). Organic micropollutants in wet and dry depositions in the Venice Lagoon. *Chemosphere* 76, 1017–1022. doi: 10.1016/J.CHEMOSPHERE.2009.04.063

Gregoris, E., Argiriadis, E., Vecchiato, M., Zambon, S., De Pieri, S., Donateo, A., et al. (2014). Gas-particle distributions, sources and health effects of polycyclic aromatic hydrocarbons (PAHs), polychlorinated biphenyls (PCBs) and polychlorinated naphthalenes (PCNs) in Venice aerosols. *Sci. Total Environ.* 476–477, 393–405. doi: 10.1016/J.SCITOTENV.2014.01.036

Gregoris, E., Barbaro, E., Morabito, E., Toscano, G., Donateo, A., Cesari, D., et al. (2016). Impact of maritime traffic on polycyclic aromatic hydrocarbons, metals and particulate matter in Venice air. *Environ. Sci. Pollut. Res.* 23, 951–959. doi: 10.1007/s11356-015-5811-x

Gurkan Ayyildiz, E., and Esen, F. (2020). Atmospheric polycyclic aromatic hydrocarbons (PAHs) at two sites, in bursa, turkey: determination of concentrations, gas–particle partitioning, sources, and health risk. *Arch. Environ. Contam. Toxicol.* 78, 350–366. doi: 10.1007/s00244-019-00698-7

Han, S., Youn, J.-S., and Jung, Y.-W. (2011). Characterization of PM10 and PM2.5 source profiles for resuspended road dust collected using mobile sampling methodology. *Atmos. Environ.* 45, 3343–3351. doi: 10.1016/J.ATMOSENV.2011.04.015

Harrison, R. M., Pope, F. D., and Shi, Z. B. (2014). *Air Pollution?*. Amsterdam: Elsevier.

Hassan, S. K., and Khoder, M. I. (2012). Gas–particle concentration, distribution, and health risk assessment of polycyclic aromatic hydrocarbons at a traffic area of Giza, Egypt. *Environ. Monit. Assess.* 184, 3593–3612. doi: 10.1007/s10661-011-2210-8

Hayakawa, K., Tang, N., Nagato, E., Toriba, A., Lin, J.-M., Zhao, L., et al. (2020). Long-term trends in urban atmospheric polycyclic aromatic hydrocarbons and nitropolycyclic aromatic Hydrocarbons: China, Russia, and Korea from 1999 to 2014. *Int. J. Environ. Res. Public Health* 17:431. doi: 10.3390/ijerph17020431

Henry, R. C., Lewis, C. W., Hopke, P. K., and Williamson, H. J. (1984). Review of receptor model fundamentals. *Atmos. Environ.* 18, 1507–1515. doi: 10.1016/0004-6981(84)90375-5

ISPRA (2017). Guidelines for the Assessment of Ascending and Reversing Trends of Pollutants in Groundwater (Ministerial Decree, 6 July 2016) [Original title (Italian): Linee Guida Per la Valutazione Delle Tendenze Ascendenti e D'inversione Degli Inquinanti Nelle Acque. Available online at: http://www.isprambiente.gov.it/it/pubblicazioni/manuali-e-linee-guida/linee-guida-per-la-valutazione-delle-tendenze-ascendenti-e-dinversione-degli-inquinanti-nelle-acque-sotterranee-dm-6-luglio-2016 (accessed July 9, 2020).

Johnson, T., Guttikunda, S., Wells, G. J., Artaxo, P., Bond, T. C., Russell, A. G., et al. (2011). *Tools for Improving Air Quality Management: A Review of Top-Down Source Apportionment Techniques and Their Application in Developing Countries*. Report No 339/11. Washington, DE: ESMAP.

Kim, J. H., Gibb, H. J., Howe, P. D., World Health Organization. Chemical Safety Team, and International Programme on Chemical Safety (2006). *Cobalt and inorganic cobalt compounds / prepared by James H. Kim, Herman J. Gibb, Paul D. Howe*. Available online at: https://apps.who.int/iris/handle/10665/43426 (accessed July 9, 2020).

Kumar, A., Sankar, T. K., Sethi, S. S., and Ambade, B. (2020). Characteristics, toxicity, source identification and seasonal variation of atmospheric polycyclic aromatic hydrocarbons over East India. *Environ. Sci. Pollut. Res.* 27, 678–690. doi: 10.1007/s11356-019-06882-5

Lai, I. C., Chang, Y. C., Lee, C. L., Chiou, G. Y., and Huang, H. C. (2013). Source identification and characterization of atmospheric polycyclic aromatic hydrocarbons along the southwestern coastal area of Taiwan - with a GMDH approach. *J. Environ. Manag.* 115, 60–68. doi: 10.1016/j.jenvman.2012.11.018

Liu, B., Xue, Z., Zhu, X., and Jia, C. (2017). Long-term trends (1990–2014), health risks, and sources of atmospheric polycyclic aromatic hydrocarbons (PAHs) in the U.S. *Environ. Pollut.* 220, 1171–1179. doi: 10.1016/J.ENVPOL.2016.11.018

Liu, H., Tian, H., Zhang, K., Liu, S., Cheng, K., Yin, S., et al. (2019). Seasonal variation, formation mechanisms and potential sources of PM2.5 in two typical cities in the Central Plains Urban Agglomeration, China. *Sci. Total Environ.* 657, 657–670. doi: 10.1016/j.scitotenv.2018.12.068

Masiol, M., Rampazzo, G., Ceccato, D., Squizzato, S., and Pavoni, B. (2010). Characterization of PM10 sources in a coastal area near Venice (Italy): An application of factor-cluster analysis. *Chemosphere* 80, 771–778. doi: 10.1016/J.CHEMOSPHERE.2010.05.008

Masiol, M., Squizzato, S., Ceccato, D., and Pavoni, B. (2015). The size distribution of chemical elements of atmospheric aerosol at a semi-rural coastal site in Venice (Italy). The role of atmospheric circulation. *Chemosphere* 119, 400–406. doi: 10.1016/J.CHEMOSPHERE.2014.06.086

Masiol, M., Squizzato, S., Ceccato, D., Rampazzo, G., and Pavoni, B. (2012a). A chemometric approach to determine local and regional sources of PM10 and its geochemical composition in a coastal area. *Atmos. Environ.* 54, 127–133. doi: 10.1016/J.ATMOSENV.2012.02.089

Masiol, M., Squizzato, S., Ceccato, D., Rampazzo, G., and Pavoni, B. (2012b). Determining the influence of different atmospheric circulation patterns on PM10 chemical composition in a source apportionment study. *Atmos. Environ.* 63, 117–124. doi: 10.1016/J.ATMOSENV.2012.09.025

Mastral, A. M., and Callén, M. S. (2000). A Review on Polycyclic Aromatic Hydrocarbon (PAH) Emissions from Energy Generation. *Environ. Sci. Technol.* 34, 3051–3057. doi: 10.1021/es001028d

Morabito, E., Contini, D., Belosi, F., Stortini, A. M., Manodori, L., and Gambaro, A. (2014). Atmospheric deposition of inorganic elements and organic compounds at the inlets of the Venice lagoon. *Adv. Meteorol.* 2014, 1–10. doi: 10.1155/2014/158902

Prodi, F., Belosi, F., Contini, D., Santachiara, G., Di Matteo, L., Gambaro, A., et al. (2009). Aerosol fine fraction in the Venice Lagoon: particle composition and sources. *Atmos. Res.* 92, 141–150. doi: 10.1016/J.ATMOSRES.2008.09.020

Raaschou-Nielsen, O., Andersen, Z. J., Beelen, R., Samoli, E., Stafoggia, M., Weinmayr, G., et al. (2013). Air pollution and lung cancer incidence in 17 European cohorts: prospective analyses from the European Study of cohorts for air pollution effects (ESCAPE). *Lancet Oncol.* 14, 813–822. doi: 10.1016/S1470-2045(13)70279-1

Ramírez, O., Sánchez de la Campa, A. M., Amato, F., Moreno, T., Silva, L. F., and de la Rosa, J. D. (2019). Physicochemical characterization and sources of the thoracic fraction of road dust in a Latin American megacity. *Sci. Total Environ.* 652, 434–446. doi: 10.1016/j.scitotenv.2018.10.214

Rampazzo, G., Masiol, M., Visin, F., Rampado, E., and Pavoni, B. (2008). Geochemical characterization of PM10 emitted by glass factories in Murano. Venice (Italy). *Chemosphere* 71, 2068–2075. doi: 10.1016/J.CHEMOSPHERE.2008.01.039

Ravindra, K., Sokhi, R., and Van Grieken, R. (2008). Atmospheric polycyclic aromatic hydrocarbons: source attribution, emission factors and regulation. *Atmos. Environ.* 42, 2895–2921. doi: 10.1016/J.ATMOSENV.2007.12.010

Riva, G., Pedretti, E. F., Toscano, G., Duca, D., and Pizzi, A. (2011). Determination of polycyclic aromatic hydrocarbons in domestic pellet stove emissions. *Biomass Bioenergy* 35, 4261–4267. doi: 10.1016/J.BIOMBIOE.2011.07.014

Squizzato, S., and Masiol, M. (2015). Application of meteorology-based methods to determine local and external contributions to particulate matter pollution: a case study in Venice (Italy). *Atmos. Environ.* 119, 69–81. doi: 10.1016/j.atmosenv.2015.08.026

Squizzato, S., Masiol, M., Agostini, C., Visin, F., Formenton, G., Harrison, R. M., et al. (2016). Factors, origin and sources affecting PM1 concentrations and composition at an urban background site. *Atmos. Res.* 180, 262–273. doi: 10.1016/j.atmosres.2016.06.002

Stortini, A. M., Freda, A., Cesari, D., Cairns, W. R. L., Contini, D., Barbante, C., et al. (2009). An evaluation of the PM2.5 trace elemental composition in the Venice Lagoon area and an analysis of the possible sources. *Atmos. Environ.* 43, 6296–6304. doi: 10.1016/j.atmosenv.2009.09.033

Thurston, G. D., and Spengler, J. D. (1985). A quantitative assessment of source contributions to inhalable particulate matter pollution in metropolitan Boston. *Atmos. Environ.* 19, 9–25. doi: 10.1016/0004-6981(85)90132-5

Tomaz, S., Shahpoury, P., Jaffrezo, J.-L., Lammel, G., Perraudin, E., Villenave, E., et al. (2016). One-year study of polycyclic aromatic compounds at an urban site in Grenoble (France): seasonal variations, gas/particle partitioning and cancer risk estimation. *Sci. Total Environ.* 565, 1071–1083. doi: 10.1016/j.scitotenv.2016.05.137

Tositti, L., Brattich, E., Masiol, M., Baldacci, D., Ceccato, D., Parmeggiani, S., et al. (2014). Source apportionment of particulate matter in a large city of southeastern Po Valley (Bologna, Italy). *Environ. Sci. Pollut. Res. Int.* 21, 872–890. doi: 10.1007/s11356-013-1911-7

US-EPA (1999). *Residual risk - Report to Congress*. Washington, DC: US-EPA.

US-EPA (2014). *EPA Positive Matrix Factorization (PMF) 5.0 Fundamentals and User Guide*. Washington, DC: US-EPA.

United States Environmental Protection Agency (1981). *Priority Pollutant List. Regulation No.: 40 CFR 423, Appendix A*. Washington, DC: US. EPA.

United States Environmental Protection Agency (1998). *Report on revisions to AP-42 Section 1.3 Fuel Oil Combustion. Citeseer*, 5th Edn. Washington, DC: US. EPA.

United States Environmental Protection Agency (2009). *Risk Assessment Guidance for Superfund Volume I: Human Health Evaluation Manual (Part F, Supplemental Guidance for Inhalation Risk Assessment)*. Washington, DC: US. EPA.

United States Environmental Protection Agency (2016). *Regional Screening Levels (RSLs)–Generic Tables*. Washington, DC: US. EPA.

Valotto, G., Squizzato, S., Masiol, M., Zannoni, D., Visin, F., and Rampazzo, G. (2014). Elemental characterization, sources and wind dependence of PM1 near Venice. *Italy. Atmos. Res.* 143, 371–379. doi: 10.1016/j.atmosres.2014.03.007

Viana, M., Amato, F., Alastuey, A., Querol, X., Moreno, T., Garcia Dos Santos-Alves, S., et al. (2009). Chemical tracers of particulate emissions from commercial shipping. *Environ. Sci. Technol.* 43, 7472–7477. doi: 10.1021/es901558t

Viana, M., Hammingh, P., Colette, A., Querol, X., Degraeuwe, B., de Vlieger, I., et al. (2014). Impact of maritime transport emissions on coastal air quality in Europe. *Atmos. Environ.* 90, 96–105. doi: 10.1016/J.ATMOSENV.2014.03.046

Wedepohl, H. K. (1995). The composition of the continental crust. *Geochim. Cosmochim. Acta* 59, 1217–1232. doi: 10.1016/0016-7037(95)00038-2

Wild, S. R., and Jones, K. C. (1995). Polynuclear aromatic hydrocarbons in the United Kingdom environment: a preliminary source inventory and budget. *Environ. Pollut.* 88, 91–108. doi: 10.1016/0269-7491(95)91052-M

Wongphatarakul, V., Friedlander, S. K., and Pinto, J. P. (1998). A comparative study of PM2.5 ambient aerosol chemical databases. *Environ. Sci. Technol.* 32, 3926–3934. doi: 10.1021/es9800582

Yunker, M. B., Macdonald, R. W., Vingarzan, R., Mitchell, R. H., Goyette, D., and Sylvestre, S. (2002). PAHs in the Fraser River basin: a critical appraisal of PAH ratios as indicators of PAH source and composition. *Org. Geochem.* 33, 489–515. doi: 10.1016/S0146-6380(02)00002-5

Zhao, M., Zhang, Y., Ma, W., Fu, Q., Yang, X., Li, C., et al. (2013). Characteristics and ship traffic source identification of air pollutants in China's largest port. *Atmos. Environ.* 64, 277–286. doi: 10.1016/J.ATMOSENV.2012.10.007

Zou, J., Liu, Z., Hu, B., Huang, X., Wen, T., Ji, D., et al. (2018). Aerosol chemical compositions in the North China Plain and the impact on the visibility in Beijing and Tianjin. *Atmos. Res.* 201, 235–246. doi: 10.1016/J.ATMOSRES.2017.09.014

**Conflict of Interest:** The authors declare that the research was conducted in the absence of any commercial or financial relationships that could be construed as a potential conflict of interest.

frontiers in Environmental Science

ORIGINAL RESEARCH
published: 06 August 2020
doi: 10.3389/fenvs.2020.00134

# An Overview of Cadmium, Chromium, and Lead Content in Bivalves Consumed by the Community of Santa Rosa Island (Ecuador) and Its Health Risk Assessment

*David Romero-Estévez[1]*, Gabriela S. Yánez-Jácome[1], Mónica Dazzini Langdon[2]*, Karina Simbaña-Farinango[1], Eduardo Rebolledo Monsalve[3], Gabriel Durán Cobo[4] and Hugo Navarrete[1]*

*[1] Centro de Estudios Aplicados en Química, Pontificia Universidad Católica del Ecuador, Quito, Ecuador, [2] "Ciudad Abierta" Project in Architecture College, Pontificia Universidad Católica del Ecuador, Quito, Ecuador, [3] Environmental Management Career, Pontificia Universidad Católica del Ecuador, Esmeraldas, Ecuador, [4] Marine Biology Career, Pontificia Universidad Católica del Ecuador, Portoviejo, Ecuador*

Santa Rosa Island community members derive their income and livelihoods from bio-aquatic resources, principally bivalves of the genus *Anadara*, both for subsistence use and commercial purposes. Bivalve mollusks have a sedentary lifestyle and feed by filtering water, meaning they absorb all surrounding substances, including harmful elements like toxic metals. This study aimed to analyze different-sized samples of *Anadara tuberculosa* and *Anadara similis*, sediment, and *Rhizophora mangle* leaves to determine their total amount of cadmium, lead, and chromium as a first approach to the evaluation of the health risk related to the consumption of bivalves. For both species from four sampling sites, the results revealed metal concentrations in the bivalves between 0.211 and 0.948 mg $kg^{-1}$, 0.038, and 0.730 mg $kg^{-1}$, and 0.067 and 0.923 mg·$kg^{-1}$ for Cd, Cr, and Pb, respectively. The calculated potential risk (>1) for cadmium, considering all body weights, showed a high health risk for consumers. In the case of lead, the results showed a high health risk in children. There was no risk found for chromium. For sediments, the mean values were 2.14, 29.99, and 12.37 mg·$kg^{-1}$ and for the *Rhizophora mangle* leaves were 2.23, 4.22, and 3.35 mg·$kg^{-1}$ for Cd, Cr, and Pb, respectively. These results did not show a relation with the metal content in bivalves.

**Keywords: *Anadara tuberculosa*, *Anadara similis*, human health, metal intake, toxicology**

OPEN ACCESS

***Edited by:***
*Bernardo Duarte, Center for Marine and Environmental Sciences (MARE), Portugal*

***Reviewed by:***
*Mário Sousa Diniz, Faculty of Sciences and Technology, New University of Lisbon, Portugal*
*Michael Edward Deary, Northumbria University, United Kingdom*

****Correspondence:***
*David Romero-Estévez*
*dfromero@puce.edu.ec*
*Mónica Dazzini Langdon*
*mdazzini435@puce.edu.ec*

***Specialty section:***
*This article was submitted to Toxicology, Pollution and the Environment, a section of the journal Frontiers in Environmental Science*

***Received:*** *22 May 2020*
***Accepted:*** *16 July 2020*
***Published:*** *06 August 2020*

***Citation:***
*Romero-Estévez D, Yánez-Jácome GS, Dazzini Langdon M, Simbaña-Farinango K, Rebolledo Monsalve E, Durán Cobo G and Navarrete H (2020) An Overview of Cadmium, Chromium, and Lead Content in Bivalves Consumed by the Community of Santa Rosa Island (Ecuador) and Its Health Risk Assessment. Front. Environ. Sci. 8:134. doi: 10.3389/fenvs.2020.00134*

## INTRODUCTION

Over the past decades, anthropogenic activities resulting from, urban and agricultural industrialization development, and waste disposal, have led to the increase of chemical pollution in coastal and marine ecosystems (da Silveira Fiori et al., 2018; Esposito et al., 2018). Coastal zones with river inflows are the most affected due to the continuous drag of contaminants,

which constantly accumulate in marine sediments and organisms. Thus, marine organisms such as bivalves that inhabit the coasts are more likely to be exposed to high levels of contaminants, including trace metals. Hence, they represent a threat to human health when used for consumption because of their bioaccumulation and biomagnification through the aquatic food web (Jiang et al., 2018).

Mangroves are one of the most complex ecosystems in the world and are located in tropical and subtropical regions of terrestrial environments, estuaries, and near marine coasts. They are unique biomes that serve as a transition from the terrestrial to the marine environment. While there are no accurate estimates of the original cover, there is a consensus that it would have been over 200,000 $km^2$ and that considerably more than 50,000 $km^2$ or one-quarter of original mangrove cover has been lost because of human intervention (Spalding et al., 2010).

Over the past 20 years, the Ecuadorian government has awarded mangroves to fishing communities and tourism entrepreneurs. These mangrove concessions are not new in Ecuador; according to the Undersecretary for Coastal and Marine Management of the Ecuadorian Ministry of the Environment (abbreviated MAE in Spanish), 91 concessions have been granted since 2001. These concessions specify the community's rights to use the mangrove ecosystem for artisanal fishery. In communities where the concessions have been implemented, local associations of fishermen have privileged access for fishing within the boundaries of their area (Beitl, 2015).

Within the Cayapas-Mataje Mangrove Reserve (REMACAM) the Association of Afro-Ecuadorian Women of Fishermen and Collectors of Bio-Aquatic Products of Santa Rosa Island has had for 10 years, a concession of 350 hectares assigned by the MAE since October 2018. The community members of Santa Rosa Island derive their livelihoods from bio-aquatic resources from the surrounding mangrove ecosystem, principally the bivalves of the genus *Anadara*, for their sustenance, also to sell them in nearby cities (Ministerio del Ambiente [MAE], 2019; USAID, 2012, p. 5). *A. tuberculosa* and *A. similis* are two bivalve species that inhabit mangroves and are found along tropical coastal regions of the Eastern Pacific, from Heroica Guaymas de Zaragoza port in Mexico to the Bay of Tumbes in Peru (Gener et al., 2009, p. 3). These species are bivalve mollusks known in Ecuador as "concha prieta," "concha negra," or "concha hembra" (Flores et al., 2014). These bivalves are harvested from the muddy, sandy substrate characteristic of the mangrove ecosystem during periods of low tide (Beitl, 2015).

Bivalve mollusks are benthic organisms, used as sentinel species because of their long-life cycle and sedentary lifestyle (da Silveira Fiori et al., 2018). They allow pollution levels of marine ecosystems to be evaluated, providing integrated information over time on the presence of pollutants in the environment (Boening, 1999; Erk et al., 2018). Bivalves are characterized by their ability to filter water to feed (Ruiz et al., 2018). Because of this feeding method, these animals absorb high concentrations of toxic non-essential metals such as cadmium (Cd), chromium (Cr), lead (Pb), and essential metals such as cobalt (Co), copper (Cu), manganese (Mn), and zinc (Zn), which bioaccumulate in their tissues (da Silveira Fiori et al., 2018).

In Ecuador, legal regulations related to bivalves (Ministerial Agreement N° 005 issued on August 2, 2005) regulate the minimum size (4.5 cm in length) for the extraction and commercialization of *A. tuberculosa* and *A. similis* (Ministerio de Acuacultura y Pesca [MAP], 2005). However, the regulation does not address threshold values for any contaminants, including toxic metals.

The European Commission Regulation (European Commission (EC), 2006) has established maximum levels for some contaminants, including heavy elements like Cd and Pb, of 1.0 and 1.5 $mg{\cdot}kg^{-1}$ (fresh weight), respectively, in bivalve mollusks for its consumption. The Food and Agriculture Organization of the United Nations (FAO) and the World Health Organization (WHO) have established threshold values only for Cd (2.0 mg $kg^{-1}$, fresh weight) in the International Food Standards (CODEX 193) (FAO/WHO, 2019). In the case of Cr, neither the European Commission Regulation nor the FAO has established threshold values.

Regarding health risk assessment, the Environmental Protection Agency of the United States (US EPA) has established oral reference doses (RfD) of 0.001 mg $kg^{-1}$ $d^{-1}$ for Cd (US EPA, 2018, 2000) and 1.5 mg $kg^{-1}$ $d^{-1}$ for Cr (III) (US EPA-IRIS, 1998). There is no US EPA RfD value for Pb, but the United States Food and Drug Administration (FDA) interim reference level for lead corresponds to 0.003 mg $d^{-1}$ for children and 0.0125 mg $d^{-1}$ for adults (FDA, 2019).

Several studies on metal contamination in sediments, mangroves, and macrobenthic organisms that evaluate environmental pollution levels and health risks have been conducted in Guayas and Esmeralda provinces (Fernández-Cadena et al., 2014; Mendoza Angulo, 2014; Calle et al., 2018; Pernía et al., 2018). Nevertheless, no studies related to Pb levels have been conducted in Santa Rosa Island. For these reasons, this study aims to: a) determine the concentration of Cd, Cr, and Pb in REMACAM bivalves (*A. tuberculosa* and *A. similis*), and b) assess the health risks associated with these metals by consuming *Anadara* spp.

# MATERIALS AND METHODS

## Study Area

The REMACAM is located in the northwest of Ecuador, in the province of Esmeraldas, and includes the southern part of the Tumbes-Chocó-Magdalena ecological region. Within REMACAM inhabit the community of Santa Rosa Island, comprising 310 members in 87 families. Most of the community is young (146 members between 0 and 19 years old), and the illiteracy level is 24%. The population maintains an income level below the poverty line of the national average set at 47.48 USD of monthly family income.

Santa Rosa Island community is located in the central part of REMACAM between the Pacific Ocean and Santa Rosa estuary. Four sampling sites were established based on their proximity to the ocean, and the fact that they are remote areas that could be impacted by the Santa Rosa Island population. The sites were denominated E1, on the southern border of the "Hondo" estuary,

300 m from where the Santa Rosa estuary begins. E2, on "la Tumba" beach, in the Santa Rosa estuary, 1500 m south of where the estuary begins. E3, on "al Otro Lado" beach, in the estuary that borders the north side of the settlement, and E4, "la Caleta" estuary, 500 m from the Santa Rosa estuary (**Figure 1**).

## Sample Collection

The samples were bought to the Santa Rosa Island community members, who carried out the sampling process using the same technique that they routinely use to collect bivalves for consumption and sale. The harvesting was done for 1 h, in which the largest possible number of bivalves were collected without considering kind or size. Four pairs of collectors were chosen for buying the samples, one for each sampling location. In addition, holes were dug to extract four surface sediment samples of about 30 cm deep using a stainless steel scoop as the SESDPROC-200-R3 reference (US EPA, 2014) and four samples of *Rhizophora mangle* leaves were collected, corresponding to each location.

## Handling Samples Before Analysis

Fifty composite samples of the different species and sizes from the four sampling locations were formed with approximately 10 bivalves randomly selected for each sample. The samples were stored in self-sealing plastic bags, labeled, stored in a refrigerator, and transferred to the Environmental Management Laboratory of the Pontificia Universidad Católica del Ecuador in Esmeraldas (PUCE-Esmeraldas), where they were classified into 18 subgroups by species, length, and width. The soft tissues were immediately extracted to transfer to the Centro de Estudios Aplicados en Química laboratory in Quito. The sediment and leaf samples were also deposited in self-sealing plastic bags and transferred to the laboratory.

## Metal Quantification

All samples including bivalves, sediment, and leaves were analyzed in triplicate, using fortifications as quality control. The lowest concentration of each metal that can be detected (detection limit) was established analytically at 0.15 mg $kg^{-1}$, 0.55 mg $kg^{-1}$, 0.45 mg $L^{-1}$ for Cd, Cr, and Pb respectively. The minimum concentration of each metal that can be reliably determined (quantification limit) was established analytically at 0.5 mg $kg^{-1}$ for Cd and 15.0 mg $kg^{-1}$ for both Cr and Pb. The calibration curves were prepared in 0.01, 0.10, 0.30, 1.00 mg $L^{-1}$ for Cd, and in 0.3, 1.0, 3.0, 5.0 for Cr, and Pb mg $L^{-1}$, considering a correlation coefficient higher than 0.99 for its acceptation. The relative standard deviation (RSD) for each triplicate and fortification recoveries (accuracy) was calculated for each sample determination.

The refrigerated soft tissues were washed with high-quality reagent water (resistivity 18.2 MΩ·cm at 25°C) to eliminate

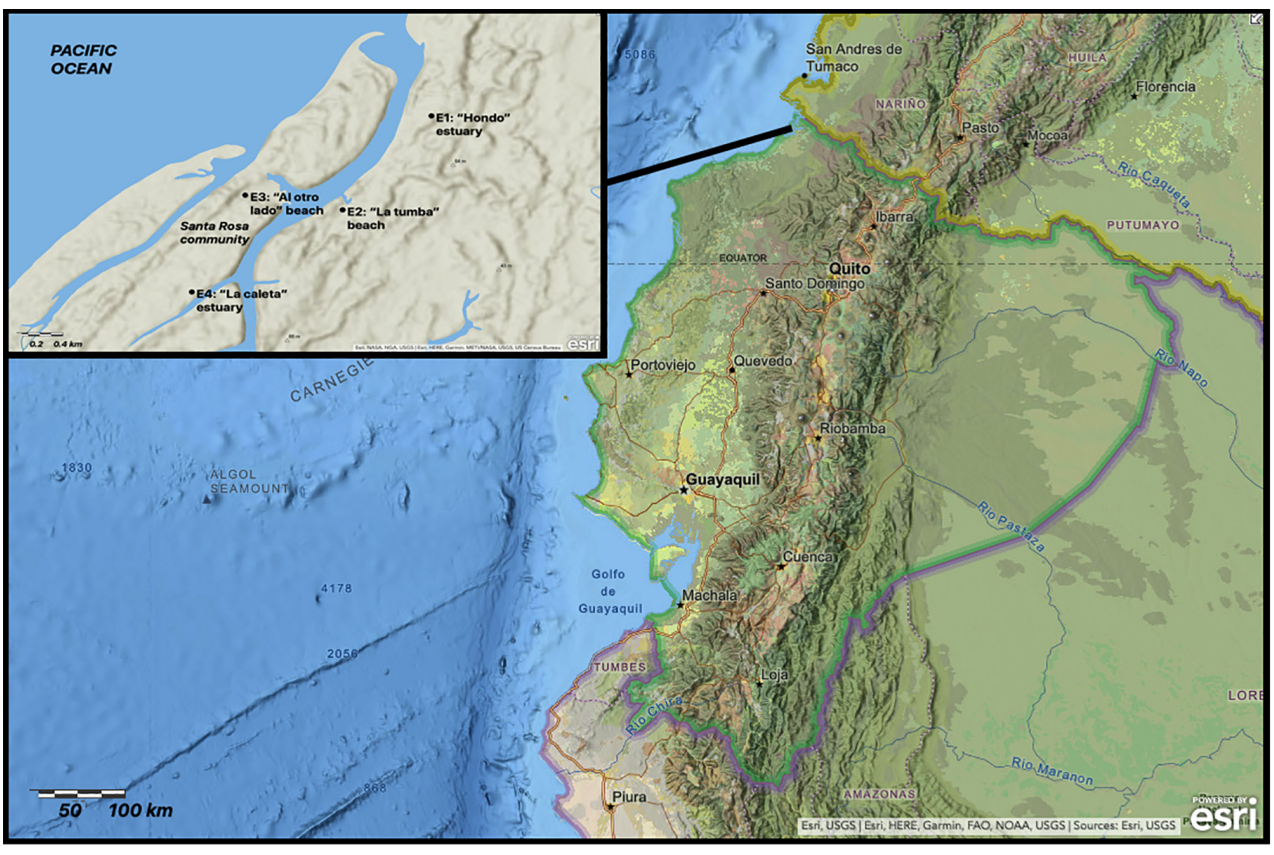


**FIGURE 1 |** Location of bivalve, sediment, and leaf sampling sites (image edited from ArcGIS online and powered by esri).

sediment residue and any other kind of impurity. Water content was determined at 105°C using an oven (Memmert UM 500). Samples were dried for 72 h at 60°C in the oven until a constant weight was achieved. The dried tissues were then milled.

Approximately 0.5 g of each sample were measured in Teflon vials, and 7 mL of 65% nitric acid were added (Fisher Chemical, Certified ACS plus, CAS# 7697-37-2). Acid digestion was performed using a CEM MARS 6 microwave, applying the analytical method IPN AC-06-00 (CIIEMAD-IPN, 2011) as a reference, validated for its use for bivalve matrix. The digested samples were then filtered and made up to a final volume of 25 $cm^3$. Metals (Cd, Cr, and Pb) were quantified with a flame atomic absorption spectrophotometer, Perkin Elmer AAnalyst 400. For blanks, samples, and calibration curve standards preparation, analytical grade reagents were employed. The triplicate analysis, fortifications of known concentrations, and certified reference material of metals in fish protein (DORM 4; National Research Council Canada) were performed as quality control. The results are presented in mg $kg^{-1}$ of fresh weight.

Sediment samples were processed according to the US EPA method 3051A (US EPA, 2007). Leaves samples were processed according to the natural food method validated for its use in plant tissues (Romero-Estévez et al., 2019). Both matrixes were analyzed using a flame atomic absorption spectrophotometer.

## STATISTICAL ANALYSES

The arithmetic mean, standard deviation, and recovery of fortifications were calculated for all the Cd, Cr, and Pb concentrations obtained from all the samples.

The RSD values and accuracy were evaluated against the acceptable limits described in the AOAC Guidelines for Single Laboratory Validation of Chemical Methods for Dietary Supplements and Botanicals (AOAC, 2002): the RSD value acceptance limits are 11% for reproducibility, and the accuracy acceptance limits are between 80 and 115%.

In addition, for the correlation analysis between the metals content in bivalves, sediments and leaves, the correlation coefficients and p-values were calculated using an alpha ($\alpha$) level of 0.05 (confidence level 95%) as an indication of statistical significance.

## CALCULATIONS

### Human Health Risk Assessment

In Ecuador, a traditional recipe for the bivalves included in the present study is the "ceviche," in which approximately 20 bivalve specimens between 40 and 50 mm are used, corresponding to an approximately intake portion between 150 and 500 g (fresh weight). Eating ceviche is common for locals, who eat between 3 and 5 portions per week. For the intake calculations, the amounts of 200 g and the 400 g (fresh weight) were selected as the intake portions for children and adults respectively, considering the average number of bivalves per portion and the mean of the general meat portion.

The exposure levels (Ex) to Cd, Cr, and Pb were calculated for children (14.5 kg of body weight) and adults (70 kg of body weight) to evaluate the human health risk from the consumption of *A. tuberculosa* and *A. similis* by the community members of Santa Rosa Island. The following US EPA (2000) formula was used:

$$\mathrm{Ex} = \frac{\mathrm{Cx} \times \mathrm{CR}}{\mathrm{BW}}, \quad (1)$$

where Ex is the exposure (mg $kg^{-1}$ $d^{-1}$); Cx is the concentration of metal in the edible portion of samples (mg $kg^{-1}$); CR is the mean amount of bivalves (kg) that are consumed daily (200 g for children and 400 g for adults), and BW is body weight (kg).

Likewise, the non-carcinogenic potential risk (Rx) for consumption was evaluated using the following equation (US EPA, 1986):

$$\mathrm{Rx} = \frac{\mathrm{Ex}}{\mathrm{Rfd}}, \quad (2)$$

where Ex is daily exposure (mg $kg^{-1}$ $d^{-1}$), and RfD is the oral reference dose (mg $kg^{-1}$ $d^{-1}$) (US EPA-IRIS, 1998; US EPA, 2018, 2000; FDA, 2019), which corresponds to the amount of metal that could be consumed daily without any adverse health effects.

For the evaluation, Rx values lower than 1 means imperceptible risk; if Rx values are higher than 1, the exposed populations may be at risk. As the US EPA guidelines explain, "Exposure above the RfD is not recommended. The likelihood of risk is related to the degree to which exposure exceeds the RfD" (US EPA, 2000, pp. 2–53).

Individual carcinogenic risk is equivalent to the increased probability of an individual developing cancer over his/her lifetime due to exposure to the metals included in this study. The individual carcinogenic risk for Pb was estimated using the existing cancer potency provided by the US EPA (2018): 0.0085 mg·$kg^{-1}$·$d^{-1}$. As Cd and Cr (III) do not have slope factor values for cancer potency, individual carcinogenic risks could not be estimated. To calculate individual carcinogenic risk, the following US EPA (2001) equation was used:

$$\text{Individual carcinogenic risk} = \mathrm{Ex} \times \text{cancer potency}. \quad (3)$$

Individual carcinogenic risk values lower than $10^{-6}$ were considered negligible, values between $10^{-6}$ and $10^{-4}$ were considered within an acceptable range, and values higher than $10^{-4}$ were considered intolerable (US EPA, 2001).

Besides, the allowable daily consumption rate [$CR_{lim}$ (g $d^{-1}$)] was evaluated (US EPA, 2000) to determine the approximate amount of bivalves (g) that a person can consume per day and not present health problems, based on the RfD:

$$\mathrm{CR_{lim}} = \frac{\mathrm{RfD} \times \mathrm{BW}}{\mathrm{Cx}} \times 1000, \quad (4)$$

where RfD is the oral reference dose (mg·$kg^{-1}$·$d^{-1}$), BW is the corporal weight (kg), and Cx is each metal concentration in the samples (mg·$kg^{-1}$).

The human health risk assessment was calculated applying different scenarios for the metal concentrations (mean, minimum, and maximum).

All the data calculations were done using Microsoft Office Professional Plus® Excel 2016.

# RESULTS AND DISCUSSION

## Sample Characteristics

In this research, different soft tissue content was observed among the four sampling sites. The specimens harvested from E1 of 30 to 40 mm in length had an average meat proportion of 8.63 ± 3.65 g of meat portion and 33.7 ± 7.89% of soft tissue. From E2, specimens were bigger with an average meat portion of 13.26 ± 7.12 g and 44.4 ± 9.45% of soft tissue. From E3, specimens fell between E1 and E2 with an average of meat portion of 10.51 ± 3.93 g of and 38.2 ± 10.23% of soft tissue. Finally, from E4, specimens had 9.43 ± 4.72 g of meat portion and a 35.8 ± 12.34% of soft tissue. Samples greater than 50 mm had an average of 13.4 ± 5.31 g of meat portion and 34.7 ± 3.81% of soft tissue from E1; 20.42 ± 6.52 g of meat portion and 41.7 ± 6.87% of soft tissue from E2; 12.65 ± 6.29 g of meat portion and 25.62 ± 13.14% of soft tissue from E3; and 16.44 ± 5.68 g of meat portion and 33.96 ± 6.53% of soft tissue from E4. The mean weight of the soft tissue from *A. tuberculosa* and *A. similis* specimens between 40 and 50 mm was 10.19 ± 5.03 g, and specimens greater than 50 mm reached 14.9 ± 6.57 g.

## Metals Quantification

The results of metals determination are shown in **Table 1**. For the Cr and Pb analysis of the bivalve samples, the results were below the quantification limits for each method. However, the approximate concentrations were estimated with the fortifications results, which were within the working range. The highest concentration of Cd was 0.560 mg $kg^{-1}$ from location E2 for *A. tuberculosa* and 0.948 mg $kg^{-1}$ from location E4 for *A. similis*. The highest concentration of Cr was 0.634 mg $kg^{-1}$ from location E3 for *A. tuberculosa* and 0.730 mg $kg^{-1}$ from location E4 for *A. similis*. Finally, for Pb, the highest concentration was 0.923 mg $kg^{-1}$ for *A. tuberculosa* and 0.908 mg $kg^{-1}$ for *A. similis*, both from location E3. In a study using bivalve samples from Esmeraldas Province conducted by Mendoza Angulo (2014), concentrations of 0.3 mg $kg^{-1}$ for Cd and Cr were found, which corresponds to the results in the present study. No studies related to Pb levels have been conducted at Santa Rosa Island location for comparison. The Pb results for the sediment samples were lower than the quantification limit in three of the four samples; the same results were found for all leaf samples for Cr and Pb. In these cases, the concentrations were estimated using the fortification results.

In the sampling process, other species were collected and analyzed: *Protothaca asperrima* with a mean concentration of 0.15, 0.41, and 0.49 mg $kg^{-1}$ for Cd, Cr, and Pb, respectively, and *Polymesoda inflata* with a mean concentration of 0.27, 0.74, and 0.36 mg $kg^{-1}$ for Cd, Cr, and Pb, respectively. In all the cases, the highest RSD were 5.43, 5.19, and 5.56% for Cd, Cr, and Pb, respectively, and the fortification recovery rates (accuracy) were between 81.82 and 101.82%. These species are not commonly used for consumption, thus the risk assessment related was no calculated. The metal content was in the same order as the content obtained for the *Anadara* spp. samples.

The certified reference material of fish protein recovery results were 84.91% for Cd, 86.19% for Cr, and 91.59% for Pb.

For the sediment results, the mean values of the metal concentrations were 2.14, 29.99, and 12.37 mg $kg^{-1}$ for Cd, Cr, and Pb, respectively. The RSD values were under 5.53, 2.65, and 2.93% for Cd, Cr, and Pb, respectively, and the recoveries were between 80.07 and 104.58%. The highest value corresponded to location E3.

For Cd, Cr, and Pb content, the results are varied, and no relation could be found between the bivalves and sediments metal content. For *A. tuberculosa* the correlation coefficients were 0.2186 ($p$ = 3.04E-06), 0.0887 ($p$ = 5.46E-06), and 0.1044 ($p$ = 6.75E-06), for Cd, Cr, and Pb, respectively. In the case of *A. similis* the correlation coefficients were 0.3356 ($p$ = 0.0019), 0.8393 ($p$ = 0.0009), and 0.0105 ($p$ = 0.0011) for Cd, Cr, and Pb, respectively. For all cases, the $p$-values were lower than $\alpha = 0.05$.

The results of the present study are in agreement with some authors who concluded that there is no correlation between the metal content between sediment and bivalve species

**TABLE 1 |** Concentration ranges of cadmium (Cd), chromium (Cr), and lead (Pb) in *A. tuberculosa* and *A. similis* (mg $kg^{-1}$), rates of the standard deviation of the triplicates (%), and accuracy (%) of the samples collected in four locations near the Isla Santa Rosa community in Esmeraldas.

| Location of harvesting | Cd | RSD | Accuracy | Cr | RSD | Accuracy | Pb | RSD | Accuracy |
|---|---|---|---|---|---|---|---|---|---|
| *Anadara Tuberculosa* | | | | | | | | | |
| E1: "Estero Hondo" | 0.346* | 4.08 | 114.38 | 0.059* | 6.93 | 94.12 | 0.381* | 4.90 | 97.17 |
| E2: "Playa la Tumba" | 0.560* | 4.05 | 98.04 | 0.038* | 10.83 | 94.66 | 0.311* | 3.94 | 98.26 |
| E3: "Playa al otro lado" | 0.211–0.321 | 1.97–4.00 | 86.31–113.33 | 0.238–0.634 | 3.03–5.58 | 86.01–100.78 | 0.067–0.923 | 1.42–6.19 | 87.47–95.78 |
| E4: "Estero la Caleta"4 | 0.245–0.531 | 0.75–3.98 | 92.95–104.58 | 0.306–0.405 | 3.63–5.81 | 93.03–100.32 | 0.304–0.512 | 4.03–4.87 | 93.27–99.46 |
| *Anadara Similis*** | | | | | | | | | |
| E3: "Playa al otro lado" | 0.243–0.439 | 2.44–4.32 | 90.91–106.67 | 0.310–0.503 | 2.96–4.06 | 91.01–100.00 | 0.164–0.908 | 3.13–4.83 | 91.92–97.33 |
| E4: "Estero la Caleta"4 | 0.330–0.948 | 3.56–4.58 | 89.51–114.38 | 0.668–0.730 | 3.95–5.49 | 90.64–100.11 | 0.483–0.545 | 4.35–4.81 | 91.67–98.04 |
| Threshold values[a] | 1.0 | – | – | – | – | – | 1.5 | – | – |

**One determination of bulk samples available. **Anadara Similis were not available in locations E1 and E2. [a]European Commission (EC) (2006). Commission Regulation No 1881/2006: Setting maximum levels for certain contaminants in foodstuffs (Text with EEA relevance). Official Journal of the European Union, 30(15), 127–129. https://doi.org/10.1093/nq/s9-VI.153.423. RSD, relative standard deviation.*

(Chu et al., 1990; Amiard et al., 2007; Lias et al., 2013). This difference may be related to sediment properties such as acid-volatile sulfides, organic matter, texture, geology, organism behaviors among others those influencing the bioavailability of metals (Zhang et al., 2014). On the other hand, the presence of metals in the sediments is related to other parameters as pH, salinity, conductivity, and temperature. The pH contributes to the efficiency of the interaction between the metal ion and the adsorbent surface (Saranya et al., 2018); water salinity is another important factor because the $Cl^-$ ion can form various complexes with metals, allowing the exchange, increase or decrease of metals in sediment-aquatic environment (Harter and Naidu, 2001); the electrical conductivity is proportional is directly related to cations or anions content including metals; the temperature has a direct influence on the solubility of heavy metals.

The mean concentrations from the *Rhizophora mangle* leaves were 2.21, 4.38, and 3.29 $mg{\cdot}kg^{-1}$ for Cd, Cr, and Pb, respectively. The RSD values were under 5.88, 5.83, and 5.00% for Cd, Cr, and Pb, respectively, and the recoveries were between 80.89 and 106.10%. In this case, the highest values corresponded to locations E1, E2, and E3 for Pb, Cr, and Cd, respectively, and did not show a relation to sediment or bivalve results.

In the comparison between the metal content of leaves and bivalve samples, there was not a correlation between the results of the three metals. The correlation coefficients were 0.0731 ($p$ = 0.0025), 0.0722 ($p$ = 0.0004), and 0.0778 ($p$ = 4.57E-07), for Cd, Cr, and Pb, respectively for *A. tuberculosa*. In the case of *A. similis* the correlation coefficients were 0.3356 ($p$ = 0.0480), 0.8393 ($p$ = 0.0108), and 0.0105 ($p$ = 5.05E-05) for Cd, Cr, and Pb, respectively. For all cases, the p values were lower than $\alpha = 0.05$. Nevertheless, *Rhizophora mangle* leaves can be used as important bioindicators of metal contamination in mangrove ecosystems (Pinheiro et al., 2012).

Location E3 is nearest to the community of Santa Rosa Island, and in this location, there is little water flow, in a curved area where sediment can accumulate. Location E4 is farther away from the community and belongs to the "La Caleta" estuary riverbed. The trace metal contamination is assumed to be from the natural composition of soils and erosion (Soborino-Figueroa et al., 2007; Aouini et al., 2018; Arumugam et al., 2018; Fasano et al., 2018), There is also illegal mining in localities upstream of river beds that flow into the area (Global Initiative against Transnational Organized Crime, 2016). Also, the inadequate management of household waste, incorrect final disposal of fuels for the repair of boats and outboard motors, pollutants that are dumped directly into the mangrove (Echeverría, 2019).

Ecuadorian laws do not have specific regulations related to metal concentrations in bivalves; nevertheless, when applying the European Commission and FAO regulations, the results of the present study are lower than the Cd and Pb threshold values.

Regarding mangrove sediments, Ecuadorian regulations do not establish specific acceptance limits for contaminants; however, Ministerial Agreement N° 097 established regulation for soil quality in general, and the maximum acceptable limits for Cd, Cr, and Pb are 0.5, 54, and 19 $mg{\cdot}kg^{-1}$, respectively (Ministerio del Ambiente [MAE], 2015). The Canadian interim sediment quality guidelines (ISQGs) also set maximum limits for these metals: 0.7 $mg{\cdot}kg^{-1}$ for Cd (Canadian Council of Ministers of the Environment [CCME], 1999), 52.3 $mg{\cdot}kg^{-1}$ for Cr (Canadian Council of Ministers of the Environment [CCME], 1995), and 30.2 $mg{\cdot}kg^{-1}$ for Pb (Canadian Council of Ministers of the Environment [CCME], 1999). The concentrations obtained in the present study were 2.14, 29.99, and 12.37 $mg{\cdot}kg^{-1}$ for Cd, Cr, and Pb, respectively. Thus, the concentrations found were lower than the Ecuadorian and Canadian regulations for both Cr and Pb. In the case of Cd, the average concentration was approximately four times the limit established in Ecuadorian regulations and three times the limit established in Canadian regulations, which may be due to the presence of cadmium in water and soils (Fernández-Cadena et al., 2014; Echeverría, 2019).

## Human Health Risk Assessment

As Acosta and Lodeiros (2004) mention, the consumption of mollusks, like bivalves, contributes to a potentially toxic metal intake. Toxic metals can elevate the risk of chronic poisoning for people living in coastal areas, and also to mangroves (Acosta and Lodeiros, 2004; Fernández-Cadena et al., 2014; Aguirre-Rubí et al., 2018a,b; Loaiza et al., 2018; Pernía et al., 2018).

For the Ex results, all Cd levels for *A. tuberculosa* and *A. similis* exceeded the respective RfD value (0.001 $mg{\cdot}kg^{-1}{\cdot}d^{-1}$). Exposure to Cd is mainly associated with increased urinary excretion of low molecular weight proteins, with repercussions on kidney dysfunction and bone disease (Itai Itai disease) in exposed populations, and also with the development of cancer (Godt et al., 2006).

In Cr, all results were quite lower than the RfD value (1.5 $mg{\cdot}kg^{-1}{\cdot}d^{-1}$), and for Pb, the results were lower than the RfD values (0.003 $mg{\cdot}d^{-1}$ for children and 0.0125 $mg{\cdot}d^{-1}$ for adults), except in children for the mean and maximum Pb concentration scenarios for both bivalve species. Moreover, the results show that in all cases (children and adults for *A. similis* and *A. tuberculosa*), Cd potential risk levels are higher than those for Cr and Pb; therefore, more Cd toxicity exists per amount of bivalves ingested (**Tables 2** and **3**). The individual carcinogenic risk showed values lower than $10^{-4}$ for *A. tuberculosa* and *A. similis*, which is considered within an acceptable range. The higher value was in children for the maximum Pb concentration scenario in *A. tuberculosa*. Exposure to elevated levels of Pb has serious consequences on the health of children, attacks the brain and central nervous system. When there is contamination at lower levels, there are no obvious symptoms, however, it can affect the brain development of children, reduced IQ, changes in behavior, attention disorders, antisocial behavior. Furthermore, exposure to lead also causes anemia, hypertension, kidney failure, immunotoxicity, and toxicity to the reproductive organs, irreversible neurological, and behavioral effects (WHO, 2019). Counter et al. (2015) have found that the blood Pb levels observed in Ecuadorian infants (33.6 ± 28.9 $\mu g\ dl^{-1}$) and young children (27.9 ± 22.5 $\mu g\ dl^{-1}$) are higher than the World Health Organization level of concern (10 $\mu g\ dl^{-1}$), and Centers for Disease Control and Prevention current reference value (5 $\mu g\ dl^{-1}$). This worrying situation means that pediatric

**TABLE 2 |** *Anadara tuberculosa* exposure levels (mg $kg^{-1}$ $d^{-1}$), non-carcinogenic potential risk (no units), individual carcinogenic risk for Pb (no units), and the allowable daily consumption rate (g $d^{-1}$) for Cd, Cr, and Pb, considering the mean, minimum, and maximum metal concentrations for child and adult mean body weights (kg).

| General portions of consumption: 200 g for children and 400 g for adults | | | | | | | | | | |
|---|---|---|---|---|---|---|---|---|---|---|
| | Cd | | | Cr | | | Pb | | | |
| BW | Ex | Rx | $CR_{lim}$ | Ex | Rx | $CR_{lim}$ | Ex | Rx | $CR_{lim}$ | Individual carcinogenic risk |
| **Mean metal concentrations** | | | | | | | | | | |
| 14.5 | 0.00475 | 4.75 | 42.1 | 0.00414 | 0.00 | 72453.3 | 0.00617 | 2.06 | 97.3 | 5.24E-05 |
| 70 | 0.00197 | 1.97 | 203.1 | 0.00172 | 0.00 | 349774.7 | 0.00256 | 0.20 | 1956.5 | 2.17E-05 |
| **Minimum metal concentrations** | | | | | | | | | | |
| 14.5 | 0.00291 | 2.91 | 68.7 | 0.00052 | 0.00 | 577734.4 | 0.00093 | 0.31 | 647.3 | 7.88E-06 |
| 70 | 0.00121 | 1.21 | 331.4 | 0.00022 | 0.00 | 2789062.5 | 0.00038 | 0.03 | 13020.8 | 3.26E-06 |
| **Maximum metal concentrations** | | | | | | | | | | |
| 14.5 | 0.00772 | 7.72 | 25.9 | 0.00875 | 0.01 | 34290.5 | 0.01273 | 4.24 | 47.1 | 1.08E-04 |
| 70 | 0.00320 | 3.20 | 125.0 | 0.00362 | 0.00 | 165540.5 | 0.00527 | 0.42 | 948.1 | 4.48E-05 |
| **Oral reference doses** | | | | | | | | | | |
| 14.5 | 0.00100 | – | – | 1.50000 | – | – | 0.00300 | – | – | – |
| 70 | | | | | | | 0.01250 | | | |

*BW, body weight; Ex, levels of exposure; Rx, non-carcinogenic potential risk; $CR_{lim}$, allowable daily consumption rate.*

**TABLE 3 |** *Anadara Similis* exposure levels (mg $kg^{-1}$ $d^{-1}$), non-carcinogenic potential risk (no units), individual carcinogenic risk for Pb (no units), and the allowable daily consumption rate (g $d^{-1}$) for Cd, Cr, and Pb, considering the mean, minimum, and maximum metal concentrations for child and adult mean body weights (kg).

| General portions of consumption: 200 g for children and 400 g for adults | | | | | | | | | | |
|---|---|---|---|---|---|---|---|---|---|---|
| | Cd | | | Cr | | | Pb | | | |
| BW | Ex | Rx | $CR_{lim}$ | Ex | Rx | $CR_{lim}$ | Ex | Rx | $CR_{lim}$ | Individual carcinogenic risk |
| **Mean metals concentrations** | | | | | | | | | | |
| 14.5 | 0.00635 | 6.35 | 31.5 | 0.00711 | 0.00 | 42200.4 | 0.00665 | 2.22 | 90.2 | 5.65E-05 |
| 70 | 0.00263 | 2.63 | 151.9 | 0.00295 | 0.00 | 203726.0 | 0.00276 | 0.22 | 1814.8 | 2.34E-05 |
| **Minimum metals concentrations** | | | | | | | | | | |
| 14.5 | 0.00335 | 3.35 | 59.6 | 0.00428 | 0.00 | 70093.5 | 0.00226 | 0.75 | 265.1 | 1.92E-05 |
| 70 | 0.00139 | 1.39 | 287.9 | 0.00177 | 0.00 | 338382.2 | 0.00094 | 0.08 | 5333.2 | 7.97E-06 |
| **Maximum metals concentrations** | | | | | | | | | | |
| 14.5 | 0.01307 | 13.07 | 15.3 | 0.01007 | 0.01 | 29800.8 | 0.01252 | 4.17 | 47.9 | 1.06E-04 |
| 70 | 0.00541 | 5.41 | 73.9 | 0.00417 | 0.00 | 143866.0 | 0.00519 | 0.42 | 963.8 | 4.41E-05 |
| **Oral reference doses** | | | | | | | | | | |
| 14.5 | 0.00100 | – | – | 1.50000 | – | – | 0.00300 | – | – | – |
| 70 | | | | | | | 0.01250 | | | |

*BW, body weight; Ex, levels of exposure; Rx, non-carcinogenic potential risk; $CR_{lim}$, allowable daily consumption rate.*

Pb intoxication persists in developing countries where Pb contamination exists.

Finally, the allowable daily consumption rate ($CR_{lim}$) in grams of *A. tuberculosa* was estimated considering that Cd poses the highest potential risk. For the mean, minimum, and maximum Cd concentration scenarios, child $CR_{lim}$ values were 42.1, 68.7, and 25.9 g, respectively, and adult values were 203.1, 331.4, and 125.0 g, respectively. In the case of *A. similis* (**Table 3**), for each scenario, the child $CR_{lim}$ values were 31.5, 59.6, and 15.3 g of bivalves; the adult $CR_{lim}$ values were 151.9, 287.9, and 73.9 g of bivalves. The higher results indicate that more consumption of bivalves than those obtained in the calculations could imply a high risk to any health for both children and adults. The FDA recommendations cited by Soborino-Figueroa et al. (2007) suggest the consumption of mollusks from 28 to 83 g as a safe portion. In the case of this study, the recommended values are higher than those recommended by Soborino-Figueroa et al. (2007).

## CONCLUSION

There is heterogeneity in the content of Cd, Cr, and Pb found in the bivalve samples of the present study. Additionally, when comparing the results of the content of metals in the sediments and the leaves collected in the same locations of bivalves, no correlation was found. These may be an indication that the presence of metals in mangrove substrates (sediments) is not the

only aspect to be considered to explain a high intake by natural species as bivalves (*Anadara* spp.), and vegetation (*Rhizophora mangle*). In addition, these sediments results can be used as a baseline that indicates no metal enrichment of any sort in the locations areas. On the other hand, the present study is aimed to be the first approach to determine a possible contamination of Cd, Cr, and Pb, in the area inside the REMACAM natural reserve. The results obtained suggest that more studies should be done to a wider evaluation of metals contamination including other locations within the REMACAM area.

As seen in the health risk assessment results for children (portion corresponding to 200 g) and adults (portion corresponding to 400 g), it is evident that consumption of a bivalve portion contains concentrations of Cd exceeding the RfD values from US EPA (2018, 2000). In the case of Pb, the concentration values for children (mean and maximum scenarios) were above de FDA (2019) values. In all cases, the consumption of bivalves could imply a health risk to the community members of Santa Rosa Island.

Many communities that derive their livelihoods from bio-aquatic resources are isolated; this fact is a limiting factor for the periodic monitoring and hinders the implementation of treatment systems as depuration for the elimination of Cd, Cr, and Pb. Furthermore, economic limitations make development activities depend on external resources, which, in most cases, are difficult to achieve.

In Santa Rosa Island, the sources of trace metal contamination cannot be completely determined because they are both natural and anthropogenic. This first approach aimed to have a general evaluation about the metals presence and the community risk exposure, but further investigations are needed to find out the principal source of contamination.

It is necessary to continue the studies related to toxic metals content in bio-aquatic resources and its relationship with public safety associated with the consumption of food that contains toxic metals. It also imperative to keep monitoring the locations where it is presumed that metal contamination exists.

## DATA AVAILABILITY STATEMENT

The raw data supporting the conclusions of this article will be made available by the authors, without undue reservation.

## AUTHOR CONTRIBUTIONS

DR-E and MD: conceptualization. DR-E, HN, and MD: visualization. MD and HN: resources. MD: project administration and funding acquisition. DR-E: methodology and validation. DR-E, KS-F, ER, and GD: formal analysis and investigation. DR-E and GY-J: data curation, writing – original draft, review, and editing. All authors contributed to the article and approved the submitted version.

## ACKNOWLEDGMENTS

The authors would like to thank to the Pontificia Universidad Católica del Ecuador Quito, Esmeraldas and Manabí headquarters for the support for the project "Ciudad Abierta."

## SUPPLEMENTARY MATERIAL

The Supplementary Material for this article can be found online at: https://www.frontiersin.org/articles/10.3389/fenvs.2020.00134/full#supplementary-material

## REFERENCES

Acosta, V., and Lodeiros, C. (2004). Heavy metals in the clam *Tivela mactroides* Born, 1778 (Bivalvia: Veneridae) from coastal localities with different degrees of contamination in Venezuela. *Ciencias Mar.* 30, 323–333. doi: 10.7773/cm.v30i2.183

Aguirre-Rubí, J., Luna-Acosta, A., Etxebarría, N., Soto, M., Espinoza, F., Ahrens, M. J., et al. (2018a). Chemical contamination assessment in mangrove-lined Caribbean coastal systems using the oyster *Crassostrea rhizophorae* as biomonitor species. *Environ. Sci. Pollut. Res.* 25, 13396–13415. doi: 10.1007/s11356-017-9159-2

Aguirre-Rubí, J., Luna-Acosta, A., Ortiz-Zarragoitia, M., Zaldibar, B., Izagirre, U., Ahrens, M. J., et al. (2018b). Assessment of ecosystem health disturbance in mangrove-lined Caribbean coastal systems using the oyster *Crassostrea rhizophorae* as sentinel species. *Sci. Total Environ.* 618, 718–735. doi: 10.1016/j.scitotenv.2017.08.098

Amiard, J.-C., Geffard, A., Amiard-Triquet, C., and Crouzet, C. (2007). Relationship between the lability of sediment-bound metals (Cd, Cu, Zn) and their bioaccumulation in benthic invertebrates. *Estuar. Coast. Shelf Sci.* 72, 511–521. doi: 10.1016/j.ecss.2006.11.017

AOAC (2002). *Guidelines for Single Laboratory Validation of Chemical Methods for Dietary Supplements and Botanicals. AOAC Int. 1–38*. Available online at: http://members.aoac.org/aoac_prod_imis/AOAC_Docs/StandardsDevelopment/SLV_Guidelines_Dietary_Supplements.pdf. (accessed May 15, 2020)

Aouini, F., Trombini, C., Volland, M., Elcafsi, M., and Blasco, J. (2018). Assessing lead toxicity in the clam *Ruditapes philippinarum*: bioaccumulation and biochemical responses. *Ecotoxicol. Environ. Saf.* 158, 193–203. doi: 10.1016/j.ecoenv.2018.04.033

Arumugam, G., Rajendran, R., Shanmugam, V., Sethu, R., and Krishnamurthi, M. (2018). Flow of toxic metals in food-web components of tropical mangrove ecosystem, Southern India. *Hum. Ecol. Risk Assess.* 24, 1367–1387. doi: 10.1080/10807039.2017.1412819

Beitl, C. M. (2015). Mobility in the mangroves: catch rates, daily decisions, and dynamics of artisanal fishing in a coastal commons. *Appl. Geogr.* 59, 98–106. doi: 10.1016/j.apgeog.2014.12.008

Boening, D. W. (1999). An evaluation of bivalves as biomonitors of heavy metals pollution in marine waters. *Environ. Monit. Assess.* 55, 459–470. doi: 10.1023/A:1005995217901

Calle, P., Monserrate, L., Medina, F., Calle, D. M., Tirapé, A., Montiel, M., et al. (2018). Mercury assessment, macrobenthos diversity and environmental quality conditions in the Salado Estuary (Gulf of Guayaquil, Ecuador) impacted by anthropogenic influences. *Mar. Pollut. Bull.* 136, 365–373. doi: 10.1016/j.marpolbul.2018.09.018

Canadian Council of Ministers of the Environment [CCME] (1995). *Canadian Sediment Quality Guidelines for the Protection of Aquatic Life: Chromium. Can. Counc. Minist. Environ. EPC-98E 35*. Available online at: http://ceqg-rcqe.ccme.ca/download/en/233. (accessed May 15, 2020)

Canadian Council of Ministers of the Environment [CCME] (1999). *Canadian Sediment Quality Guidelines for the Protection of Aquatic Life: Cadmium.*

*Can. Environ. Qual. Guidel. 5*. Available online at: http://ceqg-rcqe.ccme.ca/download/en/231. (accessed May 15, 2020)

Chu, K. H., Cheung, W. M., and Lau, S. K. (1990). Trace metals in bivalves and sediments from Tolo Harbour, Hong Kong. *Environ. Int.* 16, 31–36. doi: 10.1016/0160-4120(90)90202-h

CIIEMAD-IPN (2011). *Método General por Microondas de Digestión Ácida en Matrices Ambientales 0, 1–15*. Available online at: https://www.ciiemad.ipn.mx/assets/files/ciiemad/docs/sgc/procedimientos/IPN_AC-06-00.pdf. (accessed May 15, 2020)

Counter, S. A., Buchanan, L. H., and Ortega, F. (2015). Blood lead levels in Andean infants and young children in Ecuador: an international comparison. *J. Toxicol. Environ. Part A* 78, 778–787. doi: 10.1080/15287394.2015.1031050

da Silveira Fiori, C., de Castro Rodrigues, A. P., Castro Vieria, T., Sabadini-Santos, E., and Dausacker Bidone, E. (2018). An alternative approach to bioaccumulation assessment of methyl-Hg, total- Hg, Cd, Pb, Zn in bivalve Anomalocardia brasiliana from Rio de Janeiro bays. *Mar. Pollut. Bull.* 135, 418–426. doi: 10.1016/j.marpolbul.2018.07.045

Echeverría, K. M. (2019). *Metales Pesados en Agua, Sedimentos y Raíces de Rhizophora mangle* de la Reserva Ecológica Manglares Cayamas Mataje, Provincia de Esmeraldas. Ph. D. Thesis, Pontificia Universidad Católica del Ecuador sede Ibarra, Ecuador.

Erk, M., Ivankoviæ, D., Župan, I., Èulin, J., Dragun, Z., Puljas, S., et al. (2018). Changes in the tissue concentrations of trace elements during the reproductive cycle of Noah's Ark shells (Arca noae Linnaeus, 1758). *Mar. Pollut. Bull.* 133, 357–366. doi: 10.1016/j.marpolbul.2018.05.054

Esposito, G., Meloni, D., Abete, M. C., Colombero, G., Mantia, M., Pastorino, P., et al. (2018). The bivalve Ruditapes decussatus: A biomonitor of trace elements pollution in Sardinian coastal lagoons (Italy). *Environ. Pollut.* 242(Pt B), 1720–1728. doi: 10.1016/j.envpol.2018.07.098

European Commission (EC) (2006). Commission regulation No 1881/2006: setting maximum levels for certain contaminants in foodstuffs (Text with EEA relevance). *Off. J. Eur. Union.* 30, 127–129.

FAO/WHO (2019). *General Standard for Contaminants and Toxins in Food and Feed CXS 193-1995*. Available online at: http://www.fao.org/fao-who-codexalimentarius/sh-proxy/en/?lnk=1&url=https%253A%252F%252Fworkspace.fao.org%252Fsites%252Fcodex%252FStandards%252FCXS%2B193-1995%252FCXS_193e.pdf . (Accessed May 15, 2020)

Fasano, E., Arnese, A., Esposito, F., Albano, L., Masucci, A., Capelli, C., et al. (2018). Evaluation of the impact of anthropogenic activities on arsenic, cadmium, chromium, mercury, lead, and polycyclic aromatic hydrocarbon levels in seafood from the Gulf of Naples, Italy. *J. Environ. Sci. Heal. Part A* 53, 786–792. doi: 10.1080/10934529.2018.1445075

FDA (2019). *Lead in Food, Foodwares, and Dietary Supplements*. Available online at: https://www.fda.gov/food/metals-and-your-food/lead-food-foodwares-and-dietary-supplements. (Accessed May 15, 2020)

Fernández-Cadena, J. C., Andrade, S., Silva-Coello, C. L., and De la Iglesia, R. (2014). Heavy metal concentration in mangrove surface sediments from the north-west coast of South America. *Mar. Pollut. Bull.* 82, 221–226. doi: 10.1016/j.marpolbul.2014.03.016

Flores, L., Licandeo, R., Cubillos, L. A., and Mora, E. (2014). Intra-specific variability in life-history traits of *Anadara tuberculosa* (Mollusca: Bivalvia) in the mangrove ecosystem of the Southern coast of Ecuador. *Rev. Biol. Trop.* 62, 473–482.

Gener, R. L., Rivas, F., and Argüello, G. (2009). *Estudio de Mercado de la Concha negra (Anadara similis y Anadara tuberculosa) en Nicaragua: Comercialización con Garantía de Inocuidad*. Ph. D. Thesis, Universidad Centroamericana, Managua.

Global Initiative against Transnational Organized Crime (2016). *Organized Crime and Illegally Mined Gold in Latin America. Ginebra, Suiza: Global Initiative*. Available online at: https://arcominero.infoamazonia.org/GIATOC-OC_Illegally-Mined-Gold-in-Latin-America-3c3f978eef80083bdd8780d7c5a21f1e.pdf. (accessed May 15, 2020).

Godt, J., Scheidig, F., Grosse-Siestrup, C., Esche, V., Brandenburg, P., Reich, A., et al. (2006). The toxicity of cadmium and resulting hazards for human health. *J. Occup. Med. Toxicol.* 1:22. doi: 10.1186/1745-6673-1-22

Harter, R., and Naidu, R. (2001). An assessment of environmental and solution parameter impact on trace-metal sorption by soils. *Soil. Sci. Soc. Am. J.* 65:597. doi: 10.2136/sssaj2001.653597x

Jiang, Q., He, J., Ye, G., and Christakos, G. (2018). Heavy metal contamination assessment of surface sediments of the East Zhejiang coastal area during 2012 – 2015. *Ecotoxicol. Environ. Saf.* 163, 444–455. doi: 10.1016/j.ecoenv.2018.07.107

Lias, K., Jamil, T., and Nor Aliaa, S. A. (2013). A preliminary study on heavy metal concentration in the marine bivalves marcia marmorata species and sediments collected from the coastal area of Kuala Perlis, North Of Malaysia. *IOSR-JAC.* 4, 48–54. doi: 10.9790/5736-0414854

Loaiza, I., De Troch, M., and De Boeck, G. (2018). Potential health risks via consumption of six edible shellfish species collected from Piura – Peru. *Ecotoxicol. Environ. Saf.* 159, 249–260. doi: 10.1016/j.ecoenv.2018.05.005

Mendoza Angulo, H. (2014). *Niveles de Acumulación de Metales Pesados y Contaminantes Orgánicos en Moluscos Bivalvos del Género Anadara y su Vinculación con Actividades Económicas en la Provincia de Esmeraldas como base para una Propuesta de Regulación de Límites Máximos Permisibles*. Ph. D. Thesis, Pontificia Universidad Católica del Ecuador sede Esmeraldas, Ecuador.

Ministerio de Acuacultura y Pesca [MAP] (2005). *Acuerdo Ministerial No 005*. Available online at: http://acuaculturaypesca.gob.ec/subpesca93-acuerdo-ministerial-n-005-concha.html.(accessed May 15, 2020)

Ministerio del Ambiente [MAE] (2015). *Acuerdo Ministerial 097: Norma de Calidad Ambieltal del Recurso Suelo y Criterios de Remediación para Suelos Contaminados*. Avaialable online at: http://faolex.fao.org/docs/pdf/ecu112181.pdf. (Accessed May 15, 2020)

Ministerio del Ambiente [MAE] (2019). *Plan de Manejo para el Uso Sostenible y Custodia de Manglar para la Asociación de Mujeres Afroecuatorianas de Pescadoras y Recolectoras de Productos Bioacuáticos 18 de octubre del Manglar de Santa Rosa*. Esmeraldas: Ministerio del Ambiente de Ecuador.

Pernía, B., Mero, M., Cornejo, X., Ramírez, N., and Ramírez, L. (2018). Determinación de cadmio y plomo en agua, sedimento y organismos bioindicadores en el Estero Salado, Ecuador (Determination of cadmium and lead in water, sediment and bioindicator organisms in Estero Salado, Ecuador). *Enfoque UTE* 9, 89–105. doi: 10.29019/enfoqueute.v9n2.246

Pinheiro, M. A. A., Silva, P. P. G. E., Duarte, L. F., de, A., Almeida, A. A., and Zanotto, F. P. (2012). Accumulation of six metals in the mangrove crab Ucides cordatus (Crustacea: Ucididae) and its food source, the red mangrove *Rhizophora mangle* (Angiosperma: Rhizophoraceae). *Ecotoxicol. Environ. Saf.* 81, 114–121. doi: 10.1016/j.ecoenv.2012.05.004

Romero-Estévez, D., Yánez-Jácome, G. S., Simbaña-Farinango, K., Vélez-Terreros, P. Y., and Navarrete, H. (2019). Evaluation of two sample preparation methods for the determination of cadmium, nickel and lead in natural foods by Graphite Furnace Atomic Absorption Spectrophotometry. *Uni. Sci.* 24, 497–521. doi: 10.11144/Javeriana.SC24-3.eots

Ruiz, M. D., Iriel, A., Yusseppone, M. S., Ortiz, N., Di Salvatore, P., Fernández Cirelli, A., et al. (2018). Trace metals and oxidative status in soft tissues of caged mussels (Aulacomya atra) on the North Patagonian coastline. *Ecotoxicol. Environ. Saf.* 155, 152–161. doi: 10.1016/j.ecoenv.2018.02.064

Saranya, J., Parthasarathi, C., Darwin, R., Kartheek, C., and Sucharita, C. (2018). Effect of pH on transport and transformation of Cu-sediment complexes in mangrove systems. *Mar. Pollut. Bull.* 133, 920–929. doi: 10.1016/j.marpolbul.2018.03.054

Soborino-Figueroa, A., Cáceres-Martínez, C., and Rosas-Cedillo, R. (2007). Evaluación del riesgo por consumir moluscos contaminados con cadmio, cromo y plomo. *Rev. Hidrobiológica.* 17, 49–58.

Spalding, M., Kainuma, M., and Collins, L. (2010). *World Atlas of Mangroves. A collaborative project of ITTO, ISME, FAO, UNEP-WCMC, UNESCO-MAB, UNU-INWEH and TNC. London (UK): Earthscan, London. 319 pp. Data layer from the World Atlas of Mangroves. In Supplement to: Spalding et al. Cambridge (UK): UNEP World Conservation Monitoring Centre*. Available online at: http://data.unep-wcmc.org/datasets/22. (Accessed May 15, 2020)

US EPA (1986). Guidelines for the health risk assessment of chemical mixtures. *Risk Assess. Forum* 51, 34014–34025.

US EPA (2000). Guidance for assessing chemical contaminant data for use in fish advisories. *Risk Assess. Fish Consump. Limits* 3:34.

US EPA (2001). *Risk Assessment Guidance for Superfund: Part A, Process for Conducting Probabilistic Risk Assessment 3*. Available online at: https://www.epa.gov/sites/production/files/2015-09/documents/rags3adt_complete.pdf. (accessed May 15, 2020)

US EPA (2007). *Method 3051A. Microwave Assisted Acid Digestion of Sediments, Sludges, Soils, and Oils*. Available online at: https://www.epa.gov/esam/us-epa-

method-3051a-microwave-assisted-acid-digestion-sediments-sludges-and-oils. (accessed May 15, 2020)

US EPA (2014). *Sediment Sampling. SESDPROC-200-R4*. Available online at: https://www.epa.gov/sites/production/files/2015-06/documents/Sediment-Sampling.pdf (Accessed May 15, 2020)

US EPA (2018). *Regional Screening (RBL) Summary Table*. Available online at: https://www.epa.gov/risk/regional-screening-levels-rsls-generic-tables. (accessed May 15, 2020)

US EPA-IRIS (1998). *Chromium (III), insoluble salts; CASRN 16065-83-1. Integr. Risk Inf. Syst. U.S. Chem. Assess. Summ. Natl. Cent. Environ. Assess*. Available online at: https://cfpub.epa.gov/ncea/iris/iris_documents/documents/subst/0028_summary.pdf (accessed May 15, 2020).

USAID (2012). *Co-manejo de Bivalvo "Concha Negra" (Anadara ssp) en Aserradores, Nicaragua. Programa Reg. USAID para el manejo Recur. acuáticos y Altern. económicas*. Available online at: http://repositorio.concytec.gob.pe/bitstream/20.500.12390/200/3/2016_Pretell_Identificacion-bacterias-cultivables.pdf. (accessed May 15, 2020)

WHO (2019). *Lead poisoning and health*. Available online at: https://www.who.int/news-room/fact-sheets/detail/lead-poisoning-and-health (accessed May 15, 2020)

Zhang, C., Yu, Z., Zeng, G., Jiang, M., Yang, Z., Cui, F., et al. (2014). Effects of sediment geochemical properties on heavy metal bioavailability. *Environ. Int.* 73, 270–281. doi: 10.1016/j.envint.2014.08.010

**Conflict of Interest:** The authors declare that the research was conducted in the absence of any commercial or financial relationships that could be construed as a potential conflict of interest.

frontiers in Marine Science

ORIGINAL RESEARCH
published: 04 September 2020
doi: 10.3389/fmars.2020.00717

# Challenges in Harmonized Assessment of Heavy Metals in the Adriatic and Ionian Seas

*Daniela Berto[1]*, Malgorzata Formalewicz[1], Giordano Giorgi[2], Federico Rampazzo[1], Claudia Gion[1], Benedetta Trabucco[2], Michele Giani[3], Marina Lipizer[3], Slavica Matijevic[4], Helen Kaberi[5], Christina Zeri[5], Oliver Bajt[6], Nevenka Mikac[7], Danijela Joksimovic[8], Andriana F. Aravantinou[9], Mateja Poje[10], Magdalena Cara[11] and Loredana Manfra[2]*

*[1] Department for the Monitoring and Protection of the Environment and for Biodiversity Conservation, Higher Institute for Environmental Protection and Research (ISPRA), Chioggia, Italy, [2] Department for the Monitoring and Protection of the Environment and for Biodiversity Conservation, Higher Institute for Environmental Protection and Research (ISPRA), Rome, Italy, [3] National Institute of Oceanography and Applied Geophysics (OGS), Trieste, Italy, [4] Institute of Oceanography and Fisheries (IOF), Split, Croatia, [5] Hellenic Centre for Marine Research (HCMR), Anavyssos, Greece, [6] National Institute of Biology (NIB), Marine Biology Station, Piran, Slovenia, [7] Ruder Boskovic Institute (RBI), Zagreb, Croatia, [8] University of Montenegro - Institute of Marine Biology (UoM-IMBK), Kotor, Montenegro, [9] Region of Western Greece (RWG), Patras, Greece, [10] Slovenian Environment Agency (ARSO), Ljubljana, Slovenia, [11] Faculty of Agriculture and Environment, Agriculture University of Tirana (AUT), Tirana, Albania*

OPEN ACCESS

***Edited by:***
*Senthil Kumar Ponnusamy, SSN College of Engineering, India*

***Reviewed by:***
*Paolo Cocci, University of Camerino, Italy*
*Thadickal V. Joydas, King Fahd University of Petroleum and Minerals, Saudi Arabia*

****Correspondence:***
*Daniela Berto*
*daniela.berto@isprambiente.it*

***Specialty section:***
*This article was submitted to Marine Pollution, a section of the journal Frontiers in Marine Science*

***Received:*** *08 June 2020*
***Accepted:*** *05 August 2020*
***Published:*** *04 September 2020*

***Citation:***
*Berto D, Formalewicz M, Giorgi G, Rampazzo F, Gion C, Trabucco B, Giani M, Lipizer M, Matijevic S, Kaberi H, Zeri C, Bajt O, Mikac N, Joksimovic D, Aravantinou AF, Poje M, Cara M and Manfra L (2020) Challenges in Harmonized Assessment of Heavy Metals in the Adriatic and Ionian Seas. Front. Mar. Sci. 7:717. doi: 10.3389/fmars.2020.00717*

The Adriatic-Ionian region (ADRION Region) shows strong development in terms of urban expansion in coastal and inland areas as well as increasing maritime traffic and offshore hydrocarbon extraction activities. A serious risk of pollution arises from hazardous substances requiring reliable and coherent monitoring and assessment programs. EU Directives (WFD – Water Framework Directive, MSFD – Marine Strategy Framework Directive) and Barcelona Convention protocols, aim to assess the level of pollution with the objective to implement measures to prevent and/or mitigate impacts on the marine environment. This high level integration process has to be based on common and agreed protocols for monitoring of contaminants. Aiming to share best practices to encourage a harmonized implementation of monitoring and assessment of contaminants, an extensive review of monitoring and analytical protocols adopted by six EU and non-EU countries along the Adriatic and Ionian seas was carried out in the framework of the Interreg Adrion project HarmoNIA (Interreg V-B Adriatic-Ionian (ADRION), 2018–2020). This paper presents a methodological proposal to define a common protocol for the evaluation of the metal contamination of seawater, sediment and biota. Contaminants have been chosen following preliminary consultations among countries of the ADRION area, considering objectives of WFD and MSFD, as well as Environmental Impact Assessment (EIA) procedures for offshore platforms. Information was gathered relative to matrix characteristics and quality assurance/quality control of the analytical performance (sample preservation, analytical methodology, reference materials, limit of detection, and limit of quantification, accuracy, reproducibility, etc.). The comparison of information provided by laboratories of nine institutions highlighted the request for harmonization in terms of sampling procedures, matrix characterization, preservation procedures, analytical methods and LOQ values. Although appropriate environmental quality standards for biota and sediment matrices should be established

at national level and also through regional and sub-regional cooperation, as required by the WFD and MSFD, the proposed LOQ values, even if challenging, represent a benchmark and a stimulus to optimize analytical performance, to ensure the best level of protection to the coastal and offshore environment in the ADRION Region.

**Keywords: hazardous substances, harmonized protocols, integrated approach, monitoring, assessment of contaminants, heavy metals, Adriatic-Ionian Sea region**

## INTRODUCTION

According to the Marine Strategy Framework Directive 2008/56/EC, 2008, European Union Member States should develop and follow a common approach in environmental monitoring at the level of marine region or sub-region, as well as in definition and assessment of good environmental status (GES). The new Commission Decision 2017/848/Eu (2017) has recently revised criteria and methodological standards for monitoring and assessment of GES. For contaminants, full compliance is required with Water Framework Directive (WFD) through the application of Environmental Quality Standards fixed by EU Directive 2013/39/EU, 2013 or, where these are not available, Member States shall establish threshold values through regional or sub-regional cooperation. Furthermore, countries of the Mediterranean region ratified the Mediterranean Action Plan of United Nations Environment Program (UNEP-MAP), aiming to reach and maintain GES toward the Ecosystem Approach (EcAp) by implementing an Integrated Monitoring and Assessment Programme (IMAP) coherent and consistent with MSFD for EU countries. In the Adriatic-Ionian Sea region (ADRION Region), a serious risk of pollution arises from hazardous substances due to the development of coastal urbanization, riverine inputs, increase in marine transport and offshore oil and gas extraction. EU Directives (WFD, MSFD), Barcelona Convention protocols (Dumping Protocol, Land Based Sources Protocol LBS, Offshore Protocol, Prevention and Emergency Protocol, Hazardous Wastes Protocol) and control and prevention plans defined at national level aim to assess the level of pollution with the main objective to plan, agree and implement measures to prevent, mitigate or remove impacts on the marine environment. Such measures usually require to modify the Business as Usual (BAU) scenario with socio-economic costs on human activities, so coherence and consistency between countries in the monitoring and the assessment methodology is of the utmost importance to avoid different level of environmental protection and application of the precautionary and "polluter pay" principles.

In fact, since the ratification of Barcelona Convention by Mediterranean Contracting Parties, specific monitoring and assessment programs have been developed for each Protocol with a high level of heterogeneity between them. The implementation process of WFD and MSFD, started in 2000 and 2008, respectively, by EU countries, has added a new set of activities, many of which overlap with those required by Barcelona Convention Protocols. In order to assure coherence between EU and non-EU countries in the Mediterranean region, Barcelona Convention has developed and adopted a fully and integrated ecosystem approach (EcAp) through the definition of Common Indicators grouped by Ecological Objectives. This strictly resembles MSFD Descriptors with the sole exception of the coastal zone, which is not specifically addressed by any of the EU Directives. Monitoring protocols and assessment for each of the Common Indicators have been further developed in the Integrated Monitoring and Assessment Programme (IMAP, 2016). The recent Commission Decision 2017/848/Eu (2017) on criteria and methodological standards on MSFD good environmental status has reinforced an integrated and intelligible assessment process between MSFD and WFD, aiming to harmonize the two directives regarding the spatial scale and rules of procedure to assess a "good chemical status" for the coastal and marine environment.

However, such high level integration approach would be useless if not soundly based on common and agreed protocols for monitoring contaminants. Such issue is far from being standardized for marine environment due to the different methodologies available and adopted during each monitoring survey and laboratories involved therein, with differences in sampling, storage, laboratory quality assurance (QA) process and so on.

In this context, the Interreg ADRION project HarmoNIA (Harmonization and Networking for contaminant assessment in the Ionian and Adriatic Seas) aimed to share best practices to encourage a harmonized implementation of marine environmental directives in countries bordering Adriatic-Ionian Seas. For such a scope, information on sampling procedures, analytical methodologies and quality assurance/quality control (QA/QC) procedures were collected for a list of selected pollutants in water, sediment and biota, by a questionnaire submitted to the project partners, located in 6 countries bordering the ADRION Region (Italy, Slovenia, Croatia, Montenegro, Albania and Greece). Among the various contaminants selected for the investigation, heavy metals represent a group of particular importance, considering their introduction into the environment from widespread sources, such as atmospheric fall out, riverine input and point sources pollution from coastal cities and industrial plants (Gallmetzer et al., 2017; Joksimovic et al., 2020; Cukrov et al., 2011; Igwe et al., 2013). In fact the Directive 2013/39/EU, 2013 and amended Directive 2008/105/EC, 2008 and Directive 2000/60/Ec (2000), imposed environmental quality standards (EQS – the concentration of a contaminant that should not be exceeded to protect human health and environment) for cadmium (Cd), mercury (Hg), lead (Pb), nickel (Ni) and their compounds in water. Moreover, Cd and Hg have been recognized as priority hazardous substances and EQS for mercury in biota has been introduced. Therefore, such heavy metals play a major role in

GES assessment according to Descriptor 8 of MSFD, which requires that concentrations of contaminants be at levels not giving rise to pollution effects. Hg, Cd and Pb, as well as their organic compounds, are considered hazardous substances of priority also in the framework of Barcelona Convention (UNEP-MAP). Assessment criteria, such as Background Concentration (Med BCs), Background Assessment Criteria (Med BACs) and Environmental Assessment Criteria (EACs) for mussel (*Mytilus galloprovincialis*), fish and sediments have been also developed by UNEP-MAP as an instrument to assess and monitor the achievement of GES.

This paper has the purpose to propose a harmonized methodology for sampling procedures, matrix characterization, sample preservation procedures, analytical methods and limit of quantification (LOQ) values for selected metals, derived from the information provided by the laboratories of the six ADRION countries and assuring coherence with EU legislation and decisions adopted by countries of Barcelona Convention. We hope that such a proposal will pave the way for future legislation and regulations in the ADRION basin.

## MATERIALS AND METHODS

### Study Area

The Adriatic-Ionian Sea region has a strategic geographical position, being located on the intersection of main ways of transport system between Mediterranean, Eastern Europe and Asia. Its rich heritage, both natural and cultural, makes it one of the world's most attractive destinations for tourism. However, this region shows significant differences. On the one hand, some areas are characterized by high competitiveness due to excellent performance in terms of research, development and product quality certification systems. On the other hand, in the region there are numerous territories characterized by limited research capacity and low manufacturing productivity. Some regions suffer from the increase in the production of household waste and poor air quality. Imbalances are present in transport links between different states in the region (Interreg V-B Adriatic-Ionian (ADRION), 2018–2020). Despite these differences, the whole Adriatic-Ionian basin suffers from pollution of marine and coastal environment due to human activities such as the exploitation of various resources, agriculture (land runoff), urban development in the coastal area and activities related to maritime transport (harbor activities, ballast water management etc.). In particular, heavy metal pollution in ADRION Region originates from sources such as land mining activities, like mercury mine of Idrija, Slovenia (Horvat et al., 2014; Gallmetzer et al., 2017), metallurgic industries, like Taranto industrial plants (Di Leo et al., 2013), oil refinery plants (Cukrov et al., 2011; Traven et al., 2015), old-type chlor-alkali plants (Mikac et al., 2006; Kljaković-Gašpić et al., 2006; Acquavita et al., 2012), municipal-sewage outflows (Cozzi et al., 2008; Cukrov et al., 2011; Joksimovic et al., 2020), harbors (container terminals, Cukrov et al., 2011), cruise tourism (Carić and Mackelworth, 2014; Joksimovic et al., 2019), by means of produced water discharge in offshore oil and gas extraction plants (Igwe et al., 2013). The presence of metals in the coastal environment of the Adriatic-Ionian basin is also due to natural, geogenic sources: the metals contained in the eroded rocky material are transported through rivers, as observed, for example, in the case of nickel in Koper Bay, Slovenia (Rogan Šmuc et al., 2018), or in the case of chromium and nickel in the lagoon area of Amvrakikos Gulf, Greece (Vasileiadou et al., 2016).

Six countries of ADRION Region (Italy, Slovenia, Croatia, Montenegro, Albania, and Greece) contributed to the comparative study on sampling procedures, analytical methods and QA/QC procedures adopted in contaminant analysis, with the scope to develop a common protocol according to EQSD (Environmental Quality Standard Directive) requirements. The laboratories of the following nine institutions, belonging to research and monitoring sectors, shared their information: Italian Institute for Environmental Protection and Research (ISPRA, Italy), National Institute of Biology and Slovenian Environment Agency (NIB and ARSO, Slovenia), Institute of Oceanography and Fisheries and Ruder Boskovic Institute (IOF and RBI, Croatia), University of Montenegro – Institute of Marine Biology and Center for Eco-Toxicological Research (UoM-IMBK and CETI, Montenegro), Agriculture University of Tirana (AUT, Albania), Hellenic Center for Marine Research (HCMR, Greece) (**Figure 1**).

### Questionnaire Structure

The investigation was performed through a questionnaire, prepared considering both the contaminants monitored routinely for achieving the objectives of the WFD and MSFD, and those included in the Environmental Impact Assessment (EIA) procedures of offshore platforms. The questionnaires distributed to the participants were divided into three parts, related to environmental matrices of common interest: seawater, sediment and biota (see **Supplementary Material**). The list of metals included in the comparative study for different matrices was reported in **Table 1**.

Among types of information requested, those related to QA/QC procedures (limit of detection – LOD, limit of

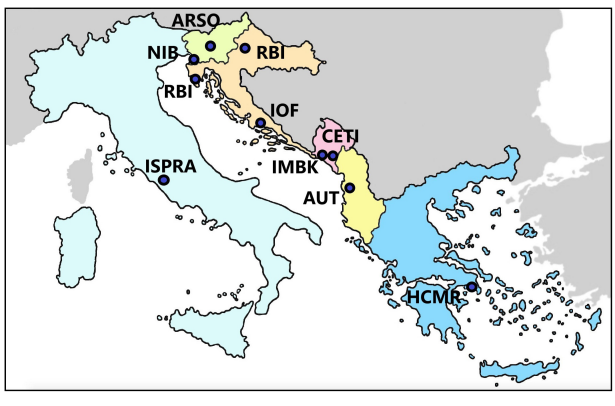


**FIGURE 1 |** Laboratories from the ADRION countries sharing information used in this study.

**TABLE 1 |** Metals considered for comparative analysis of sampling, analytical, and QA/QC procedures in different matrices.

| Elements | Seawater | Biota | Sediment |
|---|---|---|---|
| Mercury (Hg) | • | • | • |
| Cadmium (Cd) | • | • | • |
| Lead (Pb) | • | • | • |
| Vanadium (V) | | • | • |
| Chromium (Cr) | | • | • |
| Barium (Ba) | | • | • |
| Copper (Cu) | | • | • |
| Iron (Fe) | | • | • |
| Arsenic (As) | | • | • |
| Zinc (Zn) | | • | • |
| Nickel (Ni) | | • | • |
| Aluminum (Al) | | | • |

quantification – LOQ, use of reference materials, participation to intercalibration circuits, accuracy and reproducibility), as well as storage and analytical methods, were common for all three matrices. Furthermore, some specific information characteristic for each matrix is reported in **Table 2**.

The information reported by nine laboratories, from six countries of the ADRION area was compared. Most of laboratories work in respect of requirements of ISO/IEC 17025:2005. Not all of them performed the assessment of all contaminants in all three matrices. Beside the review of data collected, for the development of harmonized protocols, several technical and legislative references, such as Directive 2013/39/EU, 2013, Oslo-Paris Convention (OSPAR), Barcelona Convention documents (UNEP) and European Commission Regulations 2006/1881/EC, 2006 and its amendments), were taken into account.

# RESULTS

## Seawater Matrix

For the seawater matrix the only metals required by questionnaires were Hg, Cd, and Pb. Information on Cd and Pb was provided by one institution for each of the six countries, while information on Hg was provided by 5 of them. One of the laboratories reported additional data for nickel, copper and zinc. Among reporting laboratories, Niskin sampler made of PVC with internal silicone elastics was the most used tool for seawater sampling. Only one laboratory reported to use a home-made sampler, made of plastic such as HDPE and plexiglass with silicone seals and external closure system. Samplers employed contained external metallic parts. An acid cleaning pretreatment of the samplers was reported only by two participants. Regarding sampling cables, metal wires were mostly used, except in one case, where Kevlar cable was used. Most of the participants analyzed dissolved phase concentrations, as required by the Directive 2013/39/EU, 2013 (**Figure 2**), and one laboratory analyzed both dissolved and reactive particulate fraction. Only Hg was analyzed predominantly as total concentration.

**TABLE 2 |** Information requested for each matrix.

| Information requested | Seawater | Biota | Sediment |
|---|---|---|---|
| Storage (method, temperature, addition of preservative, etc.) | • | • | • |
| Method of analysis | • | • | • |
| Limit of detection (LOD) | • | • | • |
| Limit of quantification (LOQ) | • | • | • |
| Reference materials | • | • | • |
| Intercalibration circuit | • | • | • |
| Accuracy (% wrt certified value) | • | • | • |
| Reproducibility (RSD%) | • | • | • |
| Sample type (total, dissolved or particulate phase) | • | • | • |
| Sampling method (no filtration, filtration on 0.2, 0.45, 0.7 μm; filter type) | • | | |
| Sampling method (type of sampler) | | | • |
| Grain size (unsieved, < 2 mm, < 63 μm) | | | • |
| Thickness of sampled sediment (cm) | | | • |
| Dry or wet weight | | • | |
| Species | | • | |
| Tissue | | • | |
| Number of replicates | | • | |

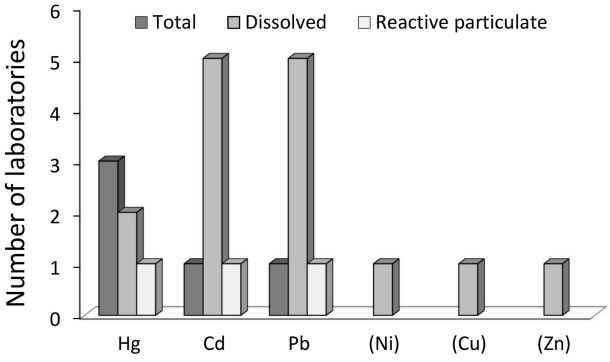


**FIGURE 2 |** Sample types for metal analysis in seawater (one laboratory analyzed two sample types).

All the participants who analyzed metals on dissolved phase, used to filter the sample through 0.45 μm pore size filters, but only one reported what type of filter was employed (cellulose acetate). Regarding storage, information was purchased by almost all reporting laboratories (only one did not provide data), highlighting that acidification and storage at 4°C were the most frequently employed procedures. Three types of analytical methods were used for Hg analysis and Cold Vapor Atomic Absorption Spectrometry (CV-AAS) was the most common. Regarding Cd and Pb, most laboratories employed Inductively Coupled Plasma Mass Spectrometry (ICP-MS), but voltammetry was also used (**Figure 3**).

LOD values were reported by only two participants for Hg (in the range 0.005–0.1 μg/l) and by three of them for Cd and Pb (0.001–1 μg/l and 0.026–2 μg/l, respectively). On the contrary, all participants reported LOQ for requested metals. That is the

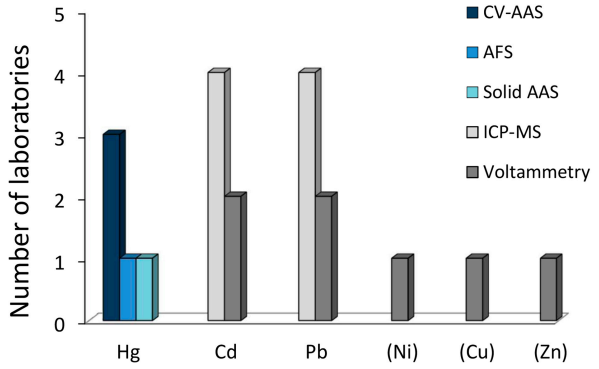


**FIGURE 3 |** Analytical methods used for metal analysis in seawater by different laboratories. CV-AAS, Cold Vapor Atomic Absorption Spectrometry; CV-AFS, Cold Vapor Atomic Fluorescence Spectrometry; Solid AAS, Solid Atomic Absorption Spectrometry; ICP-MS, Inductively Coupled Plasma Mass Spectrometry.

reason why the minimum LOQ value may appear lower than the minimum LOD, like in the case of Hg. The ranges of LOQ values were very wide, reaching up to 3 orders of magnitude (**Table 3**).

Different reference materials were used for determination of heavy metals in seawater in each institution. Two institutions reported to use reference materials for Hg: coastal seawater BCR-579 (JRC) and NIST SRM 1641d. Three different reference materials were employed by four laboratories for metals such as Cd and Pb: coastal seawater CASS-5 (NRC-CNRC), estuarine water SLEW-3 (NRC-CNRC) and open ocean seawater NASS-6 (NRC-CNRC).

Regarding the participation in intercalibration exercises, among institutions analyzing metals in seawater, only two laboratories reported to take part in such circuits – one participated in Quasimeme, while other referred to Acquacheck S11 and IELAB circuits.

Information on accuracy has been expressed in two different modes: as percentage of recovery with respect to certified value, or as the percentage of difference between the test result and the reference value. Only one laboratory responded regarding Hg: 101% with respect to certified value. For Cd and Pb, two participating institutions referred on accuracy: 96 and 100%, respectively (as% recovery), and 19 and 33%, respectively (as% difference). More information was presented regarding method reproducibility, expressed as relative standard deviation (% RSD), as three laboratories referred to produce data with reproducibility lower than 10%, and one institution declared 20% RSD at LOQ level. As additional information, one laboratory reported on measurement uncertainty: 33, 36, and 7%, respectively for Hg, Cd, and Pb.

## Sediment Matrix

For the sediment matrix the metals considered were reported in **Table 1**. In addition, Co and Mn were added as supplementary parameters by two and one institution, respectively. Metal concentrations in the sediment matrix were expressed as mg/kg on dry weight basis. Seven among nine participating institutions analyzed some of the metals, while only one performed analyses of all elements included in the questionnaire. Only Pb, Cr, Cu, and Zn were analyzed by all reporting laboratories, followed by Hg, Fe, Ni (6 laboratories), and Cd (5 laboratories), while less importance was given to the rest of the elements.

Sampling of sediments was mostly performed using box corer, followed by Van Veen grab, Ponar grab and gravity corer. The thickness of the sampled sediment layer varied among participants, while one institution reported the use of two methods for some elements. Most institutes sampled a 10 cm layer, whereas, 5 and 2 cm-thick layers were also sampled. Different grain size fractions have been chosen for metals analysis and the frequency of use was in the order 63 μm > 2 mm = unsieved > 0.5 mm. One of the laboratories measured some elements analyzing two grain size fractions.

**TABLE 3 |** Minimum and maximum values of LOD and LOQ values for metals in seawater, sediment and biota (*Mytilus galloprovincialis*) among reporting laboratories; *values expressed as wet weight (to be multiplied by a factor of 5 for the comparison with d.w. units), otherwise as dry weight (for sediment and biota); n.r. – not reported.

| Element | Seawater | | | | Sediment | | | | Biota | | | |
|---|---|---|---|---|---|---|---|---|---|---|---|---|
| | LOD [μg/l] | | LOQ [μg/l] | | LOD [mg/kg] | | LOQ [mg/kg] | | LOD [mg/kg] | | LOQ [mg/kg] | |
| | Min | Max | Min | Max | Min | Max | Min | Max | Min. | Max. | Min. | Max. |
| Hg | 0.005 | 0.1 | 0.000005 | 0.15 | 0.0003 | 0.01 | 0.0005 | 0.05 | 0.0005 | 0.002* | 0.0005 | 0.005* |
| Cd | 0.001 | 1 | 0.002 | 1.5 | 0.005 | 0.07 | 0.05 | 0.1 | 0.002* | 0.12 | 0.001 | 0.05 |
| Pb | 0.026 | 2 | 0.003 | 2.5 | 0.02 | 2 | 0.05 | 5 | 0.02 | 0.05* | 0.05 | 0.1* |
| V | | | | | 0.02 | 0.25 | 0.5 | 1 | 0.05* | n.r. | 0.1* | n.r. |
| Cr | | | | | 0.01 | 2 | 0.05 | 5 | 0.03 | 0.05* | 0.01 | 0.1* |
| Ba | | | | | 0.02 | 5 | 1 | 10 | 0.05* | n.r. | 0.01 | 0.1* |
| Cu | | | | | 0.005 | 2 | 0.02 | 5 | 0.005 | 0.4 | 0.01 | 0.1* |
| Fe | | | | | 0.2 | 20 | 0.05 | 50 | 0.1* | 1.2 | 1 | 0.5* |
| As | | | | | 0.02 | 1 | 0.001 | 3 | 0.01* | n.r. | 0.001 | 0.02* |
| Zn | | | | | 0.05 | 5 | 0.001 | 10 | 0.05 | 0.05* | 0.1 | 0.1* |
| Ni | | | | | 0.05 | 3 | 0.05 | 5 | 0.05* | n.r. | 0.01 | 0.1* |
| Al | | | | | 1 | 20 | 3 | 50 | | | | |

Regarding storage conditions, two laboratories reported the application of the SIST ISO 5667-15 method, whereas, others apply different approaches regarding both the temperature of storage (refrigeration at 1–5°C or freezing at −20°C or −40°C) and the lyophilization of samples (some referred to freeze-dry the sediments, some used the untreated sample).

More homogeneity was found among institutions in relation to the analytical instrumentation, given that for Hg most of the analyses were carried out with CV-AAS, while for the other metals the most used technique was ICP-MS, even though flame and graphite furnace AAS and Inductively Coupled Plasma Optical Emission Spectrometry (ICP-OES) have also been used (**Figure 4**). One of the laboratories applied two analytical techniques for some metals.

Regarding the method performance, not all laboratories referred to LOD and LOQ of the applied methods, whereas, differences of up to two orders of magnitude were observed between the reported values (**Table 3**). As some laboratories purchased only LOD or LOQ, for several elements small differences were observed between minimum values of both limits.

Certified reference materials (CRM) for metals in sediment were used by five institutions, which, however, used a different CRM, such as marine sediments IAEA 158 and IAEA 458 (International Atomic Energy Agency), SRM 2702 (NIST), estuarine sediment MESS-1 (NRCC) and loam soil ERM-CC141 (EU-JRC). One of the reporting laboratories used an internal reference material. Moreover, four laboratories participated in intercalibration exercises organized by IAEA, SETOC, or UNICHIM networks.

Only four laboratories reported on accuracy and/or reproducibility. Rather good accuracy was observed among all reporting laboratories; when accuracy was expressed as % recovery, it ranged between 80 and 115%, while when expressed as% difference, the values were all under 12%. Good analytical performances were confirmed also by reproducibility data, as three of four metal-analyzing institutions reported RSD values lower than 10% for all metals. Even if not requested in the questionnaire, one laboratory reported data on uncertainty lower than 20% for most metals.

## Biota Matrix

For biota, the metals considered in the questionnaire are listed in **Table 1**, and additional elements (manganese, selenium, and cobalt) were reported by only one laboratory. Six laboratories gave their contribution on the biota matrix. Cd, Cu, and Zn were analyzed by all participants, followed by Hg and Cr (5 laboratories), while less institutions determined other elements.

Participants were enquired to express their data as mg/kg. Four of them expressed their results on dry weight basis and two on wet weight basis. Mussel *Mytilus galloprovincialis* was the organism employed by all participants. Analysis was performed on whole mussel tissue by almost all institutions – only one specified that mussel muscle was used. Various institutes gave different importance to the number of analytical replicates, which ranged from 1 to 5, however, the most popular choice was 2. Regarding storage conditions, most laboratories reported keeping their samples frozen at −20°C, even if −40°C freezing and refrigeration under 5°C were also applied. Only one laboratory specified to freeze-dry the biota samples, and another to store the untreated frozen tissue.

Some commonalities were observed regarding analytical techniques used for metal determination: for Hg various atomic absorption methods were applied. Other metals were analyzed both by means of AAS (graphite furnace or flame) and ICP-MS or ICP-OES (**Figure 5**).

Only four laboratories reported values of LOD and/or LOQ. The direct comparison was not possible, as some values

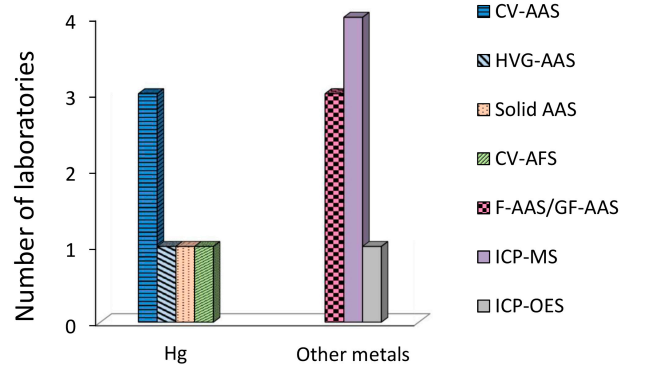


**FIGURE 4 |** Analytical methods used for metal analysis in sediment by the different laboratories. CV-AAS, Cold Vapor Atomic Absorption Spectrometry; HVG-AAS, Hydride Vapor Generation Atomic Absorption Spectrometry; Solid AAS, Solid Atomic Absorption Spectrometry; CV-AFS, Cold Vapor Atomic Fluorescence Spectrometry; F-AAS, Flame Atomic Absorption Spectrometry; GF-AAS, Graphite Furnace Atomic Absorption Spectrometry; CP-MS, Inductively Coupled Plasma Mass Spectrometry; ICP-OES, Inductively Coupled Plasma Optical Emission Spectrometry.

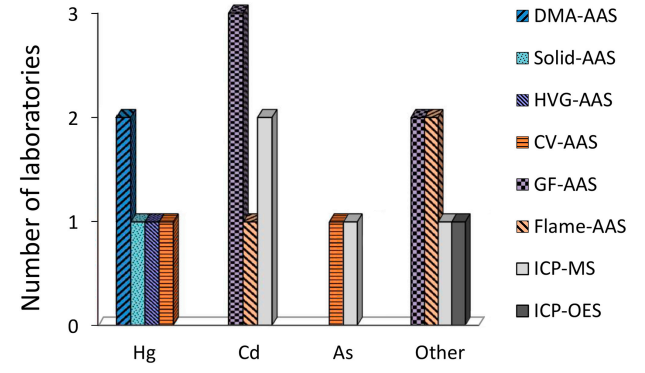


**FIGURE 5 |** Analytical methods used for metal analysis in biota by different laboratories. DMA, Direct Mercury Analyzer; Solid AAS, Solid Atomic Absorption Spectrometry; HVG-AAS, Hydride Vapor Generation Atomic Absorption Spectrometry; CV-AAS, Cold Vapor Atomic Absorption Spectrometry; GF-AAS, Graphite Furnace Atomic Absorption Spectrometry; F-AAS, Flame Atomic Absorption Spectrometry; ICP-MS, Inductively Coupled Plasma Mass Spectrometry; ICP-OES, Inductively Coupled Plasma Optical Emission Spectrometry.

were expressed on dry and other on wet weight basis. Only with the scope of comparing the values, the dry/wet weight conversion factor of 20% was assumed (w.w. units = d.w. units/5). However, w.w. data were not transformed in d.w. units, as real d.w./w.w. ratios were not known. Considering this, the minimum and maximum values of LOD and LOQ are presented in **Table 3**. The differences among LOQ values were in the range of one order of magnitude, reflecting major homogeneity of analytical performances in biota matrix. As some laboratories purchased only LOD or LOQ, for several elements values of both limits are very similar, and in some cases LOD is apparently higher than LOQ.

Certified reference materials were employed by all laboratories analyzing biota and mussel tissue SRM 2976 (NIST) was the most used. Other CRMs used were: fish tissue IAEA 407, fish protein DORM-2 and DORM-4 (NRC-CNRC), oyster tissue SRM 1566 (NIST) and mussel tissue BCR 278 (JRC). Three participants took part in intercalibration exercises (QUASIMEME, IAEA, FAPAS). Accuracy and reproducibility data were reported by four laboratories. Good analytical performances were evidenced, as accuracy values for all metals were in the range of 92–106% (as % recovery with respect to certified values), or under 12% (as % difference between the test result and the reference value). All the reproducibility data were lower than 15%. Additional information on measurement uncertainty for Hg, Cd and Pb was reported by one of the participants (21, 20, 25%, respectively).

# DISCUSSION

The comparison between sampling, analytical and QA protocols adopted by laboratories of nine institutions from six countries of the ADRION Region revealed high level of heterogeneity, pointing out the necessity to develop common and harmonized protocols for monitoring procedures to be applied for the assessment of *good environmental status*, in order to fulfill the requirements of both Marine Strategy Framework Directive 2008/56/EC, 2008 and UNEP/MAP Integrated Monitoring and Assessment Programme (IMAP). In order to establish a common protocol for the evaluation of the metal contamination, several targets for harmonization have been identified, such as matrix characteristics, measurement units, sampling procedures, and sample storage, methods of analysis and LOQ values.

## Seawater

Regarding seawater matrix, according to the Directive 2013/39/EU, 2013, measurement unit to be used is μg/l and concentrations of metals have to be determined in dissolved phase of water sample, achieved by filtration through 0.45 μm filter (or equivalent treatment), so the use of total sample has to be avoided. According to the ISO 5667-3 standard (2018), samples for metal analysis should be acidified to pH in the range 1–2 with concentrated nitric acid (possibly with purity grade for trace metals analysis), and stored cooled at 4°C. For Cd and Pb, SPE pre-concentration step may be applied, even if only one institution reported to apply this procedure. It has to be kept in mind that the risk of seawater contamination by metals has to be minimized. At this regard, the most critical step is sampling, as multiple sources of contamination may be present on the vessel such as wires, rust or antifouling paints. For this reason, it is recommended to use plastic tools and devices, preferentially made in Teflon or Teflon-coated (sampling bottles, submersible pumps). Internal metallic springs or silicone elastics should be avoided in favor of external closure systems. Non-metallic wires should be employed (made, for example, of Kevlar). On-board handling should be possibly carried out in a clean area, like a mobile laboratory container equipped with ultrapure water production system and laminar flow hoods. All sampling and storage containers, filtration apparatus and plastic material employed should be acid cleaned and rinsed with ultrapure water, and finally conditioned with seawater to be sampled (Capodaglio et al., 1995). Regarding analytical method, following the majority of questionnaire responses, CV-AAS was the preferential method for Hg determination in seawater samples, while Cd and Pb were analyzed by ICP-MS or voltammetry. Considering the wide range of LOQ values observed for metals in seawater, LOQ proposal was "harmonized" taking into account that the Article 4 of the Directive 2009/90/EC, 2009 requires that LOQ have to be equal or below 30% of environmental quality standard (EQS) values. The Directive 2013/39/EU, 2013 (EQSD) imposes MAC-EQS (maximum allowable concentration EQS for "other surface waters") of 0.07 μg/l for Hg and its compounds and AA-EQS (annual average EQS) of 0.2 and 1.3 μg/l for Cd and Pb, respectively (**Table 4**). Taking into account LOQ values reported in questionnaires by different laboratories from ADRION Region, the proposed limits should be easily reached for Hg, while for Cd and Pb some laboratories will need to improve their methods.

## Sediment

As regards the harmonization proposal for sediment matrix, consensus was reached that data should be expressed as mg/kg d.w. In view of different sampling devices used by ADRION Region laboratories, box corer was chosen as the most appropriate sampling tool, considering that its use causes minimal disturbance to the sample regardless of the sampling conditions (weather/sea state, water depth, sediment composition, etc.) (Blomqvist, 1991). According to Guidance on chemical monitoring of sediment and biota under the WFD (European Commission, 2010), the top 5–10 cm of sediment is the most dynamic layer resulting from sedimentation and

**TABLE 4 |** Proposal of harmonized monitoring procedures of metals in seawater: LOQ and EQS are expressed as μg/l.

| Elements | Hg | Cd | Pb |
|---|---|---|---|
| Sampling method | Filtration 0.45 μm | | |
| Storage | Acidification, 4°C | $HNO_3$ and SPE preconcentration | |
| Method of analysis | CV-AAS | Voltammetry/ICP-MS | |
| LOQ proposal* | 0.021 | 0.06 | 0.39 |
| EQS (2013/39/EU) | 0.07** | 0.2 | 1.3 |

**LOQ values as 30% of EQS; **MAC-EQS.*

physical and biological interactions, reflecting the actual status of pollution. However, the choice of the sediment layer thickness should depend on the sediment accumulation rate of the sampling site. ADRION laboratories agreed that in coastal as well as offshore areas the top 0–2 cm sediment layer should be sampled in order to evaluate the recent temporal trends. Even thinner depths should be sampled if measured sedimentation rates are low, such as in open water environments or coastal water with low particle deposition. Considering that various grain size classes were analyzed by different laboratories, and that one of the HarmoNIA objectives was to improve the comparability of data, it was agreed that it is advisable to analyze the grain size fraction of <2 mm. It is well known that most contaminants are preferentially linked to the fine fraction (<63 μm) and to the related organic matter, however, in areas of high hydrodynamic energy, such as coastal and offshore marine areas, fine particulate matter is mixed with coarser material (European Commission, 2010), and in sandy bottoms the < 63 μm fraction would represent a negligible fraction not representative of the bulk sediments. Nonetheless, for meaningful comparisons, it is requested to obtain also information on granulometry as metadata, in order to allow normalization to the fine fraction. Following the OSPAR approach, it is recommended to analyze Al also for the normalization of the metal concentrations (Ospar Commission, 2009). Alternatively, other elements, like Fe, may be successfully employed for normalizing the heavy metal concentrations (Villares et al., 2003; Sakan et al., 2015). For the scope of harmonization, ICP-MS technique was selected for metals determination due to its multi-element character and capacity to determine very low concentrations (Thomas, 2013); in fact, the lowest LOQ values, reported among laboratories, were obtained using this technique.

Both WFD (2000/60/EC) and MSFD (2008/56/EC), as well as their amendments and implementing decrees, consider water and biota for the assessment of GES. According to the Directive 2013/39/EU, 2013, no EQS values were laid down for sediment matrix, however, Member States have the flexibility to set EQS for alternative matrices, as long as they provide at least the same level of protection, in order to take advantage of their monitoring approach. These national EQS should be established according to WFD indications of Guidance document no. 27 (European Commission, 2011, 2018 revision). According to collected information, only Italy has set a national EQS for metals in the sediment matrix (Legislative Decree, 2015). Italian EQS values have been derived on the basis of direct hazards for the benthic communities as well as for human health via seafood consumption and the ecotoxicological criterion of Threshold Effect Level (TEL) was used as reference. Chemical and toxicological data were collected along the Italian coast in the period 2001–2008 (Tornero et al., 2019). In other ADRION countries, no national standards for sediment matrix are in force, but some international references such as Med BACs, Effect Range Low (ERL) or TEL are applied for the sediment quality assessment (**Table 5**).

Med BACs criterion was developed on the basis of Oslo-Paris Convention for the Protection of the Marine Environment of the North-East Atlantic (OSPAR) and by criteria defined by the scientific studies in the Mediterranean Sea (United Nations, 2011 and references therein). Med BACs have been calculated for the Mediterranean Sea as a whole, using Med BCs, concentrations at a pristine or remote site (United Nations, 2016; United Nations, 2019). For the purpose of this study, Med BACs for the whole Mediterranean Sea were applied as reference, even if specific BACs for Adriatic, Aegean-Levantine, Central Mediterranean and Western Mediterranean regions have been assessed. Another threshold value, often used as reference, is ERL (or ER-Low), developed by the United States Environmental Protection Agency (US EPA), defined as the lower tenth percentile of the dataset of concentrations in sediments associated with biological effects. At concentrations lower than ERL adverse effects on organisms occur rarely, thus this threshold is, in some way, of parallel significance to WFD EQS and OSPAR EACs, representing the contaminant concentration below which no chronic effects are expected to arise even in most sensitive marine species, even if these criteria are derived in a very different way (Ospar Commission, 2009). TEL, on the other hand, is a threshold value below which the negative effects on biota are expected to arise only rarely and was developed by the Canadian Council of Ministers of the Environment. In the framework of HarmoNIA project, in order to ensure the best analytical performance and maintain a precautionary approach, LOQ values proposed for sediment matrix (**Table 5**) were based on the lowest values reported by laboratories in the questionnaires, considering also that values proposed would be sufficient to determine concentrations at international threshold levels. The proposed LOQ values for sediments may be challenging to reach, considering that differences of 2 orders of magnitude were observed among values reported in the questionnaires by the ADRION Region laboratories, however, until adequate EQS for the sediment matrix are developed, it seems appropriate to stimulate the development and optimization of analytical methods.

## Biota

With regard to biota, it was agreed to express the concentrations of contaminants on the basis of wet weight, in order to favor the comparison with both the EQS values of Directive 2013/39/EU, 2013 and the maximum levels for metals in foodstuffs of the Commission Regulation 2006/1881/Ec (2006) and Commission Regulation 2008/629/Ec (2008). However, considering that the differences in the water content could affect the comparison of the different samples, it is always recommended to carefully measure both wet and dry weight (Guidance No. 25 - European Commission, 2010) and include this information among metadata. Since all laboratories use bivalve mollusk *M. galloprovincialis* for the evaluation of metal contamination in the biota matrix, it was shared that the analysis must be carried out on total samples (whole soft tissues), as indicated by the Guidance No. 25 (European Commission, 2010). However, considering that the threshold values for metals established by legislation are related to fish (EQS for Hg of Directive 2013/39/EU, 2013) or to fish and bivalve mollusks (Commission Regulation 2006/1881/Ec, 2006; Commission Regulation 2008/629/Ec, 2008), it is important

**TABLE 5 |** Proposed harmonized monitoring procedures of metals in sediment. LOQ values and international reference thresholds are expressed as mg/kg d.w.

| Elements | Hg | Cd | Pb | V | Cr | Ba | Cu | Fe | As | Zn | Ni | Al |
|---|---|---|---|---|---|---|---|---|---|---|---|---|
| Grain size | <2 mm | | | | | | | | | | | |
| Sampling method | Box corer | | | | | | | | | | | |
| Thickness of sediment | 0–2 cm | | | | | | | | | | | |
| Storage | −20°C or 4°C if freeze-dried | | | | | | | | | | | |
| Method of analysis | ICP-MS | | | | | | | | | | | |
| LOQ proposal | 0.0005 | 0.05 | 0.05 | 0.5 | 0.05 | 1 | 0.02 | 0.05 | 0.001 | 0.001 | 0.05 | 3 |
| Med BAC[a] | 0.0795 | 0.1275 | 25.425 | – | – | – | – | – | – | – | – | – |
| ERL[b] | 0.15 | 1.2 | 46.7 | – | 81 | – | 34 | – | 8.2 | 150 | 21 | – |
| TEL[c] | 0.13 | 0.67 | 30 | – | 52 | – | 19 | – | 7.2 | 120 | – | – |
| Italian AA-EQS[d] | 0.3 | 0.3 | 30 | – | 50 | – | – | – | 12 | – | – | – |

[a](United Nations, 2016); [b](Tornero et al., 2019); [c](Canadian Council of Ministers of the Environment [CCME], 2007); [d](Legislative Decree, 2015).

**TABLE 6 |** Proposal of harmonized monitoring procedures of metals in biota.

| Elements | Hg | Cd | Pb | V | Cr | Ba | Cu | Fe | As | Zn | Ni |
|---|---|---|---|---|---|---|---|---|---|---|---|
| Weight basis | Wet weight | | | | | | | | | | |
| Number of replicates | 3 | | | | | | | | | | |
| Storage | −20°C | | | | | | | | | | |
| Method of analysis | CV-AAS | ICP-OES/ICP-MS | | | | | | | | | |
| LOQ proposal | 0.006* | 0.001∞ | 0.05∞ | 0.1 | 0.01∞ | 0.01∞ | 0.01∞ | 1∞ | 0.001∞ | 0.1∞ | 0.01∞ |
| EQS[a] | 0.02* | – | – | – | – | – | – | – | – | – | – |
| Med BAC[b] | 0.101*/0.173∞ | 0.016*/1.095∞ | 0.040*/2.313∞ | – | – | – | – | – | – | – | – |
| OSPAR BAC[c] | 0.035*/0.090∞ | 0.026*/0.96∞ | 0.026*/1.3∞ | – | – | – | 6∞ | – | – | – | – |
| Maximum levels in foodstuffs[d] | 0.5-1*/0.5 | 0.05-0.30*/1 | 0.3*/1.5 | – | – | – | – | – | – | – | – |

*Proposed LOQ values and some international reference thresholds expressed as mg/kg (*concentration values referred to fish tissue, otherwise in bivalve mollusk; ∞ values expressed as dry weight, otherwise as wet weight).* [a](Directive 2013/39/EU, 2013); [b](United Nations, 2016); [c](Tornero et al., 2019); [d](Commission Regulation 2006/1881/Ec, 2006).

to remember that the choice of the tissue to be analyzed must be relative to the purpose of the monitoring (European Commission, 2010). If the objective is to protect the ecosystem, the use of the whole fish tissue is suggested, while if the aim of monitoring is the human health protection, edible tissues should be analyzed. In this context, it has to be underlined that muscle concentrations reflect long-term accumulation processes and do not reveal current bioaccumulation nor recent temporal changes in contamination level, which on the contrary are better reflected in the liver tissue (Guidance No. 25 European Commission, 2010). According to WFD Common Implementation Strategy, for each sample 3–5 replicates should be prepared and stored at −20°C, and consensus was reached that analysis should be performed on at least 3 replicates. For each sample, biometric measurements of each individual should be registered (weight and length of shell, weight of tissues). Considering that different analytical techniques were applied by different institutions, the use of CV-AAS was proposed to harmonize Hg determination, as this technique features good sensitivity, relative freedom of interferences, simplicity of use and low cost (Krata and Bulska, 2005; Ferreira et al., 2015), while ICP-MS and ICP-OES were recommended for other metal analyses, due to their multi-elemental character coupled with good precision, accuracy and recovery (Thomas, 2013; Park et al., 2018). Hg (and its compounds) is the only metal with biota EQS imposed by the Directive 2013/39/EU, 2013 (20 μg/kg w.w. in fish tissue) thus, according to what already discussed for water matrix, the LOQ proposed for its harmonized assessment was 30% of EQS, according to the Directive 2009/90/EC, 2009 (**Table 6**). For other metals, the lowest values reported among questionnaires, as listed in **Table 3**, were proposed as LOQ in order to obtain the best analytical performance in terms of QA/QC and to maintain the precautionary approach. Considering that Hg, Cd and Pb are trace metals of common concern among Commission Regulation 2006/1881/Ec, 2006, OSPAR Convention and UNEP-MAP, it has been taken into account that the proposed LOQs are sufficient to determine these metals' concentrations at the maximum levels in the foodstuffs and at the levels of OSPAR BACs and Med BACs (**Table 6**).

According to the Common Implementation Strategy of WFD, isotopic analysis of biota should be performed to determine the trophic levels if different species have to be monitored (Guidance No. 25 European Commission, 2010).

## General Indications

In addition to the harmonization indications described above, some general proposals have been suggested regarding all matrices. Laboratories involved in the comparison from all around the ADRION Region were invited to make an effort to attempt the analysis of all the substances included in the

questionnaires, with the aim of allowing the evaluation of the relative contamination in the whole area. Although the use of certified reference materials was quite common, especially in sediment and biota, all participants were invited to use adequate reference materials, similar to the sample matrix, in order to be able to verify analytical performances, especially considering the scarcity of information related to essential characteristics of method validation, such as accuracy and reproducibility. In this regard, it is important to remember, that according to the Association of Official Analytical Chemists (AOAC) recommendations, for concentrations from 0.1 to 10 mg/kg the mean recovery is expected in the range of 80–110%, with relative standard deviation (RSD%) of 15–7.3%, while for concentrations from 10 to 100 mg/kg the mean recovery should remain in the narrower range of 90–107%, with RSD of 7.3–5.3% (Aoac, 2016). In order to ensure that assessment of contaminants is coherent in the region, it was also suggested that all involved laboratories take part in the intercalibration tests or proficiency tests.

## CONCLUSION

A general lack of homogeneity emerged from the investigation on the sampling and preservation protocols and on the analytical methods used by various laboratories responsible for research and monitoring of heavy metals in different environmental compartments in the ADRION region, also due to the lack of completeness of some information. In particular, differences were related to the sampling characteristics (filtration for seawater, sample thickness and grain size for sediments, tissue and weight basis for biota), to the storage procedures (preservative addition, cooling, freezing, freeze-drying), to the analytical technique and to the achievable LOQ values. In order to enable the coherent assessment of the state of the environment and of the impacts on the coastal and off-shore areas of the Adriatic and Ionian Seas, a harmonized methodological proposal was developed and shared based on the requirements of the EU legislation and taking into account the decisions adopted by Barcelona Convention (UNEP-MAP) and OSPAR. Although appropriate environmental quality standards for biota and sediment matrices should be established at national level through regional and sub-regional cooperation, as required by the WFD and MSFD, the proposed LOQ values, even if challenging, represent a benchmark and a stimulus to optimize analytical performance, to ensure the best level of protection of the coastal and offshore environment in the ADRION Region.

## DATA AVAILABILITY STATEMENT

The raw data supporting the conclusions of this article will be made available by the authors, without undue reservation, to any qualified researcher.

## AUTHOR CONTRIBUTIONS

GG, DB, and ML directed this part of the project. DB, GG, ML, and FR conceived the form of this study. DB, CG, FR, and MF gathered and confronted the data. MG contributed to the discussion of the results. MF, DB, CG, FR, GG, BT, and ML wrote the manuscript and designed figures and tables with input and revisions from all authors. All authors contributed to the article and approved the submitted version.

## FUNDING

This work was financed by the Adriatic-Ionian Program INTERREG V-B Transnational 2014-2020, 2018-2020 within the Interreg Adrion project HarmoNIA (Harmonization and Networking for contaminant assessment in the Ionian and Adriatic Seas) granted to ML and BT. The content of the publication is the sole responsibility of beneficiaries of the project and can under no circumstances be regarded as reflecting the position of the European Union and/or ADRION programme authorities.

## SUPPLEMENTARY MATERIAL

The Supplementary Material for this article can be found online at: https://www.frontiersin.org/articles/10.3389/fmars.2020.00717/full#supplementary-material

## REFERENCES

Acquavita, A., Covelli, S., Emili, A., Berto, D., Faganeli, J., Giani, M., et al. (2012). Mercury in the sediments of the marano and grado lagoon (northern Adriatic Sea): sources, distribution and speciation. *Estuar. Coast Shelf Sci.* 113, 20–31. doi: 10.1016/j.ecss.2012.02.012

Aoac (2016). *Appendix F: Guidelines for Standard Method Performance Requirements, 20th Ed. of the Official Methods of Analysis of AOAC International*. Washington, D.C: AOAC.

Blomqvist, S. (1991). Quantitative sampling of soft-bottom sediments: problems and solutions. *Mar. Ecol. Prog. Ser.* 72, 295–304. doi: 10.3354/meps072295

Capodaglio, G., Scarponi, G., Toscano, G., Barbante, C., and Cescon, P. (1995). Speciation of trace metals in seawater by anodic stripping voltammetry: critical analytical steps. *Fresenius J. Anal. Chem.* 351, 386–392. doi: 10.1007/BF00322907

Carić, H., and Mackelworth, P. (2014). Cruise tourism environmental impacts - The perspective from the Adriatic Sea. *Ocean Coast. Manag.* 102, 350–363. doi: 10.1016/j.ocecoaman.2014.09.008

Canadian Council of Ministers of the Environment [CCME] (2007). "Protocol for the derivation and use of sediment quality guidelines for the protection of aquatic life," in *Report prepared by the Task Force on Water Quality Guidelines of the Canadian Council of Ministers of the Environment Water Quality Branch*, Environment Canada, Ottawa.

Commission Decision 2017/848/Eu (2017). *2017/848/EU Laying Down Criteria and Methodological Standards on Good Environmental Status of Marine Waters and Specifications and Standardised Methods for Monitoring and Assessment, and Repealing Decision 2010/477/EU*. EU: EEA.

Commission Regulation 2006/1881/Ec (2006). *(EC) No 1881/2006 Setting Maximum Levels for Certain Contaminants in Foodstuffs*. EU: EEA.

Commission Regulation 2008/629/Ec (2008). *(EC) No 629/2008 Amending Regulation (EC) No 1881/2006 Setting Maximum Levels for Certain Contaminants in Foodstuffs*. EU: EEA.

Cozzi, S., Reisenhofer, E., Di Monte, L., Cantoni, C., and Adami, G. (2008). Effect of environmental forcing on the fate of nutrients, dissolved organic matter and heavy metals released by a coastal wastewater pipeline. *Chem. Ecol.* 24, 87–107. doi: 10.1080/02757540801919354

Cukrov, N., Frančišković-Bilinski, S., Hlača, B., and Barišić, D. (2011). A recent history of metal accumulation in the sediments of Rijeka harbor, Adriatic Sea, Croatia. *Mar. Pollut. Bull.* 62, 154–167. doi: 10.1016/j.marpolbul.2010.08.020

Di Leo, A., Annicchiarico, C., Cardellicchio, N., Spada, L., and Giandomenico, S. (2013). Trace metal distributions in Posidonia oceanica and sediments from Taranto Gulf (Ionian Sea. Southern Italy). *Mediterranean Mar. Sci.* 14, 204–213. doi: 10.12681/mms.316

Commission Directive 2009/90/Ec (2009). *Laying Down, Pursuant to Directive 2000/60/EC of the European Parliament and of the Council, Technical Specifications for Chemical Analysis and Monitoring of Water Status*. Brussels: EU.

Directive 2000/60/Ec (2000). *Directive 2000/60/EC of the European Parliament and of the Council establishing a framework for Community action in the field of water policy*. EU: EEA.

Directive 2008/56/Ec (2008). *Directive 2008/56/EC of the European Parliament and of the Council establishing a framework for community action in the field of marine environmental policy (Marine Strategy Framework Directive)*. Brussels: EU.

Directive 2008/105/Ec, (2008). *Directive 2008/105/EC of the European Parliament and of the Council on environmental quality standards in the field of water policy, amending and subsequently repealing Council Directives 82/176/EEC, 83/513/EEC, 84/156/EEC, 84/491/EEC, 86/280/EEC and amending Directive 2000/60/EC of the European Parliament and of the Council*. Brussels: EU.

Directive 2013/39/Eu, (2013). *Directive 2013/39/EU of the European Parliament and of the Council amending Directives 2000/60/EC and 2008/105/EC as regards priority substances in the field of water policy*. Brussels: EU.

European Commission (2010). *Common Implementation Strategy for the Water Framework Directive (2000/60/EC). Guidance Document No. 25. Guidance on chemical monitoring of sediment and biota under the Water Framework Directive*. Brussels: EU.

European Commission (2011). *Common Implementation Strategy for the Water Framework Directive-Guidance Document No. 27-Technical Guidance for Deriving Environmental Quality Standards*; European Commission Technical Report; Brussels: EU.

European Commission (2018). *Common Implementation Strategy for the Water Framework Directive (2000/60/EC). Guidance Document No: 27, Updated Version 2018, Document endorsed by EU Water Directors at their meeting in Sofia on 11-12 June 2018. Technical Guidance for Deriving Environmental Quality Standards*.

Ferreira, S. L. C., Lemos, V. A., Silva, L. O. B., Queiroz, A. F. S., Souza, A. S., da Silva, E. G. P., et al. (2015). Analytical strategies of sample preparation for the determination of mercury in food matrices — a review. *Microchem. J.* 121, 227–236. doi: 10.1016/j.microc.2015.02.012

Gallmetzer, I., Haselmair, A., Tomašovych, A., Stachowitsch, M., and Zuschin, M. (2017). Responses of molluscan communities to centuries of human impact in the northern Adriatic Sea. *PLoS One* 12:e0180820. doi: 10.1371/journal.pone.0180820

Horvat, M., Degenek, N., Lipej, L., Snoj, Tratnik, J., and Faganeli, J. (2014). Trophic transfer and accumulation of mercury in ray species in coastal waters affected by historic mercury mining (Gulf of Trieste, northern Adriatic Sea). *Environ. Sci. Pollut. Res.* 21, 4163–4176. doi: 10.1007/s11356-013-2262-0

Igwe, C. O., Saadi, A. A. L., and Ngene, S. E. (2013). Optimal options for treatment of produced water in offshore petroleum platforms. *J. Pollut. Eff. Cont.* 1:102. doi: 10.4172/2375-4397.1000102

IMAP (2016). *Integrated Monitoring and Assessment Programme of the Mediterranean Sea and Coast and Related Assessment Criteria, UNEP/MAP*. Athens: United Nations.

Interreg V-B Adriatic-Ionian (ADRION) (2018–2020). *Cooperation Programme* Avaliable online at: https://www.adrioninterreg.eu/

Joksimovic, D., Castelli, A., Pestorić, B., and Perosevic, A. (2019) An assessment of trace metal contamination in surface sediments of the Montenegrin coast by using pollution indexes and statistical analysis. *Fresenius Environ. Bull.* 28, 879–884.

Joksimovic, D., Perošević, A., Castelli, A., Pestorić, B., Šuković, D., and Đurović, D. (2020). Assessment of heavy metal pollution in surface sediments of the Montenegrin coast: a 10-year review. *J. Soils Sediments* 20, 2598–2607. doi: 10.1007/s11368-019-02480-7

Kljaković-Gašpić, Z., Odžak, N., Ujević, I., Zvonarić, T., Horvat, M., and Barić, A. (2006). Biomonitoring of mercury in polluted coastal area using transplanted mussels. *Sci. Total Environ.* 368, 199–209. doi: 10.1016/j.scitotenv.2005.09.080

Krata, A., and Bulska, E. (2005). Critical evaluation of analytical performance of atomic absorption spectrometry and inductively coupled plasma mass spectrometry for mercury determination. *Spectrochim. Acta B* 60, 345–350. doi: 10.1016/j.sab.2004.11.011

Legislative Decree of 13 October 2015, no. 172. Implementation of Directive 2013/39/EU amending Directive 2000/60/EC as regards priority substances in the field of water policy. (15G00186) (GU General Series No. 250 of 27-10-2015)]. Rome: Ministry of Economy and Finance.

Mikac, N., Foucher, D., Kwokal, Ž, and Barišić, D. (2006). Mercury and radionuclides in sediments of the Kaštela bay (Croatia) – evaluation of the sediment pollution history. *Croat. Chem. Acta* 79, 85–93.

OSPAR (2009). *Agreement on CEMP Assessment Criteria for the QSR 2010. Agreement 2009-2*.

Park, Y. M., Choi, J. Y., Nho, E. Y., Lee, C. M., Hwang, I. M., Khan, N., et al. (2018). Determination of macro and trace elements in canned marine products by inductively coupled plasma—optical emission spectrometry (ICP-OES) and ICP—mass spectrometry (ICP-MS). *Anal. Lett.* 52, 1018–1030. doi: 10.1080/00032719.2018.1510938

Rogan Šmuc, N., Dolenec, M., Kramar, S., and Mladenović, A. (2018). Heavy metal signature and environmental assessment of nearshore sediments: port of koper (Northern Adriatic Sea). *Geosciences* 8:398. doi: 10.3390/geosciences8110398

Sakan, S., Dević, G., Relić, D., Anđelković, I., Sakan, N., and Đorđević, D. (2015). Evaluation of sediment contamination with heavy metals: the importance of determining appropriate background content and suitable element for normalization. *Environ. Geochem. Health* 37, 97–113. doi: 10.1007/s10653-015-9766-0

Thomas, R. (2013). *Practical guide to ICP-MS: a tutorial for beginners. 3rd edition*. Boca Raton, FL: CRC Press.

Tornero, V., Hanke, G., and the Msfd Expert Network on Contaminants. (2019). *Marine chemical contaminants – support to the harmonization of MSFD D8 methodological standards: Matrices and threshold values/reference levels for relevant substances*. Luxembourg: Publications Office of the European Union.

Traven, L., Furlan, N., and Cenov, A. (2015). Historical trends (1998–2012) of nickel (Ni), copper (Cu) and chromium (Cr) concentrations in marine sediments at four locations in the Northern Adriatic Sea. *Mar. Pollut. Bull.* 98, 289–294. doi: 10.1016/j.marpolbul.2015.07.001

United Nations (2019). *UNEP/MED WG.463/Inf.7*, Podgorica, Montenegro (accessed March 2, 2019).

United Nations (2016). *UNEP(DEPI)/MED WG.427/7. Agenda item 5. Review of Proposed Background Concentrations (BC)/Background Assessment Criteria (BACs)/Environmental Assessment Criteria (EACs) for Contaminants and Biomarkers at Mediterranean and Regional Scales. Proposal of Assessment Criteria for Hazardous Substances and Biological Markers in the Mediterranean Sea Basin and its Regional Scales*. Marseille: UNEP.

United Nations (2019). *Podgorica, Montenegro, 2- 3, 2019*.

Vasileiadou, K., Pavloudi, C., Kalantzi, I., Apostolaki, E., Chatzigeorgiou, G., Chatzinikolaou, E., et al. (2016). Environmental variability and heavy metal concentrations from five lagoons in the Ionian Sea (Amvrakikos Gulf. W Greece). *Biodivers. Data J.* 4, e8233. doi: 10.3897/BDJ.4.e8233

Villares, R., Puente, X., and Carballeira, A. (2003). Heavy Metals in Sandy Sediments of the Rías Baixas (NW Spain). *Environ. Monit. Assess.* 83, 129–144. doi: 10.1023/A:1022542416249

**Conflict of Interest:** The authors declare that the research was conducted in the absence of any commercial or financial relationships that could be construed as a potential conflict of interest.

frontiers in Marine Science

BRIEF RESEARCH REPORT
published: 16 September 2020
doi: 10.3389/fmars.2020.571365

# Heavy Metals in the Adriatic-Ionian Seas: A Case Study to Illustrate the Challenges in Data Management When Dealing With Regional Datasets

*Maria Eugenia Molina Jack[1]*, Rigers Bakiu[2], Ana Castelli[3], Branko Čermelj[4], Maja Fafanđel[5], Christina Georgopoulou[6], Giordano Giorgi[7], Athanasia Iona[8], Damir Ivankovic[9], Martina Kralj[1], Elena Partescano[1], Alice Rotini[7], Melita Velikonja[10] and Marina Lipizer[1]*

[1] Istituto Nazionale di Oceanografia e di Geofisica Sperimentale (OGS), Trieste, Italy, [2] Department of Aquaculture and Fisheries, Faculty of Agriculture and Environment, Agricultural University of Tirana, Tirana, Albania, [3] Public Institution University of Montenegro – Institute of Marine Biology (UoM-IMBK), Kotor, Montenegro, [4] National Institute of Biology, Marine Biology Station Piran, Piran, Slovenia, [5] Center for Marine Research, Ruder Boskovic Institute, Zagreb, Croatia, [6] Region of Western Greece, Patras, Greece, [7] Istituto Superiore per la Protezione e la Ricerca Ambientale (ISPRA), Rome, Italy, [8] Hellenic Centre for Marine Research, Anavyssos, Greece, [9] Institute of Oceanography and Fisheries, Split, Croatia, [10] Slovenian Environment Agency, Ljubljana, Slovenia

OPEN ACCESS

**Edited by:**
*Dragana S. Đorđević, University of Belgrade, Serbia*

**Reviewed by:**
*Giuseppe Bonanno, University of Catania, Italy*
*J. German Rodriguez, Technological Center Expert in Marine and Food Innovation (AZTI), Spain*

***Correspondence:**
*Maria Eugenia Molina Jack*
*mmolinajack@inogs.it*

**Specialty section:**
*This article was submitted to Marine Pollution, a section of the journal Frontiers in Marine Science*

**Received:** *10 June 2020*
**Accepted:** *25 August 2020*
**Published:** *16 September 2020*

**Citation:**
*Molina Jack ME, Bakiu R, Castelli A, Čermelj B, Fafanđel M, Georgopoulou C, Giorgi G, Iona A, Ivankovic D, Kralj M, Partescano E, Rotini A, Velikonja M and Lipizer M (2020) Heavy Metals in the Adriatic-Ionian Seas: A Case Study to Illustrate the Challenges in Data Management When Dealing With Regional Datasets. Front. Mar. Sci. 7:571365. doi: 10.3389/fmars.2020.571365*

Harmonization of monitoring protocols and analytical methods is a crucial issue for transnational marine environmental status assessment, yet not the only one. Coherent data management and quality control become very relevant when environmental status is assessed at regional or subregional scale (e.g., for the Mediterranean or the Adriatic Sea), thus requiring data from different sources. Heavy metals are among the main targets of monitoring activities. Significant efforts have been dedicated to share best practices for monitoring and assessment of ecosystem status and to strengthen the network of national, regional and European large data infrastructures in order to facilitate the access to data among countries. Data comparability and interoperability depend not only on sampling and analytical protocols but also on how data and metadata are managed, quality controlled and made accessible. Interoperability is guaranteed by using common metadata and data formats, and standard vocabularies to assure homogeneous syntax and semantics. Data management of contaminants is complex and challenging due to the high number of information required on sampling and analytical procedures, high heterogeneity in matrix characteristics, but also to the large and increasing number of pollutants. Procedures for quality control on heterogeneous datasets provided by multiple sources are not yet uniform and consolidated. Additional knowledge and reliable long time-series of data are needed to evaluate typical ranges of contaminant concentration. The analysis of a coherent and harmonized regional dataset can provide the basis for a multi-step quality control procedure, which can be further improved as knowledge increases during data validation process.

**Keywords: contaminants, data management, harmonization, Adriatic Sea, Ionian Sea, pollution, assessment, heavy metals**

## INTRODUCTION

The increased human use of the marine and coastal areas may compromise marine ecosystems through several kinds of physical, chemical and biological disturbances and contamination by hazardous substances. In particular, in the Adriatic and Ionian Seas, the overall increase in maritime transport, the increasing coastal urbanization and the foreseen growth in offshore oil and gas extraction pose serious risks of pollution from hazardous substances for several coastal countries (Mosetti et al., 2014). Several relevant and growing economic maritime activities such as coastal and maritime tourism, fishery and aquaculture rely on the preservation of ecosystem services and reduction of pollution. Besides, this region is a hotspot of biodiversity (Coll et al., 2012) and hosts natural protected areas, sites of conservation interest of global importance (National Marine Protected Areas, NATURA 2000 sites) and other areas with different protection regimes according to the IUCN categorization.

Due to the environmental regulations in place in the Mediterranean (MSFD, 2008/56/EC, European Commission, 2008; WFD, 2000/60/EC, European Commission, 2001; IMAP, UNEP/MAP, United Nations, 2016b), there is already a comprehensive coastal and marine monitoring undertaken in the Adriatic and Ionian seas. The ecosystem-based approach and the management at sea basin scale increase the needs of data availability, sharing and comparability.

European Marine Board (2008) highlighted a series of challenges related to marine data that are still valid: data availability, quality assurance and tools for policymaking.

Concerning marine contaminants, in particular, cost-effective measurements are still a challenging issue as *in situ* monitoring and complex analytical procedures are expensive and time-consuming. In this sense, data sharing becomes extremely valuable. However, sampling and analytical procedures may vary from country to country and efforts on standardization and harmonization of sampling and analysis, at least at regional or subregional level, are required to improve considerably the comparability of data. In addition, if data management is based on commonly agreed and standardized approaches, it will facilitate data sharing and access.

The setup of the FAIR - Findable, Accessible, Interoperable and Reusable- principles (Wilkinson, 2016) in ocean data management has contributed to considerably improve the work of the European marine data infrastructures (Tanhua et al., 2019).

Thanks to consolidated European data infrastructures, the accessibility of data has improved. However, quality of available data as well as data comparability are still critical issues. Environmental assessment needs information about protocols applied in the monitoring network of the different countries, to evaluate the comparability of data that are being collected. Without this information, the datasets may be unusable for assessment purposes. There is high heterogeneity in the procedures related to contaminants sampling and laboratory analysis (Berto et al., 2020) and, besides, these aspects require improvement in relation to contaminant data management and storage. Lastly, procedures for quality control of data of marine contaminants need to be agreed and consolidated.

Analysis of a harmonized regional dataset can be a good basis to understand the overall approach, from monitoring/sampling to data quality control aspects on a regional scale. The analysis of a regional case study will allow us to understand the benefits provided by a large data infrastructure that integrates heterogeneous data from multiple sources, but also to identify the specific aspects of data management related to contaminants that need improvement. The experience and knowledge gained with this exercise can lead to the definition of best practices that might be further implemented at a wider scale.

The aim of this study is to evaluate heterogeneity in data of heavy metals collected in seawater, sediment and biota in the Adriatic–Ionian subregions, to verify the comparability of data made available from different sources and to propose guiding principles to improve a harmonized approach of data management.

## BACKGROUND AND RATIONALE

The Adriatic and Ionian Seas are bounded by both EU and non-EU countries, which determines a number of implications in terms of the implementation of the environmental legal framework. The coastal States that share a marine region or subregions are meant to cooperate to ensure coherent management with an ecosystem-based approach.

The existing legal framework has been defined by the EU (Marine Strategy Framework Directive- MSFD-, Water Framework Directive- WFD-, Maritime Spatial Planning Directive- MSP-, etc.). and UNEP/MAP as Regional Sea Convention (Offshore Protocol, land-based sources and Activities Protocol, Protocol on Integrated Coastal Zone Management- ICZM-, etc.). and cover various aspects of environmental protection. However, they overlap to some extent and are not binding on all coastal states, which leads to several issues in their implementation.

The assessment of EU Member States reporting for the first MSFD cycle underlined that the level of coherence in the ADRION marine subregions concerning the implementation of EU environmental policies and MEDPOL program (Programme for the Assessment and Control of Marine Pollution in the Mediterranean) is considered low (Palialexis et al., 2014), particularly in the case of pollution from hazardous substances.

The descriptors 8 and 9 of the MSFD and the Ecological Objective (EO) 9 of the Ecosystem Approach of the UNEP/MAP deal with pollution from contaminants. Namely, heavy metals are a wide group of contaminants that continues to accumulate due to new productive activities. As defined by IUPAC, the term heavy metals "is often used as a group name for metals and semimetals (metalloids) that have been associated

with contamination and potential toxicity or ecotoxicity" (Duffus, 2002). Heavy metals are a natural part of the marine environment whose concentrations have been constantly increasing due to anthropogenic activities (Ansari et al., 2004). Several metals and metalloids are directly linked to sea-based sources of pollution, such as shipping, offshore oil- and gas-industry, mariculture (Tornero and Hanke, 2016, 2018) and are, therefore, included in the guidelines for environmental status assessment by EU and UNEP/MAP directives. Sediment and biota are highly conservative environmental matrices, representative of the state of contamination of the marine environment. Sediments are considered the main sink for heavy metals in aquatic environments, while heavy metals are known to accumulate in marine organisms and even be biomagnified through the trophic web (DeForest et al., 2007; Rainbow and Luoma, 2011). Due to heavy metal toxicity, their persistence and tendency to accumulate into sediment and biota, these two matrices, should be preferred for monitoring and assessment purposes with respect to water. Furthermore, besides chemical investigations, biological tools such as biomarkers and bioassays on selected target species may add information on the bioavailability and possible toxic effects of these contaminants, at the molecular, cellular or physiological level, and can be usefully associated/integrated to chemical approaches. However, heterogeneity in monitoring and analytical protocols may limit data comparability, although the environmental assessment and large geographic scale requires consistency. To improve the comparability of the data, storage of the proper documentation related to monitoring and analytical protocols is fundamental. With this in mind, assessments at regional or subregional seas levels require proper archiving of complete metadata together with data and suitable mechanisms of data discovery and access.

In the last few years, research and monitoring efforts have been strongly influenced by environmental policies implementation. However, besides environmental status assessment, also scientific research on heavy metals needs standard data. Biota interspecific differences, tissue, stage of development (Cenov et al., 2018), geographic location (Perić et al., 2012), grain size classes (Živković, 2010), among others, are variables that influence the accumulation of metals both in biota and sediment (Oros and Gomoiu, 2012). Consequently, diverse scientific approaches would benefit from using a wider range of data accurately documented and acquired.

A shared and agreed approach to data management may assist to discover, obtain and analyze large scale datasets. This might lead to an improvement of the knowledge base in the field of marine pollution.

The use of data infrastructures, that work on the basis of standardized procedures and vocabularies and provide tools for data discovery, can help to handle the heterogeneity of existing data and to promote access to data collected by different institutions. Data structured in a unique way, defined by common and harmonized parameters are the basis for the creation of data collections that are needed to bolster the quality control methodologies for contaminants and to assess pollution coherently in different areas.

# MATERIALS AND METHODS

## Data Infrastructures

The use of large data infrastructures to manage data and required for supplying fragmented marine data offers an enormous advantage when dealing with large scale studies (e.g., basin scale, European scale, global scale) (Benson et al., 2018). They are the link between observations, data management and users and are fundamental to:

- Give access to managers and policymakers to updated data and information for decision making.
- Provide scientists with a framework to integrate individual observations in order to build a strong network of knowledge.

In Europe, the consolidated EU initiative EMODnet (European Marine Observation and Data Network) is an important reference (Martín Míguez et al., 2019) for *in situ* measurements. EMODnet Chemistry, in particular, constitutes the spatial data infrastructure in charge of providing access to marine chemical (eutrophication, ocean acidification, contaminants and marine litter) data (Giorgetti et al., 2018). EMODnet Chemistry relies on SeaDataNet standards, established through a Pan-European infrastructure for ocean and marine data management (Schaap and Maudire, 2009), and adopts FAIR principles to guide the whole data management approach. Interoperability is guaranteed by the use of controlled vocabularies, the utilization of standard metadata and data formats (Vinci et al., 2017), the use of common and transparent quality control procedures and quality flagging schema, all developed in a framework of international cooperation. Particularly, the use of controlled vocabularies represents an important prerequisite to allow consistency and interoperability. Taking into consideration the high heterogeneity in marine chemical data with regard to sampled matrix characteristics, sampling and analytical protocols, a very specific vocabulary (Parameter Usage Vocabulary, P01)[1] was implemented by the British Oceanographic Data Centre (BODC). The P01 vocabulary was initially introduced during the EU/FP5 SeaSearch project and further developed in the framework of SeaDataNet for labeling measured substances and to keep relevant information linked to the data. It allows to label parameters with a standard description and is updated upon data originators needs, as new parameters are made available.

Lastly, the adoption of a standard data policy, consistent with the data providers' policies, regulating data access, allows to appropriately acknowledge data originators and encourages data sharing. All these standards allow data to be reusable, taking advantage of the already invested efforts in monitoring.

Data comparability and interoperability depend not only on sampling and analytical protocols but also on how data and metadata are archived. For data to be usable, the information about what, how, when, where and why must be on hand (Ma et al., 2014; Benson et al., 2018).

[1] https://www.bodc.ac.uk/resources/vocabularies/parameter_codes/

## ADRION Regional Data Collection of Heavy Metals

In order to evaluate the advantages of using large data management infrastructures and the needs of improvements in data management related to contaminants, a data collection of heavy metals available for the Adriatic and Ionian (ADRION) Seas has been analyzed in this study.

The used data collection consisted of all data (restricted and non-restricted) made available in the framework of HarmoNIA project[2] (INTERREG VB-ADRION, 2018–2020) by institutions listed in **Supplementary Table 1**, and unrestricted data available through EMODnet Chemistry infrastructure, covering the Adriatic and Ionian Seas. The ADRION Regional Data Collection, thus, includes over 5500 datasets related to marine contaminants, provided by six neighboring coastal countries of the subregion (Italy, Slovenia, Croatia, Montenegro, Albania and Greece). Specifically, related to heavy metals, there are around 5000 datasets with a temporal coverage spanning from 1981 to 2018.

## Data Management

Datasets are compiled by data originators using standard "Ocean Data View (ODV) format," which contains three types of columns: metadata, primary variable and data. Metadata columns provide information on cruise, station, data originator, bottom depth, project and access policy. The primary variable can be time, in cases of monitoring stations repeated in time, or depth, when data are available as vertical profiles. Metadata and data comply with common vocabularies[3] set up within SeaDataNet infrastructure, which is a fundamental part of the standardization process. Data are accompanied by quality control flags (QF) (according to SeaDataNet quality flag scale) defined by data originators (more details in **Supplementary Material**).

The ADRION Regional Data Collection has been processed and validated with ODV software[4], which is continuously being adapted to fit the needs of management of data from different disciplines. From the original ADRION Regional Data Collection, ODV was used to obtain three data collections, one for each matrix (seawater, sediment, biota). A built-in "harmonization tool," specifically implemented to handle the heterogeneity in measurement units, has been used to convert concentrations to standard units, defined according to recent EU Directives (European Commission, 2013, 2017). The resulting "harmonized and transposed matrix," provided as an optional data output format specific for data of chemical contaminants, was used to explore metadata completeness and data heterogeneity and to perform data Quality Control (QC).

A stepwise and iterative QC approach was adopted to obtain a harmonized validated regional dataset. The applied QC procedure included:

- Harmonization of measurement units and parameter naming.
- Metadata completeness and dataset format control.
- Inspection related to checks for inconsistent measurement units.
- Verification of quality flagging for data and metadata.
- Screening of data ranges to search for clearly impossible values (e.g., different orders of magnitude).

The results of the first validation cycle are reported to data originators who are in charge of revising, correcting encountered issues and, possibly, providing missing metadata needed to make data comparable and fit for further use.

[2]https://harmonia.adrioninterreg.eu

**TABLE 1 |** Example of P01 codes representing Lead concentration in the sediment, present in ADRION Regional Data Collection.

| Chemical substance | P01 code | P01 description |
|---|---|---|
| Lead in the sediment | CONPBS01 | Concentration of lead {Pb CAS 7439-92-1} per unit dry weight of sediment <2000 um |
| | CONPBS02 | Concentration of lead {Pb CAS 7439-92-1} per unit dry weight of sediment <63 um |
| | IC000041 | Concentration of lead {Pb CAS 7439-92-1} per unit dry weight of sediment <500 um |
| | MPBSP012 | Concentration of lead {Pb CAS 7439-92-1} per unit dry weight of sediment |
| | MTSDM004 | Concentration of lead {Pb CAS 7439-92-1} per unit dry weight of sediment <63 um by inductively-coupled plasma mass spectrometry |
| | PBCNAAWF | Concentration of lead {Pb CAS 7439-92-1} per unit dry weight of sediment <63 um by wet sieving, acid digestion and atomic absorption spectroscopy |
| | PBCNICXT | Concentration of lead {Pb CAS 7439-92-1} per unit dry weight of sediment by inductively-coupled plasma mass spectrometry |
| | PBCNPEXT | Concentration of lead {Pb CAS 7439-92-1} per unit dry weight of sediment by acid digestion and inductively-coupled plasma atomic emission spectroscopy |
| | PBCNXTXT | Concentration of lead {Pb CAS 7439-92-1} per unit dry weight of sediment by compression into pellets and X-ray fluorescence |

# RESULTS

Comparing the different countries, data distribution was heterogeneous and there were differences in the number of substances and matrixes monitored by the different countries (**Figure 2**). The geographical data coverage was mainly associated with coastal waters (**Figure 1**).

Only 11 "heavy metals" (As, Cd, Cu, Cr, Fe, Hg, Mn, Ni, Pb, Ag, and Zn) were measured in all three matrices and only three were measured by all countries (Cu, Pb, Zn) (**Figures 2**, **3**), out of a total of 34 metal elements.

## Sediment Collection

The largest part of data were available for the sediment matrix, for the whole Adriatic – Ionian Seas (**Figure 2**). This collection contained 133 different parameters (P01 codes) related to 52 different metal and metalloid compounds, but only Cu, Pb, and Zn were measured by all ADRION countries in this matrix.

[3]https://www.seadatanet.org/Standards/Common-Vocabularies
[4]https://odv.awi.de/

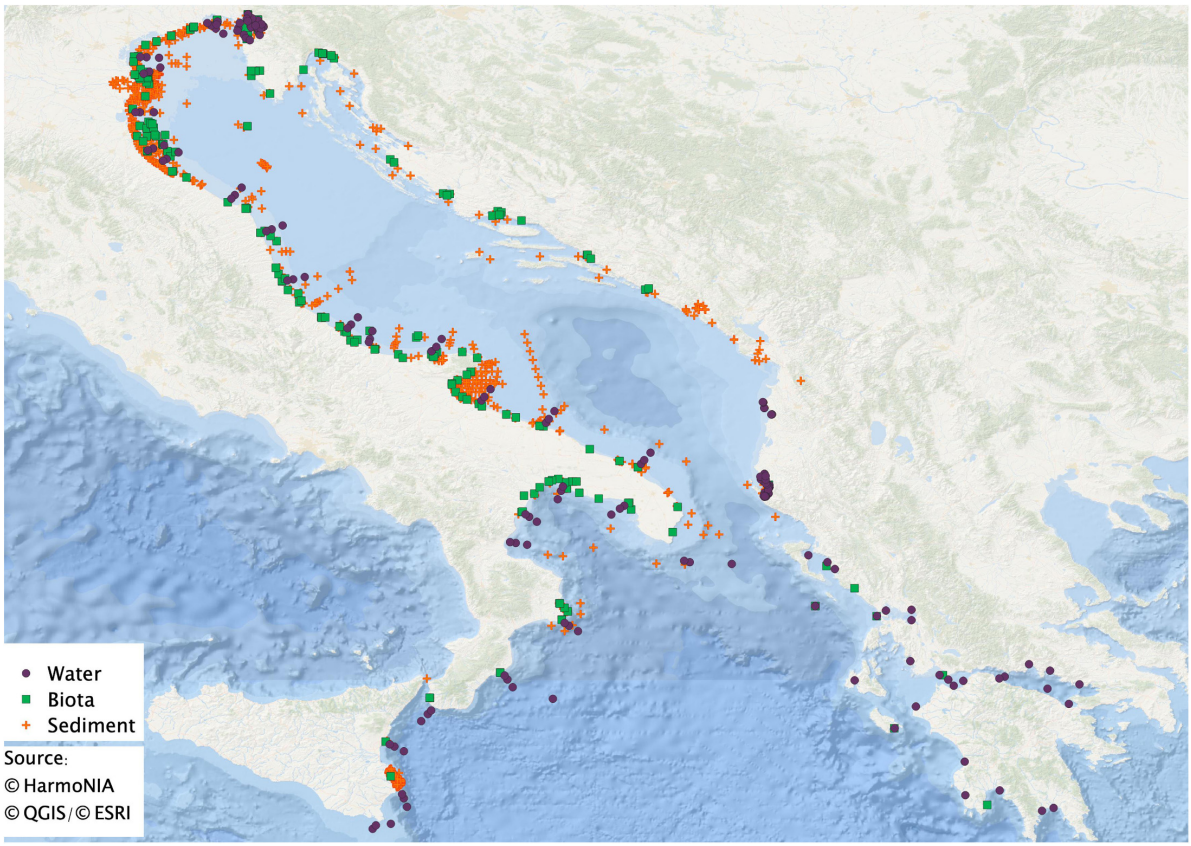


**FIGURE 1 |** Map of sampling stations in the ADRION area. Data are available for water (violet, dots), biota (green, square), and sediment (orange, crosses).

Contaminant concentrations in the sediment were reported on dry weight basis (with the exception of data related to sediment pore waters, which were removed from the sediment-matrix collection) and referred to different sediment grain sizes (total sediment, <2000 μm, <500 μm, and <63 μm).

Within the regional data collection, information related to sampling (sampled sediment depth, instrument and thickness), matrix characteristics (i.e., specific sediment grain size), sample pre-treatment and analytical techniques is not always complete, which limits data comparability and, in the worst case, possibility for use of data. In particular, the lack of specific metadata such as information on sampled thickness, which was directly linked to deposition history, may hinder a solid data comparability.

With regard to contaminant concentration values, after quality control of the regional data collection, around 83% of data are flagged as "good," 3% are below limit of detection or, when provided, below limit of quantification, 11% are flagged as "probably bad" due to values outside ranges reported for the region and 3% still have to be verified by data providers.

## Biota Collection

The data collection related to biota contains 68 parameters, related to 12 heavy metals (Ag, As, Cd, Cu, Cr, Fe, Hg, Mn, Ni, Pb, Se, and Zn). Only four countries provided data on heavy metals in biota and only two substances (Hg and Cd) were common to all four countries (**Figure 3**). Data were related to 8 different species among fishes, mollusks and annelids and were mainly reported on dry weight basis. Information about the analyzed tissue was mostly included, conversely, size class of the organisms was rarely provided. As in the case of sediment, sample pre-treatment and method of analysis details were not always described. After data QC, 4% of data result below the limit of detection or quantification, 90% of the data are flagged as good, while 5% still need to be validated by data originators.

## Water Collection

For water matrix, the data collection contained 57 different parameters associated to 16 metals and metalloids (Ag, Al, As, Ba, Cd, Cr, Co, Cu, Fe, Hg, Mn, Mo, Ni, Pb, V, and Zn). Data on heavy metal concentration in the water matrix were available for four countries and only Cd, Cu, and Hg were measured by all four countries. Heavy metal concentration refers to the water volume and data are mainly related to the dissolved phase, mostly filtered up to 0.4/0.45 um, although a minority of data were related to total, i.e., dissolved plus reactive particulate, or to the particulate phase (>0.4/0.45 um). Availability of correct information on the sampled phase is fundamental to allow comparability of data from several sources. However, indications on sampling depth, sample preparation and analytical methodology are not always complete or even provided. After QC procedure, 23% of data

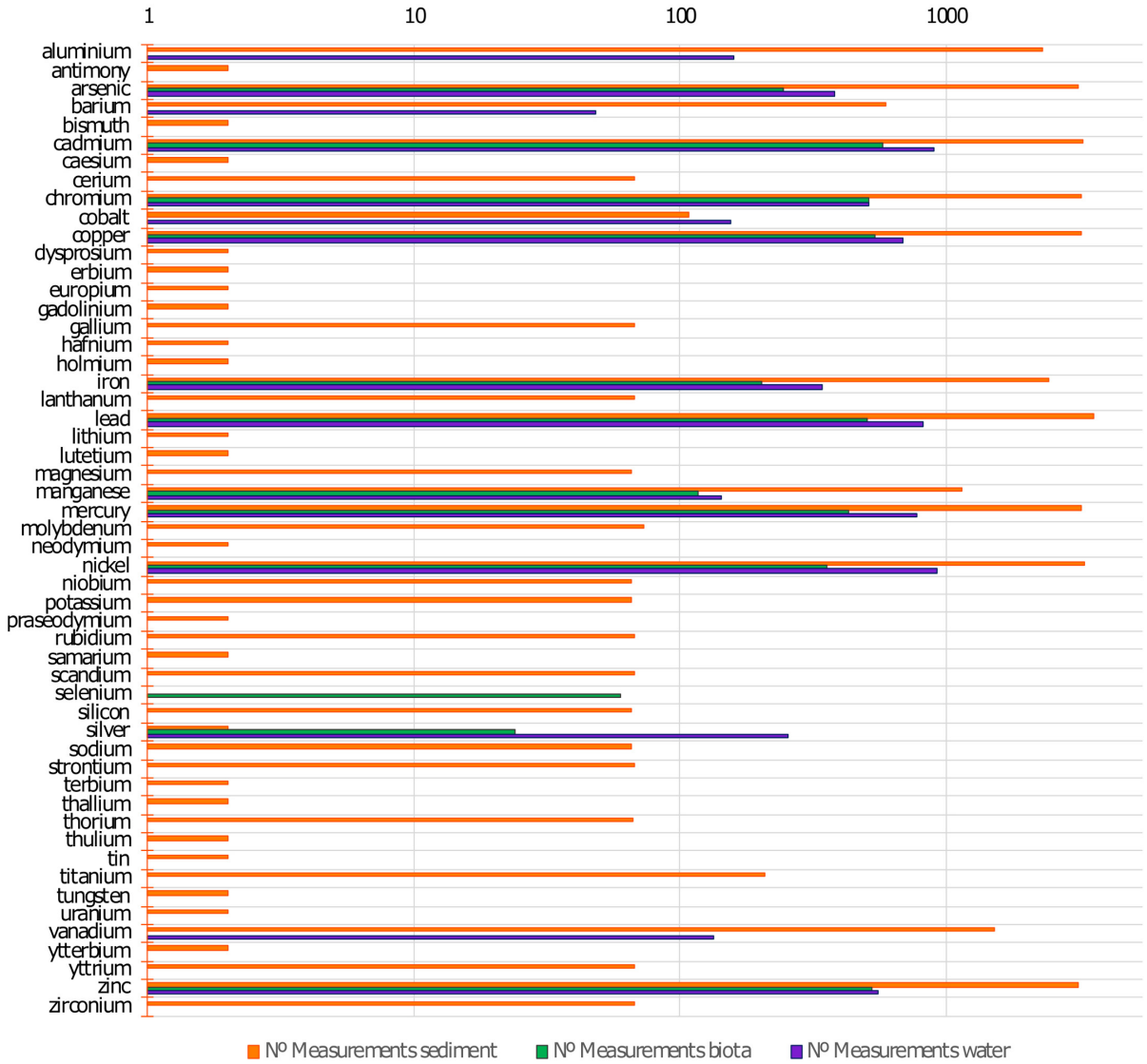


**FIGURE 2 |** Number of data available for heavy metals in sediment (orange), biota (green), and water (violet). Note the logarithmic scale.

were below detection or quantification limit, 9% were labeled as "good" data, while for the 68% of the data the quality control has not yet been finalized as additional verification by the data originators is needed.

## DISCUSSION

Despite the ongoing improvements in observing capability and consequent growing number of data, the availability of frameworks to similarly increase the conversion of data to information, which requires data of known quality, origin, use and attribution conditions, is still a challenge (Buck et al., 2019). Anthropogenic contaminants, in particular, represent high gaps in terms of geographical and temporal data availability (Astiaso Garcia et al., 2019), and data comparability and quality assurance are still limiting environmental status assessment at subregional and regional scale (United Nations, 2017). The ADRION Regional Data Collection represents the largest, harmonized and validated accessible dataset on contaminants, in particular on heavy metals, for the Adriatic-Ionian Seas. Access to marine data of known-quality is a key issue for sustainable economic development and for marine environmental management (European Commission, 2010, 2012; EEA, 2015). By improving monitoring data validation, coherence and accessibility, this product contributes to the need of improved data availability, integration and flows underlined by both scientific community and monitoring authorities (United Nations, 2017; Astiaso Garcia et al., 2019; Painting et al., 2019) and can represent a valuable resource to improve addressing environmental threats and pressures in the ADRION area. The standardization and harmonization of the datasets, produced by different laboratories,

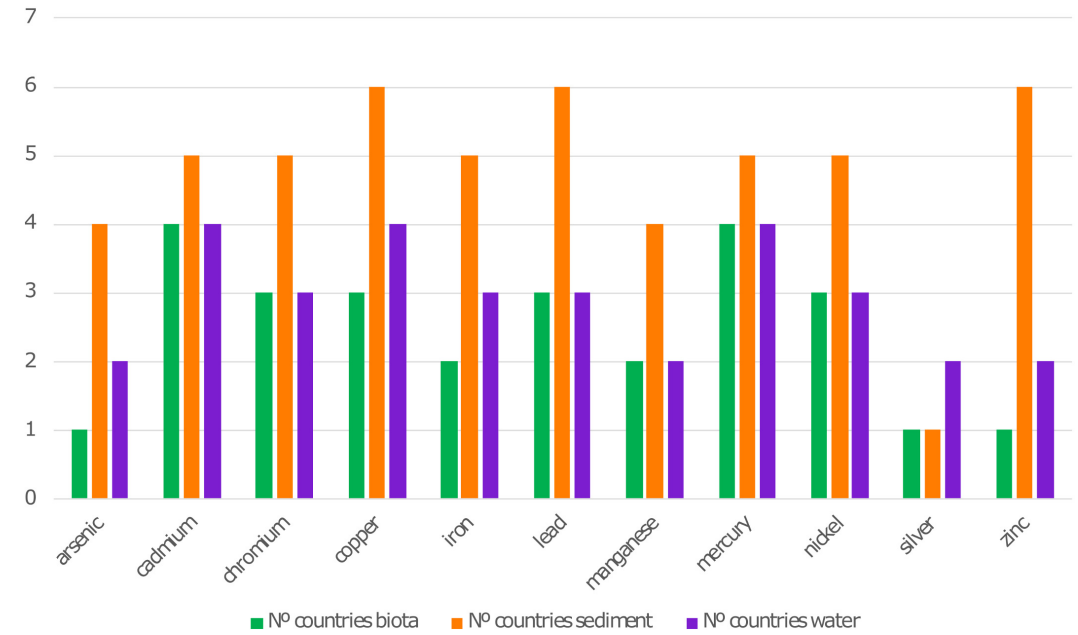


**FIGURE 3 |** Substances monitored in all three matrices and number of countries providing data.

have made it possible to obtain a homogeneous product that shows the high heterogeneity in terms of matrix properties (water phase, sediment grain size, biota taxa, target organs, size of the sampled individuals, etc.) as well as in the measured parameters and analysis protocols. At the same time, the analysis of the harmonized regional data collection allowed to identify several aspects of data management that need to be improved. In particular, the need of more complete and accurate metadata related to the sampling and analysis has been identified as an important field of improvement; the lack of relevant information such as sampling depth, the thickness of sediment samples, sample preparation, analysis methodology or normalization parameters may limit the comparability and usefulness of the data. To address these issues, the establishment of the data Quality Control feedback process (Vinci et al., 2017 and **Supplementary Material**), which is carried out in contact with the data originators, enables to obtain additional relevant metadata and promotes continuous improvement of the data at all times.

The vocabulary (P01), adopted by SeaDataNet, EMODnet Chemistry and HarmoNIA, allows to keep several kinds of information (e.g., matrix characteristics, sampling, analytical protocols, etc.) associated to the measured substance compacted in just one code, thus allowing to maintain relevant metadata connected to the data (IODE/UNESCO, 2019). This approach is fundamental to enable the comparison of the same type of monitoring data where "type" is identified by the whole set of information related to substance, matrix, sampling, etc. (**Supplementary Material**). On the other hand, such approach shows some limitations. In fact, the multiple combinations of the information mentioned above result in a huge list of parameters included in the datasets, which makes the data structure quite complex (**Table 1**). This is particularly striking for data related to biota, including bioassays and biomarkers. For these specific data, several additional parameters (e.g., age, stage of development or size of individuals, protocol details regarding organism exposure or handling, endpoint, etc.) are required to correctly evaluate the contamination status (Bajt et al., 2019). However, their inclusion into P01 expands considerably such vocabulary. The use of standard vocabularies represents an important prerequisite toward consistency and interoperability and assures data comparability (Astiaso Garcia et al., 2019). At the same time, the complexity of specific data types, such as contaminants, may require *ad hoc* adaptations to facilitate data processing by users. To better meet users' needs, specific tools were implemented to manage the complexity of contaminant parameters and allow to decompose the P01 terms on its subcomponents (i.e., matrix type and characteristics, chemical substance, sample treatment and analytical method, etc.). The "decomposition tool," thus, enables to obtain a dataset format suitable to filter data according to the user needs. This "decomposed" dataset format can be particularly useful if contaminant concentrations need to be compared, for example, between different areas but in the same sediment fractions, as required by MSFD and Barcelona Convention Protocols, and can support refining the definition of threshold values (United Nations, 2016a) required for environmental status assessment (United Nations, 2017). This specific dataset format helps to overcome the high complexity and facilitates the processing of highly heterogeneous datasets such as those related to marine contaminants measured by multiple laboratories.

Achievement of a harmonized regional dataset derived from multiple and heterogeneous data sources, thus, requires a step-wise approach consisting in data collection, standardization (same metadata, controlled vocabularies, same dataset formats,

standard Quality Flag scale), harmonization (measurement unit conversion), Quality Control loop engaging data providers, parameter decomposition (P01 subcomponents) and dataset format transposition.

The final product meets the requirements of standardized, validated and interoperable data indicated by scientific and environmental status assessment community.

## CONCLUSION

The use of data infrastructures for data archiving and management provides a standard and harmonized framework to improve access to information supplied by multiple and heterogeneous sources. Harmonized and validated data and information availability (particularly in the field of marine contaminants) are fundamental to support, both, environmental status assessment and scientific research needed to evaluate effects of contaminants on the ecosystem. The analysis focused on the ADRION Regional Data Collection allowed to identify the specific needs of data management related to contaminants and the specific metadata required to enable data comparability and fitness for use.

Data related to contaminants are complex and their management and validation protocols still have to be improved. However, the use of available data is fundamental, considering that *in situ* measurements related to pollution are expensive and difficult to obtain. Further improvements in data and metadata completeness and harmonization are crucial issues to be addressed and developed.

## DATA AVAILABILITY STATEMENT

Publicly available datasets were analyzed in this study. This data can be found here: http://harmonia.maris2.nl/search.

## AUTHOR CONTRIBUTIONS

MM contributed to data and metadata quality control and led the writing. ML developed the idea of the manuscript, participated to the writing, and coordinated the project. MK contributed to data quality control and manuscript revision. EP contributed to metadata preparation and manuscript revision. GG, AR, DI, AI, BČ, MF, AC, and RB contributed with data and to manuscript revision. CG and MV contributed to manuscript revision. All authors contributed to the article and approved the submitted version.

## FUNDING

This work was supported by the project "HarmoNIA (https://harmonia.adrioninterreg.eu/) – ADRION 340 (2018–2020)", funded by the European Regional Development Fund and IPA II fund, in the framework of INTERREG VB Adriatic-Ionian (ADRION) Cooperation Programme. The content of the publication is the sole responsibility of beneficiaries of the project and can under no circumstances be regarded as reflecting the position of the European Union and/or ADRION programme authorities.

## ACKNOWLEDGMENTS

We acknowledge the contribution of the whole HarmoNIA partnership for sharing data and information.

## SUPPLEMENTARY MATERIAL

The Supplementary Material for this article can be found online at: https://www.frontiersin.org/articles/10.3389/fmars.2020.571365/full#supplementary-material

## REFERENCES

Ansari, T. M., Marr, I. L., and Tariq, N. (2004). Heavy metals in marine pollution perspective–a mini review. *J. Appl. Sci.* 4, 1–20. doi: 10.3923/jas.2004.1.20

Astiaso Garcia, D., Amori, M., Giovanardi, F., Piras, G., Groppi, D., Cumo, F., et al. (2019). An identification and a prioritisation of geographic and temporal data gaps of Mediterranean marine databases. *Sci. Total Environ.* 668, 531–546. doi: 10.1016/j.scitotenv.2019.02.417

Bajt, O., Ramšak, A., Milun, V., Andral, B., Romanelli, G., Scarpato, A., et al. (2019). Assessing chemical contamination in the coastal waters of the Adriatic Sea using active mussel biomonitoring with *Mytilus galloprovincialis*. *Mar. Pollut. Bull.* 141, 283–298. doi: 10.1016/j.marpolbul.2019.02.007

Benson, A., Brooks, C. M., Canonico, G., Duffy, E., Muller-Karger, F., Sosik, H. M., et al. (2018). Integrated observations and informatics improve understanding of changing marine ecosystems. *Front. Mar. Sci.* 5:428. doi: 10.3389/fmars.2018.00428

Berto, D., Formalewicz, M., Giorgi, G., Rampazzo, F., Gion, C., Trabucco, B., et al. (2020). Challenges in harmonized assessment of heavy metals in the Adriatic and Ionian seas. *Front. Mar. Sci.* (in press). doi: 10.3389/fmars.2020.00717

Buck, J. J. H., Bainbridge, S. J., Burger, E. F., Kraberg, A. C., Casari, M., Casey, K. S., et al. (2019). Ocean data product integration through innovation-the next level of data interoperability. *Front. Mar. Sci.* 6:32. doi: 10.3389/fmars.2019.00032

Cenov, A., Perić, L., Glad, M., Žurga, P., Lušić, D. V., Traven, L., et al. (2018). A baseline study of the metallothioneins content in digestive gland of the Norway lobster Nephrops norvegicus from Northern Adriatic Sea: body size, season, gender and metal specific variability. *Mar. Pollut. Bull.* 131, 95–105. doi: 10.1016/j.marpolbul.2018.03.002

Coll, M., Piroddi, C., Albouy, C., Ben Rais Lasram, F., Cheung, W. W. L., Christensen, V., et al. (2012). The Mediterranean Sea under siege: spatial overlap between marine biodiversity, cumulative threats and marine reserves. *Glob. Ecol. Biogeogr.* 21, 465–480. doi: 10.1111/j.1466-8238.2011.00697.x

DeForest, D. K., Brix, K. V., and Adams, W. J. (2007). Assessing metal bioaccumulation in aquatic environments: the inverse relationship between bioaccumulation factors, trophic transfer factors and exposure concentration. *Aquat. Toxicol.* 84, 236–246. doi: 10.1016/j.aquatox.2007.02.022

Duffus, J. H. (2002). *"Heavy metals"-A Meaningless term? (IUPAC Technical Report)*. Research Triangle Park: W. A. Temple. doi: 10.1351/pac200274050793

EEA (2015). *State of Europe's Seas*. EEA Report No 2/2015. Copenhagen: EEA.

European Commission (2001). Directive 2000/60/EC of the European Parliament and of the Council of 23 October 2000 establishing a framework for Community action in the field of water policy. *Off. J. Eur. Union* 327, 1–73.

European Commission (2008). Directive 2008/56/EC of the European Parliament and of the Council of 17 June 2008 establishing a framework for community

action in the field of marine environmental policy (Marine Strategy Framework Directive). *Off. J. Eur. Union* 164, 19–40.

European Commission (2010). *Marine knowledge 2020 - Marine Data and Observation for Smart and Sustainable Growth*. Available at: https://op.europa.eu/en/publication-detail/-/publication/008821e5-977d-4c50-8e44-4f099a7fc556 (accessed July 7, 2020).

European Commission (2012). *Marine Knowledge 2020 from Seabed Mapping to Ocean Forecasting. Green Paper*. Available at: https://ec.europa.eu/maritimeaffairs/sites/maritimeaffairs/files/docs/body/marine-knowledge-2020-green-paper_en.pdf (accessed July 7, 2020).

European Commission (2013). Directive 2013/39/EU of the european parliament and of the council of 12 August 2013 amending Directives 2000/60/EC and 2008/105/EC as regards priority substances in the field of water policy. *Off. J. Eur. Union* 226, 1–17.

European Commission (2017). Commission Decision (EU) 2017/ 848 - of 17 May 2017 - laying down criteria and methodological standards on good environmental status of marine waters and specifications and standardised methods for monitoring and assessment. *Off. J. Eur. Union* 125, 43–74.

European Marine Board (2008). "1st Marine Board Forum," in *Marine Data Challenges: from Observation to Information*, eds European Science, and Foundation (Oostende: European Marine Board).

Giorgetti, A., Partescano, E., Barth, A., Buga, L., Gatti, J., Giorgi, G., et al. (2018). EMODnet chemistry spatial data infrastructure for marine observations and related information. *Ocean Coast. Manag.* 166, 9–17. doi: 10.1016/j.ocecoaman.2018.03.016

IODE/UNESCO (2019). *Ocean Data Standards, Volume 4: Technology for SeaDataNet Controlled Vocabularies for describing Marine and Oceanographic Datasets-A joint Proposal by SeaDataNet and ODIP projects*. Paris: UNESCO.

Ma, X., Fox, P., Tilmes, C., Jacobs, K., and Waple, A. (2014). Capturing provenance of global change information. *Nat. Clim. Chang.* 4, 409–413. doi: 10.1038/nclimate2141

Martín Míguez, B., Novellino, A., Vinci, M., Claus, S., Calewaert, J.-B., Vallius, H., et al. (2019). The European marine observation and data network (EMODnet): visions and roles of the gateway to marine data in Europe. *Front. Mar. Sci.* 6:313. doi: 10.3389/fmars.2019.00313

Mosetti, R., Lipizer, M., Scarcella, D., Barbanti, A., Tagliapietra, D., Grati, F., et al. (2014). *ADRIPLAN - Initial Assessment*. Report Number WP 1: Set up of MSP - AIP-1.2-1.1. Sgonico: OGS.

Oros, A., and Gomoiu, M.-T. (2012). A review of metal bioaccumulation levels in the romanian black sea biota during the last decade-a requirement for implementing marine strategy MISIS project view project IRIS-SES integrated regional monitoring implementation strategy in the South European. *Artic. J. Environ. Prot. Ecol.* 13, 1730–1743.

Painting, S. J., Collingridge, K. A., Durand, D., Grémare, A., Créach, V., Arvanitidis, C., et al. (2019). Marine monitoring in Europe: is it adequate to address environmental threats and pressures?. *Ocean Sci. Discuss.* 16, 235–252. doi: 10.5194/os-2019-75

Palialexis, A., Tornero, V., Barbone, E., Gonzalez, D., Hanke, G., Cardoso, A. C., et al. (2014). *In-Depth Assessment of the EU Member States' Submissions for the Marine Strategy Framework Directive under articles 8, 9 and 10*. Brussels: Office of the European Union.

Perić, L., Fafanđel, M., Glad, M., and Bihari, N. (2012). Heavy metals concentration and metallothionein content in resident and caged mussels Mytilus galloprovincialis from Rijeka bay, Croatia. *Fresenius Eironmental Bull.* 9, 2785–2794.

Rainbow, P. S., and Luoma, S. N. (2011). Metal toxicity, uptake and bioaccumulation in aquatic invertebrates-Modelling zinc in crustaceans. *Aquat. Toxicol.* 105, 455–465. doi: 10.1016/j.aquatox.2011.08.001

Schaap, D. M. A., and Maudire, G. (2009). SeaDataNet-Pan-European infrastructure for marine and ocean data management: unified access to distributed data sets. *Geophys. Res. Abstr.* 11, 2009–1487.

Tanhua, T., Pouliquen, S., Hausman, J., O'Brien, K., Bricher, P., de Bruin, T., et al. (2019). Ocean FAIR data services. *Front. Mar. Sci.* 6:440. doi: 10.3389/fmars.2019.00440

Tornero, V., and Hanke, G. (2016). Identification of marine chemical contaminants released from sea-based sources: a review focusing on regulatory aspects. *Eur. Comm. Jt. Res. Cent. JRC* 102452, 1–130. doi: 10.2788/258216

Tornero, V., and Hanke, G. (2018). *Marine Chemical Contaminants-Support to Harmonized MSFD Reporting Substances Considered for MSFD Descriptor 8*. Brussels: Office of the European Union.

United Nations (2016a). *Integrated Monitoring and Assessment Guidance (UNEP(DEPI)/MED IG.22/Inf.7)*. New York, NY: United Nations.

United Nations (2016b). *Integrated Monitoring and Assessment Programme of the Mediterranean Sea and Coast and Related Assessmnt Criteria IMAP*. Available at: www.inforac.org (accessed April 13, 2020).

United Nations (2017). *2017 Mediterranean Quality Status Report*. New York, NY: United Nations.

Vinci, M., Giorgetti, A., and Lipizer, M. (2017). The role of EMODnet chemistry in the European challenge for good environmental status. *Nat. Hazards Earth Syst. Sci.* 17, 197–204. doi: 10.5194/nhess-17-197-2017

Wilkinson, M. D. (2016). The FAIR guiding principles for scientific data management and stewardship. *Sci. Data* 3:160018. doi: 10.1038/sdata.2016.18

Živković, S. (2010). *Organic Pollutants and Metals in Sediment of Bakar Bay and Rječina River*. master's thesis, Ruđer Bošković Institute, Zagreb.

**Conflict of Interest:** The authors declare that the research was conducted in the absence of any commercial or financial relationships that could be construed as a potential conflict of interest.

frontiers in Marine Science

ORIGINAL RESEARCH
published: 23 September 2020
doi: 10.3389/fmars.2020.552893

# Species, Spatial-Temporal Distribution, and Contamination Assessment of Trace Metals in Typical Mariculture Area of North China

*Dawei Pan[1,2,3,4]*, Xiaoyan Ding[1,4], Haitao Han[1,2], Shenghui Zhang[1,2] and Chenchen Wang[1,2]*

*[1] CAS Key Laboratory of Coastal Environmental Processes and Ecological Remediation, Yantai Institute of Coastal Zone Research, Chinese Academy of Sciences, Yantai, China, [2] Shandong Key Laboratory of Coastal Environmental Processes, Research Center for Coastal Environment Engineering Technology of Shandong Province, Yantai Institute of Coastal Zone Research, Chinese Academy of Sciences, Yantai, China, [3] Center for Ocean Mega-Science, Chinese Academy of Sciences, Qingdao, China, [4] University of Chinese Academy of Sciences, Beijing, China*

OPEN ACCESS

**Edited by:**
*Dragana S. Đorđević, University of Belgrade, Serbia*

**Reviewed by:**
*Periyadan K. Krishnakumar, King Fahd University of Petroleum and Minerals, Saudi Arabia*
*Huamao Yuan, Institute of Oceanology (CAS), China*

***Correspondence:**
*Dawei Pan*
*dwpan@yic.ac.cn*

**Specialty section:**
*This article was submitted to Marine Pollution, a section of the journal Frontiers in Marine Science*

**Received:** *17 April 2020*
**Accepted:** *24 August 2020*
**Published:** *23 September 2020*

**Citation:**
*Pan D, Ding X, Han H, Zhang S and Wang C (2020) Species, Spatial-Temporal Distribution, and Contamination Assessment of Trace Metals in Typical Mariculture Area of North China. Front. Mar. Sci. 7:552893. doi: 10.3389/fmars.2020.552893*

The species, spatial-temporal distribution, sources, correlations with physiochemical factors, and the contamination of trace metals (Cu, Pb, Cd, and Zn) were investigated in a typical mariculture area of North China. The concentrations of three species of trace metals, including total dissolved, dissolved reactive, and dissolved inert, were obtained. The total dissolved concentrations of Cu, Pb, Cd, and Zn ranged within 1.75–8.08, 0.43–2.75, 0.07–0.29, and 2.58–30.28 μg/L, respectively. These ranges were measured over 5 months (March, May, July, September, and November) and their concentrations decreased in the following order: Zn > Cu > Pb > Cd. The concentrations of Cu, Pb, Cd, and Zn decreased from nearshore to offshore, showing a distinctly regional variation. All concentrations of trace metals over the whole mariculture area were lower than the grade-II seawater quality standard of China. The relationships between trace metals with micronutrient metal (Fe) and other environmental factors (i.e., temperature, chlorophyll *a*, salinity, dissolved oxygen, and conductivity) were studied in detail. Discharged industrial and aquaculture effluents, uptake by organisms, and atmospheric deposition were found to be possible sources of trace metals in the studied area. Sea current and physicochemical parameters were factors that possibly influenced the spatial-temporal distribution of trace metals.

**Keywords: metal species, spatial-temporal distribution, contamination, trace metals, mariculture**

## INTRODUCTION

Trace metals (TMs) are important micronutrients in marine systems and are essential for the growth of organisms (Morel et al., 2003; Li et al., 2017; Posacka et al., 2017). Whether TMs are essential or toxic mainly depends on their concentrations (Herrero et al., 2014). On the one hand, a number of TMs can be limiting factors to the primary production of an ecosystem if their concentrations are too low (Martin et al., 1994; Maldonado et al., 2006). On the other hand, if their

concentrations exceed a certain threshold, they may become toxic for marine organisms (Sunda et al., 1987; Moffett et al., 1997; Hook and Fisher, 2001; Rivera-Duarte et al., 2005; Dong et al., 2015). Although many TMs can be found at extremely low concentrations in seawater, through biological accumulation, TM concentrations in seafood can be hundreds of times greater than in seawater (Maity et al., 2017). Once excess TM enters the body through the food chain, it will be detrimental for human health.

Marine metal pollution has become the focus of many scholars (Ellwood and Van den Berg, 2000; Fitzwater et al., 2000; Ellwood, 2008; Croot et al., 2011; Zhang et al., 2014; Heller and Croot, 2015). TM pollutants not only gradually deteriorate the seawater quality, but also cause serious pollution of aquatic products. With the continuing industrial development and population growth, human activities release large amounts of TMs into the marine environment, which seriously harms marine ecosystems (Maity et al., 2017). As a result, the determination and analysis of TMs in seawater are urgently needed. In seawater, only dissolved TMs can be directly absorbed and utilized by organisms. These dissolved TMs can be subdivided into total dissolved TMs, dissolved reactive TMs, and dissolved inert TMs. The total dissolved TM concentration is the sum of the dissolved reactive TM and the dissolved inert TM (Han et al., 2018). So far, environmental measurements have only established the total concentration of target metals in samples (Kot and Namieśnik, 2000), which was proved to be inadequate for assessing their bioavailability, behavior, and toxicity (Huang et al., 2003; Adnívia et al., 2016). In the water body, the degree of TM contamination and its effect on both their biological activity and toxicity are directly related to the TM species present. Hence, it is essential to determine the species of TMs in marine environments. In this experiment, the concentrations of total dissolved TM, dissolved reactive TM, and dissolved inert TM were determined by at least three measurements.

There are many techniques for separation and detection of TMs, including gas chromatography (Wang and Cui, 2016), capillary zone electrophoresis (Kubáň and Timerbaev, 2014), supercritical fluid chromatography (Henry and Yonker, 2006), atomic absorption spectrometry (Ribeiro et al., 2017), inductively coupled plasma mass spectrometry (Zhu et al., 2017), and atomic emission spectrometry (Vidal et al., 2016). Among the analytical techniques, electroanalytical techniques are the most universal analytical tool due to the simultaneous quantitative and qualitative determinations of TMs in various matrices with high levels of convenience and rapid and straightforward analytical processes.

Yantai Sishili Bay is a typical mariculture area of North China and is located in Shandong Province. Its area of about 87 $km^2$ include a shallow sea aquaculture area of about 53 $km^2$, and mariculture activities are pursued throughout the year. It is an important breeding ground for fish, shrimp, crab, and shellfish, and mainly cultures seafood for the local area, especially scallops. As Sishili Bay is a semi-closed sea area, its water exchange capacity is poor, cargo throughput increases, and mariculture, industrial, agricultural, and domestic sewage discharges exert great pressure on the marine ecosystem of Sishili Bay (Wang et al., 1995; Tang, 2004; Liu et al., 2009; Zhang et al., 2012). Effluent discharge from the sewage treatment plant of Xinan River and Zhifu Island, aquatic animal feed residues and excrement, as well as domestic waste from workers of aquatic farms all contain a certain level of TMs, which pollute the marine environment of Sishili Bay. Chemical drugs are often used in mariculture to control pests, and the residues of these drugs also cause TM pollution of both the marine environment and the marine ecosystem. For example, $CuSO_4$ is widely used to treat shrimp diseases along the Pearl River Delta, resulting in severe Cu pollution in the aquatic environment of this region (Hu et al., 2007). As a mariculture area, it is very important to investigate the pollution level of seawater, especially the metal levels. Although various studies investigated TMs in seawater (Nimmo et al., 1989; Meng et al., 2008; Mao et al., 2009; Tian et al., 2009; Wang et al., 2012; Su et al., 2015, 2016, 2017; Han et al., 2018), little information is available on the spatial-temporal distributions and species of TMs. However, studying the spatial-temporal distributions and species of TM is helpful to achieve a better understanding of the TM pollution degree in seawater and provides effective data support for aquaculture.

Although Cu, Pb, Cd, and Zn are essential metals for the growth of organisms in marine environments, they are also the main elements that cause marine metal pollution. Once these metal elements occur excess, they cause serious harm to aquatic animals, aquatic plants, and the human body. Excessive Cu and Zn can harm the normal reproduction and growth of aquatic animals and plants, excessive Cu and Pb are teratogenic and carcinogenic, and excessive Cd can lead to kidney damage (Xie et al., 2014). Therefore, the pollutions of Cu, Pb, Cd, and Zn must not be ignored. This study investigated species, spatial-temporal distribution, sources, correlations with physiochemical factors, and contamination of specific TMs (Cu, Pb, Cd, and Zn) in the typical mariculture area of North China. Different species of Cu, Pb, Cd, and Zn were simultaneously analyzed by anodic stripping voltammetry (ASV) with different procedures. The relationships between different species of metals with the micronutrient metal Fe, chlorophyll *a*, salinity, dissolved oxygen (DO), conductivity, pH, and temperature were investigated in detail.

# MATERIALS AND METHODS

## Sample Collection

Samples were collected from the surface seawater of Sishili Bay (Yellow Sea, China, see **Figure 1**), covering 12 stations and 5 months of 2018 (March, May, July, September, and November). Cleaning procedures are strictly followed with GEOTRACES manual when collecting water samples. All seawater samples were collected with a 2.5-L sample collector (Taiheng Plastics Corporation, Henan, China) into individual polypropylene bottles (Xiangyun Plastic Products Factory, Hebei, China). These polypropylene bottles had been cleaned with 1 M HCl (analytical grade) and thoroughly rinsed with deionized water (18.2 MΩ cm specific resistance). Following collection, they were filtered through 0.45-μm cellulose acetate membranes (Shanghai Xingya Purification Material Factory, Shanghai, China) and were stored in polypropylene bottles at 4°C until further analysis. Chlorophyll

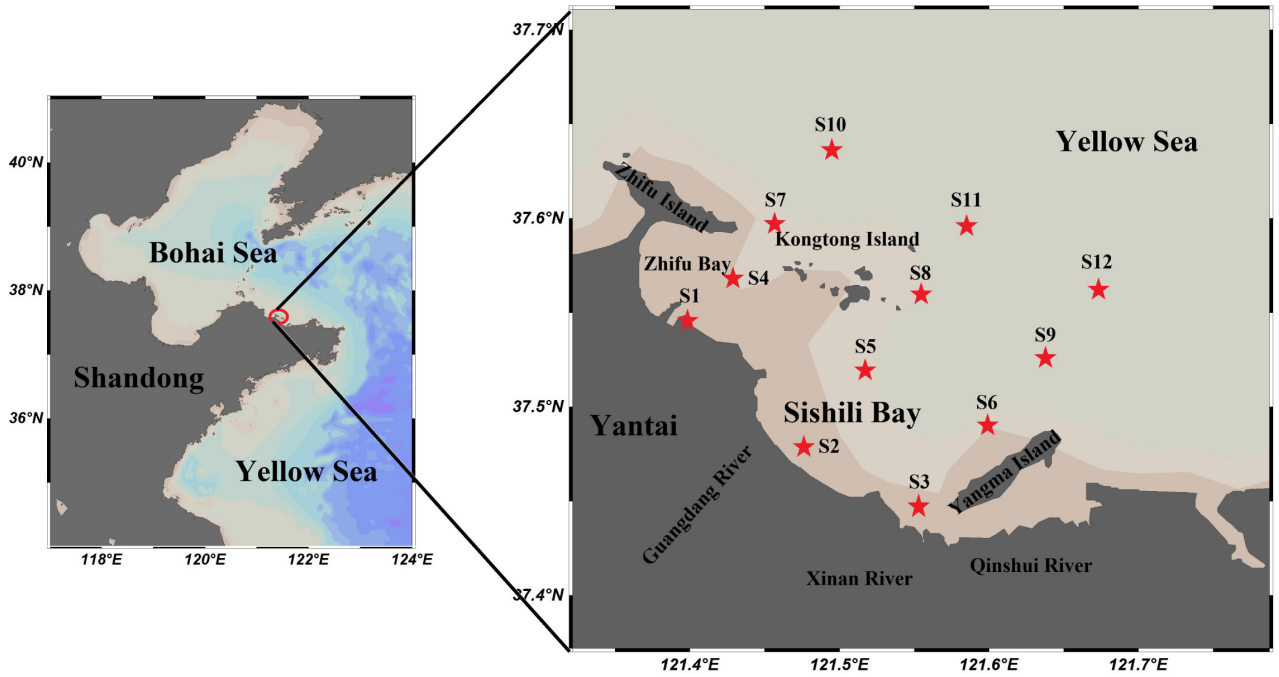


**FIGURE 1 |** Map of the sampling stations in Sishili Bay. The red stars mark the sampling stations.

*a* (Chl *a*) was collected from all seawater samples and stored in 0.45-μm cellulose acetate membranes wrapped with aluminum foil (Xuhuacheng Plastic Co., Ltd., Shanghai, China), and stored at −20°C until use. The temperature, salinity, DO, conductivity, and pH in surface seawater were measured by an YSI MI-parameter Meter (ProPlus, United States).

All containers used in the experiment were soaked in nitric acid ($HNO_3$, 5 wt%, analytical grade) for at least 24 h before use, and rinsed thoroughly with deionized water before starting the experiment. All reagents used were of analytical grade and purchased from Shanghai Sinopharm Chemical Reagent Co., China. All deionized water was sourced from the Pall Cascada's laboratory water system (Port Washington, New York, United States).

## Sampling Stations

The semi-closed Sishili Bay is located on the eastern shore of Yantai city and is one of the most intensive scallop aquaculture areas of North China (Dong et al., 2019). The average water depth is less than 15 m. The quality of the marine environment is not only affected by mariculture, but also by industrial, agricultural, and domestic sewage discharges by local Zhifu and Laishan districts. Studies showed that a large quantity of industrial materials and wastewater are discharged by the Zhifu Island sewage treatment plant every year (Sheng et al., 2012). In this experiment, all sampling stations were located in Sishili Bay within the area from 37°26′49.44″N to 37°38′10.14″N and 121°24′0.00″E to 121°40′27.85″E. The details can be found in **Supplementary Table S1**. The locations of the 12 sampling stations (S1–S12) in this study are shown in **Figure 1**. These were situated in the nearshore areas (S1–S3, where S3 is near the Xinan River sewage treatment plant), port areas (S4 is near Yantai port), mariculture areas (S5, S6, S8, and S9), sewage outfall areas (S7 is near the Zhifu Island sewage treatment plant), and offshore areas (S10–S12). These locations are severely affected by human activities (Li et al., 2013; Dong et al., 2019).

## Determination of Different Species of Cu, Pb, Cd, and Zn

In this study, all voltammetric measurements were carried out using the 797 VA Computrace system with software (version 1.3) from Metrohm (Beijing, China). A three-electrode system was used, consisting of a working electrode, a reference electrode, and a counter electrode. A standard addition method (Illuminati et al., 2010) was adopted for all TM detections.

The concentrations of different species of Cu, Pb, Cd, and Zn in seawater samples were determined by ASV, which imposes detection limits of 28.87, 1.06, 2.97, and 12.70 ng $L^{-1}$, respectively (Han et al., 2018). Seawater samples were pretreated, as shown in **Figure 2**. The filtered samples were transferred to quartz tubes, and then, UV digested for 45 min. When the sample had cooled, 10 mL were transferred into the voltammetric cell and DO was removed with high-purity nitrogen for 5 min. Finally, the total dissolved TM concentration was obtained by ASV (Achterberg and van den Berg, 1994). The UV digestion apparatus was provided by van den Berg's research group (Oceanography Laboratories, University of Liverpool, United Kingdom). Dissolved reactive TM concentrations were obtained via direct electrochemical

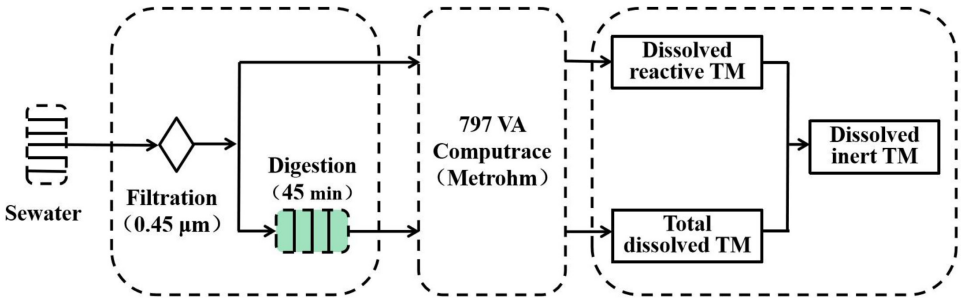


**FIGURE 2 |** Diagram showing the speciation analysis processes for trace metals (TMs).

detection of the filtered samples. Filtered samples (10 mL) were placed into the voltammetric cell and DO was removed with high-purity nitrogen for 5 min; then, the dissolved reactive TM concentration was obtained by ASV (Han et al., 2018). Dissolved inert TMs were obtained via the difference between total dissolved TMs and dissolved reactive TMs (Florence, 1986).

The detailed parameters of the differential pulse voltammetry were as follows: deposition time was 60 s, deposition potential was −1.15 V, initial potential was −1.15, termination potential was 0.02 V, sweep rate of 0.03 $Vs^{-1}$, and the peak positions of Cu, Pb, Cd, and Zn were −0.17, −0.41, −0.58, and −1.0 V, respectively (Han et al., 2018). The accuracy and reliability of the method have been verified in certified reference materials (CASS-6 and NASS-6) (Han et al., 2018).

## Determination of Total Dissolved Fe

Cathode stripping voltammetry (CSV) was used to determine the total dissolved Fe concentration in a 797 VA Computrace system, which imposes a detection limit of 0.84 nM (Lin et al., 2016). Detection details followed were described in Lin et al. (2016). Seawater samples were pretreated, as shown in **Supplementary Figure S1**. First, concentrated nitric acid was added to maintain the pH value of the water sample to less than 2.0, and added $H_2O_2$. Next, NaOH was added to maintain the pH at 8.0 after 90 min of UV digestion. 10 mL seawater samples, 100 μL 1 M HEPPS/0.5 M NaOH (Buffer solution, pH value of the system was about 8.0), 10 μL 0.02 M DHN (Complexing ligand) and 500 μL 0.4 M $KBrO_3$ (Oxidant) were added successively in the voltammetric cell and then remove dissolved oxygen with high-purity nitrogen for 5 min (Lin et al., 2016). The detailed parameters of DPV were as follows: the deposition potential was −0.1 V, deposition time was 60 s, initial potential was −0.1 V, termination potential was −1.1 V, with a sweep rate of 0.024 $Vs^{-1}$ (Lin et al., 2016). The accuracy and reliability of the method have been verified in certified reference materials (CASS-5 and NASS-6) (Lin et al., 2016).

## Determination of Chl *a*

The concentration of Chl *a* was determined by using a Turner Designs Trilogy fluorometer (George et al., 2015). The filter membrane was cut into pieces and extracted with a 90% acetone solution at 4°C for 24 h, then centrifuged at 4000 r speed for 10 min. The supernatant was taken for the concentration determination of Chl *a* (Zhang et al., 2016). The whole process was done in dark light.

## Evaluation of the Trace Metal Contamination Level

In this study, both the contamination factor ($C_f$) and the contamination degree ($C_d$) were used to evaluate the surface seawater quality (Hakanson, 1980; Lü et al., 2015). $C_f$ and $C_d$ reflect the contamination level of a single TM and overall TMs in the medium, respectively (Wang et al., 2018).

$$C_f = \frac{C_c}{C_b} \quad C_d = \sum_{i=1}^{n} C_f$$

where $C_c$ represents the concentration of TM, and $C_b$ represents the background value of corresponding TM in the seawater. The background concentrations used the grade-I seawater quality standard for China (5 μg/L Cu, 1 μg/L Pb, 1 μg/L Cd, and 20 μg/L Zn; GB 3097–1997) (Aqsiq, 1997). $C_f$ and $C_d$ values were interpreted as recommended by Hakanson (1980).

# RESULTS AND DISCUSSION

## Species of TMs

The concentrations of TMs (Cu, Pb, Cd, and Zn) in different species in the surface seawater of Sishili Bay during the five investigated months are listed in **Supplementary Table S2**. The total dissolved Cu, Pb, Cd, and Zn concentrations ranged within 1.75–8.08, 0.43–2.75, 0.07–0.29, and 2.58–30.28 μg/L, respectively. The dissolved reactive Cu, Pb, Cd, and Zn concentrations ranged within 1.05–5.55, 0.15–1.59, 0.04–0.23, and 1.62–20.14 μg/L, respectively. The dissolved inert Cu, Pb, Cd, and Zn concentrations have ranges of 0.22–2.94, 0.02–1.56, 0.01–0.07, and 0.43–16.96 μg/L, respectively. The concentrations of different species of TMs followed (in decreasing order): Zn > Cu > Pb > Cd.

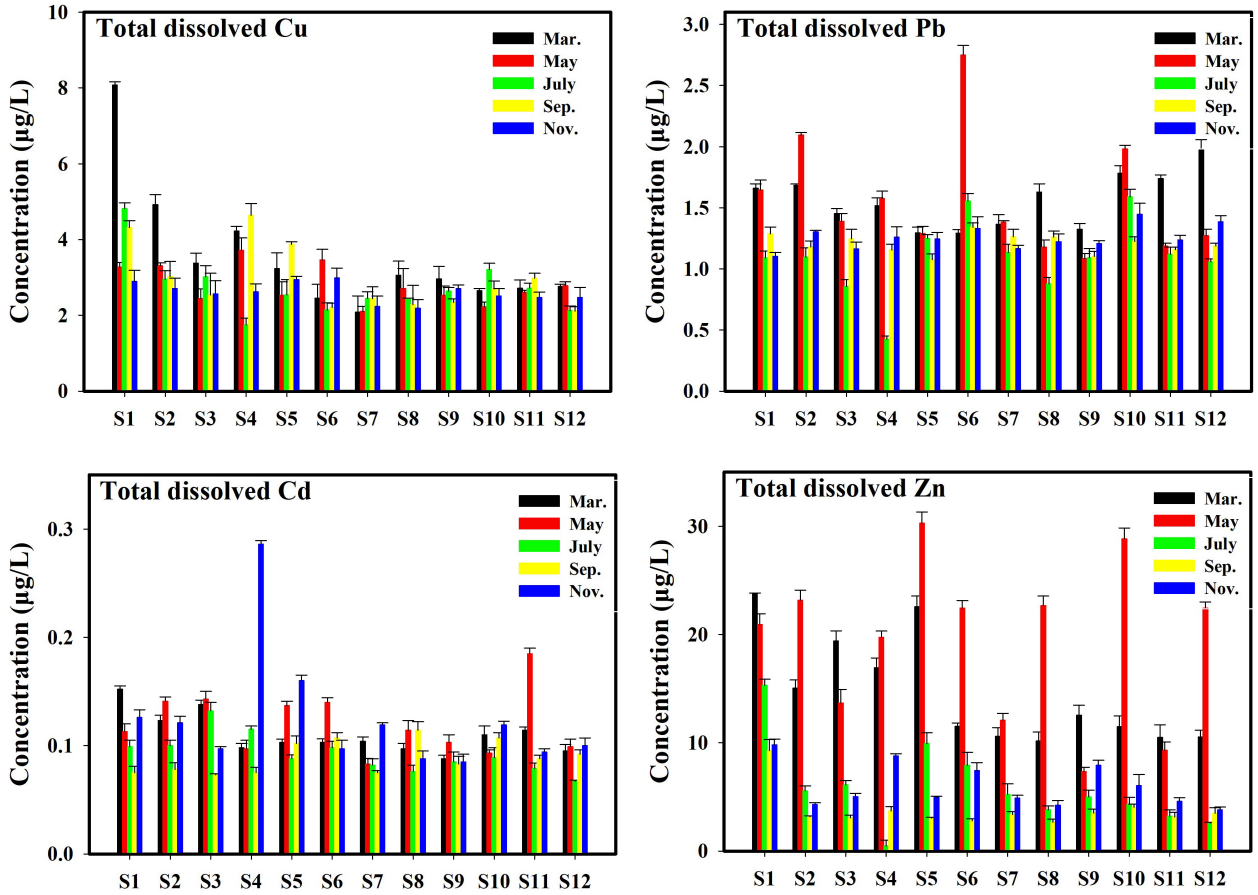


**FIGURE 3 |** Concentrations of total dissolved TMs at all sampling stations in different months.

The concentrations of total dissolved Cu, Pb, Cd, and Zn in all samples for different months are shown in **Figure 3**. The statistical results identified significant differences in TM concentrations for all stations in different months. In March, the highest values of total dissolved Cu, Cd, and Zn were found at station S1, and the highest value of total dissolved Pb was found at station S12. In May, the highest values of total dissolved Cu, Pb, Cd, and Zn were found at stations S4, S6, S11, and S5, respectively. In July, the highest value of total dissolved Cu and Zn was found at station S1, and the highest values of total dissolved Pb and Cd were found at stations S10 and S3, respectively. In September, the highest values of total dissolved Cu, Pb, Cd, and Zn were found at stations S4, S6, S8, and S1, respectively. In November, the highest values of total dissolved Cu, Pb, Cd, and Zn were found at stations S6, S10, S4, and S1, respectively. In summary, the maximum values of dissolved Cu, Pb, Cd, and Zn were 8.08 (station S1 in March), 2.75 (station S6 in May), 0.29 (station S4 in November), and 30.28 μg/L (station S5 in May), respectively.

The annual mean concentrations of total dissolved Cu, Pb, Cd, and Zn in Sishili Bay were compared with those from other marine areas (**Table 1**). The results for all dissolved concentrations of Cu, Pb, Cd, and Zn found values of the same order of magnitude as those reported for Bohai Bay (Meng et al., 2008; Mao et al., 2009), Jinzhou Bay (Wang et al., 2012), the North Yellow Sea (Tian et al., 2009), the San Francisco Bay (Flegal et al., 1991), Boston Harbor (Li et al., 2010), and the Weser estuary (Turner et al., 1992). The concentrations of Cu in Sishili Bay were comparable with those in Bohai Bay, Jinzhou Bay, and the Weser estuary but higher than concentrations in the North Yellow Sea, the San Francisco Bay, and Boston Harbor. The concentrations of Pb in Sishili Bay were higher than in other sea areas, but lower than in Bohai Bay. The concentrations of Cd in Sishili Bay were lower than in Jinzhou Bay but higher than in Boston Harbor and San Francisco Bay. The concentrations of Zn were lower than in Bohai Bay but higher than in the North Yellow Sea, Boston Harbor, and San Francisco Bay.

The annual mean percentages of dissolved reactive and dissolved inert concentrations of Cu, Pb, Cd, and Zn in the total dissolved concentrations are presented in **Figure 4**. The proportions of dissolved reactive TMs are higher, which is consistent with previous observations by Han et al. (2018). The mean percentages of the dissolved reactive concentrations of Cu, Pb, Cd, and Zn were 65.67, 59.92, 72.56, and 64.29%, respectively,

**TABLE 1 |** Comparison of the annual mean concentrations (μg/L) of dissolved Cu, Pb, Cd, and Zn in the seawater of other regions of the world [parentheses present the range of trace metals (TMs)].

| Region | Cu | Pb | Cd | Zn | Reference |
|---|---|---|---|---|---|
| Sishili Bay, China | 2.93 (1.75–8.08) | 1.34 (0.43–2.75) | 0.12 (0.07–0.29) | 5.97 (2.58–30.28) | This work |
| Bohai Bay, China | 2.54 (1.60–4.10) | 7.18 (3.63–12.65) | 0.12 (0.08–0.19) | 26.9 (3.00–55.00) | Meng et al. (2008) |
| Bohai Bay, China | 3.22 | 4.43 | 0.2 | 43.92 | Mao et al. (2009) |
| Jinzhou Bay, China | 3.06 (1.26–6.49) | 0.61 (0.21–1.39) | 0.92 (0.56–2.04) | 11.87 (1.58–25.73) | Wang et al. (2012) |
| North Yellow Sea, China | 0.80 | 0.35 | 0.14 | 3.80 | Tian et al. (2009) |
| San Francisco Bay, United States | 2.16 | 0.03 | 0.07 | 0.65 | Flegal et al. (1991) |
| Boston Harbor, United States | 0.93 (0.51–3.44) | 0.09 (0.04–0.15) | 0.04 (0.01–0.05) | 1.36 (0.37–3.35) | Li et al. (2010) |
| Weser Estuary, Germany | 2.98 | 0.07 | 0.16 | 7.03 | Turner et al. (1992) |

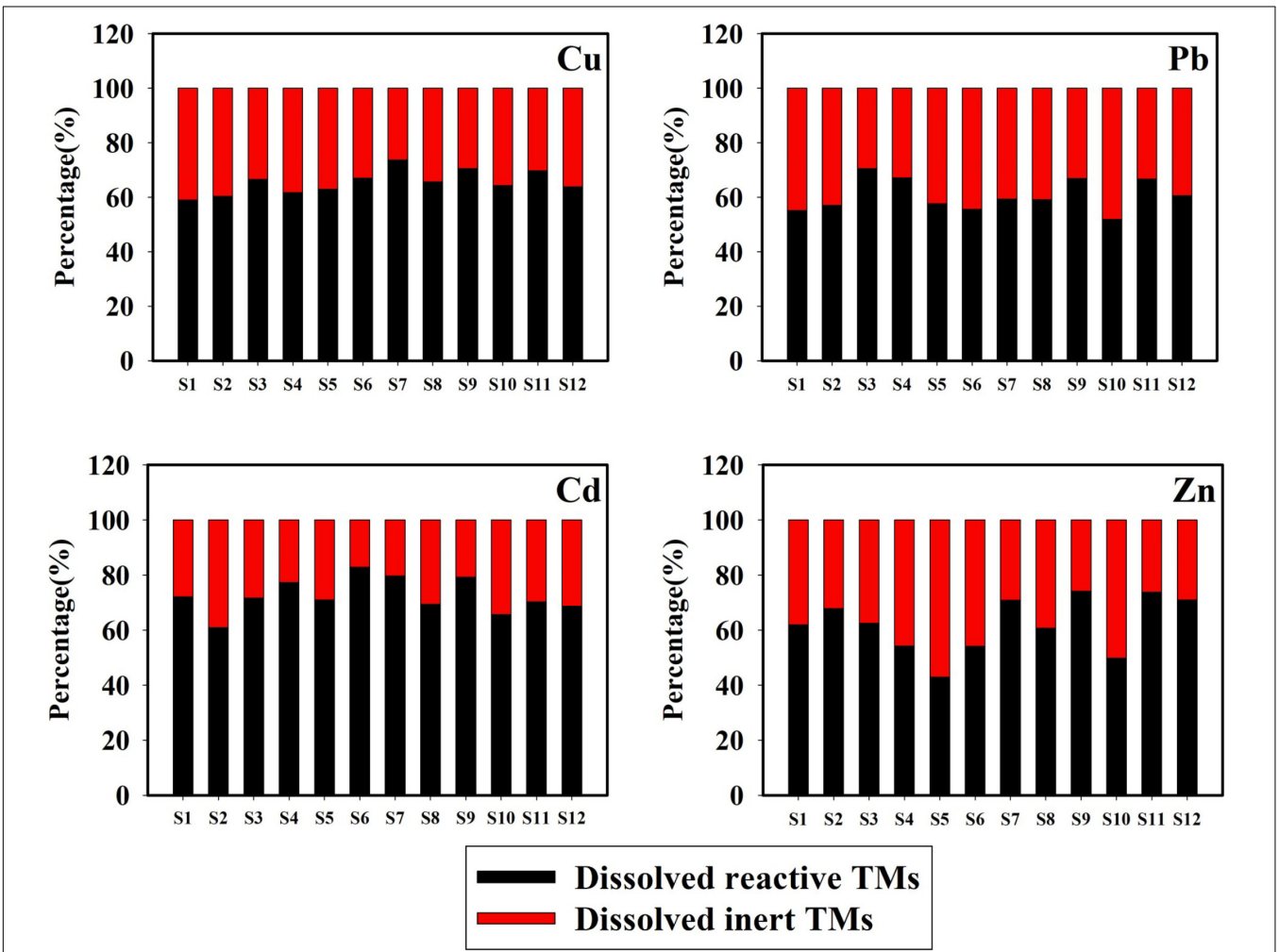


**FIGURE 4 |** Annual mean percentage of the dissolved reactive and inert concentrations of Cu, Pb, Cd, and Zn in surface seawater of Sishili Bay.

following (in decreasing order): Cd > Cu > Zn > Pb. The dissolved reactive TMs (detected by ASV) were classified as free ions, inorganic complexes, and weak organic complexes (Achterberg et al., 2003). Moreover, only free ions, a number of inorganic complexes, and a small number of organic complexes are responsible for the uptake processes by the cells of organisms (Huang et al., 2003). These results indicate that the dissolved reactive TMs had high bioavailability and toxicity for marine organisms. The lowest annual mean percentages of the dissolved reactive Cu, Pb, Cd, and Zn were found at stations S1, S10, S2, and S5, respectively. Considering that the chlorophyll *a* level was the highest at station S1, uptake by phytoplankton could explain the low proportion of the dissolved reactive Cu (Su et al., 2015). The low proportion of the dissolved

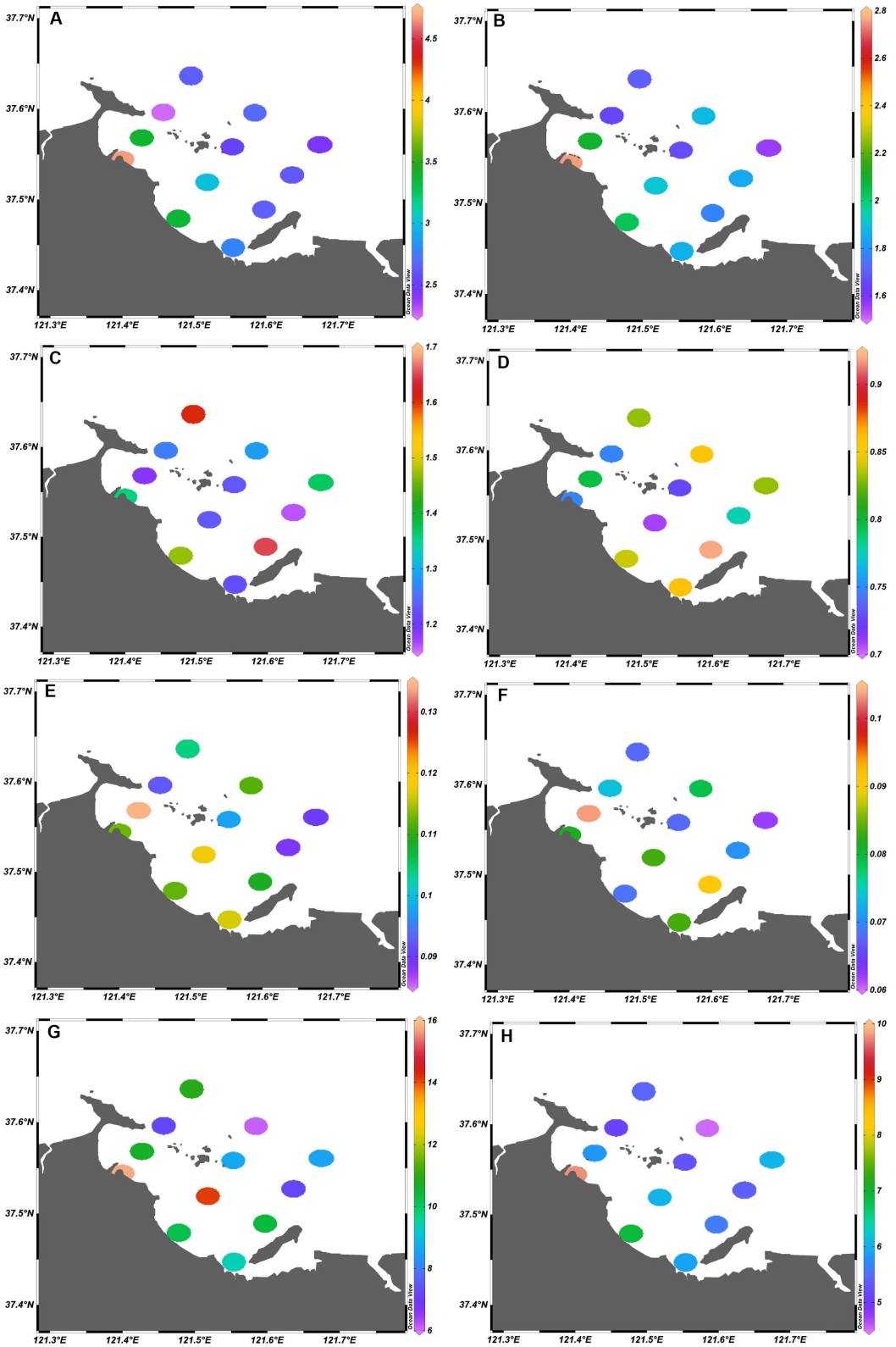


**FIGURE 5 |** Spatial distribution of the concentrations of total dissolved and dissolved reactive TMs (annual average values) in the surface seawater of Sishili Bay. **(A)** Total dissolved Cu (μg/L), **(B)** dissolved reactive Cu (μg/L), **(C)** total dissolved Pb (μg/L), **(D)** dissolved reactive Pb (μg/L), **(E)** total dissolved Cd (μg/L), **(F)** dissolved reactive Cd (μg/L), **(G)** total dissolved Zn (μg/L), and **(H)** dissolved reactive Zn (μg/L).

reactive Pb at station S10 may have been caused by pollutions from the sewage outfall area, influenced by tidal currents that contained a large amount of dissolved inert Pb. At station S2, higher biological activity may have been the cause for the low proportion of dissolved reactive Cd. Station S5 was an intensive scallop mariculture, and uptake from scallops could be an explanation for the low proportion of dissolved reactive Zn (Zhang et al., 2012).

## Spatial-Temporal Distribution Characteristics of TMs

### Spatial Distribution Characteristics and Sources of TMs

The spatial distributions of TMs (annual average values) in the surface seawater of Sishili Bay are presented in **Figure 5**. The spatial distributions of total dissolved Cu, Cd, and Zn were similar, indicating that they might have the same or similar input sources. The concentrations decreased from nearshore to offshore and were higher in the west than in the east. The total dissolved Pb concentrations were also higher at nearshore stations than at offshore stations, but lower in the west than in the east. The spatial distribution patterns of the tested metals implied that they may have been affected by anthropogenic pollution and coastal sources. The highest concentrations of total dissolved Cu and Zn were found at station S1, near nearshore areas, where Zhifu Bay coastal industrial and agricultural activities may cause higher Cu and Zn concentrations. The highest total dissolved Cd concentration was found at station S4, near Yantai port, suggesting vessel traffic and vessel sewage as the main reasons for the high concentration of Cd (Liu et al., 2012; Han et al., 2018). Pb is a atmophile-type metal, and its atmospheric deposition is widely considered to be an important source of Pb in seawater (Stumm and Morgan, 1996; Bruland and Lohan, 2003). Therefore, the higher Pb concentration at offshore stations may have been caused by atmospheric deposition. The highest Pb concentration was found at station S6, near mariculture areas, suggesting that feed residues, chemical drug residues, and household waste from aquaculture workers may contribute to the high levels of Pb. Pb at S10 station was also relatively high, which may have been caused by pollutants from sewage outfall areas, which were carried by oceanic currents (Liu et al., 2012).

Further study showed that the spatial distributions of dissolved reactive TMs and total dissolved TMs were similar (**Figure 5**). The highest concentrations of dissolved reactive Cu, Pb, Cd, and Zn were found at stations S1, S6, S4, and S1, respectively. These results indicated that the factors and sources of dissolved reactive TMs and total dissolved TMs may be similar. At station S2, the concentration of dissolved reactive Cd was low. According to the data results, the percentage of dissolved inert Cd at station S2 was highest (**Figure 4**), which can explain the lower dissolved reactive Cd.

### Temporal Distribution Characteristics

The temporal variation of TMs (monthly average values) in Sishili Bay were significant (as presented in **Figure 6**). The temporal

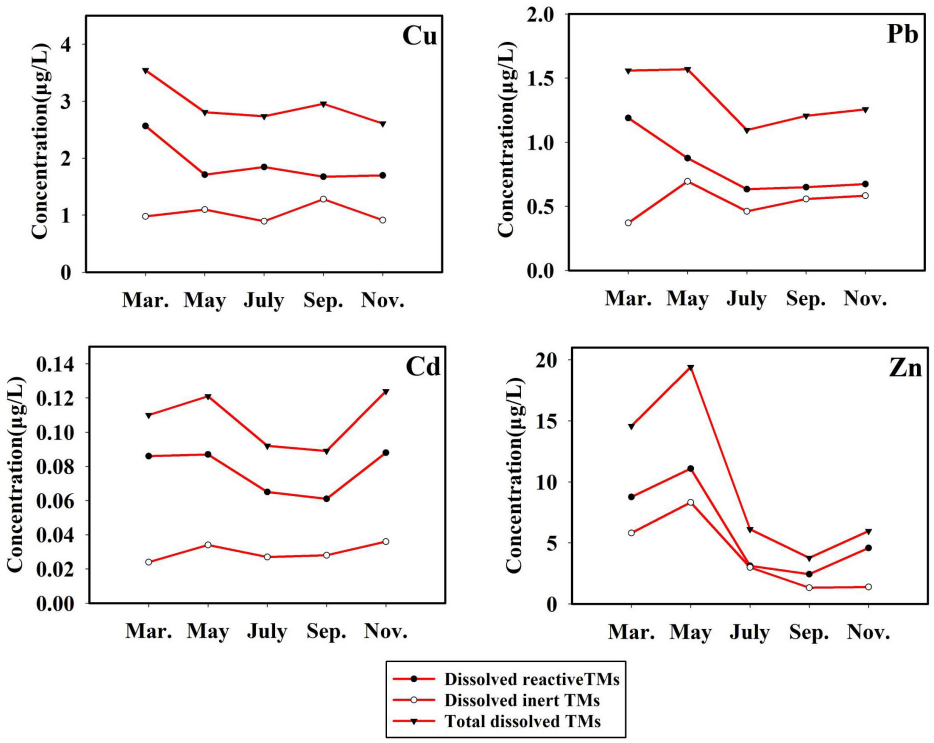


**FIGURE 6 |** Temporal variation of different species of Cu, Pb, Cd, and Zn (μg/L, monthly average values) in the surface seawater of Sishili Bay.

variations of total dissolved TMs and dissolved reactive TMs were similar, indicating that they might have the same or similar input sources. Total dissolved TM and dissolved reactive TM concentrations were highest in March, May, and November, and lowest in July and September. Aquaculture exerts a certain influence on the TM concentration, which adds complexity to the study of TM. The highest values of chlorophyll *a* were found in July, followed by September, which explains the lower concentrations of TMs in July and September (Su et al., 2015). Bioactivity decreased in March, May, and November, which may be a reason for the higher concentrations of TMs.

## Contamination Level of TMs

The total dissolved TM concentrations were assessed according to the seawater quality standards of China (**Table 2**). The concentrations of total dissolved Cd in the present study remained far below the grade-I seawater quality standard of China. In March, May, September, and November, the Pb concentrations in all locations exceeded the grade-I seawater quality of China. However, each TM level in the present study remained lower than the grade-II seawater quality standard of China. The concentrations of total dissolved TMs (annual mean values) of all 5 months were used to calculate $C_f$ and $C_d$ (**Figure 7**). The contamination levels of the total dissolved TMs were assessed according to $C_f$ and $C_d$ value standards (**Table 3**). The $C_f$ values of Cu, Pb, Cd, and Zn ranged within 0.35–1.62, 0.43–2.75, 0.07–0.29, and 0.13–1.51, respectively. $C_f$ values of Cd were all lower than 1, indicating that Cd is at a low contamination level in Sishili Bay. Pb had the highest $C_f$ value, followed by Cu, Zn, and Cd, indicating low to moderate contamination levels. These results indicate that the major contamination pressure in Sishili Bay originates from Pb, Cu, and Zn. $C_d$ values ranged from 1.11 to 4.70, which indicated a low contamination level of Sishili Bay. If the grade-I seawater quality standard is used as background data, contamination levels may rank differently. The actual pollution level might be higher than identified in the present study. In general, TM contamination in the seawater of Sishili Bay is light.

**TABLE 2 |** Rates of total dissolved TMs exceeding seawater quality standards of China among sampling locations.

| Trace metals | Cu | Pb | Cd | Zn |
|---|---|---|---|---|
| March | 8.33% (0%) | 100% (0%) | 0% (0%) | 16.67% (0%) |
| May | 0% (0%) | 100% (0%) | 0% (0%) | 58.33% (0%) |
| July | 0% (0%) | 75% (0%) | 0% (0%) | 0% (0%) |
| September | 0% (0%) | 100% (0%) | 0% (0%) | 0% (0%) |
| November | 0% (0%) | 100% (0%) | 0% (0%) | 0% (0%) |
| Grade-I | 5.00 | 1.00 | 1.00 | 20.00 |
| Grade-II | 10.00 | 5.00 | 5.00 | 50.00 |
| $C_f$ | 0.35–1.62 | 0.43–2.75 | 0.07–0.29 | 0.13–1.51 |
| $C_d$ | 1.11–4.70 | | | |

*Percentages outside of or inside parentheses present the levels of total dissolved TM that exceeded grade-I or grade-II seawater quality standards of China, respectively.*

## Relationship of TMs With Micronutrient Metal (Fe)

Fe is ubiquitous in the natural environment, an essential nutrient for almost all organisms (Kustka et al., 2002), and key to limiting

**TABLE 3 |** $C_f$ and $C_d$ standards (Hakanson, 1980; Lü et al., 2015).

| Contamination level | $C_f$ | $C_d$ |
|---|---|---|
| Low | $C_f < 1$ | $C_d < 5$ |
| Moderate | $1 \leq C_f < 3$ | $5 \leq C_d < 10$ |
| Considerable | $3 \leq C_f < 6$ | $10 \leq C_d < 20$ |
| Very high | $C_f \geq 6$ | $C_d \geq 20$ |

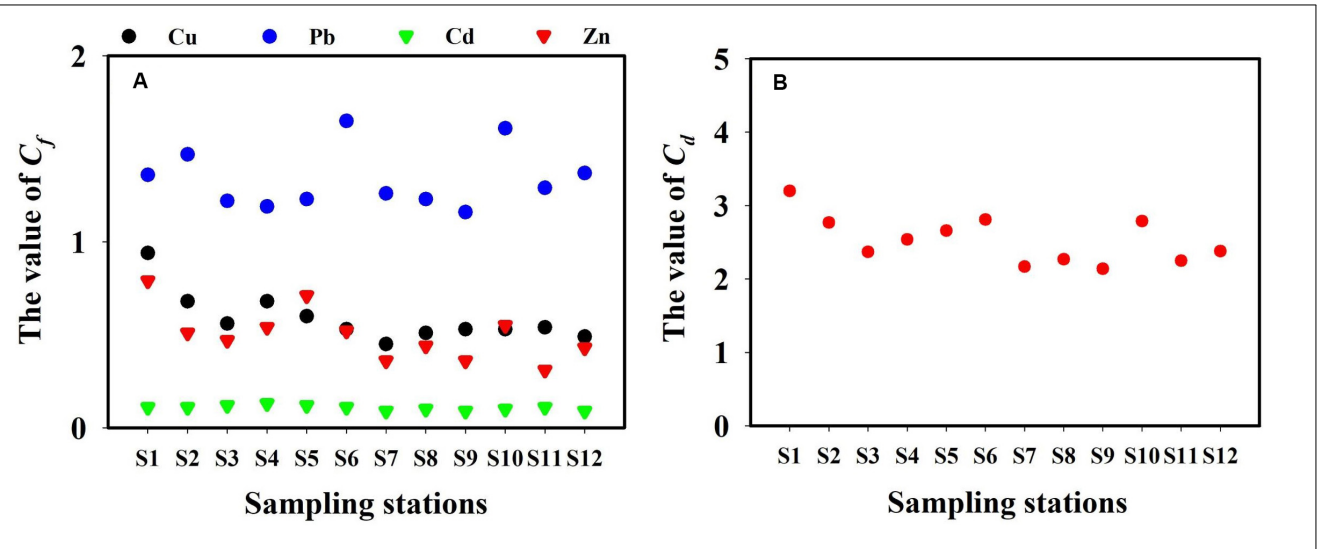


**FIGURE 7 |** $C_f$ and $C_d$ for total dissolved TMs (annual mean concentrations) in the surface seawater of Sishili Bay. **(A)** Value of $C_f$ and **(B)** the value of $C_d$.

phytoplankton growth (Martin et al., 1991). To obtain more valuable experimental data, the total dissolved Fe concentration was determined and the relationship between Fe and TMs was further analyzed. The results showed that Fe concentrations were higher in Sishili Bay than in other areas (Nimmo et al., 1989; Su et al., 2016, 2015, 2017). The spatial distribution of the total dissolved Fe (annual average values) in the surface seawater of Sishili Bay is presented in **Figure 8A**. Unlike total dissolved Cu, Pb, Cd, and Zn, a reverse distribution pattern was found for total dissolved Fe, indicating that the source of Fe might differ from the sources of Cu, Pb, Cd, and Zn. The concentrations were lower at nearshore stations than at offshore stations. The highest concentration of total dissolved Fe was found at station S12. Station S12 was located near offshore areas, where the dry-wet deposition of atmospheric aerosols was the main external source of Fe (Johnson et al., 1994; Yuan et al., 2003). This indicates that atmospheric deposition may be the cause for the higher Fe levels. However, station S12 was close to the aquaculture zone, suggesting that sewage from the aquaculture area carried by ocean currents may be responsible for the higher Fe. The temporal variation of the total dissolved Fe (monthly average values) in Sishili Bay is presented in **Figure 8B**. Significant temporal variations in total dissolved Fe were found. The total dissolved Fe concentrations were highest in March and lowest in May. The variation trends of total dissolved Cu, Pb, Cd, Zn, and Fe are shown in **Figure 8C**. From March to May, the concentration of Fe and Cu decreased obviously, while the concentrations of Pb, Cd, and Zn increased slightly. March to May is when phytoplankton begins to grow, which suggests that during this time, Fe and Cu are more readily absorbed by phytoplankton. Then, Fe and Cu started to increase, but Pb, Cd, and Zn started to decrease and did not start to increase until July. From May to July, phytoplankton began to bloom, which may be the reason why Pb, Cd, and Zn decreased rapidly. From July to September, Cd and Zn still showed a slight decrease. From September to November, only Cu followed a slight decreasing trend. Overall, except for November, Cu presented a similar tendency than Fe.

## Correlations With Physiochemical Factors of TMs

The values of the physiochemical parameters in Sishili Bay during the five investigated months are listed in **Supplementary Table S2**. Water temperature, pH, salinity, DO, conductivity, and chlorophyll *a* ranged within 3.5–25.2°C, 7.78–8.40, 28.89–32.4, 3.92–17.26 mg/L, 45.22–50.89 μS/cm, and 0.02–21.19 μg/L, respectively. The spatial distributions of the physiochemical parameters (annual average values) for Sishili Bay are presented in **Figure 9**. Significant spatial variation was found for chlorophyll *a*. The values decreased from nearshore to offshore stations, and were higher in the west than in the east, which was similar to the previously observed results by Shen et al. (2014). The highest values of temperature, pH, salinity, DO, conductivity, and chlorophyll *a* were found at stations S10, S6, S9, S11, S9, and S1, respectively. The temporal variations of physicochemical parameters (monthly average values) in Sishili Bay are presented in **Figure 10**. The temporal variations of temperature and chlorophyll *a* were similar, and were significantly positively correlated (Yu et al., 2009). Water temperature and chlorophyll *a* values differed significantly among the 5 months, where the highest values were found in July, which was followed by September. The salinity and pH values were ∼31 and 8.1, respectively. DO and conductivity were much higher in March than in the other 4 months.

The Pearson correlation test was used to determine the correlation coefficients among dissolved reactive TM concentrations and physicochemical parameters. The results are shown in **Table 4** (monthly average values). Statistical analysis showed that the concentrations of Cu, Pb, Cd, and

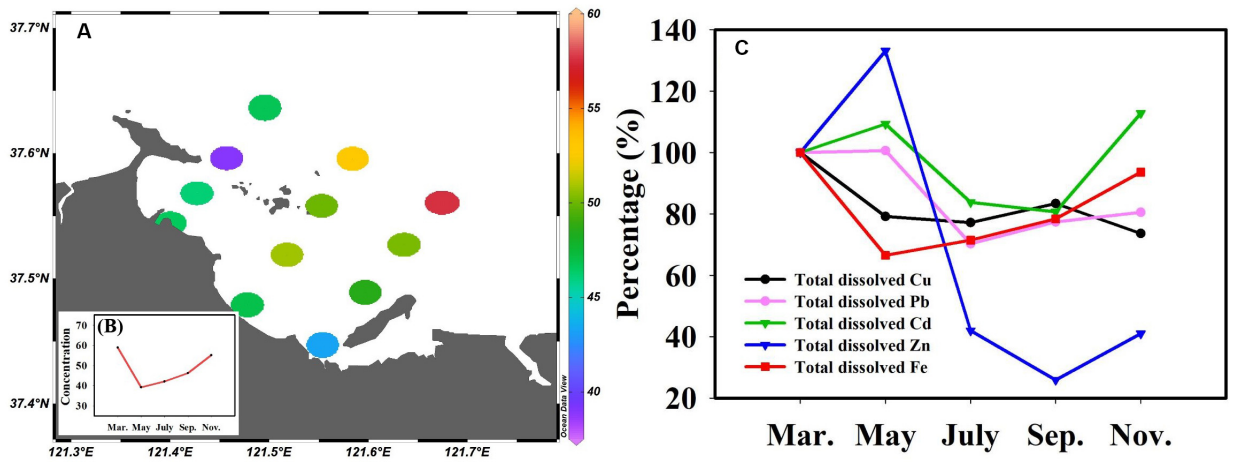


**FIGURE 8 |** Spatial-temporal distribution of total dissolved Fe concentrations in surface seawater of Sishili Bay and the change trend of Cu, Pb, Cd, Zn, and Fe. **(A)** Spatial distribution (nmol/L, annual average values), **(B)** temporal variation (nmol/L, monthly average values). **(C)** Change trend of Cu, Pb, Cd, Zn, and Fe. Percentage values indicate the change trend of the metal concentrations in other months compared with the first months (where the first month's concentration is equal to 100%).

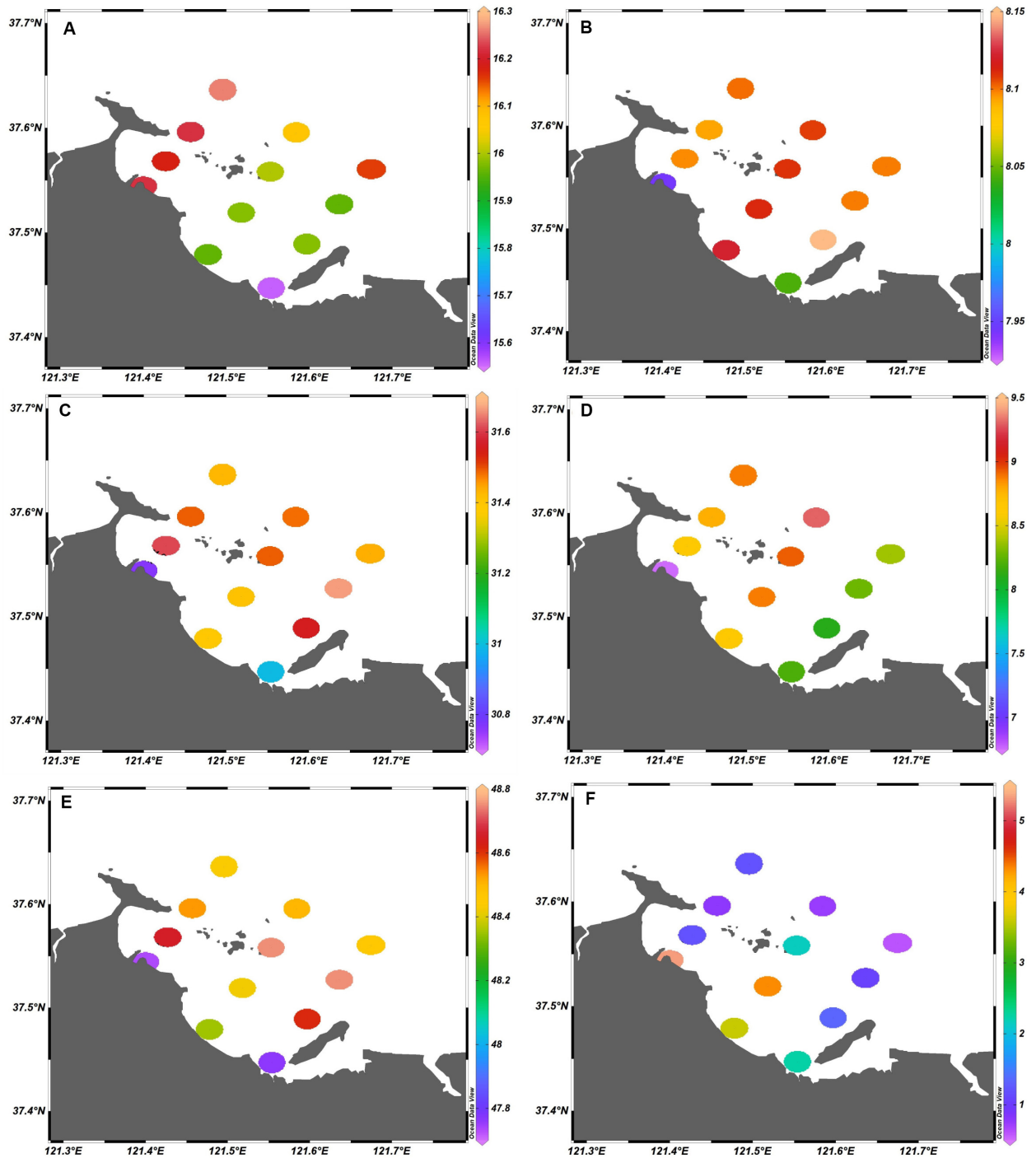


**FIGURE 9 |** Spatial distribution of physicochemical parameters (annual average values) in surface seawater of Sishili Bay. **(A)** Temperature (°C), **(B)** pH, **(C)** salinity, **(D)** dissolved oxygen (DO; mg/L), **(E)** conductivity (μS/cm), and **(F)** chlorophyll *a* (μg/L).

Zn were positively correlated with each other, indicating that these four TMs have certain homology and compound contamination. The concentrations of Cu, Pb, Cd, and Zn were negatively related to temperature and chlorophyll *a*, and positively correlated to salinity, DO, and conductivity. The concentrations of dissolved reactive TMs were significantly positively correlated with salinity, indicating that the existing species of TMs were affected by salinity. This might be because increasing salinity intensifies the adsorption competition between ions, and the electrical properties of

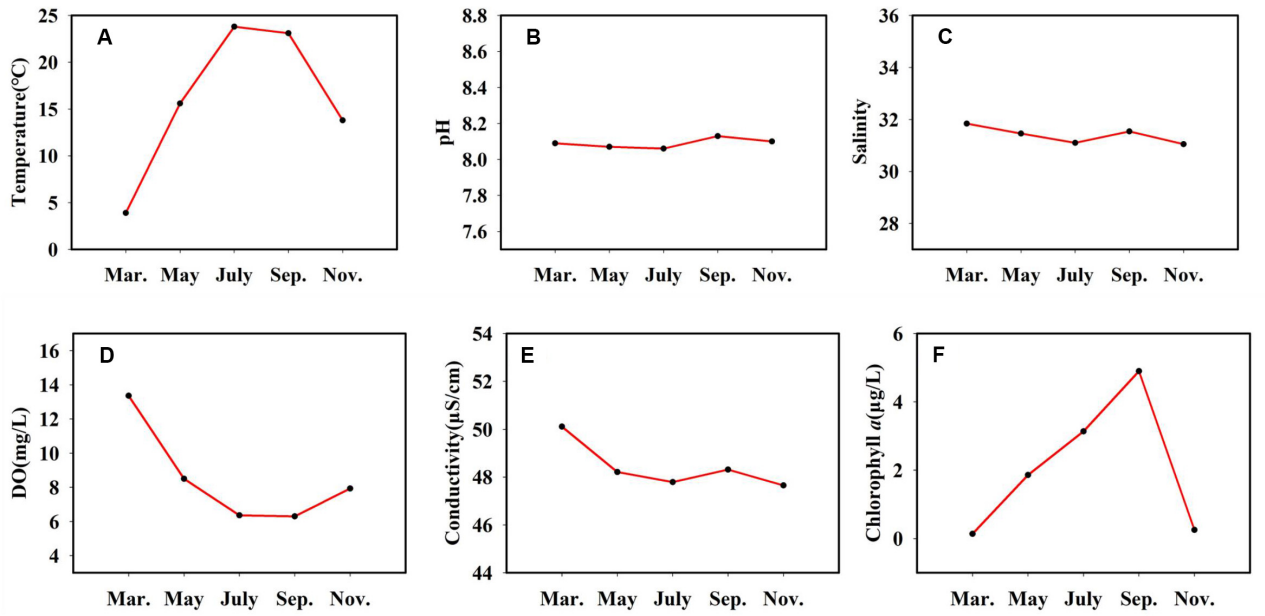


**FIGURE 10 |** Temporal variation of physicochemical parameters (monthly average values) in the surface seawater of Sishili Bay. **(A)** Temperature (°C), **(B)** pH, **(C)** salinity, **(D)** DO (mg/L), **(E)** conductivity (μS/cm), and **(F)** chlorophyll *a* (μg/L).

**TABLE 4 |** Pearson correlation matrix for the monthly average concentrations of dissolved reactive Cu, Pb, Cd, and Zn and the physicochemical parameters in the surface seawater of Sishili Bay.

| | Temperature | pH | Salinity | DO | Conductivity | Chlorophyll *a* | Cu | Pb | Cd | Zn |
|---|---|---|---|---|---|---|---|---|---|---|
| Temperature | 1 | | | | | | | | | |
| pH | 0.041 | 1 | | | | | | | | |
| Salinity | −0.558 | 0.276 | 1 | | | | | | | |
| DO | −0.960** | −0.093 | 0.706 | 1 | | | | | | |
| Conductivity | −0.761 | 0.102 | 0.907* | 0.898* | 1 | | | | | |
| Chlorophyll *a* | 0.856 | 0.304 | −0.057 | −0.725 | −0.353 | 1 | | | | |
| Cu | −0.780 | −0.134 | 0.680 | 0.906* | 0.923* | −0.517 | 1 | | | |
| Pb | −0.892* | −0.147 | 0.804 | 0.971** | 0.922* | −0.600 | 0.876 | 1 | | |
| Cd | −0.809 | −0.257 | 0.124 | 0.651 | 0.276 | −0.919* | 0.318 | 0.587 | 1 | |
| Zn | −0.658 | −0.418 | 0.484 | 0.650 | 0.465 | −0.561 | 0.373 | 0.746 | 0.762 | 1 |

*$p < 0.05$ and **$p < 0.01$.

the adsorbent will also change; this leads to the desorption of TMs and the conversion of numerous granular TMs into dissolved states (Wu, 2012). The concentrations of Cu, Pb, Cd, and Zn were negatively correlated to pH, and the correlation was weak.

## CONCLUSION

The species, spatial-temporal distributions, sources, correlations with physiochemical factors, and the contamination assessments of TMs (Cu, Pb, Cd, and Zn) were investigated in a typical mariculture area of North China. Significant spatial-temporal distributions of TMs were identified. The spatial distribution patterns of these metals implied that they may be affected by anthropogenic pollution, discharged effluent, industrial and aquaculture pollution, uptake by organisms, atmospheric deposition, and other coastal sources. The dissolved reactive TMs and total dissolved TMs have similar spatial-temporal distributions, indicating that they also have similar factors and sources. Significant differences were found in TM concentrations at all stations in different months. The mean percentages of the dissolved reactive concentrations of Cu, Pb, Cd, and Zn were 65.67, 59.92, 72.56, and 64.29%, respectively. These values indicated that the dissolved reactive TMs have high bioavailability and toxicity for marine organisms. All TMs in the surface water were below the grade-II seawater quality standard of China. The single contaminator factors of the elements follow the order: Pb > Cu > Zn > Cd. This showed that the identified contamination degree of the mariculture area was at a low pollution level.

## DATA AVAILABILITY STATEMENT

All datasets presented in this study are included in the article/**Supplementary Material**.

## AUTHOR CONTRIBUTIONS

DP and HH designed the experiments. XD performed the experiments and analyses. SZ and CW helped the data analyses. DP and XD wrote the manuscript. All authors contributed to the article and approved the submitted version.

## FUNDING

This work was financially supported by the National Key R&D Program of China (2019YFD0901103), the Original Innovation Project of Chinese Academy of Sciences (ZDBS-LY-DQC009), and the Key Research and Development Plan of Shandong Province (2017GHY215002).

## SUPPLEMENTARY MATERIAL

The Supplementary Material for this article can be found online at: https://www.frontiersin.org/articles/10.3389/fmars.2020.552893/full#supplementary-material

## REFERENCES

Achterberg, E. P., Herzl, V. M., Braungardt, C. B., and Millward, G. E. (2003). Metal behaviour in an estuary polluted by acid mine drainage: the role of particulate matter. *Environ. Pollut.* 121, 283–292. doi: 10.1016/S0269-7491(02)00216-6

Achterberg, E. P., and van den Berg, C. M. G. (1994). In-line ultraviolet-digestion of natural water samples for trace metal determination using an automated voltammetric system. *Anal. Chim. Acta.* 291, 213–232. doi: 10.1016/0003-2670(94)80017-0

Adnívia, S. C. M., Corinne, P., André, H. R., and José, P. P. (2016). Towards field trace metal speciation using electroanalytical techniques and tangential ultrafiltration. *Talanta* 152, 112–118. doi: 10.1016/j.talanta.2016.01.053

Aqsiq. (1997). *Sea Water Quality Standard (GB 3097-1997). Administration of Quality Supervision, Inspection and Quarantine*. Beijing: Standard Press of China.

Bruland, K. W., and Lohan, M. C. (2003). "Controls of trace metals in seawater," in *Treatise on Geochemistry*, ed. H. Elderfield (Amsterdam: Elsevier), 23–47. doi: 10.1016/B0-08-043751-6/06105-3

Croot, P. L., Baars, O., and Streu, P. (2011). The distribution of dissolved zinc in the Atlantic sector of the Southern Ocean. *Deep Sea Res. II Top. Stud. Oceanogr.* 58, 2707–2719. doi: 10.1016/j.dsr2.2010.10.041

Dong, Y., Rosenbaum, R. K., and Hauschild, M. Z. (2015). Assessment of metal toxicity in marine ecosystems: comparative toxicity potentials for nine cationic metals in coastal seawater. *Environ. Sci. Technol.* 50, 269–278. doi: 10.1021/acs.est.5b01625

Dong, Z. J., Liu, D. Y., Wang, Y. J., and Di, B. P. (2019). Temporal and spatial variations of coastal water quality in Sishili Bay, northern Yellow Sea of China. *Aquat. Ecosyst. Health Mgmt.* 22, 30–39. doi: 10.1080/14634988.2018.1525264

Ellwood, M. J. (2008). Wintertime trace metal (Zn, Cu, Ni, Cd, Pb and Co) and nutrient distributions in the subantarctic zone between 40–52°S; 155–160°E. *Mar. Chem.* 112:107. doi: 10.1016/j.marchem.2008.07.008

Ellwood, M. J., and Van den Berg, C. M. G. (2000). Zinc speciation in the northeastern Atlantic Ocean. *Mar. Chem.* 68, 295–306. doi: 10.1016/S0304-4203(99)00085-7

Fitzwater, S. E., Johnson, K. S., Gordon, R. M., Coale, K. H., and Smith, W. O. (2000). Trace metal concentrations in the ross sea and their relationship with nutrients and phytoplank-ton growth. *Deep Sea Res. II.* 47, 3159–3179. doi: 10.1016/S0967-0645(00)00063-1

Flegal, A. R., Smith, G. J., Gill, G. A., Sanudo-Wilhelmy, S. A., and Anderson, L. C. D. (1991). Dissolved trace element cycles in the San Francisco Bay estuary. *Mar. Chem.* 36, 329–363. doi: 10.1016/S0304-4203(09)90070-6

Florence, T. M. (1986). Electrochemical approaches to trace element speciation in waters. A review. *Analyst* 111, 489–505. doi: 10.1039/AN9861100489

George, J. A., Lonsdale, D. J., Merlo, L. R., and Gobler, C. J. (2015). The interactive roles of temperature, nutrients, and zooplankton grazing in controlling the winter–spring phytoplankton bloom in a temperate, coastal ecosystem, long Island sound. *Limnol. Oceanogr.* 60, 110–126. doi: 10.1002/lno.10020

Hakanson, L. (1980). An ecological risk index for aquatic pollution control. A sedimentological approach. *Water Res.* 14, 975–1001. doi: 10.1016/0043-1354(80)90143-8

Han, H. T., Pan, D. W., Zhang, S. H., Wang, C. C., Hu, X. P., Wang, Y. C., et al. (2018). Simultaneous speciation analysis of trace heavy metals (Cu, Pb, Cd and Zn) in seawater from Sishili Bay, North Yellow Sea, China. *Bull. Environ. Contam. Toxicol.* 101, 486–493. doi: 10.1007/s00128-018-2431-4

Heller, M. I., and Croot, P. L. (2015). Copper speciation and distribution in the Atlantic sector of the Southern Ocean. *Mar. Chem.* 173, 253–268. doi: 10.1016/j.marchem.2014.09.017

Henry, M. C., and Yonker, C. R. (2006). Supercritical fluid chromatography, pressurized liquid extraction, and supercritical fluid extraction. *Anal. Chem.* 78, 3909–3915. doi: 10.1021/ac0605703

Herrero, E., Arancibia, V., and Rojas-Romo, C. (2014). Simultaneous determination of Pb2+, Cd2+ and Zn2+ by adsorptive stripping voltammetry using Clioquinol as a chelating-adsorbent agent. *J. Electroanal. Chem.* 729, 9–14. doi: 10.1016/j.jelechem.2014.06.039

Hook, S. E., and Fisher, N. S. (2001). Sublethal effects of silver in zooplankton: importance of exposure pathways and implications for toxicity testing. *Environ. Toxicol. Chem.* 20, 568–574. doi: 10.1002/etc.5620200316

Hu, W. J., Yang, S. Y., and Zhu, X. M. (2007). The impact of mariculture on the marine ecosystem and studies on bioremediation. *Nat. Sci. S*1, 197–202.

Huang, S., Wang, Z., and Ma, M. (2003). Measuring the bioavailable/toxic concentration of copper in natural water by using anodic stripping voltammetry and *Vibrio qinghaiensis* sp. *Nov. Q*67 bioassay. *Chem. Spec. Bioavailab.* 15, 37–45. doi: 10.3184/095422903782775226

Illuminati, S., Truzzi, C., Annibaldi, A., Migliarini, B., Carnevali, O., and Scarponi, G. (2010). Cadmium bioaccumulation and metallothionein induction in the liver of the Antarctic teleost *Trematomus bernacchii* during an on-site short-term exposure to the metal via seawater. *Toxicol. Environ. Chem.* 92, 617–640. doi: 10.1080/02772240902902349

Johnson, K. S., Coale, K. H., and Elrod, V. A. (1994). Iron Photochemistry in seawater from the equatorial pacific. *Mar. Chem.* 46, 319–334. doi: 10.1016/0304-4203(94)90029-9

Kot, A., and Namieśnik, J. (2000). The role of speciation in analytical chemistry. *Trends Anal. Chem.* 19, 69–79. doi: 10.1016/S0165-9936(99)00195-8

Kubáň, P., and Timerbaev, A. R. (2014). Inorganic analysis using CE: advanced methodologies to face old challenges. *Electrophoresis* 35, 225–233. doi: 10.1002/elps.201300302

Kustka, A., Carpenter, E. J., and Sañudo-Wilhelmy, S. A. (2002). Iron and marine nitrogen fixation: progress and future directions. *Res. Microbiol.* 153, 255–262. doi: 10.1016/S0923-2508(02)01325-6

Li, B. Q., Keesing, J. K., Liu, D. Y., Han, Q. X., Wang, Y. J., Dong, Z. J., et al. (2013). Anthropogenic impacts on hyperbenthos in the coastal waters of Sishili Bay, Yellow Sea. *Chin. J. Oceanol. Limnol* 31, 1257–1267. doi: 10.1007/s00343-013-2173-4

Li, L., Pala, F., Jiang, M., Krahforst, C., and Wallace, G. (2010). Three-dimensional modeling of Cu and Pb distributions in Boston Harbor, Massachusetts and Cape Cod Bays. *Estuar. Coast. Shelf Sci.* 88, 450–463. doi: 10.1016/j.ecss.2010.05.003

Li, L., Wang, X. J., Liu, J. H., and Shi, X. F. (2017). Dissolved trace metal (Cu, Cd, Co, Ni, and Ag) distribution and Cu speciation in the southern Yellow Sea and Bohai Sea, China. *J. Geophys. Res. Oceans.* 122, 1190–1205. doi: 10.1002/2016JC012500

Lin, M. Y., Pan, D. W., Hu, X. P., Zhu, Y., Han, H. T., Li, F., et al. (2016). Speciation analysis of iron in Yantai coastal waters. *J. Environ. Chem* 35, 297–304.

Liu, D., Keesing, J. K., Xing, Q., and Shi, P. (2009). World's largest macroalgal bloom caused by expansion of seaweed aquaculture in China. *Mar. Pollut. Bull.* 58, 888–895. doi: 10.1016/j.marpolbul.2009.01.013

Liu, D. Y., Shi, Y. J., Di, B. P., Sun, Q. L., Wang, Y. J., Dong, Z. J., et al. (2012). The impact of different pollution sources on modern dinoflagellate cysts in Sishili Bay, Yellow Sea, China. *Mar. Micropaleontol.* 84, 1–13. doi: 10.1016/j.marmicro.2011.11.001

Lü, D., Zheng, B., Fang, Y., Shen, G., and Liu, H. (2015). Distribution and pollution assessment of trace metals in seawater and sediment in Laizhou Bay. *Chin. J. Oceanol. Limnol.* 33, 1053–1061. doi: 10.1007/s00343-015-4226-3

Maity, S., Sahu, S. K., and Pandit, G. G. (2017). Determination of traces of Pb, Cu and Cd in seawater around Thane Creek by anodic stripping voltammetry method. *Bull. Environ. Contam. Toxicol.* 98, 534–538. doi: 10.1007/s00128-016-2025-y

Maldonado, M. T., Allen, A. E., Chong, J. S., Lin, K., Leus, D., Karpenko, N., et al. (2006). Copper-dependent iron transport in coastal and oceanic diatoms. *Limnol. Oceanogr.* 51, 1729–1743. doi: 10.4319/lo.2006.51.4.1729

Mao, T. Y., Dai, M. X., Peng, S. T., and Li, G. L. (2009). Temporal-spatial variation trend analysis of heavy metals (Cu, Zn, Pb, Cd, Hg) in Bohai Bay in 10 years. *J. Tianjin Univ.*42, 817–825.

Martin, J. H., Coale, K. H., Johnson, K. S., Fitzwater, S. E., Gordon, R. M., Tanner, S. J., et al. (1994). Testing the iron hypothesis in ecosystems of the equatorial Pacifific-Ocean. *Nature* 371, 123–129. doi: 10.1038/371123a0

Martin, J. H., Gordon, M., and Fitzwater, S. E. (1991). The case for iron. *Limnol. Oceanogr.* 36, 1793–1802. doi: 10.4319/lo.1991.36.8.1793

Meng, W., Qin, Y., Zheng, B., and Zhang, L. (2008). Heavy metal pollution in Tianjin Bohai bay. *China. J. Environ. Sci.* 20, 814–819. doi: 10.1016/S1001-0742(08)62131-2

Moffett, J. W., Brand, L. E., Croot, P. L., and Barbeau, K. A. (1997). Cu speciation and cyanobacterial distribution in harbors subject to anthro pogenic Cu inputs. *Limnol. Oceanogr.* 42, 789–799. doi: 10.4319/lo.1997.42.5.0789

Morel, F. M. M., Milligan, A. J., and Saito, M. A. (2003). "Marine bioinorganic chemistry: The role of trace metals in the oceanic cycles of major nutrients," in *Treatise Geochemistry*, eds H. Elderfield, H. D. Holland, and K. K. Turekian (Cambridge: Elsevier), 113–143. doi: 10.1016/B978-0-08-095975-7.00605-7

Nimmo, M., van den Berg, C. M. G., and Brown, J. (1989). The chemical speciation of dissolved nickel, copper, vanadium and iron in Liverpool Bay, Irish Sea. *Estuar. Coast. Shelf Sci.* 29, 57–74. doi: 10.1016/0272-7714(89)90073-5

Posacka, A. M., Semeniuk, D. M., Whitby, H., van den Berg, C. M. G., Cullen, J. T., Orians, K., et al. (2017). Dissolved copper (dCu) biogeochemical cycling in the subarctic Northeast Pacific and a call for improving methodologies. *Mar. Chem.* 196, 47–61. doi: 10.1016/j.marchem.2017.05.007

Ribeiro, D. R. G., Faccin, H., Molin, T. R. D., de Carvalho, L. M., and Amado, L. L. (2017). Metal and metalloid distribution in different environmental compartments of the middle Xingu river in the Amazon, Brazil. *Sci. Total Environ.* 605, 66–74. doi: 10.1016/j.scitotenv.2017.06.143

Rivera-Duarte, I., Rosen, G., Lapota, D., Chadwick, D. B., Kear-Padilla, L., and Zirino, A. (2005). Copper toxicity to larval stages of three marine invertebrates and copper complexation capacity in San Diego Bay, California. *Environ. Sci. Technol.* 39, 1542–1546. doi: 10.1021/es040545j

Shen, C. Y., Shi, P., and Zhao, H. (2014). Spatial-temporal distribution characteristics of chorophyll a and the controlling facters in the Sishili Bay of Yantai. *Mar. Sci.* 38, 33–38. doi: 10.11759/hykx20130925002

Sheng, Y. Q., Sun, Q. Y., Bottrell, S. H., Mortimer, R. J. G., and Shi, W. J. (2012). Anthropogenic impacts on reduced inorganic sulfur and heavy metals in coastal surface sediments, north Yellow Sea. *Environ. Earth Sci.* 68, 1367–1374. doi: 10.1007/s12665-012-1835-4

Stumm, W., and Morgan, J. J. (1996). *Aquatic Chemistry: Chemical Equilibria and Rates in Natural Waters*. New York, NY: John wiley and Sons Inc, doi: 10.5860/choice.33-6312

Su, H., Yang, R. J., Pižeta, I., Omanović, D., Wang, S., and Li, Y. (2016). Distribution and speciation of dissolved iron in Jiaozhou Bay (Yellow Sea, China). *Front. Mar. Sci.* 3:99. doi: 10.3389/fmars.2016.00099

Su, H., Yang, R. J., Zhang, A. B., and Li, Y. (2015). Dissolved iron distribution and organic complexation in the coastal waters of the East China Sea. *Mar. Chem.* 173, 208–221. doi: 10.1016/j.marchem.2015.03.007

Su, H., Yang, R. J., Zhang, A. B., Li, Y., Qu, S. L., and Wang, X. C. (2017). Characteristics of trace metals and phosphorus in seawaters offshore the Yangtze River. *Mar. Pollut. Bull.* 124, 1020–1032. doi: 10.1016/j.marpolbul.2017.01.022

Sunda, W. G., Tester, P. A., and Huntsman, S. A. (1987). Effects of cupric ion and zinc ion activities on the survival and reproduction of marine copecods. *Mar. Biol.* 94, 203–210. doi: 10.1007/BF00392932

Tang, Q. (2004). *Study on Ecosystem Dynamics in Coastal Ocean. III, Atlas of the Resources and Environment in the East China Sea and the Yellow Sea Ecosystem*. Beijing: Science Press.

Tian, L., Chen, H. T., Du, J. T., and Wang, X. H. (2009). Factors influencing distribution of soluble heavy metals in north yellow sea surface seawaters. *Period. Ocean. Univ. Chin.* 39, 617–621. doi: 10.16441/j.cnki.hdxb.2009.04.011

Turner, A., Millward, G. E., Schuchardt, B., Schirmer, M., and Prange, A. (1992). Trace metal distribution coefficients in the Weser estuary (Germany). *Continent. Shelf Res.* 12, 1277–1292. doi: 10.1016/0278-4343(92)90064-Q

Vidal, L., Silva, S. G., Canals, A., and Nóbrega, J. A. (2016). Tungsten coil atomic emission spectrometry combined with dispersive liquid–liquid microextraction: a synergistic association for chromium determination in water samples. *Talanta* 148, 602–608. doi: 10.1016/j.talanta.2015.04.023

Wang, J., Liu, R. H., Yu, P., Tang, A. K., Xu, L. Q., and Wang, J. Y. (2012). Study on the pollution characteristics of heavy metals in seawater of Jinzhou Bay. *Proc. Environ. Sci.* 13, 1507–1516. doi: 10.1016/j.proenv.2012.01.143

Wang, X. E., Xu, Z. F., and Zhou, X. J. (1995). Animal survey in Yantai inshores. *Chin. J. Ecol.* 14, 6–10. doi: 10.13292/j.1000-4890.1995.0002

Wang, X. Y., Zhao, L. L., Xu, H. Z., and Zhang, X. M. (2018). Spatial and seasonal characteristics of dissolved heavy metals in the surface seawater of the Yellow River Estuary, China. *Mar. Pollut. Bull.* 137, 465–473. doi: 10.1016/j.marpolbul.2018.10.052

Wang, Z. F., and Cui, Z. J. (2016). Determination of arsenic species in solid matrices utilizing supercritical fluid extraction coupled with gas chromatography after derivatization with thioglycolic acidn-butyl ester. *J. Sep. Sci.* 39, 4568–4576. doi: 10.1002/jssc.201600510

Wu, Y. F. (2012). Distribution of heavy metals in the surface water of Luoyuan Bay. *J. Fujian Fish.* 5, 387–391. doi: 10.14012/j.cnki.fjsc.2012.05.005

Xie, W. P., Zhu, X. P., Zheng, G. M., and Ma, L. S. (2014). Residues and health risk assessment of HCHs, DDTs and heavy metals in water and tilapias from fish ponds of guangdong. *Environ. Sci.* 35, 4663–4670. doi: 10.13227/j.hjkx.2014.12.033

Yu, L., Hao, Y. J., and Cai, Y. Y. (2009). Annual variation of nutrient and Chla during HABs' periods in Sishili Bay. *Mar. Environ. Sci.* 5, 558–562.

Yuan, Z., Qi, J. H., and Zhang, M. P. (2003). The origin of iron in seawater and its relationship with phytoplankton. *Trans.Oceanol.Limnol.* 4, 38–48. doi: 10.13984/j.cnki.cn37-1141.2003.04.005

Zhang, G. S., Liu, D. Y., Wu, H. F., Chen, L. L., and Han, Q. X. (2012). Heavy metal contamination in the marine organisms in Yantai coast, northern Yellow Sea of China. *Ecotoxicology* 21, 1726–1733. doi: 10.1007/s10646-012-0958-4

Zhang, H. Y., Lin, M. Y., Zhang, Q., Han, H. T., and Pan, D. W. (2014). Bismuth as internal standard for reliable detection of trace lead at screen-printed electrode. *Asian J. Chem.* 26, 5217–5222. doi: 10.14233/ajchem.2014.16740

Zhang, Y., Wang, Y. J., Wang, Y. Q., and Liu, D. Y. (2016). Spatial distribution and correlation of environmental factors and chlorophyll a concentrations in the Bohai Sea during the summer of 2013. *Mar. Sci. Bull.* 5, 571–578. doi: 10.11840/j.issn.1001-6392.2016.05.011

Zhu, X. C., Zhang, R. F., Liu, S. M., Wu, Y., Jiang, Z. J., and Zhang, J. (2017). Seasonal distribution of dissolved iron in the surface water of Sanggou Bay, a typical aquaculture area in China. *Mar. Chem.* 189, 1–9. doi: 10.1016/j.marchem.2016.12.004

**Conflict of Interest:** The authors declare that the research was conducted in the absence of any commercial or financial relationships that could be construed as a potential conflict of interest.

frontiers in Environmental Science

ORIGINAL RESEARCH
published: 25 September 2020
doi: 10.3389/fenvs.2020.560415

# Ecological Risk Assessment of Heavy Metals in the Soil at a Former Painting Industry Facility

*Milena Radomirović[1], Željko Ćirović[1], Danijela Maksin[2], Tamara Bakić[1], Jelena Lukić[1], Slavka Stanković[3] and Antonije Onjia[3]**

*[1] The Innovation Center of the Faculty of Technology and Metallurgy, University of Belgrade, Belgrade, Serbia, [2] The Vinca Institute of Nuclear Sciences, University of Belgrade, Belgrade, Serbia, [3] Faculty of Technology and Metallurgy, University of Belgrade, Belgrade, Serbia*

OPEN ACCESS

**Edited by:**
*Bernardo Duarte, Center for Marine and Environmental Sciences (MARE), Portugal*

**Reviewed by:**
*Lucienne R. D. Human, South African Environmental Observation Network, South Africa*
*Miguel Caetano, Portuguese Institute of Ocean and Atmosphere (IPMA), Portugal*

***Correspondence:**
*Antonije Onjia*
*onjia@tmf.bg.ac.rs*

**Specialty section:**
*This article was submitted to Toxicology, Pollution and the Environment, a section of the journal Frontiers in Environmental Science*

**Received:** *08 May 2020*
**Accepted:** *04 September 2020*
**Published:** *25 September 2020*

**Citation:**
*Radomirović M, Ćirović Ž, Maksin D, Bakić T, Lukić J, Stanković S and Onjia A (2020) Ecological Risk Assessment of Heavy Metals in the Soil at a Former Painting Industry Facility. Front. Environ. Sci. 8:560415. doi: 10.3389/fenvs.2020.560415*

Soil samples from the site of the former largest paint and varnish factory in ex-Yugoslavia were analyzed for arsenic and eight heavy metals (Pb, Cd, Zn, Cr, Ni, Cu, Fe, and Hg). Several additional soil properties (pH, sulfur, nitrogen, phosphorus, and water content) were also measured. Multivariate analysis showed strong correlations between Pb and Zn; and a moderate correlation between Cu and Ni. There was no correlation between heavy metals and any of the analyzed soil properties parameters. A factor analysis grouped most heavy metals, except Cd, which showed different behavior, and Fe and As, which associated with soil properties. The soil samples were clustered into two distinctive groups. Positive matrix factorization receptor modeling clearly identified Zn and Pb as belonging to the traffic vehicle factor. The second factor dominating arsenic was industrial chemical emissions, while the third factor containing most of the heavy metals was attributed to natural background variation. The last non-metallic factor, dominated by sulfur, was the result of past activities in the paint facility. The average enrichment factor values were for the metals analyzed were: 0.73; 0.71; 2.4; 0.58; 2.3; 0.87; 1.6; and 0.76; for Cr, Cd, Pb, Ni, Zn, Cu, As, and Hg, respectively. Only moderate soil enrichment by Pb and Zn was found. The geoaccumulation index values showed a moderately polluted soil with Pb and Zn, but most contributing to the ecological risk were Cd with 63% and Hg with 19%. These two metals are of major concern in this case study due to their high toxicity, even though they are present at very low concentrations. Generally, a moderate ecological risk was estimated for most soil samples, except for a small number of high-risk samples. Spatial distribution mapped three severely polluted sub-areas. In general, the paint and varnish industry moderately contributes to the contamination of soil. The main ecological risk from metal contamination is not related to the paint technological production process itself, but from other activities at the site that deposit of heavy metals into the soil.

**Keywords: trace elements, enrichment, geoaccumulation, PCA, GIS, PMF**

## INTRODUCTION

Over the last few decades, many industrial plants throughout Central and Eastern Europe have ceased operations, and the land has been converted for other purposes. Many of these facilities were located in an attractive urban area, so the new use of land is often intended for housing, commerce, and city parks. Knowledge of the potential ecological risk of soil pollution is, therefore, of great importance for the management of such a site. Before re-purposing an abandoned industrial site, it should be inspected to determine whether there is any pollution originating from the previous activities. In such cases, the pollutants that are often a problem are heavy metals (Wcisło et al., 2016; Harvey et al., 2017; Khademi et al., 2019). The contamination of industrial soils is predominantly dependent on the type of industrial activity (Liang et al., 2017; Spahić et al., 2019; Li et al., 2020), but, the soil characteristics and other influences, such as urbanization (Xie et al., 2019), traffic (Chen et al., 2020), geographical factors (Dragović et al., 2014), should also be taken into account.

Duga d.o.o. Company, located in Belgrade, the capital of Serbia, was the largest paint and varnish factory in the former Yugoslavia, but it ceased operations a decade ago. There is no possibility or intention to start production at the factory again, therefore, the plant will be dismantled, and the factory site repurposed. It was founded in 1895 and operated for over a century at the same location. At the time of its establishment, the site was located out of town, while today, due to the expansion of the city, this location is part of the wider city center. Accordingly, this location can now be considered both industrial and urban. Recently, numerous studies on heavy metal contamination of urban and industrial soils have been carried out (Khademi et al., 2019; Roy et al., 2019; Xie et al., 2019; Yadav et al., 2019; Adimalla et al., 2020; Chen et al., 2020; Egbueri et al., 2020; Li et al., 2020).

Khademi et al. (2019) demonstrated that concentrations of heavy metals in soils of urban areas are higher than the background values, due to industrial activities; however, industrialization does not appear to significantly affect the level of most soil elements. Heavy metals in soils near factories generally enter the soil from industrial activities (Li et al., 2020), and the type of heavy metal contamination depends on the type of industry. For example, increased concentrations of Fe and Zn have been found in soil samples near a welding factory (Spahić et al., 2019); high levels of Pb contamination have been found in the topsoil around a lead-smelter (Li et al., 2020); soil samples near a tannery contain a high level of Cr (Dheeba and Sampathkumar, 2012); and soil highly polluted by Hg from a chlor-alkali plant has been reported (Relić et al., 2019).

The painting industry can contaminate soil with metals that make up the components of raw materials and the finished products. In addition to the production process, other activities, such as site traffic and mechanical services, can also leach metals into the soil. Jolly et al. (2012) measured the metal content in soil and plants in the vicinity of a paint factory and found that the concentrations of heavy metals in the agricultural soil were only slightly higher than those in unpolluted soil. Inobeme et al. (2014) also found moderate contamination in a number of soil samples collected from the vicinity of an industrial paint site. In this industry, the waste storage area could be contaminated with heavy metals (Yan et al., 2008). Nwajei et al. (2012) reported that metal contamination was not attributed to the activity from a paint factory, but to other anthropogenic factors. However, soil samples from the paint factory showed higher metal concentrations than those samples located a few hundred meters away. Heavy metal contamination may originate from industrial accidents (such as pouring alkali-based colors into the soil, Dobroshi et al., 2019), or via the discharge of wastes containing metal pigments (Udosen et al., 2016).

To accurately explain the relationship between the heavy metals in soil in large and complex experimental datasets, it is necessary to reduce dimensionality and classify the data. Multivariate methods of the data evaluation, such as principal component analysis (PCA) and hierarchical cluster analysis (HCA), have been extensively used to identify and apportion the sources of heavy metal contamination (Slavković et al., 2004; Relić et al., 2019; Egbueri et al., 2020). This allows for pattern recognition, and classification of the experimental data on analytes, as well as the samples. Data processed in this way, together with the knowledge of the tracer analytes, may be used to estimate potential contamination sources.

Positive matrix factorization (PMF) is a source apportionment method capable of dealing with missing data, error estimate, and the contribution rate of each source at each sampling site (Paatero and Tapper, 1994). This method is widely used nowadays (Cheng et al., 2020; Jiang et al., 2020; Jin and Lv, 2020; Li et al., 2020) and pinpoints soil metal sources, based on their composition fingerprints. The PMF approach is based on the chemical mass balance equations, using a factor analysis (FA) method with a weighted least-squares algorithm, and non-negative constraints on the factors. The uncertainties for individual data results (U) may be estimated using the following equation (Liang et al., 2017; Cheng et al., 2020; Jin and Lv, 2020):

$$U = \sqrt{(error\,fraction \times c)^2 + (0.5 \times \mathrm{MDL})^2} \qquad (1)$$

where $c$ is the concentration of individual metal, MDL is the method detection limit, and error fraction is a percentage of the measurement uncertainty. If samples are below the MDL, the $U$ value is estimated as 5/6 of the MDL.

A visualization of the spatial distribution of the trace metal contamination over the studied area is helpful in contamination tracking. By using geostatistical interpolation it is possible to get information, even for an area that is not sampled. Spatial visualization has been used extensively in risk assessment studies of heavy metals in soils (Dragović et al., 2014; Škrbić et al., 2018; Zhao et al., 2019; Cheng et al., 2020; Jiang et al., 2020; Jin and Lv, 2020).

Of the utmost importance in evaluating the site and deciding how to approach soil management is quantifying the ecological risk of soil pollution. Using soil pollution indices, such as enrichment factor (EF), geoaccumulation index ($I_{geo}$) and pollution load index (PLI), gives information on the soil quality, and the degree of contamination for each sample, based on individual metals (Müller, 1969; Tomlinson et al., 1980;

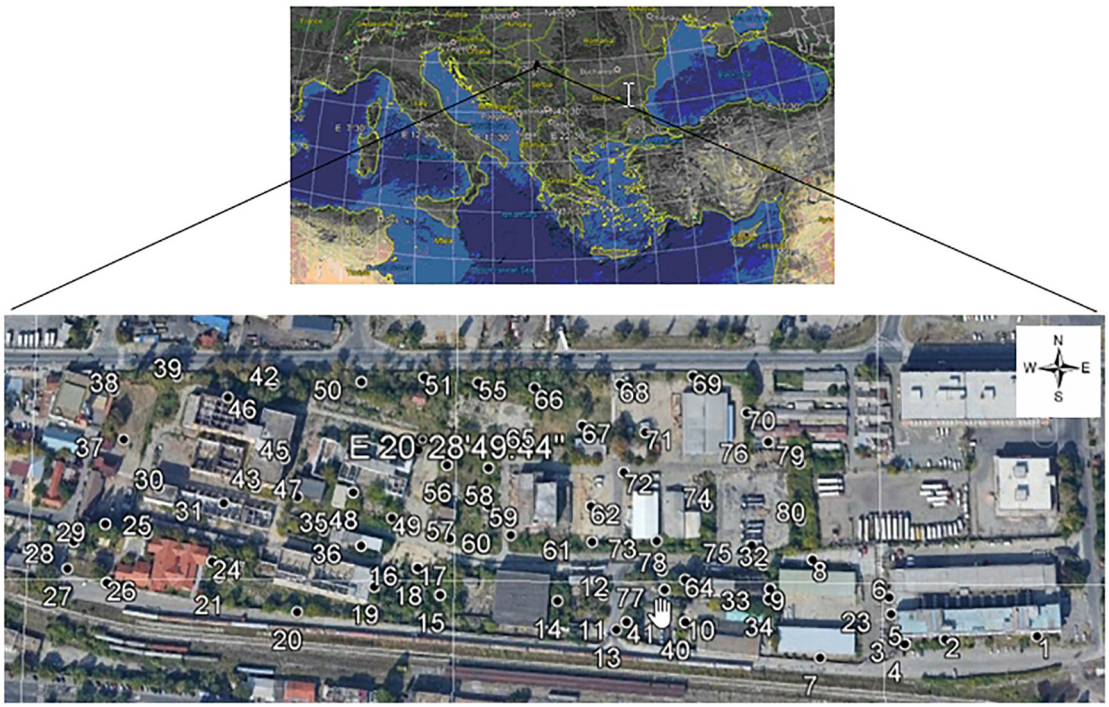


**FIGURE 1 |** Map of the study area and distribution of sampling points.

Men et al., 2018; Khademi et al., 2019; Adimalla et al., 2020; Egbueri et al., 2020; Monged et al., 2020). The potential ecological risk can be estimated based on the risk index (RI) for each sample. Also, the risks from individual metals, which contribute to the ecological risk, can be identified (Men et al., 2018; Gan et al., 2019; Li et al., 2020; Monged et al., 2020).

The main objectives of this study are to evaluate the heavy metal contamination in the soil; characterize the distribution of heavy metals, by combining multivariate analysis and geostatistical mapping; identify potential pollution sources using a PMF model; and estimate potential ecological risks in the area.

## MATERIALS AND METHODS

### Study Area and Sampling

Sampling took place at the Duga paint and varnish factory in Belgrade between December 29, 2009 and January 20, 2010. Eighty surface soil samples (up to 30 cm depth) were collected and analyzed using a soil core sampler. The facility site occupies approximately 11 ha; sampling points (**Figure 1**) were first evenly distributed, and then additional points were selected when there was a suspicion of spillage of contaminants into the soil. The longitude and latitude coordinates of the sampling points were recorded on a Trimble TDC100 GPS instrument. The sampling area was between latitude 44°49′10.399″–44°49′16.464″ and longitude 20°28′37.693″–20°29′6.97″.

Some sampling points were inside the buildings, or on areas covered by asphalt or concrete paving. To reach the soil, a core-drilling machine was used to make a hole, prior to sampling. Five subsamples were collected to make a composite soil sample (about 1 kg). After removing stones and other debris, this composite sample was divided into two to make duplicates. All samples were put into plastic jars and transported to the laboratory in a few hours.

### Sample Preparation and Measurement

Soil samples were air-dried, pulverized, and passed through a 2 mm sieve, followed by pseudo-total microwave-assisted digestion using a CEM Mars 5 oven (CEM Corporation, Matthews, NC, United States Each sample (0.5 g) was digested in acid, using a 10 mL mixture of concentrated $HNO_3$, HCl, and $H_2O_2$ (7÷2÷1). The amount of $H_2O_2$ was added slowly to prevent excessive bubbling within the tube. The microwave oven was set to the following program: ramp time 10 min and hold time 10 min, at 175°C. After digestion, sample solutions were cooled, diluted (10-fold), and filtered through a Whatman No. 41 filter. Samples were stored in 50 mL acid-washed polyethylene autosampler tubes at 4°C until analysis.

Metal concentrations (Cr, Cd, Pb, Ni, Zn, Cu, Fe) were measured by a flame atomic absorption spectrometer (AAS; Analyst 100, Perkin Elmer Inc., Waltham, MA, United States) equipped with the appropriate hollow-cathode or electrodeless discharge lamps. Deuterium background correction was used throughout. Hydride generation/cold vapor accessory was used

to determine As and Hg concentrations (MHS-15, Perkin-Elmer Inc.). Reducing solutions of $NaBH_4$ and $SnCl_2$ were used in the accessory to generate a gaseous form of As and Hg, respectively. Working standard solutions of each heavy metal were made by dilution of stock solutions (1000 mg/L; Merck KGaA, Darmstadt, Germany).

A gravimetric method was used to measure the soil water content. The difference in the mass of soil before and after drying to a constant mass at 105 ± 5°C was used to estimate the water content on a mass basis.

A Thermo Orion model 3 star pH-meter was used for the pH-value measurement. Soil pH was measured using a glass electrode in a 1:5 (v/v) suspension of soil in water. The measurement of the pH in the suspension was made at 20 ± 2°C whilst being stirred to achieve a reasonably homogeneous suspension of soil particles avoiding entrainment of air bubbles.

The content of phosphorus, which is soluble in $NaHCO_3$ solution, was determined by adding a 0.5 mol/L $NaHCO_3$ solution to the soil sample at pH 8.5, to reduce the concentration of Ca, Al, and Fe ions by precipitation and to release phosphate ions into the solution. The clear extract is analyzed for P content at 880 nm wavelength on a UV/VIS spectrometer Perkin-Elmer model Lambda 40, after forming an antimony-phosphate-molybdate complex at room temperature.

The total nitrogen content determination was based on the Kjeldahl digestion using a $TiO_2$ catalyst. After distillation, the nitrogen content in distillate was titrated with sulfuric acid.

The sulfur in the soil was analyzed by oxidation to the sulfate form by fusion. The soil sample is ignited at 550°C with $NaHCO_3$ in the presence of $Ag_2O$ catalyst, and the melt is dissolved in $CH_3COOH$. The total sulfur was determined as sulfate ($SO_4^{2-}$) by the titration with a $BaCl_2$ solution.

**TABLE 1 |** Criteria for soil classification using pollution indices.

| Index, Values | Equation, Class | References |
|---|---|---|
| Enrichment factor | $EF = [(C_x/R)_{sample}]/[(C_x/R)_{reference}]$ | Khademi et al., 2019; |
| EF < 2 | Deficiency to minimal enrichment | Relić et al., 2019; |
| 2 < EF < 5 | Moderate enrichment | Jiang et al., 2020; |
| 5 < EF < 20 | Significant enrichment | Monged et al., 2020; |
| 20 < EF < 40 | Very high enrichment | Adimalla et al., 2020 |
| EF > 40 | Extremely high enrichment | |
| Geoaccumulation index | $I_{geo} = \log_2[C_n/(1.5 \times B_n)]$ | Müller, 1969; |
| Igeo < 0 | Unpolluted | Men et al., 2018; |
| 0 < Igeo < 1 | Unpolluted to moderately polluted | Khademi et al., 2019; |
| 1 < Igeo < 2 | Moderately polluted | Monged et al., 2020; |
| 2 < Igeo < 3 | Moderately to strongly polluted | Adimalla et al., 2020; |
| 3 < Igeo < 4 | Strongly polluted | Egbueri et al., 2020 |
| 4 < Igeo < 5 | Strongly to extremely polluted | |
| Igeo > 5 | Extremely polluted. | |
| Pollution load Index | $PLI = (CF_1 \times CF_2 \times CF_3 \times CF_4 \ldots \times CF_n)^{1/N}$ | Tomlinson et al., 1980; |
| PLI < 1 | Unpolluted | Relić et al., 2019; |
| 1 < PLI < 2 | Moderately polluted | Jiang et al., 2020; |
| 2 < PLI < 10 | Strongly polluted | Egbueri et al., 2020; |
| PLI > 10 | Extremely polluted | Monged et al., 2020 |
| Risk index | $RI = \sum(T_i^i \times C_{is}^i/C_{in}^i)$ | Hakanson, 1980; |
| RI < 150 | Low ecological risk | Men et al., 2018; |
| 150 < RI < 300 | Moderate ecological risk | Gan et al., 2019; |
| 300 < RI < 600 | Significant ecological risk | Monged et al., 2020; |
| RI > 600 | Very high ecological risk. | Li et al., 2020 |

## Quality Assurance/Quality Control

Quality assurance/quality control (QA/QC) ensured that all 80 samples and their duplicates and blanks were sampled, prepared, and analyzed in the laboratory. Certified reference material NIST SRM 2711a – Montana II soil from the National Institute of Standards and Technology (NIST) was used as the standard soil sample for quality control of metal analyses. The recovery study was used for the validation of the sample preparation procedure. The following mean recoveries (±relative standard deviation) were obtained: Cr: 104 ± 3.1%; Cd: 91 ± 3.2%; Pb: 93 ± 2.9%; Ni: 95 ± 2.4%; Zn: 98 ± 2.1%; Cu: 97 ± 2.5%; As: 90 ± 3.6%; Fe: 92 ± 3.8%; and Hg: 83 ± 11.7%. The MDL for the studied metals were: Cr: 1.3 mg/kg; Cd: 0.4 mg/kg; Pb: 2.1 mg/kg; Ni: 1.5 mg/kg; Zn: 0.07 mg/kg; Cu: 0.6 mg/kg; As: 0.04 mg/kg; Fe: 1.8 mg/kg; and Hg: 0.03 mg/kg. All calibration lines were linear, with a correlation coefficient higher than 0.995. The AAS sequence included a QC sample and a blank after 10 soil samples. A second identical sequence was run with the duplicate samples.

## Data Analysis

Descriptive analysis (mean, median, skewness, kurtosis, standard deviation, maximum, minimum), Grubb's outlier tests, and pollution indices (EF, $I_{geo}$, PLI, RI) were performed in Microsoft Excel. The soil pollution indices and their equations used for risk assessment methods were presented in **Table 1**. For an adequate understanding of the methodologies, the criteria and references are also included. Symbols in **Table 1** denotes: $C_x$, $C_n$, $C_{is}$ is the measured concentration of individual metal in the soil, R is the concentration of the reference element in the unpolluted soil, $B_n$ is the background concentration or reference value of the metal n, N is the number of metals tested, $C_{in}$ denotes the background concentration of metals in uncontaminated soil; $T_{ir}$ denotes the toxic response factor of heavy metals. These factors for: Pb; Cd; As; Zn; Cr; Ni; Cu; and Hg have values: 5; 30; 10; 1; 2; 5; 5; and 40; respectively (Hakanson, 1980; Men et al., 2018; Gan et al., 2019; Li et al., 2020; Monged et al., 2020).

Minitab software package was used to perform multivariate (Pearson correlation, PCA, HCA) data analyses. Details on the multivariate procedures are described in Onjia (2016). The spatial distribution of toxic metal concentration was mapped using Golden Software Surfer. EPA PMF 5.0 software (Norris et al., 2014) was employed for the PMF data evaluation.

# RESULTS AND DISCUSSION

## Physiochemical Properties and Trace Elements Distribution

### Soil Physicochemical Properties

The characteristics of heavy metals content in soils are related to both the physical and chemical properties of soils. Therefore, the concentrations of heavy metals (Cr, Cd, Pb, Ni, Zn, Cu, Hg, As, and Fe) together with some basic soil properties (pH, phosphorus, sulfur, nitrogen, and water content) were analyzed in all samples. **Supplementary Table 1** shows the experimental results for all analytes tested in the soil samples. According to the average pH values, the soil is slightly alkaline, although, there is a maximum of pH 9.9, which classifies that soil sample as very alkaline. This indicates that there have been alkaline chemical leaks. In general, soil of this pH is not suitable for metal bioavailability, since most heavy metals are more mobile and available at a lower pH (Kim et al., 2015). Soil water content varied significantly: this is expected from surface soil, as it is strongly influenced by weather conditions. The sulfur content of some samples showed increased values, while the nutrient content (nitrogen and phosphorus) was relatively low, and well within the concentrations expected in industrial soil. The soil texture was estimated to be similar to that of Novi Sad city (Serbia), which is located on a similar river bank terrace, affected with Danube fluvial activities, therefore, quite a sandy soil (Mihailović et al., 2015), not suitable for water and nutrient retention.

### Descriptive Statistics

The results of the descriptive statistics are presented in **Table 2**. Across the study area, the concentrations of toxic metals (mg/kg dry weight) in soil samples were found in the following ranges: Cd (1.1–7.4); Pb (13–616); Ni (27–189); Zn (29–1199); Cu (16–96); Hg (<0.1–1.2); As (1.2–28); and Cr (21–89). The skewness and kurtosis of Cd, Pb, Ni, Zn, As, and Hg were found well above the one showing right-handed skewness. Based on the mean values, the metal concentrations decreased in the following order: Zn > Pb > Ni > Cr > Cu > As > Cd > Hg. The results show that besides Fe, the most abundant metals in the study area were Zn and Pb. Several studies have reported that Zn is the most abundant heavy metal in urban soil (Yadav et al., 2019; Zhao et al., 2019; Egbueri et al., 2020; Jiang et al., 2020; Jin and Lv, 2020), while in some studies, Pb is found in the highest concentration (Harvey et al., 2017; Škrbić et al., 2018; Adimalla et al., 2020). However, Chen et al. (2020) reported Cr as the most abundant toxic metal in soil. If Fe is excluded, the most abundant metal in soil is usually Mn (Men et al., 2018; Roy et al., 2019; Xie et al., 2019; Monged et al., 2020). In this study, Ni, Cr, and Cu were found in similar concentrations, while Cd and Hg were present at very low levels. Levels of Zn and Pb had high standard deviation: these metals are influenced by human activities, and their dispersion over the sampling area is less uniform.

Most soil samples exceeded the geochemical background values (Taylor and McLennan, 1995; **Table 2**). Soil pollution is not comprehensively regulated at the European level, therefore, national regulations should be considered. A comparison of the results with the Serbian limits (Official Gazette of Republic of Serbia, 2018) is shown in **Table 2**. The Serbian target and intervention values are identical to those from the Dutch list for soil pollution (Dutch Standards, 2000), which are widely applied globally (Gong, 2010). The target value implies that contamination is present and further investigation is required, while the intervention value implies significant contamination is present and cleanup is required to decrease the soil metal concentrations to below the target value. **Table 2** shows that the average content of metals in our soil samples do not exceed the intervention values. However, for all metals, except Cr, these metals are above the target values. In the case of Pb and Zn, there are a number of individual samples with concentrations well above the intervention limits. This indicates that at certain locations there has been a leakage of materials containing these metals into the soil, or intensive traffic activity as vehicle fuel

**TABLE 2 |** Descriptive statistics of soil samples ($n$ = 80) ($H_2O$, N, S, Fe in %, and all others are in mg/kg).

| No. | $C_{mean}$ | $C_{med}$ | $C_{skew}$ | $C_{kurt}$ | $C_{stdev}$ | $C_{max}$ | $C_{min}$ | $T_V$[a] | $I_V$[b] | $BG_V$[c] |
|---|---|---|---|---|---|---|---|---|---|---|
| pH | 8.1 | 8.2 | 0.1 | -0.5 | 0.6 | 9.9 | 7.1 | – | – | |
| $H_2O$ | 17 | 18 | 0.1 | 0.2 | 5.9 | 36 | 6.1 | – | – | |
| N | 0.12 | 0.13 | -1.0 | -0.14 | 0.02 | 0.14 | 0.07 | – | – | |
| S | 0.07 | 0.04 | 5.1 | 30 | 0.12 | 0.88 | 0.005 | – | – | |
| P | 6.9 | 6.8 | 0.2 | -0.7 | 1.2 | 9.3 | 4.0 | – | – | |
| Fe | 1.9 | 2.0 | 0.13 | 1.1 | 0.6 | 3.8 | 0.5 | – | – | 3.5 |
| Cd | 2.7 | 2.8 | 1.6 | 10 | 0.9 | 7.4 | 1.1 | 0.8 | 12 | 0.098 |
| Pb | 113 | 74 | 2.8 | 9.2 | 110 | 616 | 13 | 85 | 530 | 20 |
| Ni | 56 | 50 | 3.4 | 17 | 22 | 189 | 27 | 35 | 210 | 20 |
| Zn | 238 | 148 | 1.9 | 4.4 | 217 | 1199 | 29 | 140 | 720 | 71 |
| Cu | 49 | 44 | 0.8 | -0.2 | 18 | 96 | 16 | 36 | 190 | 25 |
| Hg | 0.3 | < 0.1 | 1.9 | 3.0 | 0.3 | 1.2 | <0.1 | 0.3 | 10 | 0.085[d] |
| As | 6.8 | 3.8 | 1.6 | 1.8 | 6.7 | 28 | 1.2 | 29 | 55 | 1.5 |
| Cr | 55 | 53 | 0.3 | 0.3 | 14 | 89 | 21 | 100 | 380 | 35 |

[a] *Target value.* [b] *Intervention value.* [c] *Background value.* [d] *From William and Haynes (2017).*

is a major source of Pb contamination in soils (Roy et al., 2019; Adimalla et al., 2020). These sites require remedial action, and the soil should be cleared before any further management decision is made.

A literature survey of soil metal concentration related to the painting industry was summarized in **Table 3**. At the first sign, a very high variation in the concentrations reported is notable, i.e., from below detectable levels, to >1000 mg/kg in some hot spots (Yan et al., 2008). Arsenic pollution is not a major concern because the maximum concentration of 28 mg/kg, well below the target value, was found in this study. Cooper Cr, and Ni concentrations in this study show comparable patterns, and they are highly dependent on the existence of a specific industry nearby (Nwajei et al., 2012; Ekpo et al., 2014; Spahić et al., 2019). Zinc and Pb are usually present at a higher level, therefore, they should be monitored (Yan et al., 2008; Hu et al., 2012; Dobroshi et al., 2019). Even if Cd and Hg concentrations are very low, they are of significant concern because they have very high toxicity (Hakanson, 1980). It should be noted in **Table 3** that data on Hg pollution are very scarce. This could be because in order to measure it, a different configuration of the AAS instrument must be used. It is also present at very low levels, which is difficult to detect.

## Spatial Distribution

Spatial visualization was made using geostatistical (GIS) mapping to recognize hot spots, i.e., the area with high values of toxic metals concentrations. In this study, based on the data from sampling points, a spatial interpolation using ordinary kriging enables an evaluation even for the unsampled area. This GIS approach has been used in numerous soil pollution studies (Dragović et al., 2014; Liang et al., 2017; Cheng et al., 2020; Jin and Lv, 2020). Soils concentration patterns of the studied metals are presented in **Figure 2**. Nickel, Cr, and Cu, show similar spatial distribution patterns, while the other patterns are quite varied. These maps are a worthwhile tool for identifying hot spots with high metal pollution and demarcating the safe and unsafe areas. Hot spots in this site are located in the vicinity of the car mechanic workshop, the waste store building, and the raw materials store.

## Multivariate Analysis

### Correlation Matrix

Prior to multivariate analysis, a Pearson correlation matrix was made to measure the strength of the relationships between analyte pairs within the samples. Correlation analysis may provide information about the same origin or a similar pathway. Pearson's correlation is to be performed in a normal distribution, therefore, the normality test was first made. The Ryan-Joiner test showed that Pb, Ni, Zn, and As were not normally distributed, so log-transformed data was used for further multivariate processing. The Pearson correlation coefficient matrix for metals and other soil parameters is presented in **Table 4**. Strong, moderate and weak correlations are considered as those with correlation coefficients of >0.7; 0.5 < r < 0.7; and <0.5, respectively (Egbueri et al., 2020).

Lead and Zn have a strong significant positive correlation, indicating that the method by which they reach the soil at this location is similar. The second pair of heavy metals with moderate correlation are Ni and Cu. The correlation coefficient values >0.5 are shown in bold. The Pearson correlation analysis showed that pH, soil water content, sulfur, and nutrients (nitrogen and phosphorus) did not affect the retention of metals in surface soil samples.

### Principal Component and Factor Analysis

Principal component analysis and FA are common multivariate statistical methods used to reduce the dimensions of the dataset. In this paper, Varimax rotation was applied to maximize the variation of factor loadings. From this analysis, four PCs were retained that had Eugen values above one. In most cases, PCA and FA methods make a distinction between natural

**TABLE 3 |** Comparison (min-max) of the metal content (mg/kg) in soil samples with other studies from painting industry sites.

| Location | Cr | Cd | Pb | Ni | Zn | Cu | Hg | As | References |
|---|---|---|---|---|---|---|---|---|---|
| Changchun, Jilin, China | 20.7–402 | 0.09–2.64 | 30–1000 | 13.7–36.9 | 64.3–3300 | 20.5–69.2 | n.d.–0.03 | 4.7–12.6 | Yan et al., 2008 |
| Southern Nigeria | n.a. | 0.51 | 474 | 7.3 | n.a. | 138 | n.a. | n.a. | Udosen et al., 2016 |
| Srem, Serbia | 20.1–247 | 0.16–1.27 | 5.3–95.4 | 21.7–273 | 24–192 | 13.6–553 | n.a. | 0.4–21.4 | Spahić et al., 2019 |
| Savar, Dhaka, Bangladesh | <335 | n.a. | n.a. | <45–48 | 65–84 | 56–58 | n.a. | <11.5 | Jolly et al., 2012 |
| Kaduna, Nigeria | 28.5–55.5 | n.d.–1.3 | 30.8–63.6 | 27.1–27 | 128–273 | n.a. | n.a. | n.a. | Inobeme et al., 2014 |
| Vushtrri, Serbia | n.a. | <0.01 | 104–746 | 23.2–45.2 | 100–684 | 11.0–32.1 | n.a. | n.a. | Dobroshi et al., 2019 |
| Chongqing, China | n.a. | 0.04–0.35 | 12.3–962 | 16.0–66.9 | 35.3–97.8 | n.a. | n.a. | n.a. | Hu et al., 2012 |
| Akwa Ibom, Nigeria | 7.2–15.2 | 8.2–12.3 | 14.2–18.3 | 12.5–25.3 | 42.1–58.3 | 12.5–36.3 | n.a. | n.a. | Ekpo et al., 2014 |
| Tamil Nadu, India | 8.94–10.4 | n.a. | 6.91–8.22 | n.a. | 2.21–3.75 | 1.11–2.95 | n.a. | n.a. | Dheeba and Sampathkumar, 2012 |
| Agbor, Delta, Nigeria | 0.05–0.27 | n.d.–0.01 | 5.2–10.2 | 1.66–4.90 | 3.98–9.74 | 1.8–2.3 | n.a. | n.d.–0.01 | Nwajei et al., 2012 |
| Belgrade, Serbia | 21–89 | 1.1–7.4 | 13–616 | 27–189 | 29–1199 | 16–96 | n.d.–1.2 | 1.2–28 | This study |

*n.d., not detected; n.a., not analyzed; m, mean value.*

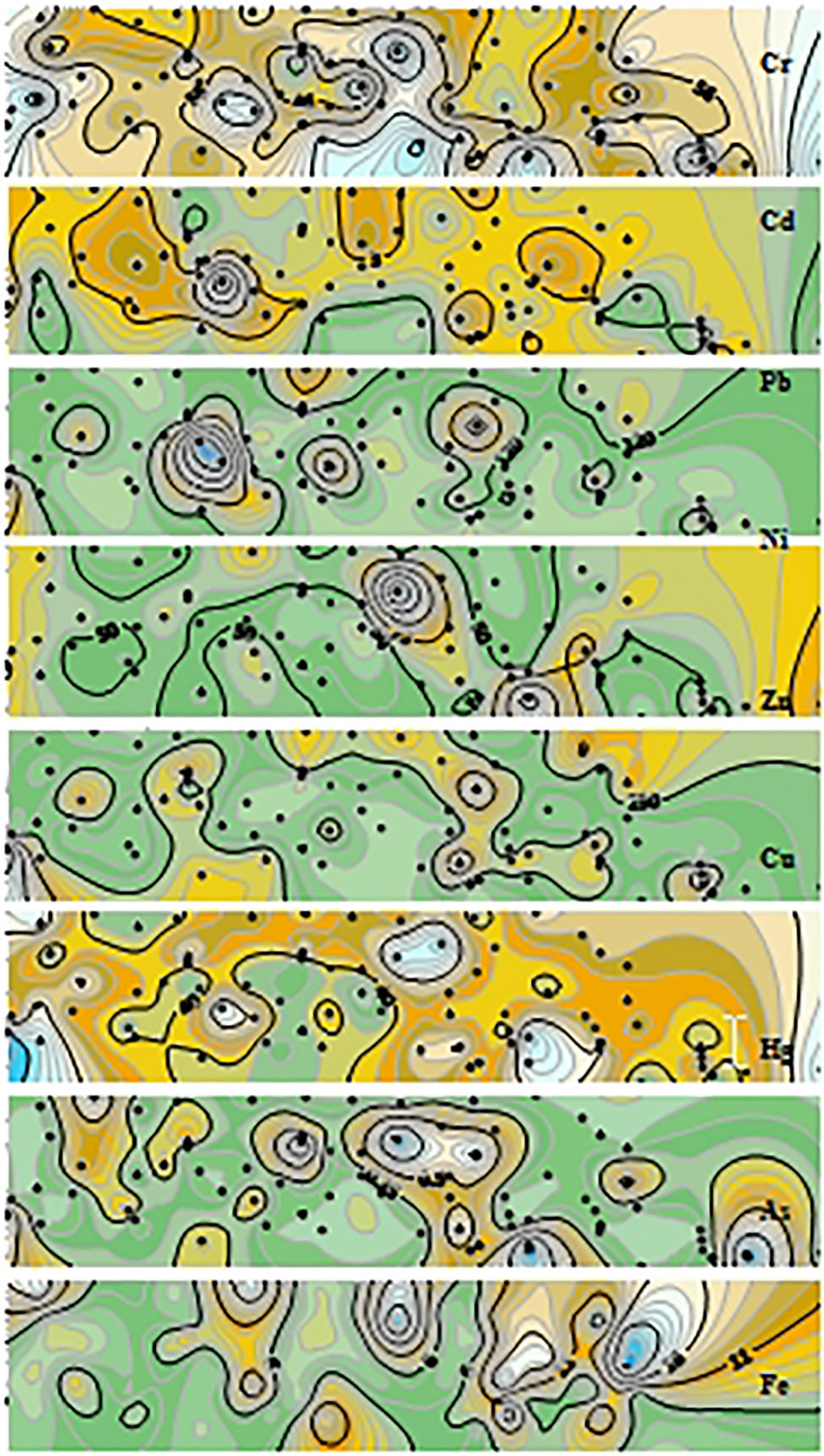


**FIGURE 2 |** Spatial distribution of Cr, Cd, Pb, Ni, Zn, Cu, As, and Hg, in soil across the study area.

and anthropogenic sources from which contaminants originate (Slavković et al., 2004; Egbueri et al., 2020). **Figure 3** presents the factor loading values for the analytes studied. Most metals are classified into one group, except Cd, which is classified by itself, and As and Fe, which are classified together with the water content, P, and pH, S and N, respectively. This shows

**TABLE 4 |** Pearson correlation coefficient matrix for metals and other soil parameters ($n$ = 80).

| | Pb | Cr | Ni | Zn | Cu | Cd | As | Hg | Fe | pH | $H_2O$ | N | S |
|---|---|---|---|---|---|---|---|---|---|---|---|---|---|
| Cr | 0.110 | | | | | | | | | | | | |
| Ni | 0.339 | 0.334 | | | | | | | | | | | |
| Zn | **0.721** | 0.029 | 0.424 | | | | | | | | | | |
| Cu | 0.370 | 0.344 | **0.517** | 0.493 | | | | | | | | | |
| Cd | −0.034 | −0.332 | −0.070 | −0.074 | −0.183 | | | | | | | | |
| As | 0.008 | 0.061 | 0.134 | 0.111 | 0.191 | 0.201 | | | | | | | |
| Hg | 0.081 | 0.026 | 0.057 | 0.107 | 0.165 | 0.223 | −0.020 | | | | | | |
| Fe | 0.240 | 0.207 | 0.352 | 0.268 | 0.269 | 0.143 | 0.236 | 0.025 | | | | | |
| pH | 0.025 | 0.123 | −0.070 | −0.125 | −0.137 | 0.071 | −0.318 | 0.047 | 0.002 | | | | |
| $H_2O$ | 0.158 | −0.131 | 0.125 | 0.182 | 0.173 | 0.246 | 0.385 | −0.043 | 0.123 | −0.256 | | | |
| N | 0.007 | 0.221 | −0.074 | 0.019 | 0.045 | −0.203 | −0.112 | 0.016 | −0.026 | 0.150 | −0.196 | | |
| S | 0.180 | 0.098 | 0.023 | 0.313 | 0.258 | 0.076 | 0.020 | 0.275 | 0.175 | 0.070 | 0.015 | −0.140 | |
| P | 0.069 | −0.048 | 0.109 | 0.151 | 0.128 | −0.069 | 0.249 | 0.187 | −0.207 | −0.281 | 0.355 | −0.200 | 0.001 |

*The significance level $p < 0.05$ (two-tailed).*

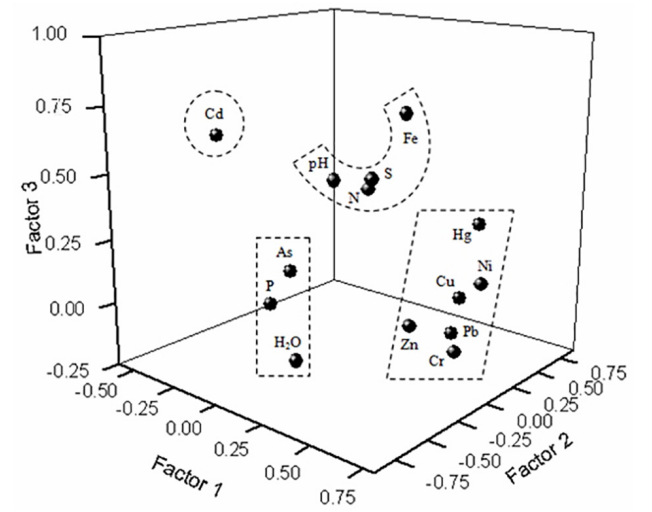


**FIGURE 3 |** Factor analysis plot loadings.

that As and Fe do not originate from the same source as the other metals.

## Hierarchical Cluster Analysis

The similarities of metals sources in soil samples were analyzed by HCA. This method differentiates the components of different sources and classifies them into several groups. For this dataset, a Ward amalgamation rule with a squared Euclidean distance was used. Hierarchical cluster analysis results are shown in the dendrogram (**Figure 4**). The soil samples were classified into two distinctive groups, which were further divided into two sub-groups. The samples with a similar pattern are presented in one class. Hierarchical cluster analysis evaluation indicates that the metals Pb and Zn may originate from the same source, likely from human activity. The left-hand group of samples in **Figure 4** is characterized by a high level of Pb and Zn. The cluster membership for all samples was given in **Supplementary Table 2**.

## Positive Matrix Factorization

In this study, the input data for the PMF model were the concentrations of all analytes, and uncertainty data associated with these concentrations. The number of factors run in the base PMF model were set to two, three, four, and five. The start seed number was chosen randomly, and the number of runs was set to 20. The Q value was shown to be the smallest and most stable when the number of source factors was set to four. In this way, most of the values in the residual matrix E were within ± five. The correlation indices between the estimated and measured concentrations ranged from 0.707 (Ni) to 0.989 (As), except for Cd (0.457) and Hg (0.346). This suggests that the PMF model apportioned metals appropriately. Four sources were identified by PMF and they agreed with the previous FA results. The source profiles of metals, together with the soil characteristics of the four factors are shown in **Figure 5**.

As seen in **Figure 5**, Fe, As, Cu, Zn, Ni, Pb, and Cr contributed to all factors by more than 50% of their total amounts. The soil pH, water content, and phosphorus content show similar behavior. The contribution of nitrogen to Factor 4, Hg to Factor 3, and sulfur to Factors 1 and 2, is negligible. The factor fingerprints of metals resulting from the PMF model are shown in **Figure 6**, while the factor contributions to the heavy metals are given in **Supplementary Figure 1**.

The first factor presented high loadings of Pb (58.2%) and Zn (73.6%). Most of the sample sites showed obvious Zn and Pb pollution, with Zn in particular reaching a level of severe contamination. Anthropogenic activities were the primary source of these two heavy metals. Traffic vehicle emission is generally considered to be the most important source of Pb and Zn (Men et al., 2018; Adimalla et al., 2020; Chen et al., 2020), although the accumulation of Pb and Zn in urban soils could, to some extent, be dependent on atmospheric deposition (Xie et al., 2019). It has also been reported that most of the risk from road dust, which is resuspended and deposited in the area, could be attributed to Pb (Roy et al., 2019). According to Harvey et al. (2017), road dust is the most significant contaminant of urban soil. The spatial variation of Zn and Pb content was similar, and some of their

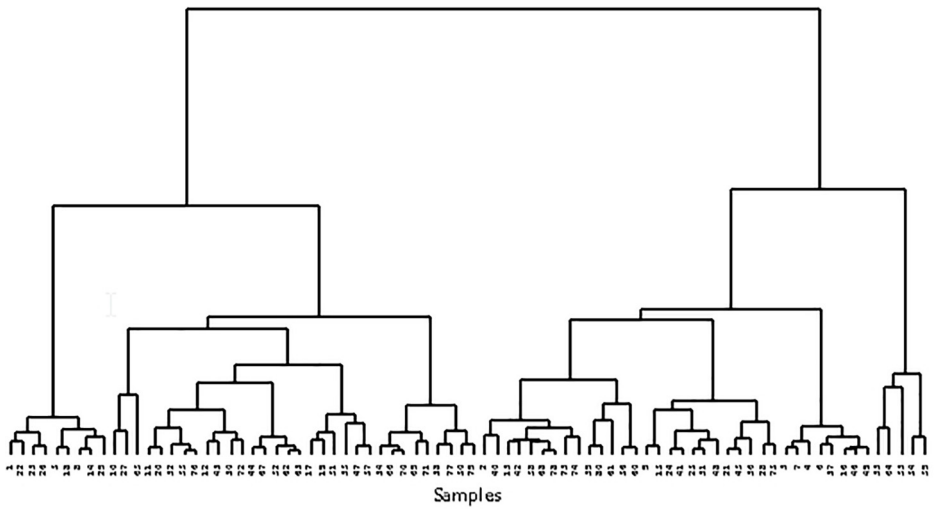


**FIGURE 4 |** Dendrogram of soil samples at the former painting production facility.

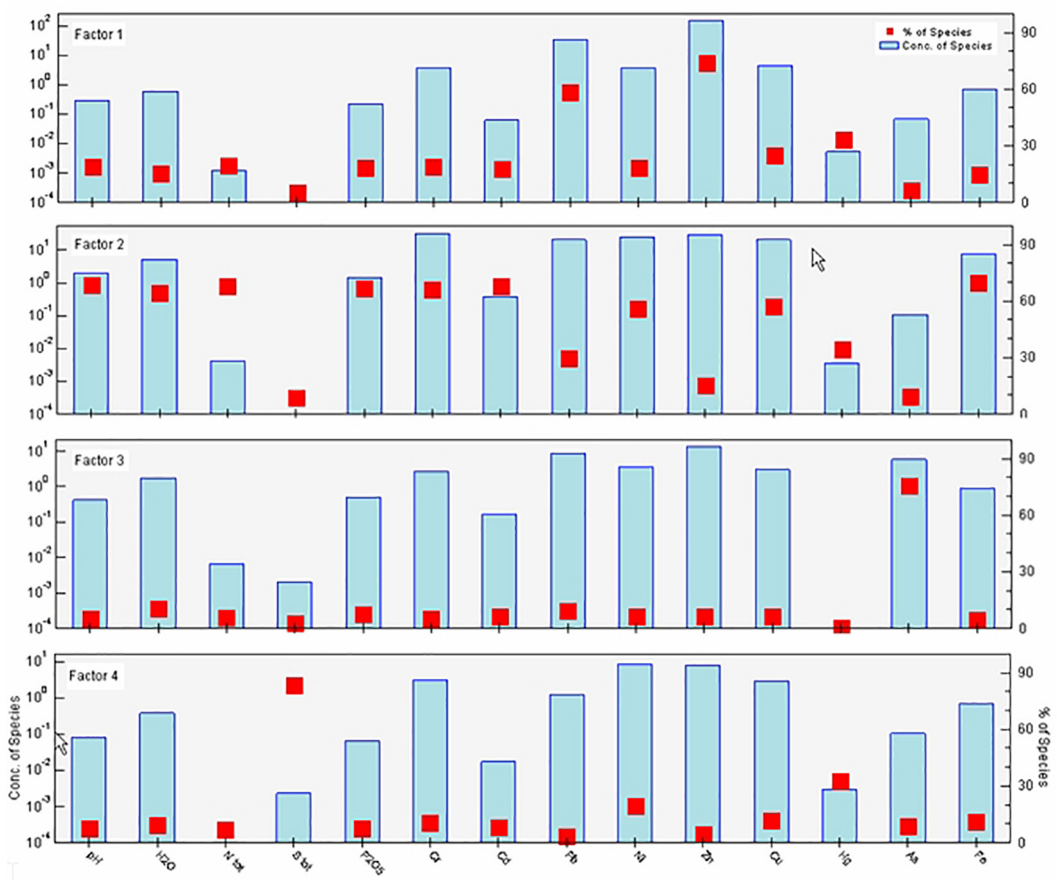


**FIGURE 5 |** Source profiles of metals and other analytes and source contribution percentages from the PMF model.

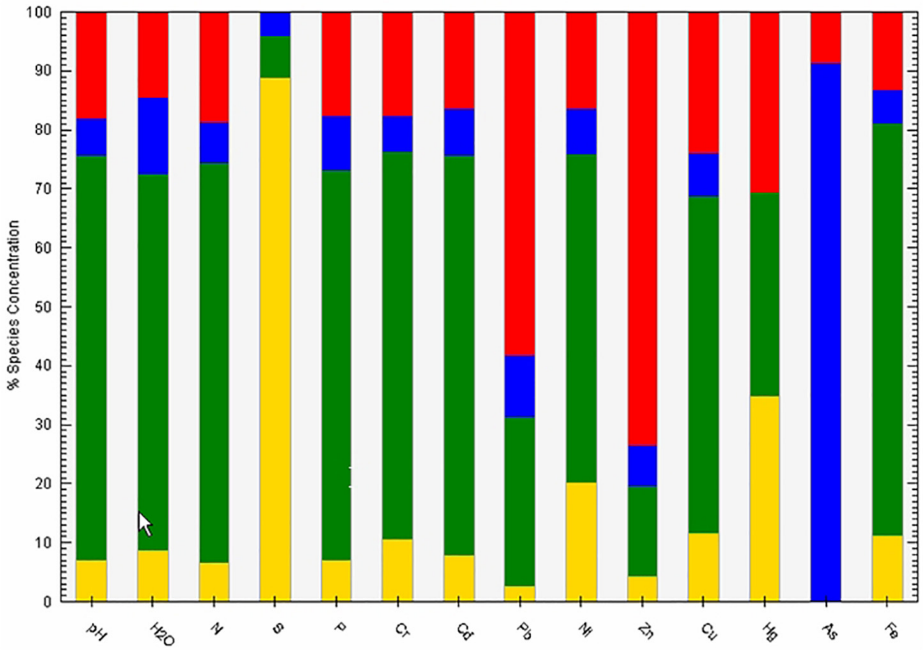


**FIGURE 6 |** Factor fingerprints of metals resulting from the PMF model. Factor 1 (red color); Factor 2 (blue color); Factor 3 (green color); Factor 4 (yellow color).

high-value areas coincided in the study area. As mentioned above, this location is currently part of the city center and surrounded by streets with heavy traffic. Besides vehicle exhaust emissions, this factor includes possible spillage of vehicle-related mineral oil or gasoline. Automobile tyres also release a large amount of Zn (Jiang et al., 2020).

The second factor accounted for 91.3% of the As contribution. This high factor load may be connected with the use of chemicals containing high levels of As (Nriagu et al., 2007). The measured concentration level of As in these soil samples is far below the target value, and does not pose a pollution threat. These changes in the soil levels of As are probably caused by industrial emission from several other industrial facilities, including a chemical manufacturing factory located northeast of the study area: spatial distribution revealed that the As high values spots were mostly in the northeast of the study area. Factor 2 was considered as an anthropogenic component, owing to the industrial As emissions.

Factor 3 was defined by Fe (69.8%), Cu (57.1%), Ni (55.8%), Cd (67.9%), Cr (65.8%), Hg (34.6%), along with P (66.1%), N (67.7%), pH (68.6%), and water content (63.9%). Copper, Ni, and Cr have been demonstrated to be the indicators of a natural origin in a soil study by Jiang et al. (2020). Nickel has also been identified as being from natural sources (Cheng et al., 2020). Chromium and Fe by Liang et al., 2017, Cr and Ni by Jin and Lv (2020). Hence, factor 3 was identified as a natural source.

The last factor was shown to be a non-metallic one, accounting for 88.9% of the sulfur contribution, the dominant analyte in this factor. This factor is attributed to the facility operation process during its lifetime. Sulfur is present in petroleum products and can reach the soil by hydrocarbon spillages, however, as sulfur is not correlated with Pb and Zn, this is not it's primary route to the soil. Atmospheric deposition may also occur, in the form of acid rain, as well as spillages of sulfuric acid. However, the measured pH values do not show soil acidity; therefore, sulfuric acid deposition is assumed to be negligible. The use of sulfur to make paints, for example in the process of sulfonation, and the addition of sulfur, as an additive, to asphalt and concrete (Saylak and Conger, 1982) which could leach into the soil, are the most likely reasons for the sulfur variations measured in our samples. Therefore, factor 4 was determined as a non-metallic historical factor.

A metal that appears to comes from several different sources is Hg. This metal equally contributes to factors 1 (30.6%), 3 (34.6%), and 4 (34.8%). Thus, Hg could be of natural origin and, to some extent, released from the production of chemicals and medical devices (Men et al., 2018).

## Ecological Risk Assessment

### Enrichment Factor

The difference between the presence of individual metals derived from anthropogenic activities, and those of natural origin or

**TABLE 5 |** The enrichment factor for studied metals in soil samples.

| EF | Cr | Cd | Pb | Ni | Zn | Cu | Hg | As |
|---|---|---|---|---|---|---|---|---|
| $EF_{avg}$ | 0.73 | 0.71 | 2.4 | 0.58 | 2.3 | 0.87 | 0.76 | 1.6 |
| $EF_{std}$ | 0.27 | 0.38 | 2.3 | 0.25 | 2.2 | 0.51 | 1.0 | 1.6 |
| $EF_{max}$ | 2.4 | 2.5 | 12 | 1.4 | 9.4 | 4.1 | 7.5 | 8.3 |
| $EF_{min}$ | 0.41 | 0.26 | 0.42 | 0.22 | 0.37 | 0.33 | n.d. | 0.21 |

*n.d., not determined.*

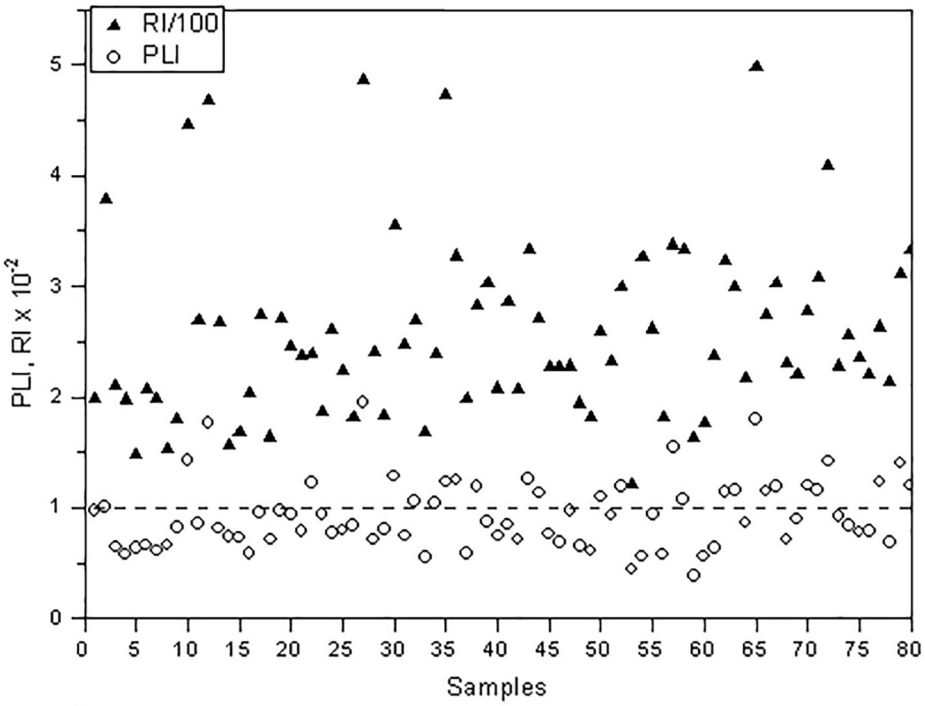


**FIGURE 7 |** PLI and RI values in the studied area at the former painting production facility.

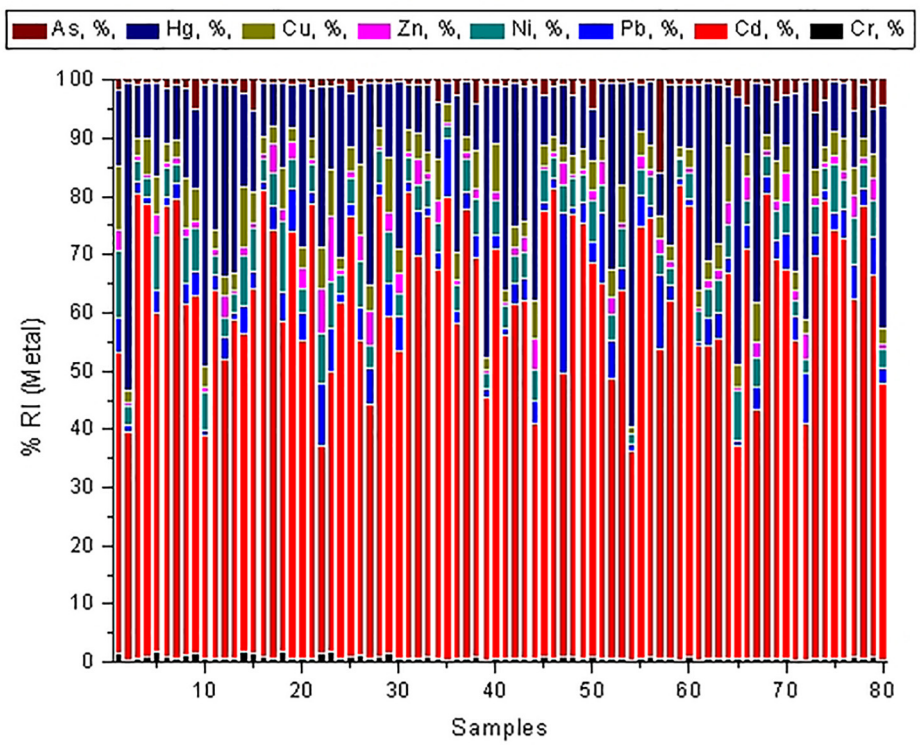


**FIGURE 8 |** The individual contribution of metals to RI in the studied soil samples.

derived from a mixed source of heavy metals can be estimated using the EF. The unpolluted Earth's crust is used as the reference for element content in the calculation of EF, commonly using Fe (Khademi et al., 2019; Monged et al., 2020), Al (Relić et al., 2019; Adimalla et al., 2020), Ti (Jiang et al., 2020), Mn (Yadav et al., 2019), or soil organic matter content (Gan et al., 2019). In any case, it is mandatory that the reference element selected is not of anthropogenic origin in the study area.

Based on the factor analysis (section"Principal Component and Factor Analysis"), it was established that the source of Fe was different from the source of the other metals. Furthermore, the Fe content in the upper continental crust is high, compared with the inputs of anthropogenic sources. Therefore, Fe can be used as the reference element in EF estimation for the trace metal data geochemical normalization. A surface soil sample from a rural area, not far from the study site (6 km southeast, GPS: 44°49′00.5″N; 20°33′25.4″E) was used to establish the background reference concentrations (in mg/kg; Cr = 28; Cd = 1,4; Pb = 17; Ni = 36; Zn = 39; Cu = 21; Hg = 0,13; As = 1.6; Fe = 6700). The EF results are presented in **Table 5**.

Five categories of soil contamination are recognized based on the EF classification (see **Table 1**). The average EF values for Zn and Pb are much higher than the others, and in terms of these metals, it can be said that most soil samples are moderately enriched in Zn and Pb. In the case of Ni, there was a lack of any significant enrichment, even in the soil sample with the maximum concentration. As discussed above, PMF identified Cr, Cd, Ni, and Cu as belonging to natural sources. It should be

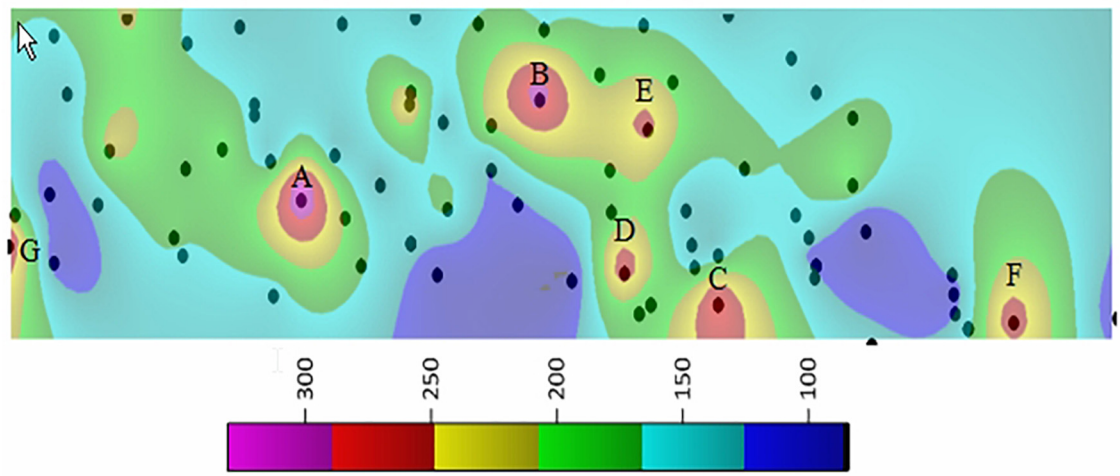


**FIGURE 9 |** Spatial distribution map of RI of soil at the former painting production facility.

**TABLE 6 |** Percentage of pollution class distribution of individual metals.

| Class | Cr | Cd | Pb | Ni | Zn | Cu | Hg | As |
|---|---|---|---|---|---|---|---|---|
| $C < T_V$ | 100 | 0 | 57 | 5 | 48 | 31 | 69 | 100 |
| $T_V < C < I_V$ | 0 | 100 | 40 | 95 | 47 | 69 | 31 | 0 |
| $C > I_V$ | 0 | 0 | 3 | 0 | 5 | 0 | 0 | 0 |
| EF < 2 | 99 | 97 | 55 | 100 | 63 | 96 | 93 | 74 |
| 2 < EF < 5 | 1 | 3 | 37 | 0 | 26 | 4 | 6 | 22 |
| 5 < EF < 20 | 0 | 0 | 8 | 0 | 11 | 0 | 1 | 4 |
| 20 < EF < 40 | 0 | 0 | 0 | 0 | 0 | 0 | 0 | 0 |
| EF > 40 | 0 | 0 | 0 | 0 | 0 | 0 | 0 | 0 |
| $I_{geo} < 0$ | 0 | 0 | 0 | 0 | 0 | 0 | 0 | 0 |
| $0 < I_{geo} < 1$ | 4 | 11 | 1 | 8 | 3 | 1 | 66 | 10 |
| $1 < I_{geo} < 2$ | 59 | 50 | 6 | 80 | 10 | 46 | 3 | 28 |
| $2 < I_{geo} < 3$ | 37 | 38 | 37 | 11 | 40 | 48 | 20 | 32 |
| $3 < I_{geo} < 4$ | 0 | 1 | 33 | 1 | 19 | 5 | 6 | 11 |
| $4 < I_{geo} < 5$ | 0 | 0 | 15 | 0 | 22 | 0 | 5 | 16 |
| $I_{geo} > 5$ | 0 | 0 | 8 | 0 | 6 | 0 | 0 | 3 |
| RI < 150 | 100 | 98 | 100 | 100 | 100 | 100 | 99 | 100 |
| 150 < RI < 300 | 0 | 2 | 0 | 0 | 0 | 0 | 1 | 0 |
| 300 < RI < 600 | 0 | 0 | 0 | 0 | 0 | 0 | 0 | 0 |
| RI > 600 | 0 | 0 | 0 | 0 | 0 | 0 | 0 | 0 |

emphasized that an EF value less than 1.0 suggests that the heavy metal in question originates entirely from the Earth's crust, or natural weathering processes (Adimalla et al., 2020).

### Geoaccumulation Index

Assessment of soil pollution can also be done by comparing current metal concentrations with pre-industrial concentration levels. This approach was proposed by Müller (1969) to identify and define metal pollution in soil and sediments, for which the $I_{geo}$ was introduced. The same rural sample used in EF formula was used for the $I_{geo}$ estimation. Factor 1.5 in the $I_{geo}$ equation is used due to of possible variations in the background values of a particular metal in the environment, i.e., lithogenic effect as well as due to possible minimal anthropogenic effects (Müller, 1969; Egbueri et al., 2020; Monged et al., 2020).

Seven classes of soil, based on $I_{geo}$, are defined in **Table 1**. The average values obtained for $I_{geo}$ were Cr, 1.9 ± 0.4; Cd, 1.8 ± 0.5; Pb, 3.3 ± 1.0; Ni, 1.6 ± 0.4; Zn, 3.2 ± 1.1; Cu, 2.1 ± 0.5; Hg, 1.4 ± 1.2; and As, 2.5 ± 0.6. Maximum $I_{geo}$ values for the same metals are 2.7; 3.3; 6.2; 3.4; 6.0; 3.2; 4.2; and 5.1, respectively. Based on the average values, it can be concluded that, in terms of Cr, Cd, Ni, and Hg, the soil belongs to the class "moderately polluted." Based on the As and Cu concentrations, the soil is classified as "moderately to strongly polluted." The presence of Pb and Zn in the soil samples assign these samples to the class "strongly polluted." In terms of maximum values of Pb, Zn, and As, the $I_{geo}$, in some cases, classifies the soil as "extremely polluted."

### Contamination Factor and Pollution Load Index

Using the model defined by Tomlinson et al. (1980), the contamination factor (CF) was determined as the ratio of the metal concentration in the analyzed soil, to the target concentration. According to Serbian regulations, the target values for analyzed metals are (in mg/kg): 85 for Pb; 100 for Cr; 0.8 for Cd; 140 for Zn; 35 for Ni; 140 for Zn; 29 for As; and 0.3 for Hg. As the regulatory values sometimes vary from country to country, CF values may be different, even if the metal concentrations are identical.

From the CF values, the PLI was derived to assess the metal pollution, the status of the soil, and the decision on the necessary actions to be taken. PLI > 1 indicates the presence of pollution. In the majority of soil samples, the analyzed PLI is below 1 (**Figure 7**), although there are those with PLIs well above one.

### Potential Ecological Risk

The ecological risk was quantified using the RI, taking into account the concentrations of heavy metals, ecological factors and toxic response factors. This index stands for the potential ecological risk factor of all metals tested together. The RI values of pollutant metals were estimated for each sample (**Figure 7**). From these results and criteria, some soil samples show a very high ecological risk. The maximum RI is 349, and the lowest ecological RI is 77. The average value of the potential ecological RI is 164, indicating moderate pollution. The average contribution of individual metals to RI (**Figure 8**) is as follows: 63% Cd; 19% Hg; 5% Ni; 5% Cu; 4% Pb; 2% Zn; 2% As; and 1% Cr. This study reveals that Cd is the metal that poses the highest ecological threat. This metal has also been at the top of the risk list of heavy metals in recently published ecological risk assessment studies (Men et al., 2018; Gan et al., 2019; Zhao et al., 2019; Egbueri et al., 2020).

The spatial distribution patterns of ecological RI values in the surface soils indicate that samples with significant risk exist in some locations (**Figure 9**). Three large spots (A, B, C) and four smaller spots (D, E, F, G) stood out. It should be pointed out that some of these spots (C, F, G) are at the edge of the study area. Except for three low ecological risk areas, most of the studied area is generally at moderate risk.

### Comparison of Ecological Risk Indices

A comparison of ecological risk indices is shown in **Table 6**. It is evident that there is a zero contamination with As and Cr, but there are three and five soil samples, which are highly contaminated with Pb and Zn, respectively. The soil is most frequently enriched with Zn. Geoaccumulation is highest for Pb and Zn. In addition, the geoaccumulation of As is significant. Although individual metal contribution rarely exceeds an RI of 150, i.e., only 2% samples for Cd and 1% samples for Hg, the total RI percentage distribution is 47% (RI < 150), 49% (150 < RI < 300), 4% (300 < RI < 600) and 0% (RI > 600). This means that nearly half of the samples have either low or moderate ecological risk, while in a small number of samples the ecological risk is significant.

## CONCLUSION

The average individual metal content in the studied soil samples is ordered, from high to low, as follows: Fe > Zn > Pb > Ni > Cr > Cu > As > Cd > Hg. Pearson's correlation coefficient analysis, PCA, FA, and HCA identified the relationship between heavy metals in soil samples and their probable origins. A heavy metals group consisting of Pb, Cr, Cu, Ni, Zn, and Hg was separated from the other analytes, as well as from Cd. No correlation between metals and other soil physicochemical parameters was found. The PMF receptor modeling used to apportion the pollution source in the studied area, derived four factors, including the traffic vehicle factor (Zn, Pb), the natural background variation (most metals and physicochemical parameters), industrial chemicals emissions (As), and a non-metallic historical factor (S).

From the evaluation of the soil pollution indices, EF, CF, $I_{geo}$, PLI, and RI, it can be seen that the studied soil samples in most cases, are either not contaminated or are slightly contaminated. However, there are a considerable number of samples with severe contamination by heavy metals. Even though the concentrations of Zn and Pb are the highest, the highest potential ecological risk is attributed to Cd and Hg, the concentrations of which are the lowest. The geostatistical technique, using spatial distribution by ordinary kriging, mapped several high-risk sub-areas, as well as uncontaminated sub-areas.

These findings are relevant for environmental agencies and land use management. In general, moderate soil pollution by heavy metals could be expected at the site of a former painting and varnish facility, provided that no metallic paints had been produced.

## DATA AVAILABILITY STATEMENT

The raw data supporting the of this article will be made available by the authors, without undue reservation.

## AUTHOR CONTRIBUTIONS

MR wrote the draft manuscript. ŽĆ performed the soil sampling in the field. DM did the data processing and interpretation of multivariate analysis results. TB performed the sample pretreatment, microwave digestion of soil samples, and pH and moisture determination. JL did the measurements of the concentrations by an atomic absorption and UV/VIS spectrometer. SS worked on data processing and interpretation of results for the Geoaccumulation Index, the Pollution Load Index and the Potential Ecological Risk Index. AO defined the scope of research and wrote parts of the discussion and processing of results. All authors contributed to the article and approved the submitted version.

## FUNDING

This work was supported by the Ministry of Education, Science and Technological Development of the Republic of Serbia (Contract No. 451-03-68/2020-14/200135).

## SUPPLEMENTARY MATERIAL

The Supplementary Material for this article can be found online at: https://www.frontiersin.org/articles/10.3389/fenvs.2020.560415/full#supplementary-material

## REFERENCES

Adimalla, N., Chen, J., and Qian, H. (2020). Spatial characteristics of heavy metal contamination and potential human health risk assessment of urban soils: A case study from an urban region of South India. *Ecotoxicol. Environ. Saf.* 194:110406. doi: 10.1016/j.ecoenv.2020.110406

Chen, B., Liu, K., Liu, Y., Qin, J., and Peng, Z. (2020). Source identification, spatial distribution pattern, risk assessment and influencing factors for soil heavy metal pollution in a high-tech industrial development zone in Central China. *Hum. Ecol. Risk Assess. Int. J* 49, 1–15. doi: 10.1080/10807039.2020.1739510

Cheng, W., Lei, S., Bian, Z., Zhao, Y., Li, Y., and Gan, Y. (2020). Geographic distribution of heavy metals and identification of their sources in soils near large, open-pit coal mines using positive matrix factorization. *J. Hazard. Mater.* 387:121666. doi: 10.1016/j.jhazmat.2019.121666

Dheeba, B., and Sampathkumar, P. (2012). Evaluation of heavy metal contamination in surface soil around industrial area, Tamil Nadu, India. *Int. J. ChemTech Res.* 4, 1229–1240.

Dobroshi, F., Mazrreku, A., Malollari, I., Dobroshi, K., and Maloku, F. (2019). Determination of heavy metals in the "ExtraColors" paint factory. *Eur. J. Engin. Technol.* 7, 28–33.

Dragović, R., Gajić, B., Dragović, S., Dordević, M., Dordević, M., Mihailović, N., et al. (2014). Assessment of the impact of geographical factors on the spatial distribution of heavy metals in soils around the steel production facility in Smederevo (Serbia). *J. Clean. Prod.* 84, 550–562. doi: 10.1016/j.jclepro.2014.03.060

Dutch Standards. (2000). *The Circular on Target Values and Intervention Values for Soil Remediation*. Netherlands: Ministry of Housing.

Egbueri, J. C., Ukah, B. U., Ubido, O. E., and Unigwe, C. O. (2020). A chemometric approach to source apportionment, ecological and health risk assessment of heavy metals in industrial soils from southwestern Nigeria. *Int. J. Environ. Anal. Chem* 98, 1–19. doi: 10.1080/03067319.2020.1769615

Ekpo, F. E., Ukpong, E. J., and Udoumoh, I. D. J. (2014). Bioaccumulations of Heavy Metals on Soil and Arable Crops Grown in Abandoned Peacock Paint Industry in Ikot Ekan, Etinan Local Government Area, Akwa Ibom State, Nigeria. *Univers. J. Environ. Res. Technol.* 4, 39–45.

Gan, Y., Huang, X., Li, S., Liu, N., Li, Y. C., Freidenreich, A., et al. (2019). Source quantification and potential risk of mercury, cadmium, arsenic, lead, and chromium in farmland soils of Yellow River Delta. *J. Clean. Prod.* 221, 98–107. doi: 10.1016/j.jclepro.2019.02.157

Gong, Y. (2010). "International experience in policy and regulatory frameworks for brownfield site management," in *Discussion Papers 57890*, (Washington: The World Bank).

Hakanson, L. (1980). An ecological risk index for aquatic pollution control. *A Sedimentol. Appr. Water Res.* 14, 975–1001. doi: 10.1016/0043-1354(80)90143-8

Harvey, P. J., Rouillon, M., Dong, C., Ettler, V., Handley, H. K., Taylor, M. P., et al. (2017). Geochemical sources, forms and phases of soil contamination in an industrial city. *Sci. Total Environ.* 58, 505–514. doi: 10.1016/j.scitotenv.2017.01.053

Hu, H., Feng, Y. Z., Yang, Y., Wang, S. G., and Li, C. L. (2012). Vertical distribution and pollution characteristics of soil heavy metals in a relocation paint factory. *Adv. Mater. Res.* 610-613, 1718–1721. doi: 10.4028/www.scientific.net/AMR.610-613.1718

Inobeme, A., Ajai, A. I., Iyaka, Y. A., Ndamitso, M., and Uwem, B. (2014). Determination of physicochemical and heavy metal content of soil around paint industries in Kaduna. *Int. J. Sci. Eng. Technol.* 3, 221–225.

Jiang, H.-H., Cai, L.-M., Wen, H.-H., Hu, G.-C., Chen, L.-G., and Luo, J. (2020). An integrated approach to quantifying ecological and human health risks from different sources of soil heavy metals. *Sci. Total Environ.* 701:134466. doi: 10.1016/j.scitotenv.2019.134466

Jin, Z., and Lv, J. (2020). Integrated receptor models and multivariate geostatistical simulation for source apportionment of potentially toxic elements in soils. *Catena* 194, 104638. doi: 10.1016/j.catena.2020.104638

Jolly, Y. N., Hossain, A., Sattar, A., and Islam, A. (2012). Impact of heavy metals on water and soil environment of a paint industry. *J. Bangladesh Chem. Soc.* 25, 159–165. doi: 10.3329/jbcs.v25i2.15068

Khademi, H., Gabarrón, M., Abbaspour, A., Martínez-Martínez, S., Faz, A., and Acosta, J. A. (2019). Environmental impact assessment of industrial activities on heavy metals distribution in street dust and soil. *Chemosphere* 217, 695–705. doi: 10.1016/j.chemosphere.2018.11.045

Kim, R. Y., Yoon, J. K., Kim, T. S., Yang, J. E., Owens, G., and Kim, K. R. (2015). Bioavailability of heavy metals in soils, definitions and practical implementation - a critical review. *Environ. Geochem. Hlth.* 37, 1041–1061. doi: 10.1007/s10653-015-9695-y

Li, J., Wang, G., Liu, F., Cui, L., and Jiao, Y. (2020). *Source Apportionment and Ecological-Health Risks Assessment of Heavy Metals in Topsoil Near a Factory, Central China*. Berlin: Springer

Liang, J., Feng, C., Zeng, G., Gao, X., and Zhong, M. (2017). Spatial distribution and source identification of heavy metals in surface soils in a typical coal mine city. *Lianyuan China. Environ. Pollut.* 225, 681–690. doi: 10.1016/j.envpol.2017.03.057

Men, C., Liu, R., Xu, F., Wang, Q., Guo, L., and Shen, Z. (2018). Pollution characteristics, risk assessment, and source apportionment of heavy metals in

road dust in Beijing. *China. Sci. Total Environ.* 612, 138–147. doi: 10.1016/j.scitotenv.2017.08.123

Mihailović, A., Budinski-Petković, L., Popov, S., Ninkov, J., Vasin, J., Ralević, N. M., et al. (2015). Spatial distribution of metals in urban soil of Novi Sad, Serbia, GIS based approach. *J. Geochem. Explor.* 150, 104–114. doi: 10.1016/j.gexplo.2014.12.017

Monged, M. H. E., Hassan, H. B., and El-Sayed, S. A. (2020). Spatial Distribution and Ecological Risk Assessment of Natural Radionuclides and Trace Elements in Agricultural Soil of Northeastern Nile Valley, Egypt. *Water. Air. Soil Pollut* 231:338. doi: 10.1007/s11270-020-04678-9

Müller, G. (1969). Index of geoaccumulation in sediments of the Rhine river. *Geol. J.* 2, 108–118.

Norris, G. A., Duvall, R., Brown, S. G., and Bai, S. (2014). *EPA/600/R-14/108 EPA Positive Matrix Factorization (PMF) 5.0 Fundamentals and User Guide*. Washington: U.S. Environmental Protection Agency.

Nriagu, J. O., Bhattacharya, P., Mukherjee, A. B., Bundschuh, J., Zevenhoven, R., and Loeppert, R. H. (2007). Arsenic in soil and groundwater, an overview. *Trace Met. Other Contam. Environ.* 9, 3–60. doi: 10.1016/S1875-1121(06)09001-8

Nwajei, G. E., Okwagi, P., Nwajei, R. I., and Obi-Iyeke, G. E. (2012). Analytical Assessment of Trace Elements in Soils, Tomato Leaves and Fruits in the Vicinity of Paint Industry, Nigeria, Res. *J. Recent Sci.* 1, 22–26.

Official Gazette of Republic of Serbia. (2018). *Rulebook on limit values of pollutants, harmful and hazardous substances in soil, Official Gazette of Republic of Serbia, No. 30/2018*. New Delhi: Gazette of India.

Onjia, A. (2016). *Chemometric approach to the experiment optimization and data evaluation in analytical chemistry*. Serbia: Belgrade University, 143.

Paatero, P., and Tapper, U. (1994). Positive matrix factorization, A non-egative factor model with optimal utilization of error estimates of data values. *Environmetrics* 5, 111–126. doi: 10.1002/env.3170050203

Relić, D., Sakan, S., Andelković, I., Popović, A., and Dordević, D. (2019). Pollution and health risk assessments of potentially toxic elements in soil and sediment samples in a petrochemical industry and surrounding area. *Molecules* 24:2139. doi: 10.3390/molecules24112139

Roy, S., Gupta, S. K., Prakash, J., Habib, G., Baudh, K., and Nasr, M. (2019). Ecological and human health risk assessment of heavy metal contamination in road dust in the National Capital Territory (NCT) of Delhi. *India. Environ. Sci. Pollut. Res.* 26, 30413–30425. doi: 10.1007/s11356-019-06216-5

Saylak, D., and Conger, W. E. (1982). A Review of the State of the Art of Sulfur Asphalt Paving Technology. *ACS Symp. Ser.* 183, 155–193. doi: 10.1021/bk-1982-0183.ch011

Škrbić, B., Buljovèić, M., Jovanović, G., and Antić, I. (2018). Seasonal, spatial variations and risk assessment of heavy elements in street dust from Novi Sad. *Serbia. Chemosp.* 205, 452–462. doi: 10.1016/j.chemosphere.2018.04.124

Slavković, L., Škrbić, B., Miljević, N., and Onjia, A. (2004). Principal component analysis of trace elements in industrial soils. *Environ. Chem. Lett.* 2, 105–108. doi: 10.1007/s10311-004-007378

Spahić, M. P., Manojlović, D., Tanèić, P., Cvetković, Ž, Nikić, Z., Kovaèević, R., et al. (2019). Environmental impact of industrial and agricultural activities to the trace element content in soil of Srem (Serbia). *Environ. Monit. Assess* 191, 1–22. doi: 10.1007/s10661-019-7268-8

Taylor, S. R., and McLennan, S. M. (1995). The geochemical evolution of the continental crust. *Rev. Geophys.* 33, 241–265.

Tomlinson, D. L., Wilson, J. G., Harris, C. R., and Jeffrey, D. W. (1980). Problems in the assessment of heavy metal level in eastuaries and the formation of a pollution index. *Helol. Mees.* 33, 566–575. doi: 10.1007/BF02414780

Udosen, E., Akpan, E., and Sam, S. (2016). Levels of some heavy Metals in Cocoyam (Colocasia esculentum) grown on soil receiving Effluent from a Paint Industry. *J. Appl. Sci. Environ. Manag.* 20:215. doi: 10.4314/jasem.v20i1.26

Wcisło, E., Bronder, J., Bubak, A., Rodríguez-Valdés, E., and Gallego, J. L. R. (2016). Human health risk assessment in restoring safe and productive use of abandoned contaminated sites. *Environ. Int.* 94, 436–448. doi: 10.1016/j.envint.2016.05.028

William, M., and Haynes. (2017). *CRC Handbook of Chemistry, and Physics, 97th edition (2016-2017)Abundance of elements in the earth's crust and in the sea*. Florida: CRC Press, 14–17.

Xie, T., Wang, M., Chen, W., and Uwizeyimana, H. (2019). Impacts of urbanization and landscape patterns on the accumulation of heavy metals in soils in residential areas in Beijing. *J. Soils Sedim.* 19, 148–158. doi: 10.1007/s11368-018-2011-6

Yadav, I. C., Devi, N. L., Singh, V. K., Li, J., and Zhang, G. (2019). Spatial distribution, source analysis, and health risk assessment of heavy metals contamination in house dust and surface soil from four major cities of Nepal. *Chemosphere* 218, 1100–1113. doi: 10.1016/j.chemosphere.2018.11.202

Yan, F., Yan, J., Wang, Y., and Chen, D. (2008). Site environmental assessment to an old paint factory in China. *Environ. Monit. Assess.* 139, 93–106. doi: 10.1007/s10661-007-9818-8

Zhao, K., Fu, W., Qiu, Q., Ye, Z., Li, Y., Tunney, H., et al. (2019). Spatial patterns of potentially hazardous metals in paddy soils in a typical electrical waste dismantling area and their pollution characteristics. *Geoderma* 337, 453–462. doi: 10.1016/j.geoderma.2018.10.004

**Conflict of Interest:** The authors declare that the research was conducted in the absence of any commercial or financial relationships that could be construed as a potential conflict of interest.

frontiers in Environmental Science

ORIGINAL RESEARCH
published: 30 September 2020
doi: 10.3389/fenvs.2020.572730

# Rhizosediments of *Salicornia tegetaria* Indicate Metal Contamination in the Intertidal Estuary Zone

*Marelé A. Nel*[1,2,3]*, *Gletwyn Rubidge*[4], *Janine B. Adams*[1,2] *and Lucienne R. D. Human*[2,3]*

[1] DSI/NRF Research Chair, Shallow Water Ecosystems, Nelson Mandela University, Port Elizabeth, South Africa, [2] Department of Botany, Nelson Mandela University, Port Elizabeth, South Africa, [3] South African Environmental Observation Network (SAEON) Elwandle Coastal Node Nelson Mandela University, Port Elizabeth, South Africa, [4] Department of Chemistry, Nelson Mandela University, Port Elizabeth, South Africa

OPEN ACCESS

**Edited by:**
*Dragana S. Đorđević, University of Belgrade, Serbia*

**Reviewed by:**
*Pedro Aboim De Brito, Instituto Português do Mar e da Atmosfera (IPMA), Portugal*
*Enrique Mateos-Naranjo, Seville University, Spain*

***Correspondence:**
*Marelé A. Nel*
*marele.anne@outlook.com*
*Lucienne R. D. Human*
*Lucienne.Human@saeon.ac.za*

**Specialty section:**
*This article was submitted to Toxicology, Pollution and the Environment, a section of the journal Frontiers in Environmental Science*

**Received:** *15 June 2020*
**Accepted:** *02 September 2020*
**Published:** *30 September 2020*

**Citation:**
*Nel MA, Rubidge G, Adams JB and Human LRD (2020) Rhizosediments of Salicornia tegetaria Indicate Metal Contamination in the Intertidal Estuary Zone. Front. Environ. Sci. 8:572730. doi: 10.3389/fenvs.2020.572730*

Metal pollution is a well-known anthropogenic impact of highly developed estuaries, with dire consequences to the ecosystem. This study investigated the metal concentrations (Al, Cr, Cu, Fe, Mn, Ni, Pb, Zn) in the sediment colonized by *Salicornia tegetaria*, a dominant salt marsh plant in the lower intertidal zone of the Swartkops Estuary. The samples were collected at five sites along the banks of the middle and lower reaches of the estuary, and analyzed using an Inductively Coupled Plasma –Optical Emission Spectrometer. Metal contamination was determined using established normalized baseline models. It was found that all the sites contained metal enrichment, with the estuary mouth experiencing the least enrichment. *Salicornia tegetaria* holds a substantial amount of anomalous metals within its rhizosediment—providing a valuable ecosystem service to a highly developed Swartkops Estuary.

**Keywords: metal pollution, Swartkops Estuary, baseline, coupled plasma optical emission spectrometer, salt marsh**

## INTRODUCTION

Estuaries are historically convenient places to build industries, as it was deemed a suitable place to dispose of large quantities of urban and industrial waste into the ocean (Forstner and Wittman, 1981). At the time it was judged to be appropriate, as rivers can transport and deposit waste into the ocean, which was considered to be so vast that it is insurmountable. Thus, metal pollution into estuaries is a well-known occurrence. Metals form part of various industrial processes, producing general products for consumers (Crane et al., 2017; Peppicelli et al., 2018). Once the waste and products are discarded, it adds to the naturally occurring metals in the sediment. Metals are commonly adsorbed onto the surface of sediment components, or dissolved in porewater (Basta et al., 2005; Almeida et al., 2008). These characteristics allows the sediment to act as a sink for metals, and mediates the release to the biological environment (Tack and Verloo, 1995; Strawn et al., 2015). The capacity for the sediments to retain the metals are limited to its physical and chemical characteristics, i.e., granulometric fraction, pH, oxidation-reduction potential and organic matter content are all important factors to include when assessing the bioavailability of metals

in sediments (Impellitteri et al., 2001; Navas et al., 2005; Carrillo −Gonzalez et al., 2006; Kabata-Pendias, 2011). However, metal behavior in sediments is far from simple, and these characteristics are not always applicable at the same extent, for other regions with different physico-chemical and biological interactions.

Wetlands play a crucial role in the biogeochemistry of trace elements in estuaries and provide a major sink for these elements (Caçador et al., 2009; Vodyanitskii and Shoba, 2015; Bonanno et al., 2018). The Swartkops Estuary is a very important socio-economic and environmental asset and has high biodiversity importance for in terms of fish, birds and plants (Turpie et al., 2002; Adams, 2020). It has a large intertidal salt marsh area and *Salicornia tegetaria* is a dominant species, but it only earns a botanical importance rating of 41–45 out of 100, due to the modifications to the system brought on by the development (Colloty et al., 2000). The accumulation of metals into the bottom sediments make these habitats particularly vulnerable to the impacts of metal toxicity. This is of concern due to the prevalent trend of environmental problems caused by metal pollution, which turns pristine environments toxic (Forstner and Wittman, 1981; Bonanno et al., 2017). However, some plant species can tolerate seemingly toxic metal levels and concentrate them into their below- or above-ground organs (Williams et al., 1994; Olguín and Sánchez-Galván, 2012). Moreover, some plant species can manipulate the bioavailability of metals in the sediments (Reboreda and Caçador, 2007; Duarte et al., 2010). Several wetland plants can also act as bioindicators of metals (Phillips et al., 2015), and can be used in ecological engineering in environmental management strategies. Estuary habitats are some of the most productive in the world and provide several crucial ecosystem services, namely: (1) nursery areas for marine fish, (2) a path for migratory marine and bird species, (3) habitat for important and endangered wetland ecosystems (saltmarsh, mangroves, seagrass beds), (4) transportation for nutrients and organic materials to coastal habitats, (5) carbon sequestration, and (6) the containment of endemic species dependent on the estuarine ecosystem (Roy et al., 2001; Turpie et al., 2002; Barbier et al., 2011; NBA, 2012; Adams, 2020).

A simple question of potential metal contamination in an area can become complicated without historical baseline data for comparison. Separating the naturally occurring metal concentrations from the contaminants is a challenge. Sediment Quality Guidelines (SQGs) are often used to compare current metal concentrations where historical data are unavailable. However, the SQGs are based on concentrations that are adverse to the ecosystem or human activity (Long et al., 1995), and cannot give an indication of *in situ* metal contamination. Sediment with comparably higher concentrations of metals compared to other areas can also not be assumed to be metal-contaminated. The research by Newman and Watling (2007) used these insights as a means to create geochemical baseline models for geological areas of the south-eastern coast of South Africa, between the Kromme Estuary in Cape St. Francis and the Nahoon Estuary in East London. Geochemical normalization compares the metal concentration with a reference element that follows crustal decomposition (Karageorgis et al., 2009). The ratio of metal: normalizer is only comparable due to the stability of the normalizer within the area. Aluminum is often used as a normalizer in estuarine and coastal sediment (Kersten and Smedes, 2002). A stable metal will have little increase or decrease in their concentration. Aluminum concentrations are naturally high in sediment, being the third most abundant element in the earth's crust (Turekian and Wedepohl, 1961; Kring, 1997). The normalizer element can only be used when it's anthropogenic input is negligible (Almeida et al., 2008). Aluminum fits these criteria as anthropogenic inputs are not likely to be significant enough to affect its levels (Schropp et al., 1990). Iron (fourth most abundant element in the earth's crust) is often not suitable, due to its close association with manganese, which concentrates iron in the metal surface (Douglas and Adeney, 2000).

The Swartkops Estuary is located within the Nelson Mandela Metropolitan, South Africa. The estuary flows through highly urbanized and industrialized developments that began in the first quarter of the 19th century (Theal, 2010). Historical data does not include metal baseline concentrations specific to the area, so it is difficult to assess the impacts of industry and urbanization on the biota. Indeed, "there is a lack of baseline data of pollutants in the sediments and biota in the estuaries of South Africa" (NBA, 2012). Instead, studies have compared the metal concentrations to other datasets available from the 1970s—more than 150 years after the initial developments. Studies agree that the rate of metal accumulation has increased throughout the Swartkops Estuary, in some cases more than 100% for Cr, Mn, Pb and Zn (Binning and Baird, 2001). In 2014 high concentrations were found in the juveniles of popular angling fish, selected invertebrates and in the eggs of gull, exceeding the international food quality guidelines, where applicable (Nel et al., 2015). Other than fishing, the estuary has important recreational and ecological importance, providing numerous essential ecosystem services originating from the diverse salt marsh and seagrass habitats. The estuary has high national botanical importance, because of the large intertidal salt marshes (Colloty et al., 2000; Adams, 2020). The ability of the salt marshes to capture and localize metals and other contaminants is important to maintain a healthy ecosystem. Assessing the extent of metal contamination in the area will provide critical information on how the salt marsh habitats are coping as metal sinks, as well as information for environmental management procedures within the estuary. *Salicornia* spp. is good at localizing metals in their roots, preventing metals from entering the food chain (Smillie, 2015). Little research has been done on *S. tegetaria*, a lower intertidal salt marsh species vulnerable to the effect of sea-level rise (Brown and Rajkaran, 2020). In this study, sediment metal concentrations within monoculture stands of *S. tegetaria*, a dominant halophyte within the Swartkops salt marshes, were assessed. The metals analyzed included Al, Cr, Cu, Fe, Mn, Ni, Pb and Zn. The objective of this paper was to investigate the levels of metal contamination within the salt marsh habitat of the Swartkops Estuary. The sediment characteristics were also determined to ascertain the behavior of metals in the salt marsh. In order to determine whether contamination was influenced by anthropogenic sources, a geochemical (normalization) model created by Newman and Watling (2007) was used. This can

potentially indicate the extent of metal contamination in the marsh, between the approximately 40-year-old datasets used for the models.

## MATERIALS AND METHODS

### Study Site and Sampling

Sediment samples were collected on 30 April 2019 and 01 May 2019 from the saltmarsh of the Swartkops Estuary (33°51′11″S; 25°36′53″E), which is a predominantly open warm temperate estuary. Five sites were chosen along the middle and lower reaches of the estuary, according to the distribution of plant species. Point source inputs from surrounding catchment activities occur in close proximity to Motherwell Canal (Site 1), Markman Canal (Site 2), Tiger Bay Launch Site (Site 3), Tipper's Creek (Site 4) and Swartkops Estuary mouth (Site 5) (**Figure 1**). The latter is close to an inactive oyster farm. At each site randomly selected *S. tegetaria* plants were carefully uprooted using a PVC corer (Diameter = 11.2 cm). Sediment samples from the rhizosediment were collected at the surface of the cores and stored in polyethylene jars. Five replicates of the sediment samples were collected at each site. The samples were transported in a cooled and insulated container, to the laboratory on the day of collection.

The Motherwell Canal (Site 1) is the furthest site from the mouth and is located just above the actual canal. The canal is connected to 14 stormwater drains and contains a series of litter traps located at regular intervals. The base of the canal is connected to an artificial wetland, which was built to extract the pollutants from the wastewater flowing down the canal. Large volumes of plastic debris and other litter enter the canal from the surrounding developments. The Motherwell township is located along the canal. Approximately 1 km downstream from Site 1 is the Markman Canal, which transports stormwater effluent from a large industrial area. Site 2 is located downstream from the canal, within a large salt marsh. The Tiger Bay Launch Site (Site 3) is located downstream, on the opposite side of the riverbank. It has an interconnected series of creeks, which contains large stands of eelgrass (*Zostera capensis)*. The Papenkuils River connects to the Swartkops Estuary close to Site 3. This river is very small but flows through a large section of Port Elizabeth (urban and industrial areas) to reach the Swartkops Estuary. The last 8 km of the Papenkuils river is reinforced with concrete, forming a canal. Site

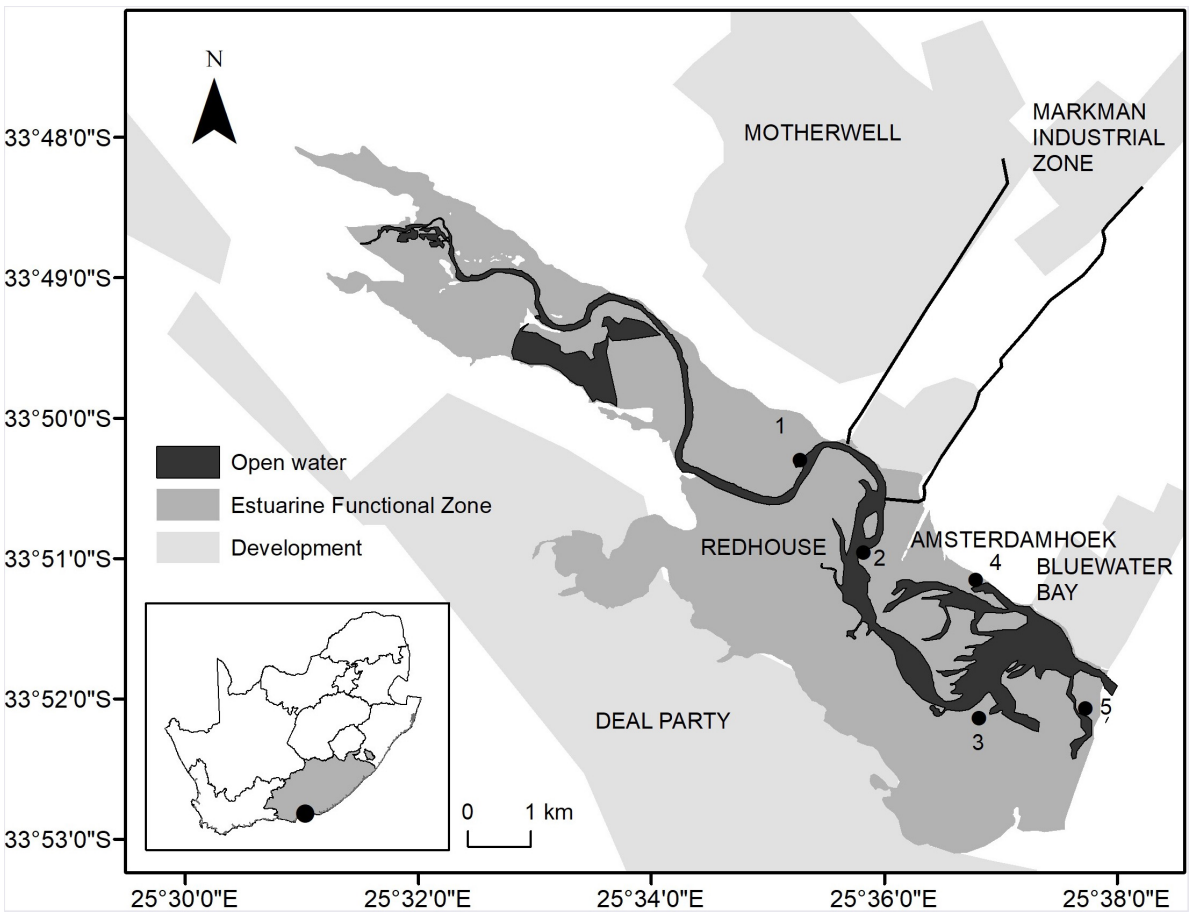


**FIGURE 1 |** Locations of the sampling sites within the Swartkops Estuary: Motherwell Canal (Site 1), Markman Canal (Site 2), Tiger Bay Launch Site (Site 3), Tipper's Creek (Site 4) and Swartkops Estuary Mouth (Site 5).

3 is located adjacent to Site 4, on the other side of the estuary, and next to the wastewater treatment works, which treats urban and industrial effluent. A busy national road is located next to Site 3, and can be followed to a dense neighborhood, Amsterdamhoek, adjacent to the riverbank and Tippers Creek (Site 4). The creek contains numerous jetties and a large mudbank. The Swartkops Estuary mouth is predominantly open. The area is subjected to higher flushing rates, due to the strong marine influence in the area, compared to the rest of the estuary. Site 5 is located next to the estuary mouth, where an inactive oyster farm was located. The catchment lacks any large-scale agricultural activities (Bornman et al., 2016).

## Metal Determination

Total metal extractions were performed using a conventional $HNO_3$ (65%, AR, Merck) digestion in 250 ml glass beakers covered with watch glasses (Du Laing et al., 2003; Phillips et al., 2015). The samples were first freeze-dried using a (Vacutec, V-FD12 Series Freeze Dryer), which dries the sediment at −60°C. The homogenized and dry sample of sediment was pushed through a 1 mm nylon mesh. Then 1.00 g was digested in 10 ml of the 65% $HNO_3$ overnight, and afterward on a hotplate for 5 h at 110°C. After evaporation to near dryness the sample was diluted with 20 ml of 2% (v/v $H_2O$) nitric acid and transferred to 50 ml volumetric flasks, after filtering with Whatman® glass fiber filters (GF/F, pore size = 0.7 μm), and diluted to the mark with Milli-Q ultra-pure water.

Extracts were analyzed for the selected metals using an Inductively Coupled Plasma-Optical Emission Spectrometer (ICP-OES, PerkinElmer®, Avio™ 200) by the aspiration of the sample into an argon generated plasma. The analytical wavelengths used were (in nanometer): Al (396.2), Cr (357.9), Cu (224.7), Fe (302.1), Mn (259.4), Ni (221.6), Pb (217.0) and Zn (206.2). Detection limits for the selected metals (in $\mu g\ L^{-1}$) were directly obtained from the ICP-OES program: Al (28), Cr (23), Cu (7.7), Fe (20), Mn (1.6), Ni (10), Pb (90) and Zn (5.9). Method blanks were prepared by using the same digestion procedure as the samples and were subtracted from the results during analysis. Blanks and concurrent analysis of standards were used to detect possible contamination during analysis. The samples were measured in triplicate and obtained in ppm. Due to the magnitude of Al and Fe, they were reported in mg $g^{-1}$, whereas the rest of the metals were reported in $\mu g\ g^{-1}$.

## Sediment Characteristics

Sediment pH was measured using a handheld Hanna (Hanna® Instruments, HI98121 Tester) *in situ*, on the surface sediment, upon collection. All instruments were calibrated and cleaned according to the manufacturer's specifications. Other sediment characteristics were measured in the laboratory; sediment organic content (%), conductivity (μS) and granulometric size. Organic content of the sediment was measured using the loss on ignition method described in Veres (2002) with 10 g of wet sediment (Eq. 1). The samples were freeze-dried using a (Vacutec, V-FD12 Series Freeze Dryer). Sediment salinity was measured conductometrically by mixing a ratio of 250 g dried sediment to 100 ml distilled water, or until saturation, according to the specification in Bernard (1990). The mixture was then filtered through Whatman No.1 filter papers and the electrical conductivity was measured using a handheld conductivity meter (CyberScan, HANNA handheld conductivity meter). Granulometric size was also determined with the dry sediment using the sieve method (Wentworth, 1922). All samples were analyzed in triplicate.

$$\%\ \mathrm{TOM} = [(\text{dry mass before combustion} - \text{dry mass after combustion})/\text{dry mass}] \times 100 \quad (1)$$

## Statistical Analysis

The analyses of variance (ANOVA, random effects) was used to test for differences in the total concentrations of metals, the percentage total organic matter (TOM), pH and salinity. Tukey's *post hoc* test was then used to compare the means where significant differences were found. The assumptions of normality were verified before analysis with the Shapiro-Wilks test accompanied with the respective histograms. Variables were log transformed (Log[M], where M is the concentration of the selected metal) if the null hypothesis for normality was rejected. Metal enrichment was determined using metal-Al baseline relationships for coastal sediment in the region that included the study site (between the Kromme Estuary and the Sundays Estuary). The regressions were modeled by Newman and Watling (2007). Scatterplots of the metal data were overlain with the straight-line equations provided. Points above the baseline are considered enrichment. Non-metric multidimensional scaling (NMDS) was performed on the metal concentrations and the environmental factors (i.e., the sediment characteristics) were overlain as vectors, to show the degree of influence of the environmental characteristics on the metals and the sites. Statistical processing was performed in RStudio (R version 3.5.1 and 4.0.2), a product of RProject using the R-commander (Version 2.6-2) with the packages Vegan, RColorBrewer, Tidyverse and Geoveg.

# RESULTS

## Metal Concentrations

Considering the metal concentration in the sediment, Site 4 had the highest concentrations of metals in the sediment with no exceptions, followed by Site 3 (**Table 1**). The lowest concentrations were measured in Site 5, with the exception of Zn, where the lowest value occurred in Site 1. These differences were for the most cases significant ($p < 0.05$), however, Zn concentrations had no statistical difference across all the sites. Other cases where Site 5 did not contain the statistically lowest concentration was: Cr and Cu (Site 1 and Site 2; $p > 0.05$), and Mn (Site 1; $p > 0.05$) Contrastingly, the metal normalizer (Al), showed statistical differences across all sites with the exception of Site 2 and Site 3 ($p > 0.05$).

**TABLE 1 |** Average metal concentrations (Al, Fe = mean mg $g^{-1}$ ± SD; Cr, Cu, Mn, Ni, Pb, Zn = mean μg $g^{-1}$ ± SD) of the surface sediment at the sampling sites ($N = 15$).

| [M] | Site 1 | Site 2 | Site 3 | Site 4 | Site 5 |
|---|---|---|---|---|---|
| Al | $8.8 \pm 0.2^{a}$ | $15.1 \pm 0.3^{b}$ | $20.3 \pm 6.4^{b}$ | $42.1 \pm 2.8^{c}$ | $2.1 \pm 0.2^{d}$ |
| Fe | $18.1 \pm 6.3^{a}$ | $24.8 \pm 1.4^{a}$ | $30.2 \pm 7.1^{a}$ | $58.0 \pm 4.6^{b}$ | $5.1 \pm 0.9^{c}$ |
| Cr | $21.7 \pm 5.6^{a}$ | $26.6 \pm 0.3^{a,c}$ | $42.3 \pm 15.0^{a}$ | $99.4 \pm 2.2^{b}$ | $14.1 \pm 2.5^{c}$ |
| Cu | $36.9 \pm 7.1^{a,c}$ | $39.7 \pm 3.9^{a,c}$ | $52.0 \pm 9.1^{a}$ | $85.6 \pm 7.6^{b}$ | $18.4 \pm 3.0^{c}$ |
| Mn | $110.9 \pm 55.6^{a,c}$ | $283.1 \pm 34.3^{a,b}$ | $286.6 \pm 49.4^{a,b}$ | $379.1 \pm 103.1^{b}$ | $33.9 \pm 0.3^{c}$ |
| Ni | $10.3 \pm 2.7^{a}$ | $10.5 \pm 0.7^{a}$ | $14.7 \pm 3.3^{a}$ | $24.4 \pm 1.8^{b}$ | $2.5 \pm 0.3^{c}$ |
| Pb | $48.3 \pm 12.9^{a}$ | $60.8 \pm 2.8^{a}$ | $89.3 \pm 27.1^{a}$ | $187.5 \pm 19.1^{b}$ | $14.8 \pm 1.8^{c}$ |
| Zn | $90.9 \pm 20.5^{a}$ | $93.4 \pm 4.9^{a}$ | $104.5 \pm 24.9^{a}$ | $136.6 \pm 16.0^{a}$ | $98.6 \pm 23.2^{a}$ |

*Different letters (a, b, c, d) indicate significant differences between values of the same element within the five sites ($p < 0.05$).*

## Sediment Characteristics

**Figure 2A** show the separation of the metal concentrations in Site 5 to the rest of the sites. The NMDS showed a good fit with a stress value <0.05. Similarities occurred between Site 2 and Site 3, seen by the overlap of the diagram in the figure. The sediment characteristics had different degree of influence on the metal concentrations in the sites. Gravel, pH and organic matter showed significant results ($p < 0.05$). The environmental vector representing percentage gravel showed the greatest influence in Site 1, while pH and total organic matter showed the greatest influence in Site 2 and Site 3. The metal concentrations all differed from each other (**Figure 2B**), but according to the environmental vectors do not point directly at the type of metals. The exception is Mn, where the significant vector, total organic matter, is directed to it.

Total organic matter (TOM) was highest at Site 3 (6.32 ± 0.008%) and the lowest at Site 5 (2.89 ± 0.003%; **Figure 3**). These sites also displayed the highest (41.53%) and lowest (1.40%) silt/clay content, respectively. The difference was significant according to statistical processing ($p < 0.05$). The other sites displayed no significant statistical differences in TOM. The grain size distribution was reasonably similar throughout the sites except for Site 3 and Site 5. The latter having a much coarser grain than the other sites. Gravel was not present in Site 1 and Site 2 and was negligible in Site 4 and Site 5 (<0.1%). Site 3 had the highest gravel content but did not exceed 2%.

The pH differed across the sites (**Figure 4A**). The lowest pH was found in Site 4 (7.3 ± 0.1), while the highest was in Site 5 (8.3 ± 0.1) and they differed significantly from each other ($p < 0.001$). The pH of Site 4 was also lower than Site 2 and Site 3 ($p < 0.05$), and Site 5 had a higher pH than Site 1 ($p < 0.05$). The salinity (μS; **Figure 4B**) did not differ significantly between sites according to statistical testing. The lowest salinity was measured in Site 1 (6.6 ± 0.9), while the highest in Site 2 and Site 4 (10.8 ± 0.6 and 10.8 ± 1.3; **Figure 4**).

## Metal Contamination

The majority of the metals are higher than the baseline (**Figure 5**). Cu, Cr, Fe, Pb, and Zn show enrichment across all the sites. Cr is notably much higher than the baseline in Site 4 compared to the other sites and does not follow the trend of the baseline (**Figure 5B**). Cu, Pb, and Fe plots deviate from the gradients of the baseline, indicating that the metal concentration increases more steeply with the metal normalizer, than the baseline suggested (**Figures 5A–C**). The majority of the points fall above the baseline for Mn and Ni however, the exceptions occur in Site 1 and Site 4 for Mn and Site 4 for Ni (**Figures 5D,E**). The plots for the latter metal, Ni follows the baseline closely.

# DISCUSSION

This study measured six of the most common metal contaminants in the Swartkops Estuary i.e., Al, Cr, Pb, Mn, Ni and Zn (Strawn et al., 2015). The average metal concentrations in this study follows a decreasing order of Fe > Al > Mn > Zn > Pb > Cu > Cr > Ni (**Table 1**). The five sites within the estuary showed a 46% average increase in metal concentrations (Cr, Cu, Mn, Pb, Zn) over the past 23 years (Binning and Baird, 2001). The same study compared the 1996 dataset with another in 1979, and found an average increase of 149% in metal concentrations between them. Previous authors agree that the anthropogenic activities surrounding the estuary are to blame for the increases (Baird et al., 1986; Binning and Baird, 2001; Phillips et al., 2015). However, metals also occur naturally in the sediment due to the weathering of rock (Kabata-Pendias, 2011). Some metals such as Al and Fe, form a large part of the sediment matrix, and occur in much higher concentrations that the other metals (Newman and Watling, 2007). The Al and Fe concentrations ranged from 2.1–42.1 mg $g^{-1}$ to 5.1–58.0 mg $g^{-1}$ (**Table 1**), respectively. Newman and Watling (2007) established that Fe contamination is prevalent in the Swartkops Estuary. The Al concentrations measured in this study were of a comparable range to previous studies (0–40 mg $g^{-1}$), which also confirms that no significant Al contamination has occurred in the middle and lower reaches of the estuary (Watling and Watling, 1979, 1982; Newman and Watling, 2007). Gyedu-Ababio (2011) reported much lower Fe concentrations in the sediment of the Swartkops Estuary (1.9 mg $g^{-1}$–16.42 mg $g^{-1}$), but is still comparable where sites correspond. Manganese concentrations ranged from 33.9 to 379.1 μg $g^{-1}$ in this study. Iron and Mn oxides play an important role in scavenging other metals such as Cu, Ni, Pb and Zn from solution (Vesper, 2012). Gyedu-Ababio (2011) also found Mn concentrations between 64 and 229 μg $g^{-1}$,

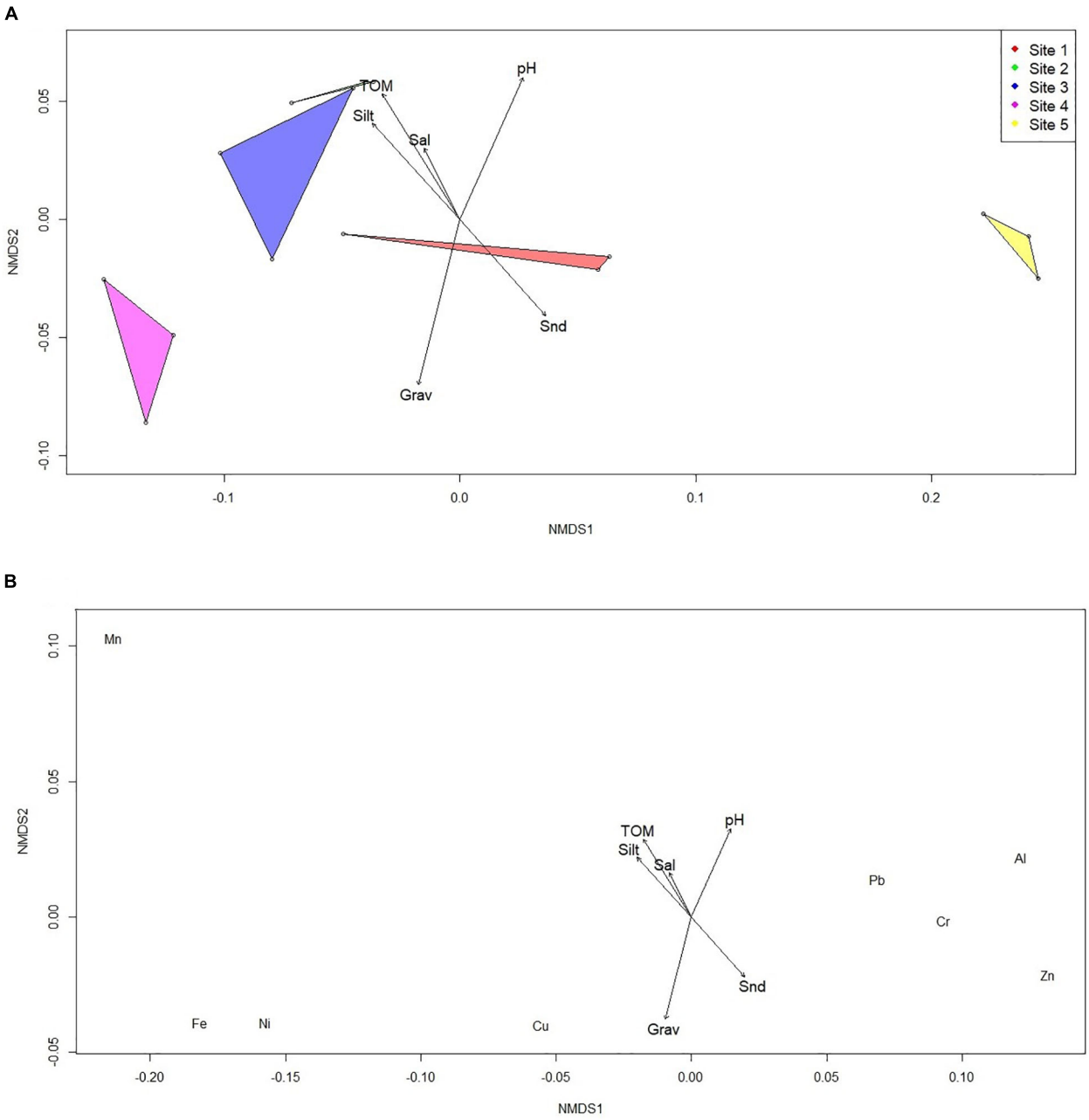


**FIGURE 2 |** NMDS of **(A)** metal concentration per site and **(B)** metal concentrations per metal type with an overlay of the sediment characteristics (where: TOM, Total Organic Matter; Sal, salinity; Silt, percentage silt and clay; Snd, percentage sand; Grav, percentage gravel, and pH).

previously in the estuary. The concentrations reported by this author are also lower for Mn, but is again comparable where the sites correspond.

Lead concentrations in this study ranged from 14.8 to 187.5 $\mu g\ g^{-1}$ of sediment, showing a 47% increase from 1996 (**Table 1**). High loads of Pb were associated with the stormwater originating from high density, low-income settlements in entering False Bay, South Africa (MacKay, 1994). This may be the case in the Swartkops Estuary, as stormwater and effluent from the Wastewater Works enters the system. Another source of Pb contamination is the highway, as automobile exhaust gas is a well-known source of Pb aerosol (Mielke et al., 2010). Site 4 was the only site in which Pb concentrations exceeded Zn concentrations—owed to its proximity to an urban roadway. Lead concentrations in this study were much higher than that reported by Phillips et al. (2015)—maximum concentrations differed by approximately 60 $\mu g\ g^{-1}$ (or 16%) of sediment. In both these cases, the maximum concentrations were located close

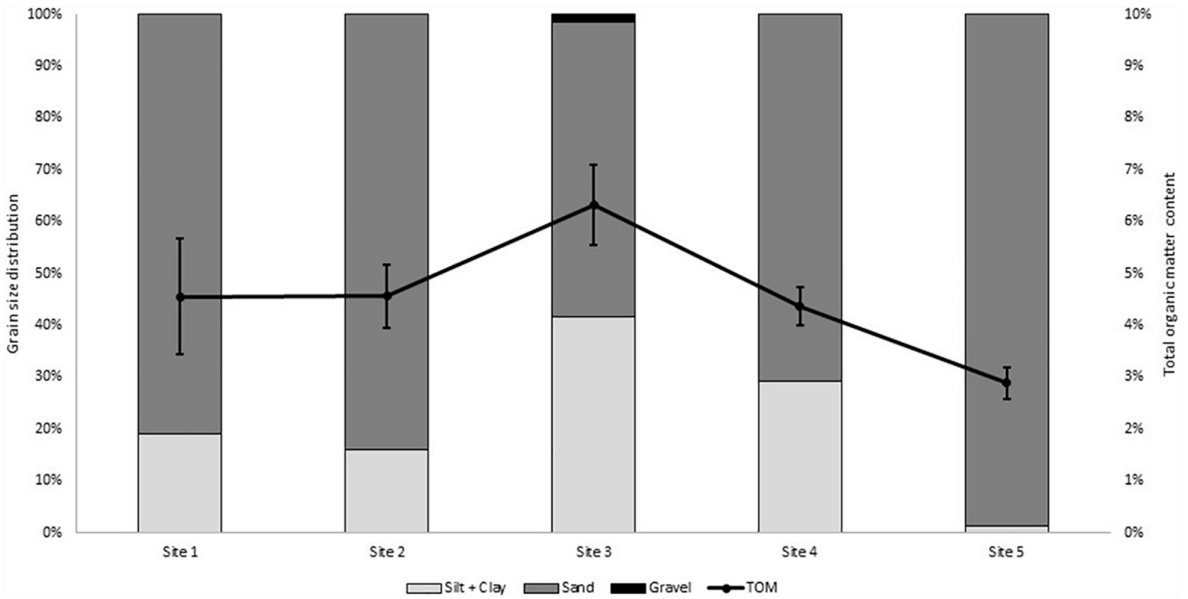


**FIGURE 3 |** Grain size distribution and average organic matter content (%TOM ± SD; $N = 15$) of the surface sediment in the salt marsh, along five sites in the estuary.

to highways and roads, that is; Redhouse and Tippers Creek (Site 4; **Figure 1** and **Table 1**). Copper, Pb, Ni and Zn are the most commonly measured metals in the estuary. Copper and Zn concentrations ranged from 18.4–85.6 $\mu g\ g^{-1}$ to 93.4–136.6 $\mu g\ g^{-1}$. Binning and Baird (2001) indicated that Cu and Zn pollution enters the system in the freshwater reaches, from the industries in Uitenhage (**Figure 1**). Phillips et al. (2015) found their highest Cu and Zn concentrations (51.5 $\mu g\ g^{-1}$ and 112.9 $\mu g\ g^{-1}$, respectively) in the Upper Markman Canal, which carries effluent from industries into the estuary.

There are multiple point sources in the Swartkops Estuary, and most prominent is the effluent from the Markman (industrial) Canal, the stormwater from the Motherwell Canal, treated effluent from the Fishwaterflats Wastewater Treatment Works, and contaminated water from the Papenkuils River. However, the data indicates that the highest metal concentrations were measured in Site 4 (Tippers Creek), which is downstream from the two point-sources mentioned first. Site 3, also downstream from the two main point sources, contained the second highest metal concentrations in the estuary. The Papenkuils River connects to the Swartkops Estuary at this site. Watling and Emmerson (1981) found higher concentrations of Cu, Zn, Cr and Pb in the Papenkuils than in the estuary. Both sites are located within creeks and between two motorway bridges, that carry heavy traffic. The bridges are one of the factors that cause heavy sediment accretion in Site 3 and Site 4 (Esterhuysen and Rust, 1987). Sediment accretion in Site 4 is further enhanced by the jetties, which also trap sediment and creates a large sand bank against the concrete wall, adjacent to the urban area, Amsterdamhoek (**Figure 1**). The obstructed flow of water entering the creek is therefore trapped between the artificial concrete bank with the jetties and the large sand bank in the middle of the estuary. According to Esterhuysen and Rust (1987), both Site 3 and Site 4 are conducive to trapping sediment and other particles that flow downstream. These conditions make the sites favorable to trap particles containing metals, as well as capturing soluble metals from the overlaying water column. The extensive root system of *S. tegetaria* can also trap sediment particles that flow down river, creating an ideal environment to act as a metal sink. The metals trapped within the creeks may most likely originate from the Motherwell Canal and the Markman Canal, which transports effluent from low-income settlements and large industries, respectively. Indeed, Watling and Watling (1982) and Nel et al. (2015) both formed the conclusion that pollutants transported into Tippers Creek (Site 4) may be incompletely flushed by tidal action and may have resulted in its build-up over time. Adams et al. (2019) recommended Tippers Creek as a long-term metal monitoring site.

Each of the five sites sampled in the estuary show distinct differences, and general similarities (**Figure 2A**). Metal concentrations in Site 2 and Site 3 are the most similar, depicted by the overlap in **Figure 2A**. Site 4 is distinctly dissimilar from Site 2 and Site 3, just emphasizing the extremely high metal concentrations found here. The lowest metal concentrations in Site 5 can also distinctly be seen, as the diagram is far removed from the other sites. The sediment characteristics of the given sites largely affect the capacity of the sediment to accumulate metals. Contrastingly, it also dictates the potential for leaching (or flushing) and the bioavailability (or mobility) of the metal to plants and other biota. Authors are still debating which sediment characteristics are the most important determinant of the element's form (Kabata-Pendias, 2011), however, pH, carbonates and Fe and Mn oxides greatly influence the behavior

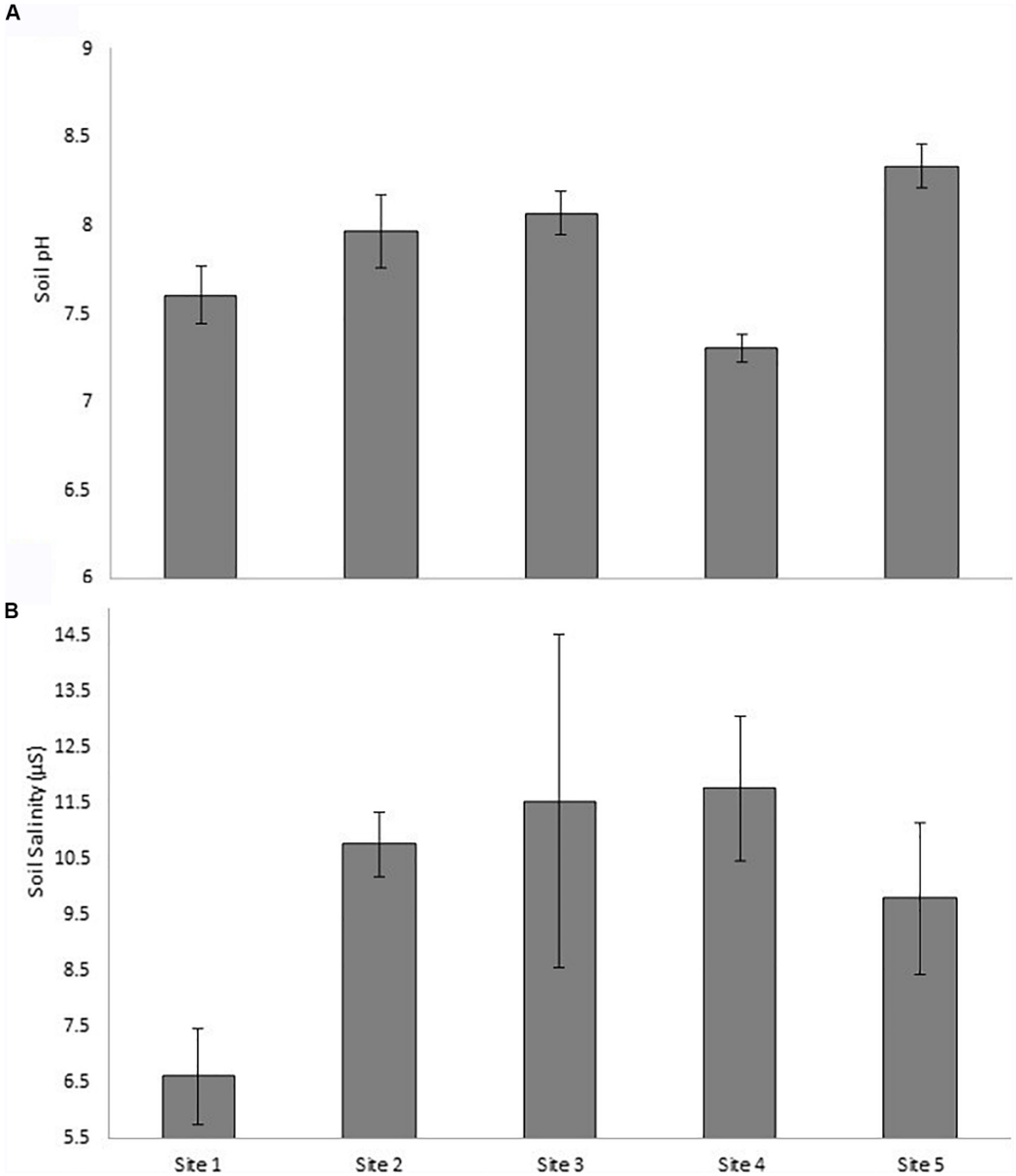


**FIGURE 4 |** Average sediment pH and salinity (µS) at each of the five sites, of the surface sediment in the salt marsh, with error bars (±SD; $N = 15$).

of chemical elements (Shine et al., 1995; Li et al., 2013). Others suggest that it is pH, redox potential and organic matter that are the most important in sediments (Hermann and Neumann-mahlkau, 1985; Strawn and Sparks, 2000). In this study, the gravel content, pH and organic matter content had the most significant effect on the metal behavior. Copper and Pb did not form a close association with the total organic matter content as would be expected (**Figure 2B**; Duarte et al., 2010; Wyatt and Stevenson, 2010; Human et al., 2020), but metal behavior in sediment is complex, and the other characteristics and unmeasured factors cannot be ignored. The pattern of the environmental vectors in **Figure 2B** would suggest that the sediment characteristics play a dynamic part in the metal form.

The study sites are dominated by the larger grain sizes, sand (Avg% sand > 50%; **Figure 3**). Bradley and Morris (1990), who studied salt marshes across the Eastern United States of America, also found that the salt marshes tend to be dominated by sand. This agrees with previous assessments of the middle and lower reaches of the Swartkops Estuary (Reddering et al., 1981; Els, 2020). Reddering et al. (1981) indicated that the sand originates by tidal transportation from the sea. Large grain size (sand) in sediments usually present lower levels of metal accumulation (Williams et al., 1994; Zhang et al., 2001). Contrastingly, higher percentages of the finer particles (clays and silt), increases the metal binding capacity of cationic metals onto the negatively charged surfaces (Ujeviæ et al., 2000). The binding capacity of

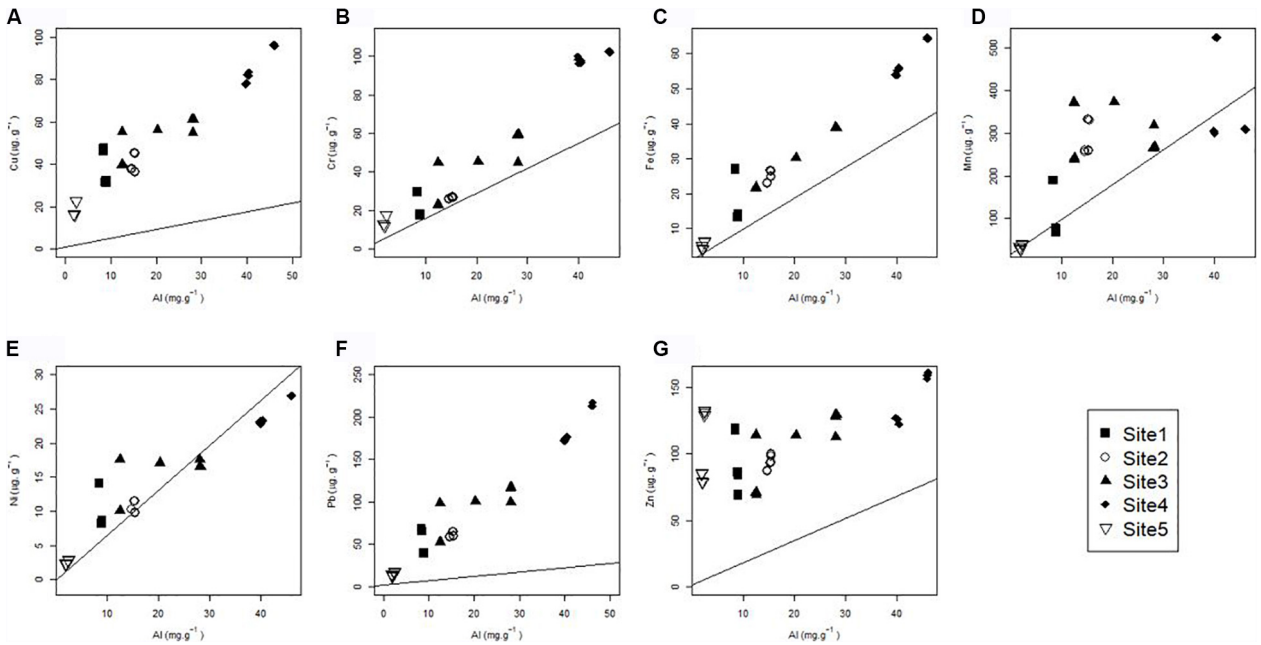


**FIGURE 5 |** Total individual metal content **(A)** Cu, **(B)** Cr, **(C)** Fe, **(D)** Mn, **(E)** Ni, **(F)** Pb and **(G)** Zn against the concentration of the metal normalizer (Al), in the surface sediment colonized by *S. tegetaria*. The scatterplot represents the different metal concentrations per site and is overlain with the linear models created by Newman and Watling (2007).

smaller sediment particles are so significant due to the high specific surface area creating more binding sites for metals (Lin et al., 2003). In this study, the estuary mouth (Site 5) had the highest sand content at 97%, while Site 3 had lowest at 57% followed by Site 4 at 82% (**Figure 3**). Site 3 and Site 4 contained the only silt and clay content above 17%; that is 41.5 and 33.8%, respectively (**Figure 3**). This may indicate a higher degree of fluvial sediment in-put in at these sites, previously established as trapping sediment and other particles flowing downstream. High sand content in the estuary increases the potential of metals to be leached to the water column and transported downstream. This may occur in Site 1 and Site 2 (% sand >80%), where two of the point sources occur (Motherwell Canal and Markman Canal). The metals may thereafter be captured and accumulated by the higher silt/clay content in Site 3 and Site 4.

The organic content of sediments in this study is very low but followed a similar pattern as the grain sizes. The highest value is 6.3% at Site 3 and the lowest value is 2.9% at Site 5 (Estuary Mouth). The organic matter content in Site 4 fell just below the average at 4.4%. Bradley and Morris (1990) indicated that these values are natural, as they found organic matter ranges from 2 to 16% in salt marshes. A recent study in the Swartkops Estuary found similar organic matter content (Els, 2020). Organic matter plays a significant role in metal accumulation. Low organic matter content in sediments usually presents lower levels of metal accumulation (Williams et al., 1994). Higher percentages of organic matter increases the metal binding capacity of cationic metals by forming insoluble complexes with the metals (Ujeviæ et al., 2000). Copper and Pb in general prefer to bind to sediment organic matter, creating complexes with the humic acids that form part of sediment organic matter (Duarte et al., 2010; Wyatt and Stevenson, 2010; Human et al., 2020). Although, Cu and Pb's association with sediment organic matter is strong, other metals also form bonds with it due to the high specific surface area provided by the sediment organic matter (Lin et al., 2003).

Lastly, the pH and salinity in the rhizosediment of the salt marsh ranged between 7.3–8.3 and 6.6–11.8 μS, respectively (**Figure 4**). The highest pH was found at the mouth (Site 5) and the lowest at Site 4, though the latter is not quite acidic. Acidity increases the mobility of cationic metals—creating conditions conducive to the leaching of these metals into the water column (Williams et al., 1994). It is due to the adsorption and desorption mechanisms onto sediment surfaces that are largely controlled by pH (Li et al., 2013). However, Eh (redox potential) also has an important relationship with metal mobility, and in cases where pH is alkaline and Eh is highly positive, metals can become immobile before reverting to a mobile anionic metal species (Hermann and Neumann-mahlkau, 1985; Kabata-Pendias, 2011). The pH requirements to form an ionic Cu species ($Cu_2O_2^{2-}$) is above 12 and did not occur in this dataset (Hermann and Neumann-mahlkau, 1985). The salinity remained fairly constant within the sites, however, Site 1, being the uppermost site showed significantly lower salinity. Fritioff et al. (2005) found that metals become more bioavailable for submersed plants (like *S. tegetaria*) with decreasing salinity and increasing temperature. Lower salinity and high sand content in upper sites, close to the point sources (Motherwell Canal and Markman Canal), creates conditions that enhance metal mobility, and therefore its transport to the lower reaches of the estuary.

For this study, the baseline models indicate that all the sites are metal enriched—where metal concentrations fall above the baseline (**Figure 5**). The exceptions are for Mn (Site 4 and Site 1), and Ni in Site 4 and Site 2 (**Figures 5D,E**). Copper, Pb and Zn in particular show high enrichment throughout all the sites, with the exception of Pb, which had low concentrations at the mouth (**Figures 5A,F,G**). The sites with the highest concentrations, Site 3 and Site 4, show anomalous Cu, Cr, Fe, Pb and Zn levels. The mouth (Site 5), which contained the lowest metal concentrations, show enrichment in Cu, Cr, Fe, Ni, Pb and Zn. Some of these data points fall close to the baseline, which may indicate that the enrichment in Site 1 is not that large, however, Cu and Zn are of particular concern (**Figures 5A,G**). An outfall, located 1 km SSW from the estuary mouth is a source of contamination, and waste is transported to Site 5 through the connected bay (Emmerson et al., 1983). The outfall contains treated urban and industrial effluent from the wastewater treatment works. However, with the presence of sediment characteristics conducive to leaching and the marine turbulence at the mouth, the contamination at the mouth has not reached critical levels. The same cannot be said for the middle and lower reaches (Site 1–Site 4) that have metal concentrations far exceeding the baseline.

## CONCLUSION

This study investigated the levels of metal contamination within the salt marsh habitat of the Swartkops Estuary. From the baseline models it is clear that the pollution is of anthropogenic origin and the estuary is highly enriched by metal contamination resulting from the vast array of urban and industrial settlements, which releases effluent into the estuary. It follows that the gravel content, pH and organic matter content had the most significant effect on the metal behavior. Considering the above observations, it can be concluded that the rhizosediment of *S. tegetaria* acts as a metal sink and localizes the contamination of metals to a large extent thereby performing an important ecosystem service. Management practices are crucial at this stage of development as high concentrations of metals leading to metal enrichment can restrict some recreational activities, in and around the estuary.

## DATA AVAILABILITY STATEMENT

The raw data supporting the conclusions of this article will be made available by the authors, without undue reservation.

## AUTHOR CONTRIBUTIONS

MN wrote the article and did the laboratory analysis. MN and LH contributed to the field analysis, while the latter also conceptualized the research. LH, JA, MN, and GR provided conceptual and editorial inputs on the manuscript and discussed field methodology. All authors contributed to the article and approved the submitted version.

## FUNDING

MN was supported by a scholarship from the National Research Foundation of South Africa (Grant Number: 116920). This work was supported by the Shallow Marine and Coastal Research Infrastructure (SMCRI) platform hosted by the South African Environmental Observation Network Elwandle Node (SAEON). The publication fees for this article was paid for by NRF Incentive Funding (Grant Number: 119449).

## ACKNOWLEDGMENTS

The authors wish to thank the Shallow Water Ecosystem research group (funded by UID 84375DSI/NRF Research Chair) for assistance in the laboratory and field.

## REFERENCES

Adams, J. B. (2020). Salt marsh at the tip of Africa: patterns, processes and changes in response to climate change. *Estuar. Coast. Shelf Sci.* 237:106650. doi: 10.1016/j.ecss.2020.106650

Adams, J. B., Pretorius, L., and Snow, G. C. (2019). Deterioration in the water quality of an urbanised estuary with recommendations for improvement. *Water SA* 45, 86–96. doi: 10.4314/wsa.v45i1.10

Almeida, C. M. R., Mucha, A. P., Bordalo, A. A., and Vasconcelos, M. T. S. D. (2008). Influence of a salt marsh plant (*Halimione portulacoides*) on the concentrations and potential mobility of metals in sediments. *Sci. Total Environ.* 403, 188–195. doi: 10.1016/j.scitotenv.2008.05.044

Baird, D., Hanekom, N., and Grindley, J. (1986). "Report No. 23: swartkops (CSE 3)," in *Estuaries of the Cape, Part 2: Synopsis of Available Information Individual Systems.*CSIR Research Report No. 422, eds A. E. F. Heydorn and J. R. Grindley (New Delhi: CSIR).

Barbier, E. B., Hacker, S. D., Kennedy, C., Koch, E. W., Stier, A. C., and Silliman, B. R. (2011). The value of estuarine and coastal ecosystem services. *Ecol. Monogr.* 81, 169–193. doi: 10.1890/10-1510.1

Basta, N. T., Ryan, J. A., and Chaney, R. L. (2005). Trace element chemistry in residual-treated soil: key concepts and metal bioavailability. *J. Environ. Qual.* 34, 49–63. doi: 10.2134/jeq2005.0049dup

Bernard, R. O. (1990). *Handbook of Standard Soil Testing Methods for Advisory Purposes*. Pretoria: Sediment Science Society of South Africa.

Binning, K., and Baird, D. (2001). Survey of heavy metals in the sediments of the Swartkops River Estuary, Port Elizabeth South Africa. *Water SA* 27, 461–466. doi: 10.4314/wsa.v27i4.4958

Bonanno, G., Borg, J. A., and Di Martino, V. (2017). Levels of heavy metals in wetland and marine vascular plants and their biomonitoring potential: a comparative assessment. *Sci. Total Environ.* 576, 796–806. doi: 10.1016/j.scitotenv.2016.10.171

Bonanno, G., Vymazal, J., and Cirelli, G. L. (2018). Translocation, accumulation and bioindication of trace elements in wetland plants. *Sci. Total Environ.* 631–632, 252–261. doi: 10.1016/j.scitotenv.2018.03.039

Bornman, T. G., Schmidt, J., Adams, J. B., Mfikili, A. N., Farre, R. E., and Smit, A. J. (2016). Relative sea-level rise and the potential for subsidence of the Swartkops Estuary intertidal salt marshes, South Africa. *S. Afr. J. Bot.* 107, 91–100. doi: 10.1016/j.sajb.2016.05.003

Bradley, P., and Morris, J. (1990). Physical characteristics of salt marsh sediments: ecological implications. *Mar. Ecol. Prog. Ser.* 61, 245–252. doi: 10.3354/meps061245

Brown, C. E., and Rajkaran, A. (2020). Biomass partitioning in an endemic southern African salt marsh species *Salicornia tegetaria* (Chenopodiaceae). *Afr. J. Aquat. Sci.* 45, 41–48. doi: 10.2989/16085914.2019.1687419

Caçador, I., Caetano, M., Duarte, B., and Vale, C. (2009). Stock and losses of trace metals from salt marsh plants. *Mar. Environ. Res.* 67, 75–82. doi: 10.1016/j.marenvres.2008.11.004

Carrillo −Gonzalez, R., Simunek, J., Sauve, S., and Adriano, D. (2006). Mechanisms and pathways of trace element mobility in soils. *Adv. Agron.* 91, 111–178. doi: 10.1016/S0065-2113(06)91003-7

Colloty, B. M., Adams, J. B., and Bate, G. C. (2000). The use of a botanical importance rating to assess changes in the flora of the Swartkops Estuary over time. *Water SA* 26, 171–180.

Crane, R. A., Sinnett, D. E., Cleall, P. J., and Sapsford, D. J. (2017). Physicochemical composition of wastes and co-located environmental designations at legacy mine sites in the south west of England and Wales: implications for their resource potential. *Resour. Conserv. Recycl.* 123, 117–134. doi: 10.1016/j.resconrec.2016.08.009

Douglas, G. B., and Adeney, J. A. (2000). Diagenetic cycling of trace elements in the bottom sediments of the Swan River Estuary, Western Australia. *Appl. Geochem.* 15, 551–566. doi: 10.1016/S0883-2927(99)00070-0

Doyle, M. O., and Otte, M. L. (1997). Organism-induced accumulation of iron, zinc and arsenic in wetland soils. *Environ. Pollut.* 96, 1–11. doi: 10.1016/S0269-7491(97)00014-6

Du Laing, G., Tack, F. M. G., and Verloo, M. G. (2003). Performance of selected destruction methods for the determination of heavy metals in reed plants (*Phragmites australis*). *Anal. Chim. Acta* 497, 191–198. doi: 10.1016/j.aca.2003.08.044

Duarte, B., Caetano, M., Almeida, P. R., Vale, C., and Caçador, I. (2010). Accumulation and biological cycling of heavy metal in four salt marsh species, from Tagus estuary (Portugal). *Environ. Pollut.* 158, 1661–1668. doi: 10.1016/j.envpol.2009.12.004

Els, J. (2020). *Carbon and Nutrient Storage of the Swartkops Estuary Salt Marsh and Seagrass Habitats*. Port Elizabeth: Nelson Mandela University.

Emmerson, W. D., McLachlan, A., Watling, H. R., and Watling, R. J. (1983). Some ecological effects of two sewrage outfalls in Algoa Bay. *Water SA* 9, 23–30.

Esterhuysen, K., and Rust, I. C. (1987). Channel migration in the lower Swartkops estuary. *S. Afr. J. Sci.* 83, 521–525.

Forstner, U., and Wittman, G. T. W. (1981). *Metal Pollution in the Aquatic Environment*. Berlin: Springer-Verlag.

Fritioff, Å, Kautsky, L., and Greger, M. (2005). Influence of temperature and salinity on heavy metal uptake by submersed plants. *Environ. Pollut.* 133, 265–274. doi: 10.1016/j.envpol.2004.05.036

Gyedu-Ababio, T. K. (2011). Pollution status of two river estuaries in the Eastern Cape, South Africa, based on benthic meiofauna analyses. *J. Water Resour. Prot.* 3, 473–486. doi: 10.4236/jwarp.2011.37057

Hermann, R., and Neumann-mahlkau, P. (1985). The mobility of zinc, cadmium, copper, lead, iron and arsenic in ground water as a function of redox potential and pH. *Sci. Total Environ.* 43, 1–12. doi: 10.1016/0048-9697(85)90027-0

Human, L., Feijão, E., de Carvalho, R. C., Caçador, I., Reis-Santos, P., Fonseca, V., et al. (2020). Mediterranean salt marsh sediment metal speciation and bioavailability changes induced by the spreading of non-indigenous *Spartina patens*. *Estuar. Coast. Shelf Sci.* 243:106921. doi: 10.1016/j.ecss.2020.106921

Impellitteri, C. A., Allen, H. E., Yin, Y., You, S. J., and Saxe, J. K. (2001). "Soil properties controlling metal partitioning," in *Heavy Metals Release in Soils*, eds H. M. Selim and D. L. Sparks (New York, NY: Lewis Publishers), 149–165. doi: 10.1201/9781420032611.ch7

Kabata-Pendias, A. (2011). *Trace Elements in Soils and Plants*, 4th Edn. Boca Raton: CRC Press.

Karageorgis, A. P., Katsanevakis, S., and Kaberi, H. (2009). Use of enrichment factors for the assessment of heavy metal contamination in the sediments of Koumoundourou Lake, Greece. *Water. Air. Soil Pollut.* 204, 243–258. doi: 10.1007/s11270-009-0041-9

Kersten, M., and Smedes, F. (2002). Normalization procedures for sediment contaminants in spatial and temporal trend monitoring. *J. Environ. Monit.* 4, 109–115. doi: 10.1039/b108102k

Kring, D. A. (1997). "Composition of Earth's continental crust as inferred from the compositions of impact melt sheets," in *Proceedings of the Twenty-Eighth Lunar and Planetary Science Conference*, Houston, TX, 1–2.

Li, Y., Kang, C., Chen, W., Ming, L., Zhang, S., and Guo, P. (2013). Thermodynamic characteristics and mechanisms of heavy metals adsorbed onto urban soil. *Chem. Res. Chin. Univ.* 29, 42–47. doi: 10.1007/s40242-013-2200-1

Lin, J. G., Chen, S. Y., and Su, C. R. (2003). Assessment of sediment toxicity by metal speciation in different particle-size fractions of river sediment. *Water Sci. Technol.* 47, 233–241. doi: 10.2166/wst.2003.0694

Long, E. R., Macdonald, D. D., Smith, S. L., and Calder, F. D. (1995). Incidence of adverse biological effects within ranges of chemical concentrations in marine and estuarine sediments. *Environ. Manage.* 19, 81–97. doi: 10.1007/BF02472006

MacKay, H. (1994). *Management of Water Quality in an Urban Estuary*. Ph.D. thesis, University of Port Elizabeth, Port Elizabeth.

Mielke, H. W., Laidlaw, M. A. S., and Gonzales, C. (2010). Lead (Pb) legacy from vehicle traffic in eight California urbanized areas: continuing influence of lead dust on children's health. *Sci. Total Environ.* 408, 3965–3975. doi: 10.1016/j.scitotenv.2010.05.017

Navas, A., Machín, J., and Soto, J. (2005). Mobility of natural radionuclides and selected major and trace elements along a soil toposequence in the central Spanish Pyrenees. *Soil Sci.* 170, 743–757. doi: 10.1097/01.ss.0000185906.18460.65

NBA (2012). *South African National Biodiversity Assessment 2011: Techinical Report. CSIR Report*, eds L. Van Niekerk and J. Turpie.(Stellenbosch: Council for Scientific and Industrial Research) doi:CSIR/ECOS/ER/2011/0045/B.

Nel, L., Strydom, N. A., and Bouwman, H. (2015). Preliminary assessment of contaminants in the sediment and organisms of the Swartkops Estuary, South Africa. *Mar. Pollut. Bull.* 101, 878–885. doi: 10.1016/j.marpolbul.2015.11.015

Newman, B. K., and Watling, R. J. (2007). Definition of baseline metal concentrations for assessing metal enrichment of sediment from the south-eastern Cape coastline of South Africa. *Water SA* 33, 675–691.

Olguín, E. J., and Sánchez-Galván, G. (2012). Heavy metal removal in phytofiltration and phycoremediation: The need to differentiate between bioadsorption and bioaccumulation. *N. Biotechnol.* 30, 3–8. doi: 10.1016/j.nbt.2012.05.020

Pedro, S., Duarte, B., Raposo, P., Almeida, D., and Caçador, I. (2015). Metal speciation in salt marsh sediments?: Influence of halophyte vegetation in salt marshes with different morphology. *Estuar. Coast. Shelf Sci.* 167, 248–255. doi: 10.1016/j.ecss.2015.05.034

Peppicelli, C., Cleall, P., Sapsford, D., and Harbottle, M. (2018). Changes in metal speciation and mobility during electrokinetic treatment of industrial wastes?: implications for remediation and resource recovery. *Sci. Total Environ.* 624, 1488–1503. doi: 10.1016/j.scitotenv.2017.12.132

Phillips, D. P., Human, L. R. D., and Adams, J. B. (2015). Wetland plants as indicators of heavy metal contamination. *Mar. Pollut. Bull.* 92, 227–232. doi: 10.1016/j.marpolbul.2014.12.038

Reboreda, R., and Caçador, I. (2007). Halophyte vegetation influences in salt marsh retention capacity for heavy metals. *Environ. Pollut.* 146, 147–154. doi: 10.1016/j.envpol.2006.05.035

Reddering, J. S. V., Esterhuysen, K., and Rust, I. C. (1981). *The Sedimentary Ecology of the Swartkops Estuary*. Port Elizabeth: University of Port Elizabeth.

Roy, P. S., Williams, R. J., Jones, A. R., Yassini, I., Gibbs, P. J., Coates, B., et al. (2001). Structure and function of south-east Australian estuaries. *Estuar. Coast. Shelf Sci.* 53, 351–384. doi: 10.1006/ecss.2001.0796

Schropp, S. J., Graham Lewis, F., Windom, H. L., Ryan, J. D., Calder, F. D., and Burney, L. C. (1990). Interpretation of metal concentrations in estuarine sediments of Florida using aluminum as a reference element. *Estuaries* 13, 227–235. doi: 10.2307/1351913

Shine, J. P., Ika, R. V., and Ford, T. E. (1995). Multivariate statistical examination of spatial and temporal patterns of heavy-metal contamination. *Environ. Sci. Technol.* 29, 1781–1788. doi: 10.1021/es00007a014

Smillie, C. (2015). Salicornia spp. as a biomonitor of Cu and Zn in salt marsh sediments. *Ecol. Indic.* 56, 70–78. doi: 10.1016/j.ecolind.2015.03.010

Strawn, D. G., Bohn, H. L., and O'Connor, G. A. (2015). *Soil Chemistry*, 4th Edn. West Sussex: John Wiley and Sons.

Strawn, D., and Sparks, D. (2000). Effects of soil organic matter on the kinetics and mechanisms of Pb (II) sorption and desorption in soil. *Soil Sci. Soc. Am. J.* 64, 144–156. doi: 10.2136/sssaj2000.641144x

Tack, F. M., and Verloo, M. G. (1995). Chemical speciation and fractionation in soil and sediment heavy metal analysis: a review. *Int. J. Environ. Anal. Chem.* 59, 225–238. doi: 10.1080/03067319508041330

Theal, G. M. (2010). *History of South Africa since September 1795*, 2nd Edn. Cambridge: Cambridge University Press.

Turekian, K. K., and Wedepohl, K. H. (1961). Distribution of the elements in some major units of the Earth's crust. *America (NY)* 72, 175–192. doi: 10.1130/0016-7606(1961)72[175:doteis]2.0.co;2

Turpie, J. K., Adams, J. B., Joubert, A., Harrison, T. D., Colloty, B. M., Maree, R. C., et al. (2002). Assessment of the conservation priority status of South African estuaries for use in management and water allocation. *Water SA* 28, 191–206. doi: 10.4314/wsa.v28i2.4885

Ujeviæ, I., Odžak, N., and Bariæ, A. (2000). Trace metal accumulation in different grain size fractions of the sediments from a semi-enclosed bay heavily contaminated by urban and industrial wastewaters. *Water Res.* 34, 3055–3061. doi: 10.1016/S0043-1354(99)00376-0

Veres, D. S. (2002). A comparitive study between loss on ignition and total carbon analysis on minerogenic sediments. *Stud. Univ. Babes Bolyai Geol.* 67, 171–182. doi: 10.5038/1937-8602.47.1.13

Vesper, D. J. (2012). *Contamination of Cave Waters by Heavy Metals*, 2nd Edn. Amsterdam: Elsevier Inc. doi: 10.1016/B978-0-12-383832-2.00024-4

Vodyanitskii, Y. N., and Shoba, S. A. (2015). Biogeochemistry of carbon, iron, and heavy metals in wetlands (Analytical review). *Moscow Univ. Soil Sci. Bull.* 70, 89–97. doi: 10.3103/S0147687415030072

Watling, R. J., and Emmerson, W. D. (1981). A preliminary pollution survey of the Papenkuils River, Port Elizabeth. *Water SA* 7, 211–215.

Watling, R. J., and Watling, H. R. (1979). *Metal Surveys in Southern African Estuaries: 1. Swartkops Estuary*. Port Elizabeth: Council for Scientific and Industrial Research.

Watling, R. J., and Watling, H. R. (1982). Metal surveys in South African estuaries. I. Swartkops River. *Water SA* 8:26.

Wentworth, C. K. (1922). A scale of grade and class terms for clastic sediments'. *J. Geol.* 30, 377–392. doi: 10.1086/622910

Williams, T. P., Bubb, J. M., and Lester, J. N. (1994). Metal accumulation within salt marsh environments: a review. *Mar. Pollut. Bull.* 28, 277–290. doi: 10.1016/0025-326x(94)90152-x

Wyatt, K. H., and Stevenson, R. J. (2010). Effects of acidification and alkalinization on a periphytic algal community in an Alaskan wetland. *Wetlands* 30, 1193–1202. doi: 10.1007/s13157-010-0101-3

Zhang, W., Yu, L., Hutchinson, S. M., Xu, S., Chen, Z., and Gao, X. (2001). China's Yangtze Estuary: I. Geomorphic influence on heavy metal accumulation in intertidal sediments. *Geomorphology* 41, 195–205. doi: 10.1016/S0169-555X(01)00116-7

**Conflict of Interest:** The authors declare that the research was conducted in the absence of any commercial or financial relationships that could be construed as a potential conflict of interest.

frontiers in Environmental Science

ORIGINAL RESEARCH
published: 11 December 2020
doi: 10.3389/fenvs.2020.581591

# Analysis of Water Pollution Using Different Physicochemical Parameters: A Study of Yamuna River

*Rohit Sharma[1], Raghvendra Kumar[2], Suresh Chandra Satapathy[3], Nadhir Al-Ansari[4]*, Krishna Kant Singh[5], Rajendra Prasad Mahapatra[6], Anuj Kumar Agarwal[7], Hiep Van Le[8]* and Binh Thai Pham[9]**

[1] Department of Electronics and Communication Engineering, Faculty of Engineering and Technology, SRM Institute of Science and Technology, Delhi- NCR Campus, Ghaziabad, India, [2] Department of Computer Science and Engineering, Gandhi Institute of Engineering and Technology University, Gunupur, India, [3] School of Computer Engineering, Kalinga Institute of Industrial Technology Deemed to Be University, Bhubaneswar, India, [4] Department of Civil, Environmental and Natural Resources Engineering, Lulea University of Technology, Lulea, Sweden, [5] Department of Electronics and Communication Engineering, Krishna Institute of Engineering and Technology, Group of Institutions, Ghaziabad, India, [6] Department of Computer Science, SRM Institute of Science and Technology, NCR Campus, Ghaziabad, India, [7] Department of Applied Sciences and Humanities, Teerthankar Mahaveer University, Moradabad, India, [8] Institute of Research and Development, Duy Tan University, Da Nang, Vietnam, [9] Geotechnical Engineering and Artificial Intelligence Research Group (GEOAI), University of Transport Technology, Hanoi, Vietnam

OPEN ACCESS

**Edited by:**
*Senthil Kumar Ponnusamy, SSN College of Engineering, India*

**Reviewed by:**
*Rakesh Bhutiani, Gurukul Kangri Vishwavidyalaya, India*
*Lalit Garg, University of Malta, Malta*

***Correspondence:**
*Nadhir Al-Ansari*
*nadhir.alansari@ltu.se*
*Hiep Van Le*
*levanhiep2@duytan.edu.vn*
*Binh Thai Pham*
*binhpt@utt.edu.vn*

**Specialty section:**
*This article was submitted to Toxicology, Pollution and the Environment, a section of the journal Frontiers in Environmental Science*

**Received:** *09 July 2020*
**Accepted:** *11 November 2020*
**Published:** *11 December 2020*

**Citation:**
*Sharma R, Kumar R, Satapathy SC, Al-Ansari N, Singh KK, Mahapatra RP, Agarwal AK, Le HV and Pham BT (2020) Analysis of Water Pollution Using Different Physicochemical Parameters: A Study of Yamuna River. Front. Environ. Sci. 8:581591. doi: 10.3389/fenvs.2020.581591*

The Yamuna river has become one of the most polluted rivers in India as well as in the world because of the high-density population growth and speedy industrialization. The Yamuna river is severely polluted and needs urgent revival. The Yamuna river in Dehradun is polluted due to exceptional tourist activity, poor sewage facilities, and insufficient wastewater management amenities. The measurement of the quality can be done by water quality assessment. In this study, the water quality index has been calculated for the Yamuna river at Dehradun using monthly measurements of 12 physicochemical parameters. Trend forecasting for river water pollution has been performed using different parameters for the years 2020–2024 at Dehradun. The study shows that the values of four parameters namely, Temperature, Total Coliform, TDS, and Hardness are increasing yearly, whereas the values of pH and DO are not rising heavily. The considered physicochemical parameters for the study are TDS, Chlorides, Alkalinity, DO, Temperature, COD, BOD, pH, Magnesium, Hardness, Total Coliform, and Calcium. As per the results and trend analysis, the value of total coliform, temperature, and hardness are rising year by year, which is a matter of concern. The values of the considered physicochemical parameters have been monitored using various monitoring stations installed by the Central Pollution Control Board (CPCB), India.

**Keywords: water quality index, Yamuna river, physico-chemical parameters, water pollution, Dehradun city**

## INTRODUCTION

Due to historical, geographical, religious, political, and sociocultural reasons, India has a unique place in the world Agarwal et al., 2016. Pollution-causing activities have caused severe changes in aquatic environments over the last few decades. Serious questions have been raised in context to the safe use of river water for drinking and other purposes in recent times. Numerous contaminants are playing a major role in polluting the river water. It is one of the main concerns for most of

the metropolitan cities of developing nations. Rivers play a vital role in shaping up the natural, cultural, and economic aspects of any country (Rafiq, 2016). The Yamuna river is one such river. The Yamuna river provides sustenance to ecology and is therefore considered holy by the people of India. It derives from the glacier called Yamunotri in the Himalayan ranges. States through which the Yamuna river flows are the Uttarakhand, Himachal Pradesh, Uttar Pradesh, Haryana, and Delhi. The Yamuna river is also divided into several tributaries such as the Hindon, Tons, Giri, Rishiganga, Hanuman Ganga, Sasur Khaderi, Chambal, Betwa, Ken, Sindh, and Baghain as it is flowing through several cities. These cities are the Yamuna Nagar, Delhi, Faridabad, Mathura, Agra, Etawah, and Prayagraj. It is a tributary of the river Ganges in India. Two of them together have had substantial importance in shaping up the history and geography of our country. The river on which our research primarily focuses is the Yamuna river. It passes through several states such as Uttar Pradesh, Himachal Pradesh, Uttarakhand, Haryana, and Delhi. It has a length of approximately 1,380 km. More than 600 lakh people are dependent on their living and income on this river (Census Reports of India 2001, 1971–1991). Such is the greatness of this river. Our research is based on the Yamuna river in Dehradun in Uttarakhand.

The process, in which the people from rustic areas shift to the town areas in search of a brighter future, thus resulting in a drastic increment in the population of people living in cities, is called urbanization. As a result, the number of cities and towns increases exponentially. There is an atrocious amount of stress on the weakening natural resources. As it is, the natural resources are facing major deterioration issues considering the unthoughtful plundering by the people. In the last few decades, the rate of spread in various segments of the world has been unprecedented and unimaginable. The proportion of the rate of infrastructure expansion has not been able to match up to the pace of urbanization in most cities. The amplified requirement of water, deficiency of sewage facilities, and scarce wastewater treatment facilities rigorously affect the water resources, and change the environment and ecology. Agricultural lands, rural unpaved areas, and natural wetlands are converted into paved and impervious urban areas, during urbanization. Augmented impervious land surface in urbanized areas leads to severe and radical changes in the natural order of things (Ahmad et al., 2017). There has been a drastic decline in the Yamuna river water quality since the last few years. The water is highly polluted, and it is a joint responsibility of the government and all the citizens to make sure that the Yamuna river is clean again. The primary step toward understanding and deliberating about the sorts of water pollution and developing effective reduction strategies is monitoring (Marale, 2012). Physical, chemical, and biological compositions determine the quality of water (Allee and Johnson, 1999). The substances such as heavy metals, pesticides, detergents, and petroleum form the chemical composition (Tiwari et al., 2020). Turbidity, color, and temperature comprise the physical composition, whereas the biological arrangement includes pigments and planktons. Observation and analysis of these water quality parameters need sampling from extensively distributed locations, which is time consuming and requires a lot of field and lab efforts to come up with statistical results (Wang et al., 2004; Icaga, 2007; Kazi et al., 2009; Amandeep, 2011; Duong, 2012; Singh et al., 2013; Nazeer and Nichol, 2015; Shi et al., 2018).

Conventionally, monitoring-based methods are used to find out the water quality parameters. They involve wide-ranging field sampling and expensive lab analysis, which is time inefficient and can only be accomplished for areas that are smaller (Song et al., 2012). Hence, these restraints and drawbacks make the conventional methods challenging for continuous water quality prediction at spatial scales (Panwar et al., 2015; Chabuk et al., 2017). For observing and analyzing water quality parameters, such as turbidity, chlorophyll, temperature, and suspended inorganic materials, techniques, such as optical remote sensing, are being used (Pattiaratchi et al., 1994; Fraser, 1998; Kondratyev et al., 1998). To calculate the measure of solar irradiance at varied wavelength bands reflected by the surface water, remote sensing satellite sensors are used (Zhang et al., 2003; Dwivedi and Pathak, 2007; Girgin et al., 2010; Ronghang et al., 2019). Amplified demand for water, poor sewage facility, and insufficient wastewater management amenities, relentlessly affect the resources of water resources. Models such as hydrological models have been used to evaluate the effect of numerous factors in rain-related procedures of the cosmopolitan areas (Trombadore et al., 2020). Knowledge and information about interconnections between climate, population, and ecology are essential for understanding and promoting sustainable development (Sharma et al., 2020). It also requires better knowledge of equipment and methodical planning. Proper management will reduce the degradation of rivers (Shukla et al., 2018). In this study, we focus on trying to find out contaminants in the river, finding the water pollution index, and subsequently enforcing measures to curb water pollution.

Contribution of the Study:

1. In the present study, water samples were collected every year from the Yamuna river canal in Dehradun, Uttarakhand, India.
2. The samples have been analyzed for 12 different physicochemical attributes like ph, BOD, COD, Total Coliform, Temp, DO, Alkalinity, Chlorides, Calcium, Magnesium, and Hardness as Calcium Carbonate and TDS.
3. The measurement of the water quality index has been taken into consideration for the years 2017, 2018, and 2019.
4. Forecasting the pollution trend for the Yamuna river water from 2016 to 2024.

# MATERIALS AND METHODS

## Mathematical Model

In this research paper, the water sample of the Yamuna river is considered for analysis. The 12 physicochemical parameters in the water are studied and analyzed. The water sample of the Holy River called the Yamuna river is considered for a certain period. The ratio of water components mainly Temperature, Total Coliform, TDS, and Hardness are varied irregularly at various locations of India. Due to the abrupt changes in the

water component, the water quality is also changed. In this research paper, a sampling distribution-based analytical model called *Equipoise Evaluator* (EE) is proposed for the discrete parameter value of the water components. The EE model is suitable to analyze random discrete parameters. The EE model can be applied for any kind of sample analysis where the analysis is based on sample molecules. To analyze the discrete sample in the form of the symmetric normal distribution for a particular location, the EE model is applied. In this research paper, the water sample varies based on the molecules of e water components. This EE model is also applicable for the analysis of metallurgy to detect the impurity of the metal. In this research paper, the EE model is deployed for the water sample of the Yamuna river.

Sampling distribution is proposed to transform the variable at different levels.

As per the linear transformation

$$Z = MW, \quad \forall W \rightarrow Z \text{ as the column vector of equal size} \quad (1)$$

Now, by applying the Jacobian transformation on a non-singular matrix M,

$$\frac{DZ}{DW} = |M| \text{ for a positive sign} \quad (2)$$

From Equation (2), the relational equation for all connected differential elements is defined as Equation (3)

$$dz_1\, dz_2 \ldots\ldots\ldots dz_n = |M|\ dw_1\, dw_2 \ldots\ldots dw_n \quad (3)$$

$$dZ = |M|\, dW \quad \text{as } M \text{ is a an orthogonal matrix, and } |M = 1| \quad (4)$$

As M is considered as an orthogonal matrix, hence Z = MW, which transformed into a quadratic form of preserving from the standard value.

$$W^I W \rightarrow Z^I Z$$
$$(W-\mu)'(W-\mu) \rightarrow (Z-\eta)'(Z-\eta) \forall\, \eta = M\mu \quad (5)$$

To determine the dissimilarity distance from a standard sample value, the partitioning matrix is deployed.

$$M = \begin{pmatrix} M_1 \\ . \\ . \\ . \\ M_k \end{pmatrix}$$
$$\forall\, M_i = n_i \times n \quad and \sum n_i = n \quad (6)$$

Assume that matrix M is partitioned into qth numbers, then $M_i M_j{}' = 0\ \ \forall i \neq j$.

As per the partitioning matrix, all q sub-matrices are orthogonal to each other except orthogonal themselves. Now, Equation (1) is rewritten as

$$Z_1 = M_1 W, \ldots\ldots\ldots, Z_k = M_q W \quad (7)$$

where, $M_1, \ldots, M_q$ are an exclusive subset of the tested variables.

Applying transformation in Equation (7)

$$\begin{aligned} W'W &\rightarrow Z_1{}' B_1 Z_1 + \ldots\ldots\ldots + Z_q{}' B_q Z_q \\ (W-\mu)'(W-\mu) &\rightarrow (Z_1-\eta_1)' B_1 (Z_1-\eta) + \ldots\ldots\ldots\ldots \\ &+ \left(Z_q-\eta_q\right)' B_q \left(Z_q-\eta_q\right) \end{aligned} \quad (8)$$

where, $B_i = (M_i M_i{}')^{-1} \quad and \quad \eta_i = M_i \mu$

Equation (8) determines the transformation of each partition into quadratic form with exclusive subsets of tested parameters. In this analysis, $M$ is considered as fully orthogonal, with each row orthogonal to every other row. The result of transforming all the variables to test bed data variables of D is then,

$$\int_D f(w_1,\ w_2, \ldots., w_n)\, dw_1\, dw_2 \ldots.. dw_n = h(D),$$
$$\text{where } D = g(w_1,\ w_2, \ldots\ldots., w_n) \quad (9)$$

It is considered that the water molecules of the sample water have symmetric normally distributed for a particular location. The mean of the water molecules is $\bar{z} = \frac{1}{q} \sum_{i=1}^{q} w_i$.

As per orthogonal transformation

$$\sum {z_i}^2 = \sum {u_i}^2 \quad (10)$$

where $u_1 = \sqrt{q}\bar{z}$ and $\sigma = {u_1}^2 + {u_2}^2 + \ldots. + {u_q}^2$.

$u_1$ and $\sigma$ are independently distributed. The sample mean and sample variance of the experimented sample water are independently distributed.

## Water Quality Index and Trend Analysis

The primary focus of this study is to measure and analyze the drastic changes in the Yamuna river water quality at Dehradun, Uttarakhand. Standardized and the universally accepted water quality index (WQI) has been adopted to measure the variation in water quality of the Yamuna river at the prime location of the study—Dehradun over 3 years. The standard method has been used to examine and evaluate the water quality for 12 Physicochemical parameters (TDS, Chlorides, Alkalinity, DO, Temperature, COD, BOD, pH, Magnesium, Hardness, Total Coliform, and Calcium). In this study, the water quality index has been calculated using the different Physicochemical parameters documented and verified from the monitored locations. The water quality index (WQI) is stated by

$$WQI = \sum_{i=1}^{P} WiIi$$

where $Ii$ signifies the ith water quality parameters, the weight associated and related to the parameters is denoted by Wi, and p notifies us about the number of water quality parameters. This WQI is based on the index introduced by the NSF (National Sanitation Foundation) (Bhutiani et al., 2016). This

index is established by the Central Pollution Control board with different advancements in terms of water quality criteria. The Water quality index is supported and developed by the National Sanitation Foundation (NSF) (Brown et al., 1970). It is also known as NSF-WQI. This water quality index is denoted as

$$WQI = \sum_{i=1}^{p} Wiqi$$

where $P$ denotes the ith parameter measured values, quality rating is denoted by $q_i$, and the relative weight of the ith parameters is denoted by $w_i$.

The water quality index arithmetic index was presented (Cude, 2001). It is a very popular and standard method used by many investors and researchers in their studies (Ramakrishniah et al., 2009; Ahmad et al., 2012).

In this study, the quality rating can be calculated using the following equation:

$$q_i = \{ \left[ \frac{V_{actual} - V_{ideal}}{V_{standard} - V_{ideal}} \right] * 100 \}$$

where $q_i$ signifies the ith parameter quality rating for n water quality parameters, water.

The quality parameters' actual and definite value is denoted by $V_{actual}$, the parameters ideal value is symbolized by $V_{ideal}$, and the standard value of the parameters, which is suggested by the WHO, is denoted by $V_{standard}$. The ideal values for DO and pH are 14.6 and 7 mg/L, whereas for the other parameters, it is equal to zero. After the calculation of quality rating, (relative weight), $Wi$ has to be calculated by inversing the standard value of the parameter. Finally, the following equation was used to calculate the overall water quality index (WQI):

$$WQI = \sum q_i W_i / \sum W_i$$

Here, signifying the relative weight and quality rating is symbolized by $Wi$ and $qi$.

## Trend Analysis

In this study, to forecast the pollution trend analysis, the linear regression model has been used. According to the linear regression model, the relationship between the two variables a and b can be expressed as:

$$B = x + yA + e$$

Where x and y are the model parameters, which are known as regression coefficients, and B is the dependent variable. A is known as an independent variable, and € is the error variable. For making a prediction using a linear regression model is

$$B = x + yA$$

The parameters x and y are calculated using the following equations:

$$x = \frac{\sum a^2 \sum b - \sum a \sum ab}{n \sum a^2 - (\sum a)\hat{2}}$$

$$y = \frac{\mathbf{n} \sum \mathbf{ab} - \sum \mathbf{a} \sum \mathbf{b}}{\mathbf{n} \sum \mathbf{a^2} - (\sum \mathbf{a})\hat{2}}$$

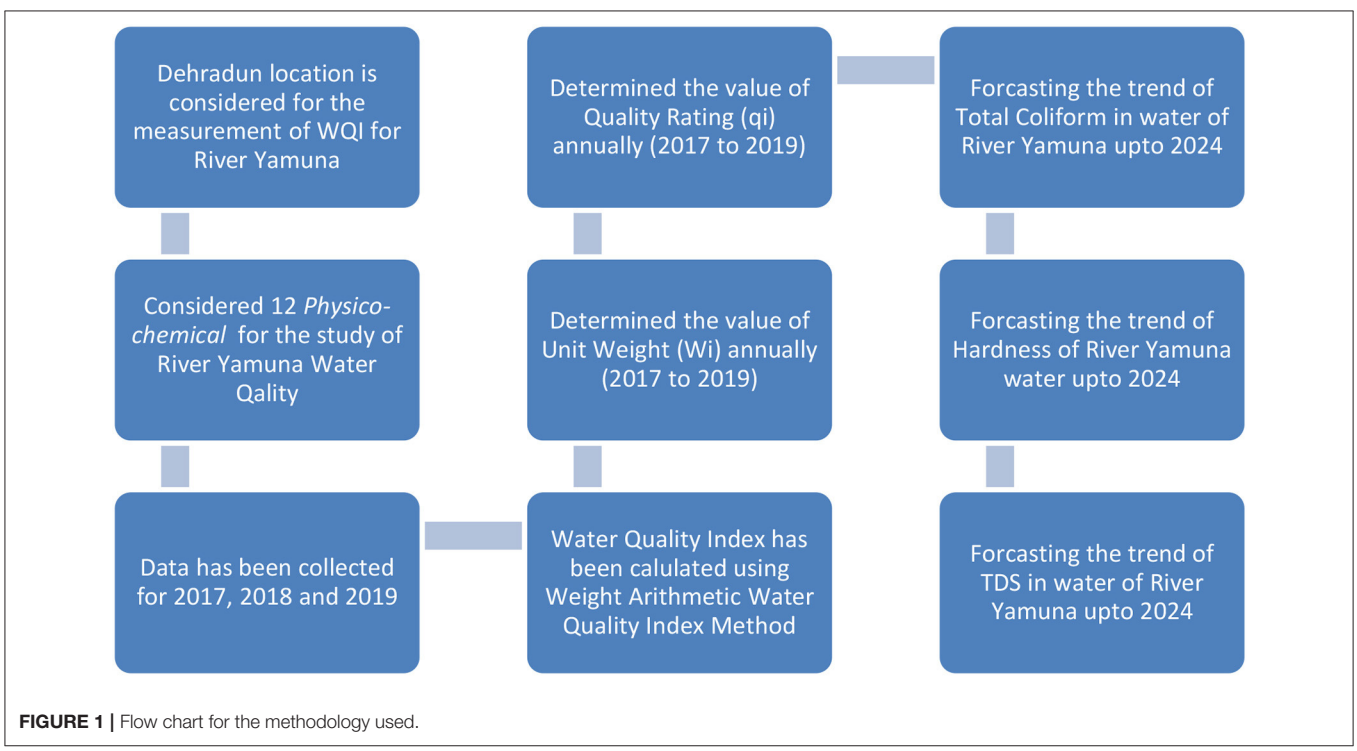


**FIGURE 1 |** Flow chart for the methodology used.

## Methodology

The flow chart for the methodology used is shown in **Figure 1**. The water quality index is calculated using the weight arithmetic water quality index method, which has been discussed in the Water Quality Index and Trend Analysis section.

The value of the water quality index has been compared with the standard values of WQI, which is shown in **Table 1**. The water quality rating is divided into five categories. The range from 0 to 25 is coming under (A) grading with excellent water quality, the range from 26 to 50 is for grading (B) with good water quality, and respectively, (C), (D), and (E) gradings are categorized for different WQI values (Chauhan and Singh, 2010).

## Dataset Collection

The most populous city of Uttarakhand is Dehradun also spelled Dear Doon. It is the capital of Uttrakhand, which is one among the 28 states in India (**Figure 2**). It is famous for its Doon Basmati Rice. Dehradun city has famous institutions like IMA (Indian Military Academy) regarded as one of the best officer training academies in India, Forest Research Institute, Indian Institute of Petroleum, and the famous ONGC training institute. This city is also famous among the tourists. It has many adventurous activities like rafting, bungee jumping, paragliding, etc. (Rafiq, 2016). The city is located about 255 km from New Delhi and 168 km from Chandigarh. The climate condition of Dehradun is humid, subtropical, and a summer temperature can reach a maximum of 44°C. This city is also located very close to Nainital, which has the famous Jim Corbett National Park attracting many tourists (Bhutiani et al., 2015).

The present study was undertaken for a period of 3 years from 2017 to 2019 to check the water quality analysis for the physicochemical attributes below. In the present study, water samples were collected on a yearly basis from the Yamuna river canal in Dehradun, Uttarakhand, India. The samples were analyzed for 12 different physicochemical attributes like ph, BOD, COD, Total Coliform, Temp, DO, Alkalinity, Chlorides, Calcium, Magnesium, and Hardness as Calcium Carbonate, and TDS (Tyagi et al., 2020). The Yamuna river plays a very crucial role in Dehradun's geography. The Yamuna river is severely polluted and needs urgent revival. The river passes through Uttarakhand. Uttarakhand has always been a tourist spot and experiences heavy tourists perennially, and Dehradun, being the capital city, also bears the brunt. The Yamuna river in Dehradun is polluted due to the exceptional tourist activities. Dehradun is also famous for the Kumaoni Holi, Jhanda Fair, Tapkeshwar Mela, and Bissu Mela. A lot of waste materials are dumped into the Yamuna river, and they contaminate the river. Water might be untreated for long spans of time. Also, a lot of industries–primarily biotechnology and food processing, are set up in Dehradun; they also mindlessly dump their waste in the Yamuna river. Industrial waste is not fully responsible for the pollution, but some poor sewage systems and human activities are also responsible for it (Bhutiani and Khanna, 2007).

Dehradun is a home to many agricultural and horticulture activities such as rice, litchi, and tea plantations. Agricultural waste also plays a major role in polluting the Yamuna river in Dehradun. The pollution is also increased by the excessive usage of insecticides and pesticides (Tiwari et al., 2020). There are also people who wash their clothes, utensils, and defecate in or around the river, thus leading to pollution. The stretch of the Yamuna river in Dehradun thus has a lot of coliform bacteria. Government projects such as road construction might also be responsible for dumping waste, although rules have been drastically upgraded in the last two decades or so. Some cattle washing activities and religious activities also polluted the Yamuna river (Bhutiani et al., 2018).

**TABLE 1 |** The standard values of water quality index (WQI) using weight arithmetic water quality index method.

| Grading | WQI value | Water quality rating |
|---|---|---|
| A | 0–25 | Excellent |
| B | 26–50 | Good |
| C | 51–75 | Poor |
| D | 76–100 | Very poor |
| E | Above 100 | Unsuitable for drinking |

# RESULTS AND DISCUSSION

The study aims to examine the alteration in the quality of water of the Yamuna river at Dehradun in the year 2017. Water quality index (WQI) is going to be used in the study so that the changes and variations in the quality of water of the Yamuna river can be measured. The conventional method by which inspection can be done for the water quality has 12 physicochemical parameters (TDS, Chlorides, Alkalinity, DO, Temperature, COD, BOD, pH, Magnesium, Hardness, Total Coliform, and Calcium). These parameters will be measured carefully, and their respective value will be found. So, the standard value and observed value will be compared with each other, and the variation is going to be measured between them. By this variation, identification of the quality of water can be done.

## Measurement of Physicochemical Parameters at Dehradun for 2017

Water samples have been taken at different months for the year 2017 (**Table 2**). The mean and standard deviation for the measured values have been also calculated. The mean is the number found by summing every data point and dividing by the number of data points. It is also called average. The standard deviation is defined as the number that is going to tell about the measurements for a group that is spread out from the mean or expected value. A low standard deviation signifies that many numbers are very close to the mean (Bisht et al., 2017). A high standard deviation signifies that the numbers are very much spread out. So, the accurate value for the quality of water can be found out easily using this.

The maximum value of pH is in the month of January when the water is a little more basic, and the minimum value is in July when it is less basic. The mean pH is 7.735, and the standard

deviation is 0.086986589. The maximum value of the biochemical oxygen demand (BOD) is in January, which indicates more polluted water, and the minimum value is in the months of April, July, and October, which indicates less polluted water. The mean of BOD is 1.05, and the standard deviation is 0.1. The maximum value of COD is in January and October, which indicates a large quantity of oxidizable organic materials in the sample, and the minimum value is in April and July which indicates a lesser quantity of oxidizable organic materials in the sample. The mean COD is 5 and the standard deviation is 1.154700538.

The maximum value of Total Coliform is in July, which indicates that the water-borne illness is increased, and the minimum value is in October which indicates that the water-borne illness is decreased. The mean of Total Coliform is 65, and the standard deviation is 17.32050808. The maximum value of Temp is in July, which indicates increased chemical reactions generally, and the minimum value is in January, which indicates decreased chemical reactions. The mean of Temp is 17.75, and the standard deviation is 2.62995564. The maximum value of DO is in October, and the minimum value is in January, April, and July. The mean of DO is 8.7, and the standard deviation is 0.2. The maximum value of Alkalinity/visual titration $CaCO_3$ is in July, which indicates greater buffering capacity against pH changes, and the minimum value is in April, which indicates lesser buffering capacity against pH changes. The mean of Alkalinity/visual titration $CaCO_3$ is 64, and the standard deviation is 5.887840578. The maximum value of Chlorides is in July, which indicates body-related diseases, and the minimum value is in April and October. The mean of Chlorides is 5.75, and the standard deviation is 0.9574271078. The maximum value of Calcium as $CaCO_3$ is in July, which has a positive effect on the body, and the minimum value is in April, which has a lesser

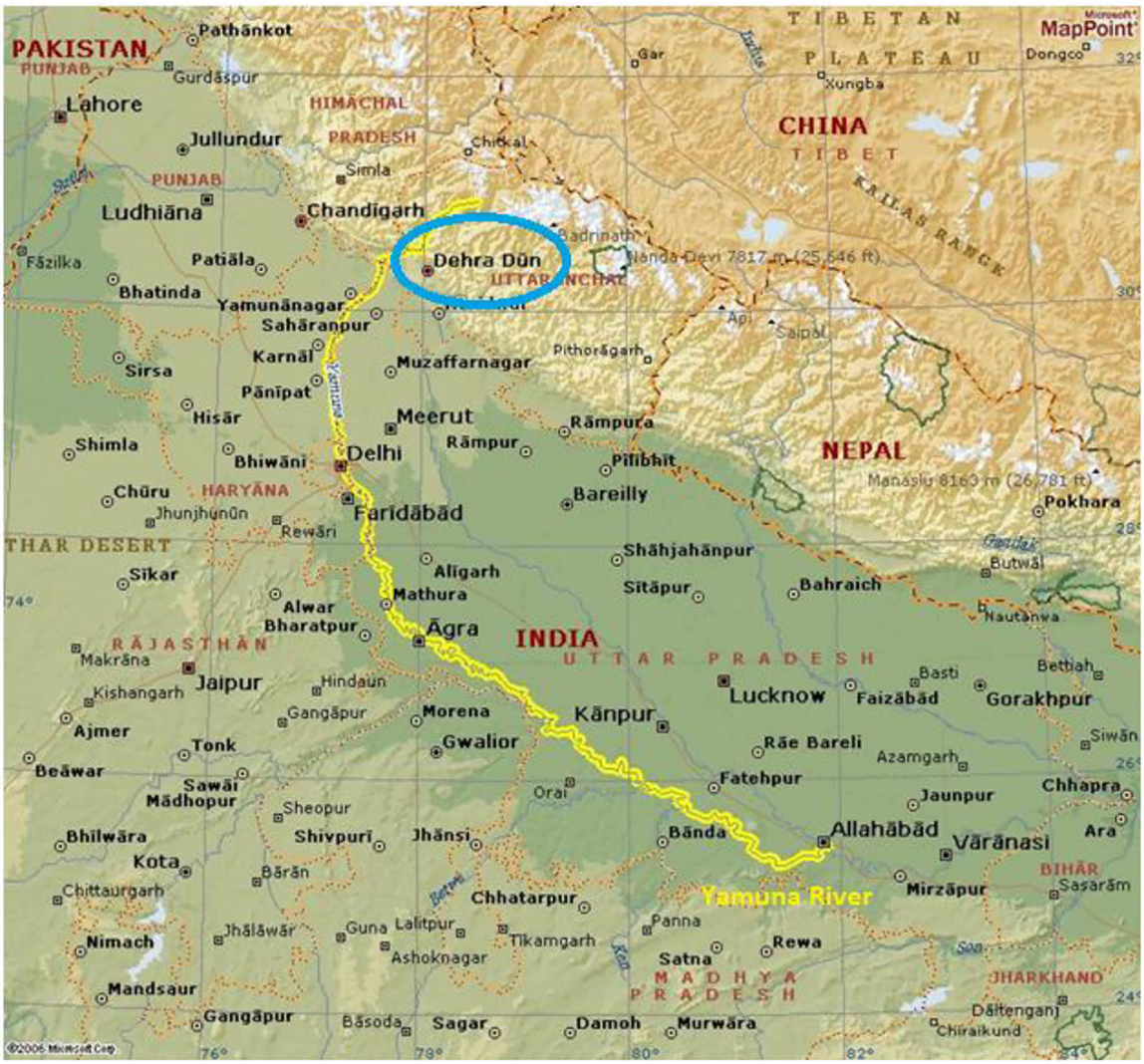


**FIGURE 2 |** Map for considering location for Yamuna, Dehradun (https://www.bcmtouring.com/forums/thread).

**TABLE 2 |** Physicochemical parameters and water quality analysis at Dehradun for 2017.

| | January | April | July | October | Mean | ST DEV | Observed value (vi) | Standard value (Si) | Unit weight (Wi) | Quality rating (qi) | Wiqi |
|---|---|---|---|---|---|---|---|---|---|---|---|
| pH | 7.82 | 7.78 | 7.62 | 7.72 | 7.735 | 0.086987 | 7.7 | 8.5 | 0.219 | 49 | 11 |
| BOD (mg/L) | 1.2 | 1 | 1 | 1 | 1.05 | 0.1 | 1.1 | 5 mg/L | 0.3723 | 21 | 7.8 |
| COD (mg/L) | 6 | 4 | 4 | 6 | 5 | 1.154701 | 5 | 25 (WPCSR) | 0.00468 | 20 | 0.1 |
| Total Coliform (MPN/100 ml) | 60 | 60 | 90 | 50 | 65 | 17.32051 | 17.32051 | 50 | — | — | — |
| Temp (°C) | 14 | 19 | 20 | 18 | 17.75 | 2.629956 | 18 | 25 | 0.00468 | 71 | 0.3 |
| DO | 8.6 | 8.6 | 8.6 | 9 | 8.7 | 0.2 | 8.7 | 5 mg/l | 0.3723 | 61 | 23 |
| Alkalinity/visualTitration $CaCO_3$ | 64 | 58 | 72 | 62 | 64 | 5.887841 | 64 | 120(WPCSR) | 0.000975 | 53 | 0.1 |
| Chlorides | 6 | 5 | 7 | 5 | 5.75 | 0.957427 | 5.8 | 250 mg/l | 0.0074 | 2.3 | 0 |
| Calcium as $CaCO_3$ | 44 | 36 | 46 | 38 | 41 | 4.760952 | 41 | 75 mg/l | 0.025 | 55 | 1.4 |
| Magnesium as $CaCO_3$ | 30 | 32 | 36 | 32 | 32.5 | 2.516611 | 2.516611 | 50 | — | — | — |
| Hardness as $CaCO_3$ | 74 | 68 | 82 | 70 | 73.5 | 6.191392 | 74 | 200 | 0.0062 | 37 | 0.2 |
| TDS | 76 | 72 | 105 | 82 | 83.75 | 14.75071 | 84 | 500 mg/l | 0.0037 | 17 | 0.1 |
| | | | | | | | 308 | | 1.01624 | 386 | 44 |
| | | | | | | | | | | WQI | 42.87 |

positive effect on the body. The mean of $CaCO_3$ is 41, and the standard deviation is 4.760952286. The maximum value of Magnesium as $CaCO_3$ is in July, which has a positive effect on the body, and the minimum value is in January, which has a lesser positive effect on the body. The mean of Magnesium as $CaCO_3$ is 32.5, and the standard deviation is 2.516611478. The maximum value of Hardness as $CaCO_3$ is in July, which has a good effect on the body, and the minimum value is in April. The mean of Hardness as $CaCO_3$ is 73.5, and the standard deviation is 6.191391874. The maximum value of TDS is in July, which specifies more toxic minerals, and the minimum value is in April, which specifies less toxic minerals. The mean of TDS is 83.75, and the standard deviation is 14.7507062. Water quality index (WQI) was used for the evaluation of the variation in the water quality of the Yamuna river at Dehradun over 3 years. The standard and prescribed methods have been used to analyze the water quality for 12 physicochemical parameters (TDS, Chlorides, Alkalinity, DO, Temperature, COD, BOD, pH, Magnesium, Hardness, Total Coliform, and Calcium). Calculations have been performed using the standardized formula and mathematical models. Detailed calculations and methodology have been used to find the water quality index as accurately as possible. The WQI of the Yamuna river in Dehradun for the year 2017 was 42.87 (**Table 2**). According to WHO, the WQI should be below 60 for its quality to be at least fair. Here, it can be easily concluded that the Yamuna river is polluted, but it is still revivable. Developmental and maintaining efforts can be adopted to make the Yamuna river clean again and improve the WQI drastically.

Total coliform is positively correlated with $CaCO_3$, chlorides, and hardness of $CaCO_3$.Temp is positively correlated with the magnesium of $CaCO_3$ and TDS and negatively correlated with pH, BOD, and COD. DO is positively correlated with COD and negatively correlated with chlorides. Alkalinity is positively correlated with chlorides, TDS, hardness, and the magnesium of $CaCO_3$ and negatively correlated with pH. Chlorides are positively correlated with calcium and hardness of $CaCO_3$ and negatively correlated with pH and DO. Magnesium ($CaCO_3$) is positively correlated with hardness and TDS, and negative with pH, BOD, and COD. Hardness ($CaCO_3$) is positive for TDS, Chlorides, Magnesium, and negative for pH. TDS is negative for pH and positive for all. The dendrogram and graphical representation for physicochemical parameters at Dehradun for 2017 are plotted between the months (January, April, July, and October) and the parameters [TDS, Total Coliform (MPN/100 ml), Alkalinity/visual titration $CaCO_3$, Hardness as $CaCO_3$, Calcium as $CaCO_3$, Magnesium as $CaCO_3$, Temp, BOD, pH, DO, COD, and Chlorides] (**Figures 3**, **4**).

Cluster 1 (blue) represents lightly polluted, and the parameters include TDS, Total Coliform (MPN/100 ml), Alkalinity/visual titration $CaCO_3$, and Hardness as $CaCO_3$. Cluster 2 (red) represents moderately polluted, and the parameters include Calcium as $CaCO_3$, Magnesium as $CaCO_3$, Temp, BOD, pH, DO, COD, and Chlorides. Cluster 3 (black) represents heavily polluted and the parameters include Total Coliform (MPN/100 ml), Alkalinity/visual titration $CaCO_3$, Hardness as $CaCO_3$, Calcium as $CaCO_3$, Magnesium as $CaCO_3$, and Temp.

## Measurement of Physicochemical Parameters at Dehradun for 2018

Water samples have been taken in different months for the year 2018 (**Table 3**). Mean and standard deviation for the measured values have been also calculated. The maximum value of pH is in October so the water is a little more basic, and the minimum value is in January, which means the water is less basic. The mean pH is 7.6325, and the standard deviation is 0.420585. The maximum value and minimum value of BOD are equal every month. The mean of BOD is 1, and the standard deviation is 0.

The maximum value of COD is in April indicating a large quantity of oxidizable organic material in the sample, and the

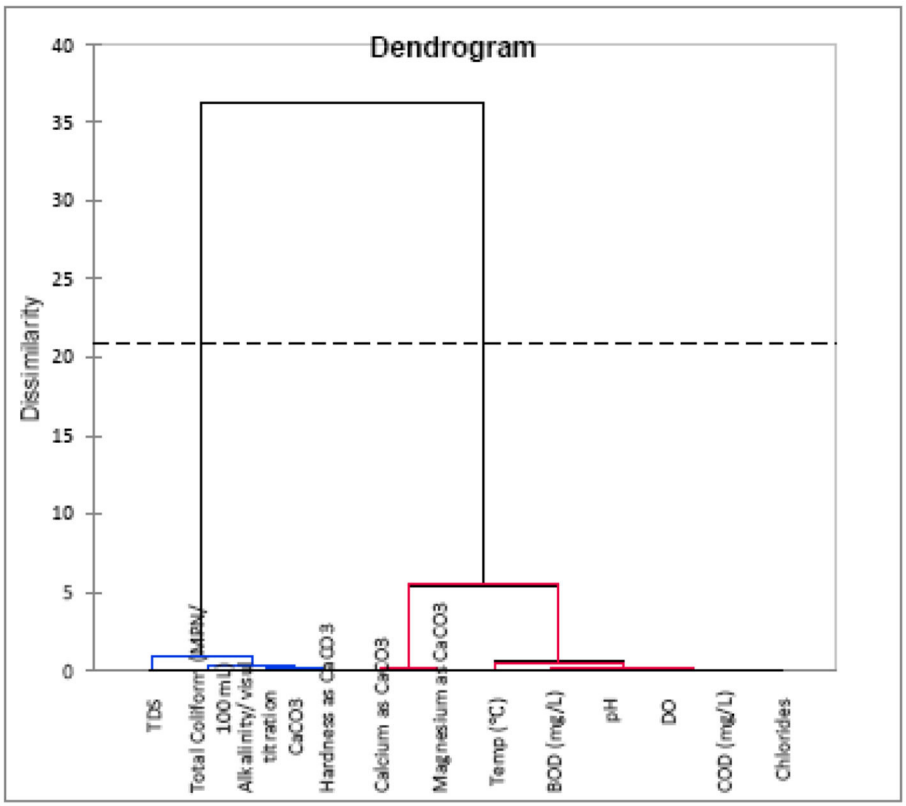


**FIGURE 3 |** Dendrogram for physicochemical parameters at Dehradun for 2017.

minimum value is in January, July, and October indicating a lesser quantity of oxidizable organic materials in the sample. The mean of COD is 4.5, and the standard deviation is 1. The maximum value of Total Coliform is in July indicating the water-borne illness is increased, and the minimum value is in January, April, and October indicating the water-borne illness is decreased. The mean of Total Coliform is 50, and the standard deviation is 20. The maximum value of Temp is in July indicating increased chemical reactions generally, and the minimum value is in January indicating decreased chemical reactions. The mean of Temp is 18.25, and the standard deviation is 1.707825. The maximum value of DO is in April, and the minimum value is in January and July. The mean of DO is 8.85, and the standard deviation is 0.251661. The maximum value of Alkalinity/visual titration $CaCO_3$ is in July indicating higher buffering capacity against pH changes, and the minimum value is in April indicating lower buffering capacity against pH changes. The mean of Alkalinity/visual titration $CaCO_3$ is 64.5, and the standard deviation is 6.608076.

The maximum value of Chlorides is in January, July, and October indicating body-related diseases, and the minimum value is in April. The mean of Chlorides is 5.75, and the standard deviation is 0.5. The maximum value of Calcium as $CaCO_3$ is in July, which has a positive effect on the body, and the minimum value is in January, April, and October, which has a less positive effect on the body. The mean of $CaCO_3$ is 41.5, and the standard deviation is 3. The maximum value of Magnesium as $CaCO_3$ is in July, which has a positive effect on the body, and the minimum value is in April, which has a less positive effect on the body. The mean of Magnesium as $CaCO_3$ is 33, and the standard deviation is 2.581989. The maximum value of Hardness as $CaCO_3$ is in July, which has a good effect on the body, and the minimum value is in April. The mean of Hardness as $CaCO_3$ is 74.5, and the standard deviation is 5.259911. The maximum value of TDS is in July specifying the presence of toxic minerals, and the minimum value is in January specifying the presence of less toxic minerals. The mean of TDS is 87.5, and the standard deviation is 15.60983.

Water quality index (WQI) was used in the evaluation of the variation in water quality of the Yamuna river at Dehradun over 3 years. The standard and prescribed method has been used to analyze the water quality for the 12 physicochemical parameters (TDS, Chlorides, Alkalinity, DO, Temperature, COD, BOD, pH, Magnesium, Hardness, Total Coliform, and Calcium). Calculations have been performed using the standardized formula and mathematical models. Detailed calculations and methodology have been used to find the water quality index as accurately as possible. The WQI of the Yamuna river in Dehradun for the year 2018 was 40.47 (**Table 3**). According to WHO, the WQI should be below 60 for its quality to be at least fair. Here, it can be easily concluded that the

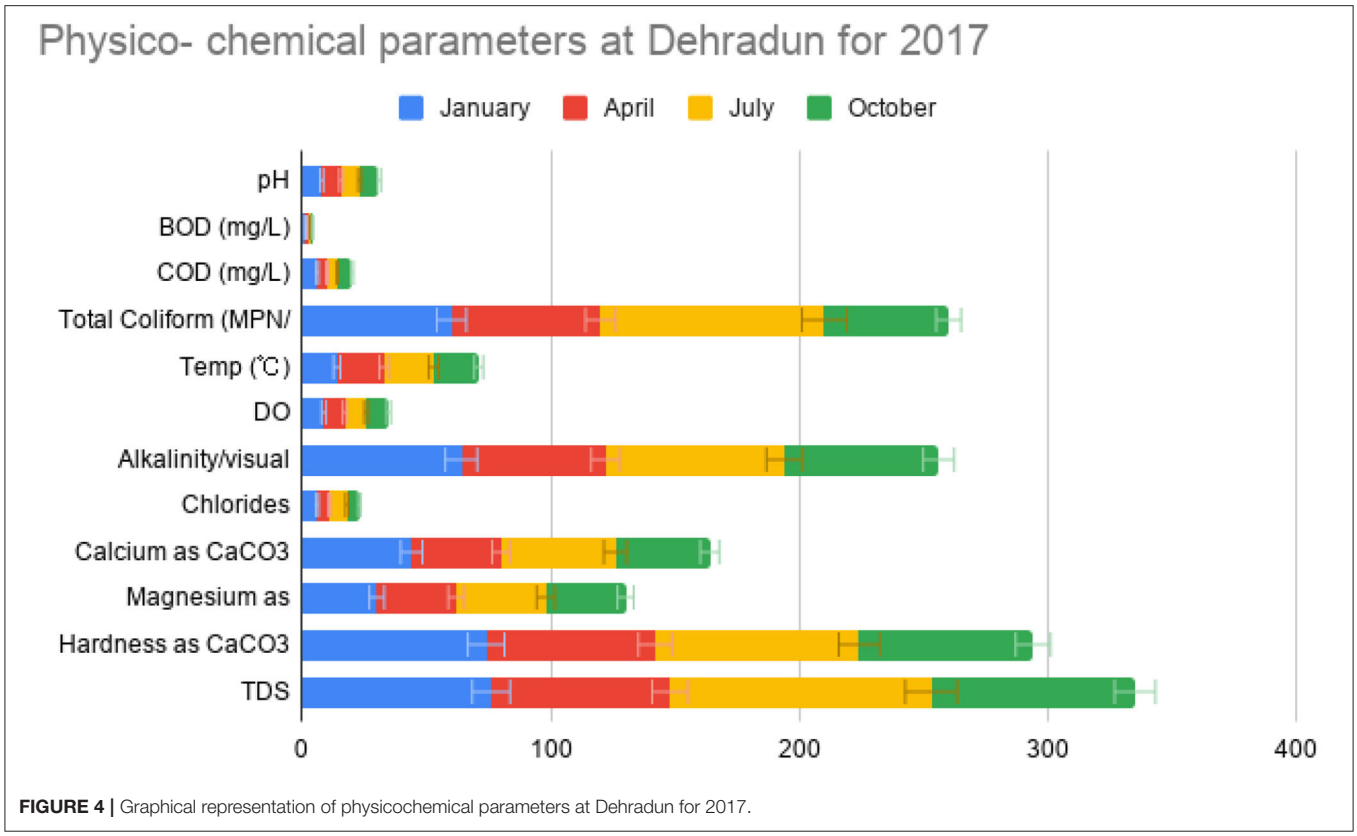


**FIGURE 4 |** Graphical representation of physicochemical parameters at Dehradun for 2017.

**TABLE 3 |** Physicochemical parameters and water quality analysis at Dehradun for 2018.

| | January | April | July | October | Mean | ST DEV | Observed value (vi) | Standard value (Si) | Unit weight (Wi) | Quality rating (qi) | Wiqi |
|---|---|---|---|---|---|---|---|---|---|---|---|
| pH | 7.12 | 7.64 | 7.62 | 8.15 | 7.6325 | 0.420585 | 7.6 | 8.5 | 0.219 | 42 | 9.2 |
| BOD (mg/L) | 1 | 1 | 1 | 1 | 1 | 0 | 1 | 5 mg/L | 0.3723 | 20 | 7.4 |
| COD (mg/L) | 4 | 6 | 4 | 4 | 4.5 | 1 | 4.5 | 25 (WPCSR) | 0.00468 | 18 | 0.1 |
| Total Coliform (MPN/100 ml) | 40 | 40 | 80 | 40 | 50 | 20 | 50 | 50 | — | — | — |
| Temp (°C) | 16 | 19 | 20 | 18 | 18.25 | 1.707825 | 18 | 25 | 0.00468 | 73 | 0.3 |
| DO | 8.8 | 9.2 | 8.8 | 8.6 | 8.85 | 0.251661 | 8.9 | 5 mg/l | 0.3723 | 60 | 22 |
| Alkalinity/ visual titration $CaCO_3$ | 64 | 56 | 72 | 66 | 64.5 | 6.608076 | 65 | 120 (WPCSR) | 0.000975 | 54 | 0.1 |
| Chlorides | 6 | 5 | 6 | 6 | 5.75 | 0.5 | 5.8 | 250 mg/l | 0.0074 | 2.3 | 0 |
| Calcium as $CaCO_3$ | 40 | 40 | 46 | 40 | 41.5 | 3 | 42 | 75 mg/l | 0.025 | 55 | 1.4 |
| Magnesium as $CaCO_3$ | 32 | 30 | 36 | 34 | 33 | 2.581989 | 33 | 50 | — | — | — |
| Hardness as$CaCO_3$ | 72 | 70 | 82 | 74 | 74.5 | 5.259911 | 75 | 200 | 0.0062 | 37 | 0.2 |
| TDS | 76 | 78 | 110 | 86 | 87.5 | 15.60983 | 88 | 500 mg/ | 0.0037 | 18 | 0.1 |
| | | | | | | | | | 1.01624 | 379 | 41 |
| | | | | | | | | | | WQI | 40.47 |

Yamuna river is polluted, but it is still revivable. Developmental and maintaining efforts can be adopted to make the Yamuna river clean again and improve the WQI severely. Moreover, it is a positive sign that the WQI of the Yamuna river has improved greatly for the year 2018 compared to the year 2017.

The dendrogram and graphical representation for the physicochemical parameters at Dehradun for 2018 are plotted between the months (January, April, July, and October) and also the parameters [TDS, Total Coliform (MPN/100 ml), Alkalinity/visual titration $CaCO_3$, Hardness as $CaCO_3$, Calcium as $CaCO_3$, Magnesium as $CaCO_3$, Temp, BOD, pH, DO, COD,

and Chlorides] (**Figures 5**, **6**). Cluster 1 (blue) represents lightly polluted and the parameters include Temp, BOD, pH, DO, COD, and Chlorides.

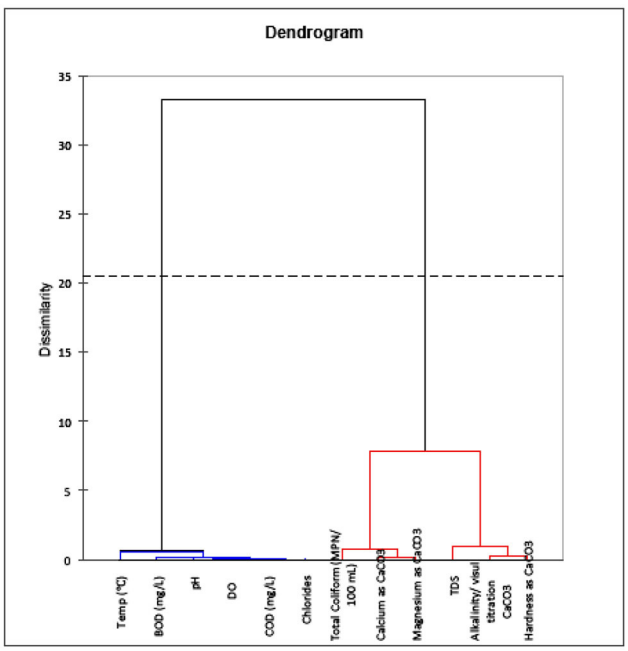


**FIGURE 5 |** Dendrogram for physicochemical parameters at Dehradun for 2018.

Cluster 2 (red) represents moderately polluted, and the parameters include Total Coliform (MPN/100 ml), Calcium as $CaCO_3$, Magnesium as $CaCO_3$, TDS, Alkalinity/visual titration $CaCO_3$, Hardness as $CaCO_3$. Cluster 3 (black) represents heavily polluted, and the parameters include BOD, pH, DO, COD, Chlorides, Total Coliform (MPN/100 ml), Alkalinity/visual titration $CaCO_3$, Hardness as $CaCO_3$, Calcium as $CaCO_3$, and Magnesium as $CaCO_3$.

## Measurement of Physicochemical Parameters at Dehradun for 2019

Water samples have been taken in different months for the year 2019 (**Table 4**). The mean and standard deviation for the measured values have been also calculated. The mean is the number found by summing every data point and dividing by the number of data points. Standard deviation is defined as the number that is going to tell about the measurements for a group that is spread out from the mean or expected value. Comparing the values of this year with those of the previous years leads to the outcomes being observed.

The maximum value of pH is in the month of January when the, water is a little more basic and the minimum value is in the month of October when the water is less basic. The mean pH is 7.6225, and the standard deviation is 0.411208. The maximum value of BOD is in July when there is a large quantity of polluted water, and the minimum value is in January, April, and October when there is less quantity of polluted water. The mean of BOD is 1.05, and the standard deviation is 0.1. The maximum value of COD is in July and October indicating a greater amount of

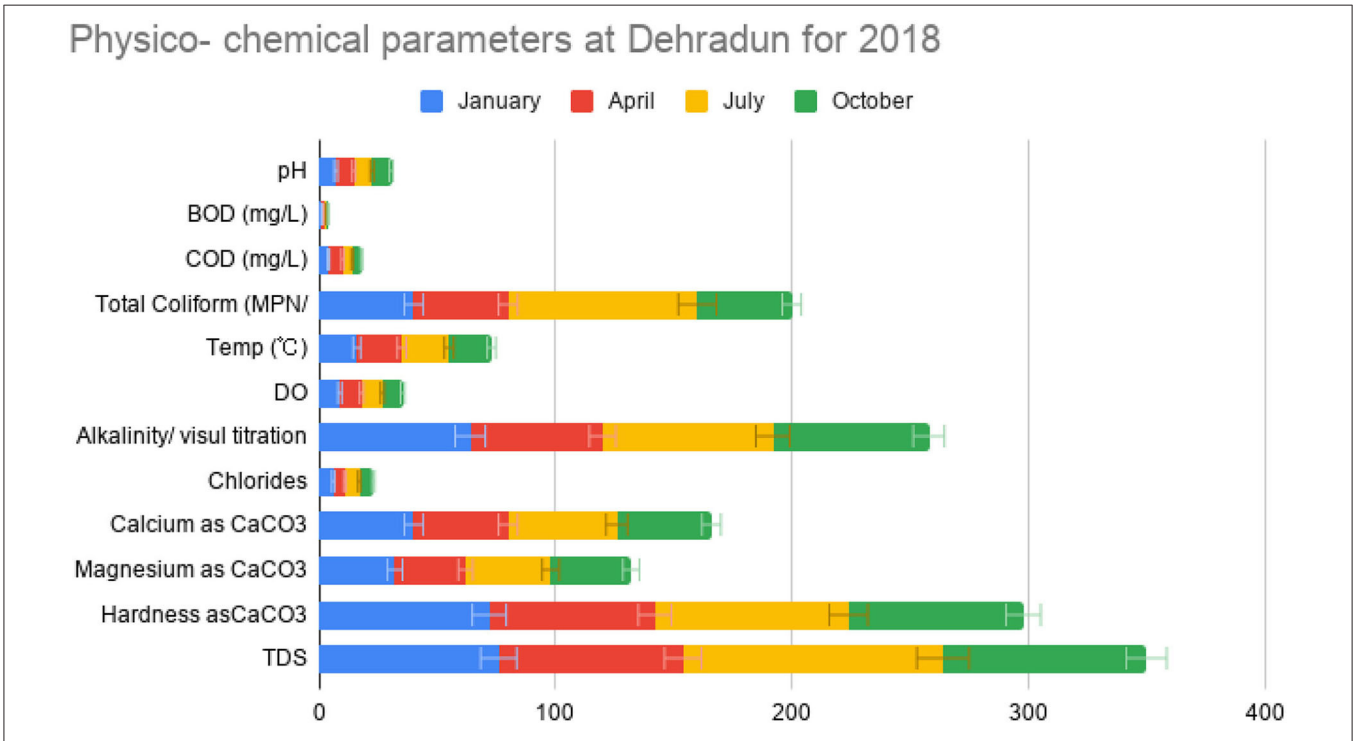


**FIGURE 6 |** Graphical representation of physicochemical parameters at Dehradun for 2018.

**TABLE 4 |** Physicochemical parameters and water quality analysis at Dehradun for 2019.

| | January | April | July | October | Mean | ST DEV | Observed value (vi) | Standard value (Si) | Unit weight (Wi) | Quality rating (qi) | Wiqi |
|---|---|---|---|---|---|---|---|---|---|---|---|
| pH | 7.98 | 7.72 | 7.76 | 7.03 | 7.6225 | 0.411208 | 7.6 | 8.5 | 0.219 | 42 | 9.1 |
| BOD (mg/l) | 1 | 1 | 1.2 | 1 | 1.05 | 0.1 | 1.1 | 5 mg/l | 0.3723 | 21 | 7.8 |
| COD (mg/l) | 4 | 4 | 6 | 6 | 5 | 1.154701 | 5 | 25 (WPCSR) | 0.00468 | 20 | 0.1 |
| Total Coliform (MPN/ 100 ml) | 60 | 280 | 220 | 170 | 182.5 | 93.22911 | 182.5 | 50 | — | — | — |
| Temp | 17 | 18 | 19 | 20 | 18.5 | 1.290994 | 18.5 | 25 | 0.00468 | 74 | 0.3463 |
| DO | 9 | 9.2 | 8.6 | 8.8 | 8.9 | 0.258199 | 19 | 25 | 0.00468 | 74 | 0.3 |
| Alkalinity/visual titration $CaCO_3$ | 70 | 72 | 70 | 60 | 68 | 5.416026 | 8.9 | 5 mg/l | 0.3723 | 59 | 22 |
| Chlorides | 6 | 6 | 6 | 12 | 7.5 | 3 | 68 | 120(WPCSR) | 0.000975 | 57 | 0.1 |
| Calcium as $CaCO_3$ | 46 | 44 | 46 | 62 | 49.5 | 8.386497 | 49.5 | 75 mg/l | 0.025 | 66 | 1.65 |
| Magnesium as $CaCO_3$ | 32 | 36 | 30 | 18 | 29 | 7.745967 | 29 | 50 | — | — | — |
| Hardness as $CaCO_3$ | 78 | 80 | 76 | 80 | 78.5 | 1.914854 | 7.5 | 250 mg/l | 0.0074 | 3 | 0 |
| TDS | 98 | 105 | 112 | 82 | 99.25 | 12.84199 | 50 | 75 mg/l | 0.025 | 66 | 1.7 |
| | | | | | | | | | | 1.01624 | 401 |
| | | | | | | | | | | WQI | 40.82 |

oxidizable organic materials in the sample, and the minimum value is in January and April indicating a lesser amount of oxidizable organic materials in the sample. The mean of COD is 5, and the standard deviation is 1.154701. The maximum value of Total Coliform is in April indicating that water-borne illness is increased, and the minimum value is in January indicating that water-borne illness is decreased. The mean of Total Coliform is 182.5, and the standard deviation is 93.22911. The maximum value of Temp is in October indicating increased chemical reactions generally, and the minimum value is in January indicating decreased chemical reactions. The mean of Temp is 18.5, and the standard deviation is 1.290994. The maximum value of DO is in April, and the minimum value is in July. The mean of DO is 8.9, and the standard deviation is 0.258199. The maximum value of Alkalinity/visual titration $CaCO_3$ is in April indicating higher buffering capacity against pH changes, and the minimum value is in October indicating lower buffering capacity against pH changes. The mean of Alkalinity/visual titration $CaCO_3$ is 68, and the standard deviation is 5.416026.

The maximum value of Chlorides is in October indicating body-related diseases, and the minimum value is in January, July, and April. The mean of Chlorides is 7.5, and the standard deviation is 3. The maximum value of Calcium as $CaCO_3$ is in October, which has a positive effect on the body, and the minimum value is in April, the month which has a less positive effect on the body. The mean of $CaCO_3$ is 49.5, and the standard deviation is 8.386497. The maximum value of Magnesium as $CaCO_3$ is in April, which has a positive effect on the body, and the minimum value is in October, which has a less positive effect on the body. The mean of Magnesium as $CaCO_3$ is 29, and the standard deviation is 7.745967. The maximum value of Hardness as $CaCO_3$ is in April and October, which has a good effect on the body, and the minimum value is in July. The mean of Hardness as $CaCO_3$ is 78.5, and the standard deviation is 1.914854. The maximum value of TDS is in July specifying the presence of toxic minerals, and the minimum value is in October specifying the presence of less toxic minerals. The mean of TDS is 99.25, and the standard deviation is 12.84199.

Water quality index (WQI) was used to evaluate the variation in water quality of the Yamuna river at Dehradun over 3 years. The standard and prescribed method has been used to analyze the water quality for 12 physiochemical parameters (TDS, Chlorides, Alkalinity, DO, Temperature, COD, BOD, pH, Magnesium, Hardness, Total Coliform, and Calcium). Calculations have been performed using the standardized formula and mathematical models. Detailed calculations and methodology have been used to find the water quality index as accurately as possible. The WQI of the Yamuna river in Dehradun for the year 2019 was 40.82 (**Table 4**). According to WHO, the WQI should be below 60 for its quality to be at least fair. Here, it can be easily concluded that the Yamuna river is polluted, but it is still revivable. Developmental and maintaining efforts can be adopted to make the Yamuna river clean again and improve the WQI drastically. Moreover, it is a positive sign that the WQI of the Yamuna river has improved for year 2019 compared to the year 2017, whereas the WQI has increased again in 2019 compared to 2018. It can be documented that the Yamuna river was the cleanest in the year 2018, and its water quality in 2019 has improved in collation to the year 2017.

The correlation coefficients between the inspected parameters of the Yamuna river water at Dehradun in the year 2019 are shown in **Table 5**. Ph is positive for TDS, alkalinity, and Magnesium ($CaCO_3$) and negative for COD, Temp, and Calcium ($CaCO_3$). BOD is positive for COD and TDS and negative for DO and hardness ($CaCO_3$). COD is positive for Temp, Chlorides, and Calcium and negative for DO, magnesium ($CaCO_3$), and alkalinity. Temp is positive for calcium ($CaCO_3$) and negative for alkalinity. DO is positive for Magnesium ($CaCO_3$). Alkalinity is positive for TDS and negative for Calcium, Magnesium, and hardness of $CaCO_3$. The dendrogram

**TABLE 5 |** Correlation table for physicochemical parameters at Dehradun for 2019.

| | pH | BOD (mg/l) | COD (mg/l) | Total Coliform | Temp(°C) | DO | Alkalinity | Chlorides | Calcium | Magnesium | Hardness | TDS |
|---|---|---|---|---|---|---|---|---|---|---|---|---|
| pH | 1 | | | | | | | | | | | |
| BOD | 0.222921 | 1 | | | | | | | | | | |
| COD | −0.63884 | 0.57735 | 1 | | | | | | | | | |
| Total Coliform | −0.1889 | 0.268157 | 0.15482 | 1 | | | | | | | | |
| Temp | −0.88221 | 0.258199 | 0.894427 | 0.373884 | 1 | | | | | | | |
| DO | 0.26058 | −0.7746 | −0.89443 | 0.096933 | −0.6 | 1 | | | | | | |
| Alkalinity | 0.915985 | 0.246183 | −0.6396 | 0.21125 | −0.76277 | 0.381385 | 1 | | | | | |
| Chlorides | −0.96059 | −0.33333 | 0.57735 | −0.08939 | 0.774597 | −0.2582 | −0.98473 | 1 | | | | |
| Calcium | −0.93516 | −0.27823 | 0.619586 | −0.1684 | 0.769686 | −0.33866 | −0.99806 | 0.993661 | 1 | | | |
| Magnesium | 0.880112 | 0.086066 | −0.74536 | 0.226177 | −0.8 | 0.533333 | 0.985245 | −0.94673 | −0.97494 | 1 | | |
| Hardness | −0.53552 | −0.87039 | −0.30151 | 0.177384 | 0.13484 | 0.6742 | −0.38569 | 0.522233 | 0.435895 | −0.22473 | 1 | |
| TDS | 0.762995 | 0.661891 | −0.20231 | 0.391871 | −0.41217 | −0.05026 | 0.881827 | −0.8955 | −0.88982 | 0.800882 | −0.65743 | 1 |

and graphical representation for physicochemical parameters at Dehradun for 2017 are plotted between months (January, April, July, and October) and parameters (TDS, Total Coliform (MPN/100 ml), Alkalinity/visual titration $CaCO_3$, Hardness as $CaCO_3$, Calcium as $CaCO_3$, Magnesium as $CaCO_3$, Temp, BOD, pH, DO, COD, and Chlorides) (**Figures 7**, **8**).

Cluster 1 (blue) represents lightly polluted, and the parameters include BOD, pH, DO, COD, Chlorides, Temp, and Magnesium as $CaCO_3$. Cluster 2 (red) represents moderately polluted, and the parameters include Total Coliform (MPN/100 ml), TDS, Calcium as $CaCO_3$, Alkalinity/visual titration $CaCO_3$, and Hardness as $CaCO_3$. Cluster 3 (black) represents heavily polluted, and the parameters include COD, Chlorides, Temp, Magnesium as $CaCO_3$, Total Coliform (MPN/100 ml), and TDS.

In **Table 6**, the variations in the 12 physicochemical parameter values for Yamuna water at Dehradun for 2017, 2018, and 2019 are shown.

## Trend Forecasting

This section is briefing about the Yamuna river water pollution trend in the next 4 years. The study demonstrates the trend of six physicochemical parameters for the years 2020 to 2024. The considered parameters for calculating the trend forecasting are Temp, Total Coliform, TDS, Hardness, pH, and DO. The forecasting for the said parameters are shown in **Figures 9**–**11**.

According to the trend analysis, the values of four parameters named Temperature, Total Coliform, TDS, and Hardness are increasing yearly, whereas the values of pH and DO are not rising year by year. The trend forecasting is verifying whether the exceptional tourist activity, poor sewage facility, and insufficient wastewater management amenities, is degrading the water of the Yamuna river at Dehradun year by year.

# DISCUSSION

The dendrogram of the mean is plotted between years (2017, 2018, and 2019) and parameters [TDS, Total Coliform (MPN/100 ml), Alkalinity/visual titration $CaCO_3$, Hardness as $CaCO_3$, Calcium as $CaCO_3$, Magnesium as $CaCO_3$, Temp, BOD, pH, DO, COD, and Chlorides] (**Figure 12**). Cluster 1 (blue) represents lightly polluted, and the parameters include Total Coliform (MPN/100 ml), TDS, Alkalinity/visual titration $CaCO_3$, and Hardness as $CaCO_3$. Cluster 2 (red) represents moderately polluted, and the parameters include Calcium as $CaCO_3$ and Magnesium as $CaCO_3$. Cluster 3 (black) represents heavily polluted, and the parameters include TDS, Alkalinity/visual titration $CaCO_3$, Hardness as $CaCO_3$, Calcium as $CaCO_3$, Magnesium as $CaCO_3$, and Temp. Cluster 4 (green) represents equal parameters, and it includes Temp, BOD, pH, DO, COD, and Chlorides.

The variation in observed values, quality rating, and Wiqi can be analyzed using **Tables 2**, **4**, **6**.

According to WHO, the WQI should be below 60 for its quality to be at least fair. If it is more than 60, then the quality of the water is surely poor. If the WQI is <30, then the water quality is good. The WQI of the Yamuna river in Dehradun for the year 2017 was 42.87. It can be easily said that the Yamuna river was quite polluted back then. Developmental and maintaining plans were implemented to make the Yamuna river clean again and improve the WQI drastically. The WQI of the Yamuna river in 2017 was the highest in collation to the subsequent years. This must have set the alarm bells ringing for the government and the citizens. The government has introduced many measures to curb water pollution and revive the Yamuna river as quickly as possible. It is a positive sign that the WQI of the Yamuna river has improved significantly for the years 2018 to 40.47. It was a marked difference in comparison to that of the year 2017. Joint efforts and collaboration by the government and the citizens ensured that the Yamuna river is much cleaner than before, although in 2019, the WQI rose by a small margin to 40.82. It is a sign of relief that it is still much better than the quality of the water in the year 2017. If the measures of the government and corporation by the citizens continue to go hand in hand, the results will be for everyone to see. Even regions in the west would emulate the policies adopted to revive the rivers. Policies included a big budget for the revival project, strict norms for the industries, and appropriate penalties for the defaulters. A common concern for the degrading water quality index of the

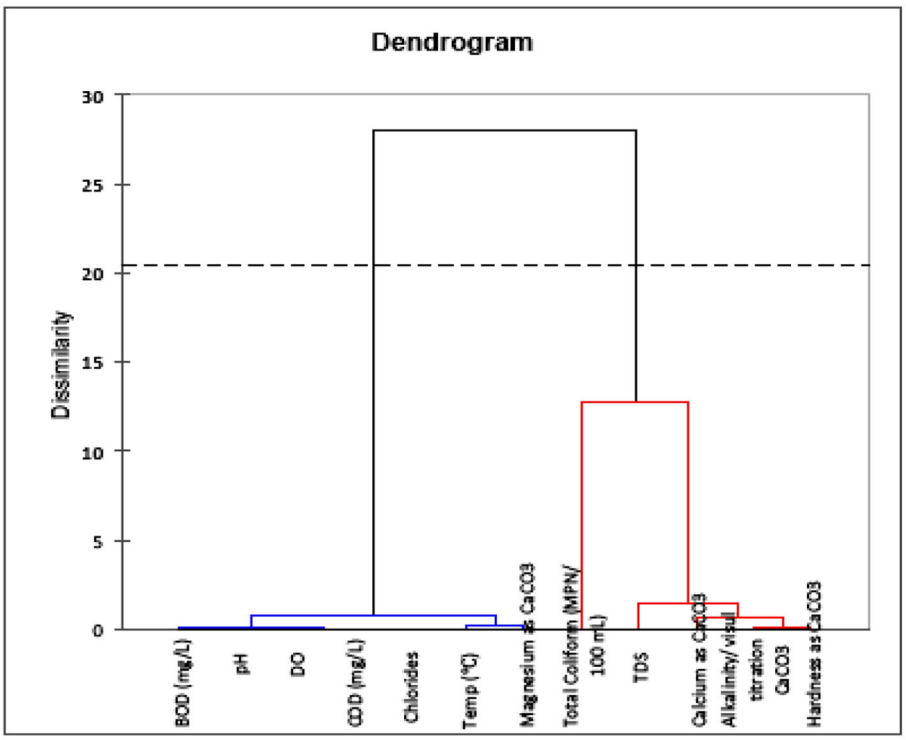


**FIGURE 7 |** Dendrogram for physicochemical parameters at Dehradun for 2019.

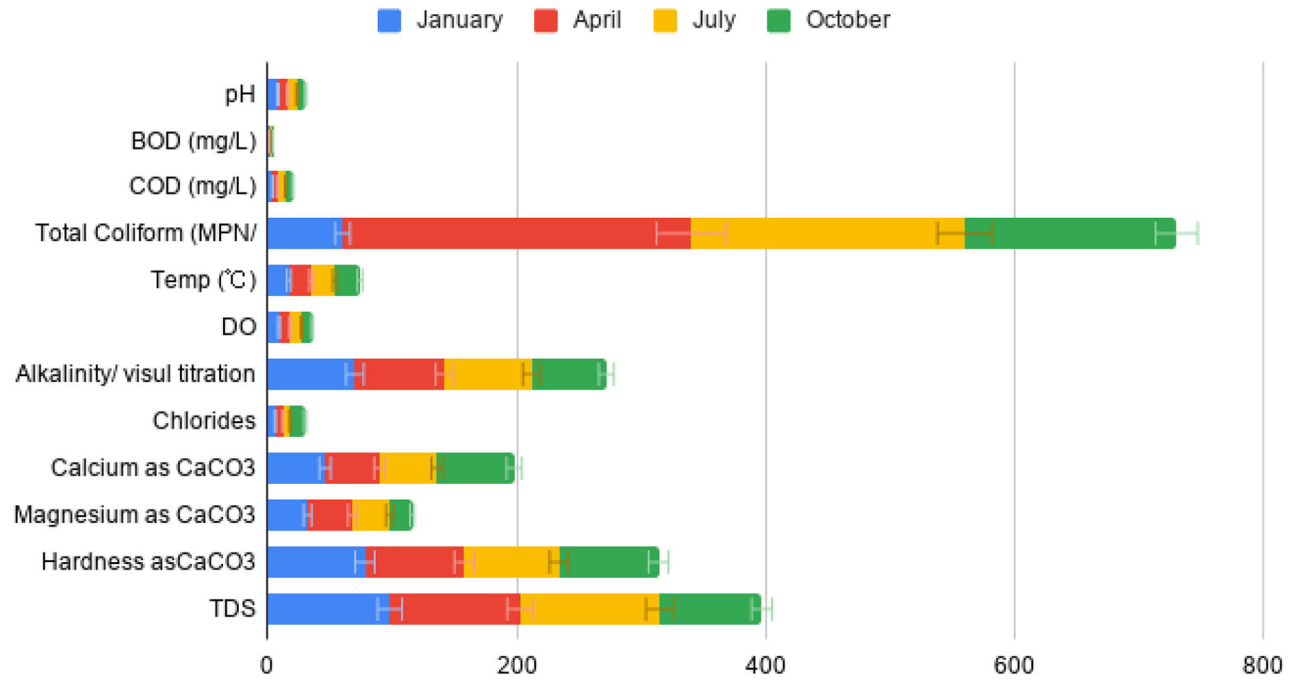


**FIGURE 8 |** Graphical representation of physicochemical parameters at Dehradun for 2019.

**TABLE 6 |** Water quality index (WQI) for Yamuna river at Dehradun for 2017, 2018, and 2019.

| | Quality rating (qi) | Wiqi | Quality Rating (qi) | Wiqi | Quality Rating (qi) | Wiqi |
|---|---|---|---|---|---|---|
| | 2017 | | 2018 | | 2019 | |
| pH | 49 | 11 | 42 | 9.2 | 42 | 9.1 |
| BOD (mg/l) | 21 | 7.8 | 20 | 7.4 | 21 | 7.8 |
| COD (mg/l) | 20 | 0.1 | 18 | 0.1 | 20 | 0.1 |
| Total Coliform (MPN/ 100 mL) | — | — | — | — | — | — |
| Temp (°C) | 71 | 0.3 | 73 | 0.3 | 74 | 0.3463 |
| DO | 61 | 23 | 60 | 22 | 74 | 0.3 |
| Alkalinity/visual titration $CaCO_3$ | 53 | 0.1 | 54 | 0.1 | 59 | 22 |
| Chlorides | 2.3 | 0 | 2.3 | 0 | 57 | 0.1 |
| Calcium as $CaCO_3$ | 55 | 1.4 | 55 | 1.4 | 66 | 1.65 |
| Magnesium as $CaCO_3$ | — | — | — | — | — | — |
| Hardness as$CaCO_3$ | 37 | 0.2 | 37 | 0.2 | 3 | 0 |
| TDS | 17 | 0.1 | 18 | 0.1 | 66 | 1.7 |
| | 386 | 44 | 379 | 41 | 1.01624 | 401 |
| WQI | 42.87 | | 40.47 | | 40.82 | |

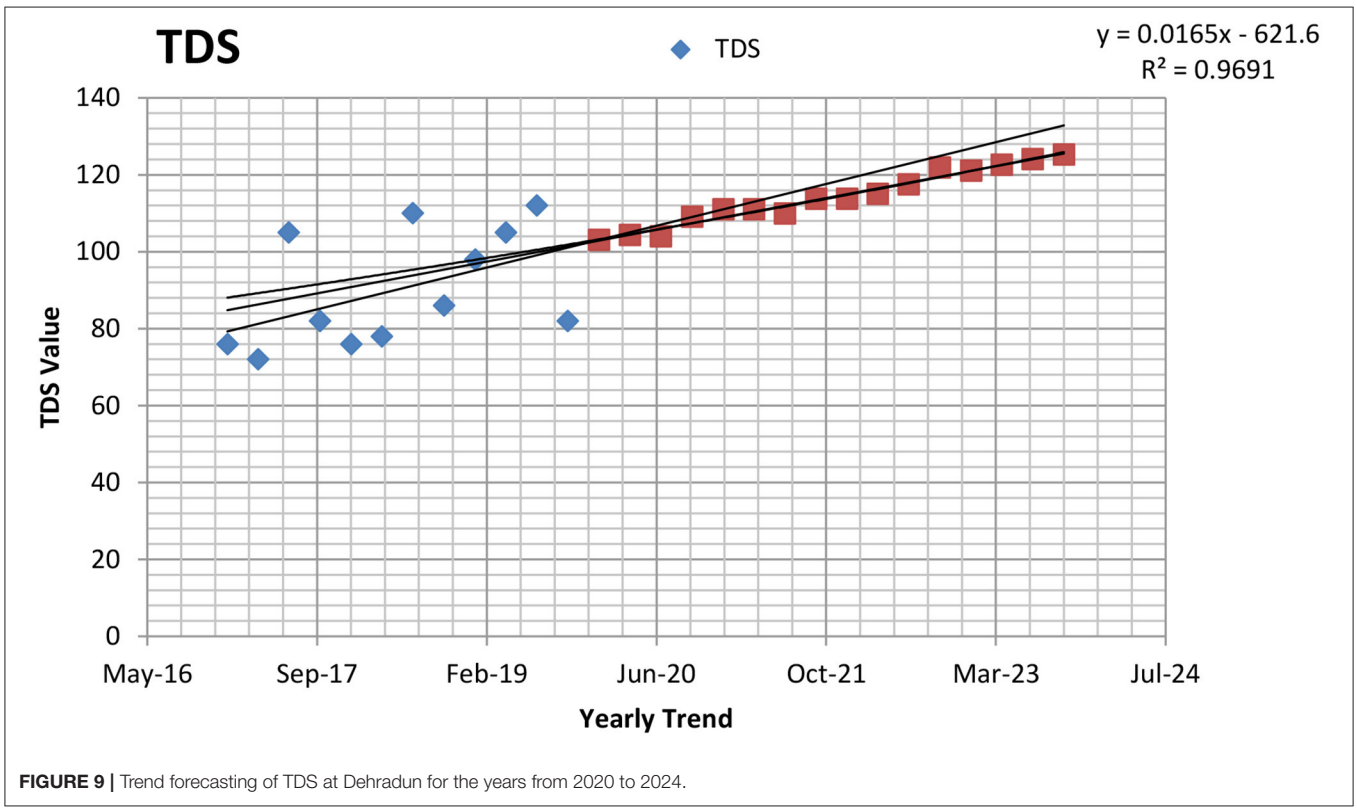


**FIGURE 9 |** Trend forecasting of TDS at Dehradun for the years from 2020 to 2024.

Yamuna river resulted in some swift actions from the citizens as well as from those who became more aware and conscious. It can be easily and comfortably said that the Yamuna river would be much cleaner and in a much-improved condition by the year 2025.

A comparative analysis is shown in **Table 7**. A comparison in description and limitations with previously published approaches are organized in this table.

## CONCLUSION

Due to historical, geographical, religious, political, and sociocultural reasons, India has a unique place in the world. Pollution-causing activities have caused severe changes in aquatic environments over the last few decades. This paper aims to calculate the water quality index of the Yamuna river in Uttarakhand using 12 physicochemical parameters for a while

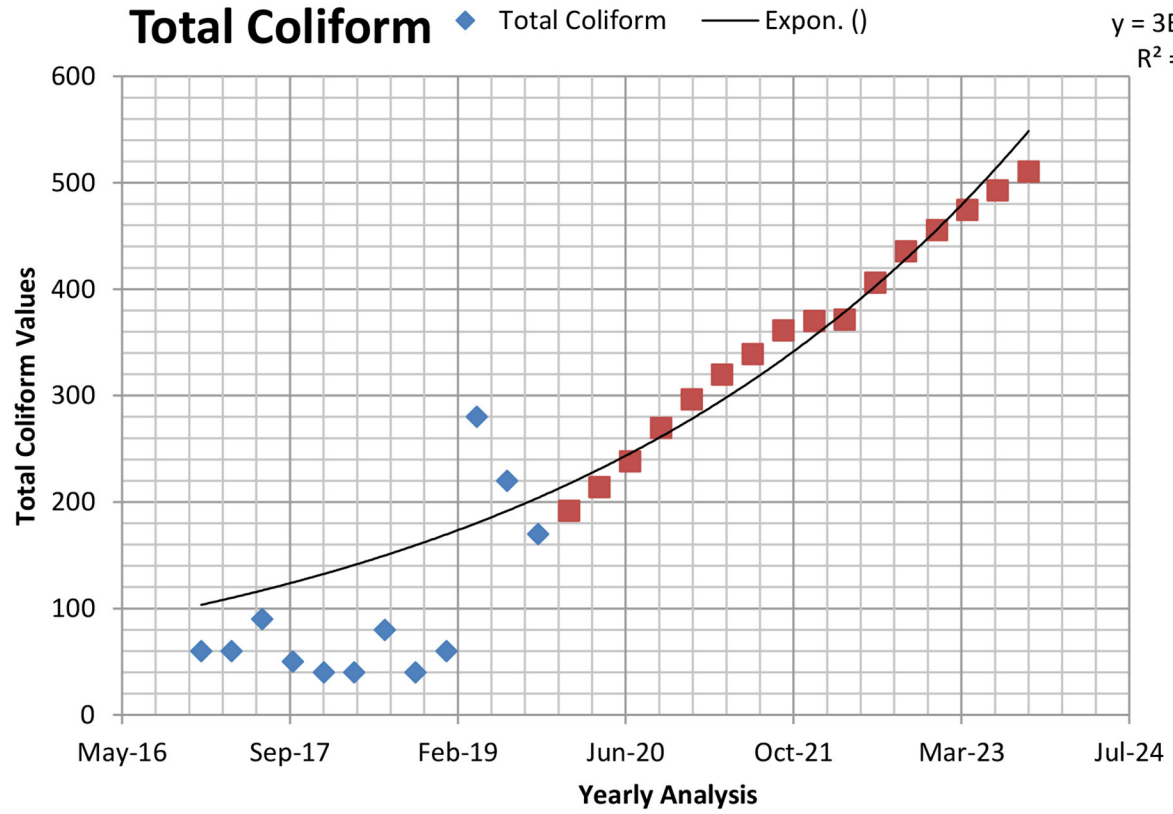


**FIGURE 10 |** Trend forecasting of total Coliform at Dehradun for the years from 2020 to 2024.

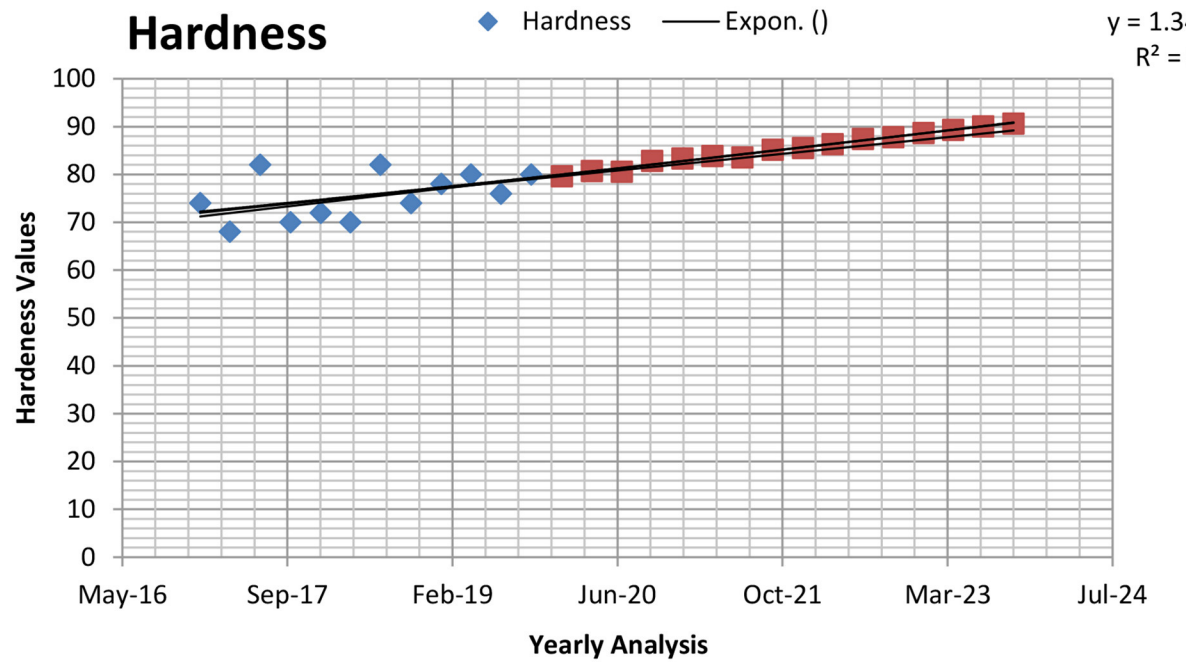


**FIGURE 11 |** Trend forecasting of hardness at Dehradun for the years from 2020 to 2024.

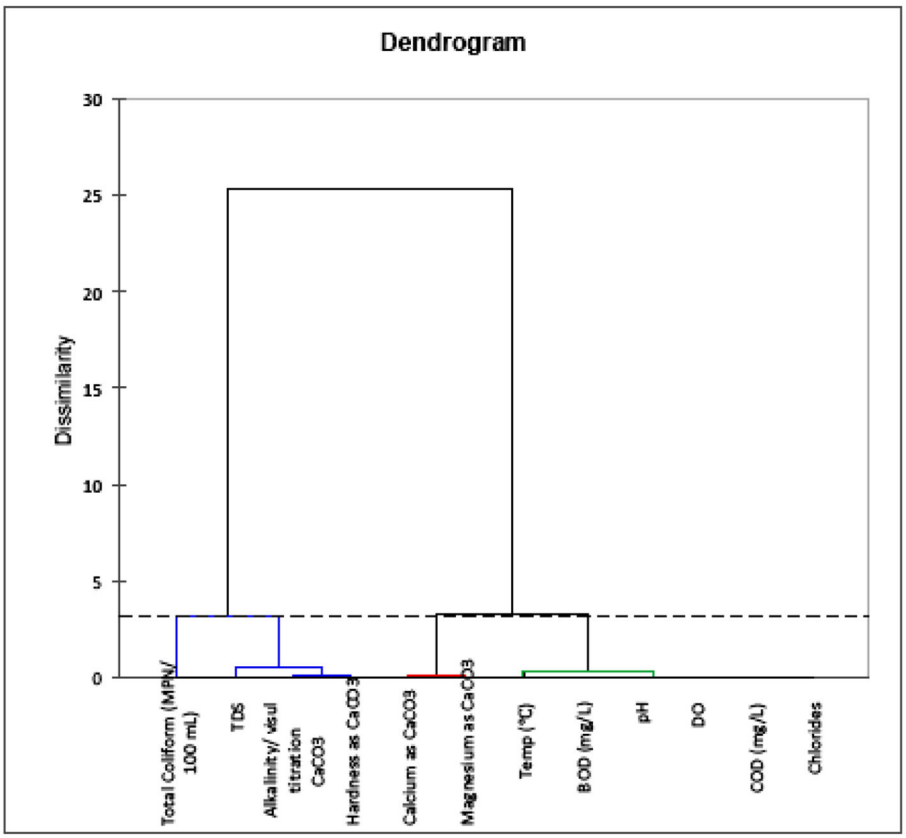


**FIGURE 12 |** Dendrogram for physicochemical parameter mean values for 2017, 2018, and 2019.

**TABLE 7 |** Comparative analysis with previous work done.

| S. No | References | Descriptions | Limitations |
|---|---|---|---|
| 1 | Zhang et al., 2003 | The estimated accuracy of these water quality variables using a neural network is much higher than the accuracy using simple and multivariate regression approaches. | This method is not yet implemented as further discussion is still required. |
| 2 | Dwivedi and Pathak, 2007 | Shifting role of ecology in solving global environmental problems. | Water quality index is calculated for only 1 year. |
| 3 | Marale, 2012 | Shifting role of ecology in solving global environmental problems. | Precautions are not mentioned. |
| 4 | Rafiq, 2016 | Causes of urban flood in India. | There is no information about the precautions taken during the flood. |
| 5 | Agarwal et al., 2016 | Demonstrates the use of a new approach for delineating the accurate flood hazard footprint in the urban regions. | The study will be done for only 2 years. |
| 6 | Ahmad et al., 2017 | Impact of urbanization on hydrological regime in Indian cities. | The study will only be done for the northern region of India. |
| 7 | Tiwari et al., 2020 | Evaluation of geogenic carbon fluxes between solid Earth and its atmosphere. | The study will only take place at Uttarakhand area |
| 8 | Ours' | Study deals with the different water quality parameters of the Yamuna river at Dehradun and calculating its water quality index. | Impact of solid waste on the water quality of the Yamuna river is absent. |

for 3 years from 2017 to 2019. The values of the considered physicochemical parameters have been monitored using the various examining stations installed by the Central Pollution Control Board (CPCB), India. According to WHO, the WQI should be below 60 for its quality to be at least fair. If it is more than 60, then the quality of the water is surely poor. If the WQI is <30, then the water quality is good. The WQI of the Yamuna river in Dehradun for the year 2017 was 42.87. It

can be easily said that the Yamuna river was quite polluted back then. Developmental and maintaining plans were implemented to make the Yamuna river clean again and improve the WQI drastically. The WQI of the Yamuna river in 2017 was the highest in collation to the subsequent years. This must have set the alarm bells ringing for the government and the citizens.

According to the trend analysis, the values of four parameters named Temperature, Total Coliform, TDS, and Hardness are increasing yearly, whereas the values of pH and DO are not rising year by year. The trend forecasting verifies whether the exceptional tourist activity, poor sewage facilities, and insufficient wastewater management amenities is degrading the water of the Yamuna river at Dehradun year by year. It is a positive sign that the WQI of the Yamuna river has improved significantly for the years 2018 to 40.47. It was a marked difference in comparison to the year 2017. Joint efforts and collaboration by the government and the citizens ensured that the Yamuna river is much cleaner than before, although in 2019, the WQI raised by a small margin to 40.82. It is a sign of relief that it is still much better than the quality of the water in the year 2017. If the measures of the government and corporation by the citizens continue to go hand in hand, the results will be for everyone to see. Even regions in the west would emulate the policies adopted to revive the rivers. A common concern for the degrading water quality index of the Yamuna river resulted in some swift actions from the citizens as well as those who became more aware and conscious.

## DATA AVAILABILITY STATEMENT

The datasets presented in this study can be found in online repositories. The names of the repository/repositories and accession number(s) can be found in the article/supplementary material.

## AUTHOR CONTRIBUTIONS

Data curation was done by RS and RK. Formal analysis was made by RS, RK, and SS. The investigation was done by RS, RK, and KS. The methodology was done by RS, NA-A, and RM. Project administration was performed by HL and AA. BP was in charge of the resources and software. BP and NA-A supervised the study. Visualization was done by BP and NA-A. RS, AA, RM, and BP wrote the original draft. All authors contributed to the article and approved the submitted version.

## REFERENCES


Agarwal, A., Rafique, F., Rajesh, E., and Ahmed, S. (2016). Urban flood hazard mapping using change detection on wetness transformed images. *Hydrol. Sci. J.* 61, 816–825. doi: 10.1080/02626667.2014.952638

Ahmad, I. K., Salih, N. M., and Nzar, Y. H. (2012). Determination of water quality index (WQI) for Qalyasan stream in Sulaimani city/Kurdistan region of Iraq. *Int. J. Plant Anim. Environ. Sci.* 2, 148–157.

Ahmad, S., Farooq, S., Zahoor-Ul-Islam, Khan, Md. A., Zaidiand, W. A., and Matloob, H. (2017). Impact of urbanization on hydro logical regime in Indian cities. *J. Environ. Res. Develop.* 2, 594–604.

Allee, R. J., and Johnson, J. E. (1999). Use of satellite imagery to estimate surface chlorophyll a and Secchi disc depth of Bull Shoals Reservoir, Arkansas, USA. *Int. J. Remote Sens.* 20, 1057–1072. doi: 10.1080/01431169912849

Amandeep, V. (2011). Identification of land and water regions in a satellite image: a texture based approach. *Int. J. Comput. Sci. Eng. Technol.* 1, 361–365.

Bhutiani, R., Ahamad, F., Tyagi, V., and Ram, K. (2018). Evaluation of water quality of River Malin using water quality index (WQI). *Environ. Conserv. J.* 19, 191–201. doi: 10.36953/ECJ.2018.191228

Bhutiani, R., and Khanna, D. R. (2007). Ecological status of river Suswa: modelling DO and BOD. *Environ. Monit. Assess.* 125, 183–195. doi: 10.1007/s10661-006-9251-4

Bhutiani, R., Khanna, D. R., Kulkarni, D. B., and Ruhela, M. (2016). Assessment of Ganga river ecosystem at Haridwar, Uttarakhand, India with reference to water quality indices. *Appl. Water Sci.* 6, 107–113. doi: 10.1007/s13201-014-0206-6

Bhutiani, R., Khanna, D. R., Tyagi, B., Tyagi, P. K., and Kulkarni, D. B. (2015). Assessing environmental contamination of River Ganga using correlation and multivariate analysis. *Pollution* 1, 265–273.

Bisht, A. K., Singh, R., Bhutiani, R., Bhatt, A., and Kumar, K. (2017). Water quality modelling of the River Ganga using artificial neural network with reference to the various training functions. *Environ. Conserv. J.* 18, 41–48. doi: 10.36953/ECJ.2017.181206

Brown, R. M., McClelland, N. I., Deininger, R. A., and Tozer, R. G. (1970). Water quality index-do we dare? *Water Sew. Works* 117, 339–343.

Census Reports of India 2001. (1971–1991). Available online at: https://censusindia.gov.in/

Chabuk, A., Al-Ansari, N., Hussain, H. M., Knutsson, S., Pusch, R., and Laue, J. (2017). Combining GIS applications and method of multi-criteriadecision-making (AHP) for landfill siting in Al-HashimiyahQadhaa, Babylon, Iraq. *Sustainability* 9, 19–32. doi: 10.3390/su9111932

Chauhan, A., and Singh, S. (2010). Evaluation of Ganga water for drinking purpose by water quality index at Rishikesh, Uttarakhand, India. *Rep. Opin.* 2, 53–61.

Cude, C. G. (2001). Oregon water quality index: a tool for evaluating water quality management effectiveness. *J. Am. Water Resour. Assoc.* 37, 125–137. doi: 10.1111/j.1752-1688.2001.tb05480.x

Duong, D. N. (2012). Water body extraction from multi spectral image by spectral pattern analysis. *J. Photogramm Remote Sens. Spat. Inf. Sci. Melb. XXXIX-B* 8, 248–259. doi: 10.5194/isprsarchives-XXXIX-B8-181-2012

Dwivedi, S. L., and Pathak, V. A. (2007). Preliminary assignment of water quality index to Mandakini river, Chitrakoot. *Indian J. Environ. Prot.* 27, 1036–1038.

Fraser, R. N. (1998). Multispectral remote sensing of turbidity among Nebraska Sand Hills Lakes. *Int. J. Remote Sens.* 19, 3011–3016. doi: 10.1080/014311698214406

Girgin, S., Kazanci, N., and Dügel, M. (2010). Relationship between aquatic insects and heavy metals in an urban stream using multivariate techniques. *Int. J. Environ. Sci. Technol.* 7, 653–664. doi: 10.1007/BF03326175

Icaga, Y. (2007). Fuzzy evaluation of water quality classification. *Ecol. Indic J. Elsevier* 7, 710–718. doi: 10.1016/j.ecolind.2006.08.002

Kazi, T. G., Arain, M. B., Jamali, M. K., Jalbani, N., Afridi, H. I., Sarfraz, R. A., et al. (2009). Assessment of water quality of polluted lake using multivariate statistical techniques: a case study. *Ecotoxicol. Environ. Saf. J.* 72, 301–309. doi: 10.1016/j.ecoenv.2008.02.024

Kondratyev, K. Y., Pozdnyakov, D. V., and Pettersson, L. H. (1998). Water quality remote sensing in the visible spectrum. *Int. J. Remote Sens.* 19, 957–979. doi: 10.1080/014311698215810

Marale, S. (2012). Shifting role of ecology in solving global environmental problems: selected practical tools. *Environ. Develop. Sustain.* 14, 869–884. doi: 10.1007/s10668-012-9362-8

Nazeer, M., and Nichol, J. E. (2015). Combininglandsat TM/ETM + and HJ-1 A/B CCD sensors for monitoring coastal water quality in Hong Kong. *IEEE Geosci. Remote Sens. Lett.* 12, 1898–1902. doi: 10.1109/LGRS.2015.2436899

Panwar, A., Bartwal, S., Dangwal, S., Aswal, A., Bhandari, A., and Rawat, S. (2015). Water quality assessment of River Ganga using remote sensing and GIS technique. *Int. J. Adv. Remote Sens. GIS* 4, 1253–1261. doi: 10.23953/cloud.ijarsg.116

Pattiaratchi, C. B., Lavery, P., Wyllie, A., and Hick, P. (1994). Estimates of water-quality in coastal waters using multi-date Landsat Thematic Mapper data. *Int. J. Remote Sens*. 15, 84–1571. doi: 10.1080/01431169408954192

Rafiq, F. (2016). Urban floods in India. *Int. J. Sci. Eng. Res*. 7, 721–734.

Ramakrishniah, C. R., Sadashivaiah, C., and Ranganna, G. (2009). Assessment of water quality index for the groundwater in Tumkur Taluk. *E-J Chem*. 6, 523–530. doi: 10.1155/2009/757424

Ronghang, M., Gupta, A., Mehrotra, I., Kumar, P., Patwal, P., Kumar, S., et al. (2019). Riverbank filtration: a case study of four sites in the hilly regions of Uttarakhand, India. *Sustain. Water Resour. Manag.* 5, 831–845. doi: 10.1007/s40899-018-0255-3

Sharma, P., Sood, S., and Mishra, S. K. (2020). Development of multiple linear regression model for biochemical oxygen demand (BOD) removal efficiency of different sewage treatment technologies in Delhi, India. *Sustain. Water Resour. Manag*. 6:29. doi: 10.1007/s40899-020-00377-9

Shi, L., Mao, Z., and Wang, Z. (2018). Retrieval of total suspended matter concentrations from high resolution WorldView-2 imagery: a case study of inland rivers. *IOP Conf. Ser. Earth Environ. Sci.* 121:032036. doi: 10.1088/1755-1315/121/3/032036

Shukla, S., Khire, M. V., and Godan, S. S. (2018). Effects of urbanization on surface and subsurface hydrologic variables of upper bhima river basin, Maharashtra, India. *Model. Earth Syst. Environ.* 4, 699–728. doi: 10.1007/s40808-018-0446-9

Singh, A., Jakubowski, A. R., Chidister, I., and Townsend, P. A. (2013). A MODIS approach to predicting stream water quality in Wisconsin. *Remote Sens. Environ*. 128, 74–86. doi: 10.1016/j.rse.2012.10.001

Song, K. S., Li, L., Li, S., Tedesco, L., Hall, B., and Li, L. H. (2012). Hyperspectral remote sensing of total phosphorus (TP) in three central Indiana water supply reservoirs. *J. Water Air Soil Pollut*. 223, 1481–1502. doi: 10.1007/s11270-011-0959-6

Tiwari, S. K., Gupta, A. K., and Asthana, A. K. L. (2020). Evaluating $CO_2$ flux and recharge source in geothermal springs, Garhwal Himalaya, India: stable isotope systematics and geochemical proxies. *Environ. Sci. Pollut. Res*. 27, 14818–14835. doi: 10.1007/s11356-020-07922-1

Trombadore, O., Nandi, I., and Shah, K. (2020). Effective data convergence, mapping, and pollution categorization of ghats at Ganga River Front in Varanasi. *Environ. Sci. Pollut. Res*. 27, 15912–15924. doi: 10.1007/s11356-019-06526-8

Tyagi, S., Dubey, R. C., Bhutiani, R., and Ahamad, F. (2020). Multivariate Statistical analysis of river ganga water at Rishikesh and Haridwar, India. *Anal. Chem. Lett*. 10, 195–213. doi: 10.1080/22297928.2020.1756405

Wang, Y. P., Xia, H., Fu, J. M., and Sheng, G. Y. (2004). Water quality change in reservoirs of Shenzhen, China: detection using LANDSAT/TM data. *Sci. Total Environ*. 328, 195–206. doi: 10.1016/j.scitotenv.2004.02.020

Zhang, Y., Pulliainen, J. T., Koponen, S. S., and Hallikainen, M. T. (2003). Water quality retrievals from combined landsat TM Data and ERS-2 SAR data in the Gulf of Finland. *IEEE Trans. Geosci. Remote Sens*. 41, 622–629. doi: 10.1109/TGRS.2003.808906

**Conflict of Interest:** The authors declare that the research was conducted in the absence of any commercial or financial relationships that could be construed as a potential conflict of interest.

frontiers in Marine Science

ORIGINAL RESEARCH
published: 22 December 2020
doi: 10.3389/fmars.2020.539827

# Toxicity Going Nano: Ionic *Versus* Engineered Cu Nanoparticles Impacts on the Physiological Fitness of the Model Diatom *Phaeodactylum tricornutum*

*Marco Franzitta[1,2]*, Eduardo Feijão[1,3], Maria Teresa Cabrita[4], Carla Gameiro[1,4], Ana Rita Matos[3,5], João Carlos Marques[6], Johannes W. Goessling[7], Patrick Reis-Santos[1,8], Vanessa F. Fonseca[1,9], Carlo Pretti[2], Isabel Caçador[1,5] and Bernardo Duarte[1,5]*

[1] MARE – Marine and Environmental Sciences Centre, Faculdade de Ciências da Universidade de Lisboa, Lisbon, Portugal, [2] Department of Veterinary Sciences, University of Pisa, Pisa, Italy, [3] BioISI – Biosystems and Integrative Sciences Institute, Plant Functional Genomics Group, Departamento de Biologia Vegetal, Faculdade de Ciências da Universidade de Lisboa, Lisbon, Portugal, [4] Instituto do Mar e da Atmosfera, Lisbon, Portugal, [5] Departamento de Biologia Vegetal, Faculdade de Ciências da Universidade de Lisboa, Lisbon, Portugal, [6] MARE – Marine and Environmental Sciences Centre, c/o Department of Zoology, Faculty of Sciences and Technology, University of Coimbra, Coimbra, Portugal, [7] International Iberian Nanotechnology Laboratory, Braga, Portugal, [8] Southern Seas Ecology Laboratories, School of Biological Sciences, The University of Adelaide, Adelaide, SA, Australia, [9] Departamento de Biologia Animal, Faculdade de Ciências da Universidade de Lisboa, Lisbon, Portugal

OPEN ACCESS

**Edited by:**
*Naser A. Anjum, Aligarh Muslim University, India*

**Reviewed by:**
*Ilaria Corsi, University of Siena, Italy*
*Tore Brembu, Norwegian University of Science and Technology, Norway*

***Correspondence:**
*Marco Franzitta*
*franzitta.marco@gmail.com*

**Specialty section:**
*This article was submitted to Marine Pollution, a section of the journal Frontiers in Marine Science*

**Received:** *02 March 2020*
**Accepted:** *04 December 2020*
**Published:** *22 December 2020*

**Citation:**
*Franzitta M, Feijão E, Cabrita MT, Gameiro C, Matos AR, Marques JC, Goessling JW, Reis-Santos P, Fonseca VF, Pretti C, Caçador I and Duarte B (2020) Toxicity Going Nano: Ionic Versus Engineered Cu Nanoparticles Impacts on the Physiological Fitness of the Model Diatom Phaeodactylum tricornutum. Front. Mar. Sci. 7:539827. doi: 10.3389/fmars.2020.539827*

Increasing input of Metal Engineered Nano Particles (MeENPs) in marine ecosystems has raised concerns about their potential toxicity on phytoplankton. Given the lack of knowledge on MeENPs impact on these important primary producers, the effects of Copper Oxide (CuO) ENPs on growth, physiology, pigment profiles, fatty acid (FA) metabolism, and oxidative stress were investigated in the model diatom *Pheodactylum tricornutum*, to provide suitable biomarkers of CuO ENP exposure versus its ionic counterpart. Diatom growth was inhibited by CuO ENPs but not Ionic Cu, suggesting CuO ENP cytotoxicity. Pulse Modulated Amplitude (PAM) phenotyping evidenced a decrease in the electron transport energy flux, pointing to a reduction in chemical energy generation following CuO ENPs exposure, as well as an increase in the content of the non-functional Cu-substituted chlorophyll *a* (CuChl *a*). A significant decrease in eicosapentaenoic acid (C20:5) associated with a significant rise in thylakoid membranes FAs reflected the activation of counteractive measures to photosynthetic impairment. Significant increase in the omega 6/omega 3 ratio, underline expectable negative repercussions to marine food webs. Increased thiobarbituric acid reactive substances reflected heightened oxidative stress by CuO ENP. Enhanced Glutathione Reductase and Ascorbate Peroxidase activity were also more evident for CuO ENPs than ionic Cu. Overall, observed molecular changes highlighted a battery of possible suitable biomarkers to efficiently determine the harmful effects of CuO ENPs. The results suggest that the occurrence and contamination of these new forms of metal contaminants can

impose added stress to the marine diatom community, which could have significant impacts on marine ecosystems, namely through a reduction of the primary productivity, oxygen production and omega 6 production, all essential to sustain heterotrophic marine life.

**Keywords: CuO nanoparticles, photobiology, oxidative stress, lipid metabolism, phytoplankton, cytotoxicity, marine systems**

## INTRODUCTION

Trace metal pollution poses a serious threat to marine environments. Poor management of anthropogenic waste and the accumulation of trace metals in sediments and seawater can lead to detrimental alterations in metabolic pathways of marine organisms, as well as in entire coastal ecosystems (Prosi, 1981; Pan and Wang, 2012). A large part of metal pollution affects marine life through direct toxic effects of metal elements (e.g., Pb, Cd, and Hg), or by altering the equilibrium of essential trace metals (e.g., Fe, Cu, and Zn), which can become toxic at high concentrations (Sunda, 1989; Ansari et al., 2004; Wei et al., 2014). Considering that higher human population densities and associated anthropogenic activities generally occur near estuarine and coastal areas, these regions are among the most immediately affected ecosystems by human-generated waste (UNEP, 2006). Metals are typical contaminants, often emerging from local or upstream industries (Duarte et al., 2010; Cabrita et al., 2014; Duarte et al., 2017). Nowadays, new anthropogenic metal forms occur in marine environments as a consequence of increasing use of nanoparticles in a variety of industrial application (UNEP, 2006).

Although metal nanoparticles can arise from both natural (aquatic colloids, volcanic activity, and atmospheric dust) and anthropogenic (industrial emissions) sources (Nowack and Bucheli, 2007), and organisms have always been exposed to them (Klaine et al., 2008), Metal Engineered Nano Particles (MeENPs) should be considered and investigated separately (Oberdörster et al., 2005). The increasing use of MeENPs is raising concerns related to their potential role as new or emerging contaminants in marine ecosystems. Copper nanoparticles, as conductive material, have many applications such as catalyst and solid lubricant, in optical and electronic applications, in particular medical applications, in manufacturing of nanofluids, conductive films, and as antimicrobial agents (Din and Rehan, 2017; Zhang et al., 2018). The increasing interest in this type of nanoparticles at the industrial and commercial level is reflected by their escalating values from 2016 (10.92 Billion USD) to projected values of 25.26 Billion USD by 2022 (Research And Markets.com., 2018). Besides the current level of exposure of organisms, the increasingly widespread use of different types of MeENPs, and the predicted exponential increase in production volumes (Royal Commission on Environmental Pollution., 2008), will undoubtedly lead to greater impact over biota within all environmental compartments (Rip et al., 1995).

In principal, copper is an essential nutrient for microalgae at trace concentrations. It is component of several proteins and enzymes (e.g., plastocyanin, cytochrome oxidase, ascorbate oxidase, and Cu/Zn superoxide dismutase) and involved in a variety of metabolic pathways (Twining and Baines, 2013). However, in excess presence, copper interferes with numerous physiological, biochemical, and structural processes inducing high toxicity in cells (Fernandes and Henriques, 1991; Hook et al., 2014). Previous studies reported microalgal growth inhibition (Cid et al., 1995), production of reactive oxygen species (ROS) and altered fatty acid (FA) production (Morelli and Scarano, 2004) in Cu-exposed microalgae. However, knowledge of the effects of MeENPs in microalgae as important primary producers of marine environments is limited.

Using variable fluorescence signals of chlorophyll *a* (Chl *a*) from photosystem II as a proxy, pulse modulated amplitude (PAM) represents a fast, non-invasive, quantitative and qualitative methodology to evaluate the photonic energy harvest and its transformation processes into electronic energy (Kumar et al., 2014). FAs that compose the lipidic fraction of membranes of phytoplankton organisms are widely used as biomarkers to evaluate exposure of multiple abiotic and biotic stressors including contaminants (Feijão et al., 2018; Duarte et al., 2019). FA profiles, depicting levels of linolenic acid 18:2 (omega-6), linoleic acid C18:3 and omega-3 FAs, such as the long-chain polyunsaturated (LC-PUFAs), eicosapentaenoic acid (EPA), and docosahexaenoic acid (DHA), are not only important structural elements controlling the cell metabolism (Fan et al., 2007), but are also of ecological importance due to their essential character for higher trophic levels (Arts et al., 2001; Parrish, 2009). The n-3 LC-PUFA originates from phytoplankton and its biomagnification through the food web is fundamental to sustain marine ecosystems (Saito and Aono, 2014). A decrease in the synthesis of these key biomolecules can have dangerous cascading effects on entire marine food webs (Gladyshev et al., 2013). Therefore, it is worth investigating if FAs have the potential to be efficient biomarkers of nanoparticle stress, as found for other stressors in marine organisms (Filimonova et al., 2016; Feijão et al., 2018).

The present work expands on the work done by Zhu et al. (2017), by providing an integrative and comprehensive approach to assess the effects of Copper Oxide (CuO) ENP on diatom physiology. It examines the photosynthetic metabolic pathway, the oxidative stress responses, the variations in lipid metabolism and the production of Cu substituted chlorophylls in the marine diatom *P. tricornutum*. This species is a cosmopolitan marine pennate diatom and is a common model organisms to study the effects of pollutant exposure due to its rapid response to trace element changes in the environment (Chen et al., 2012; Cabrita et al., 2018, 2016, 2013, 2014; Feijão et al., 2018). In order to evaluate the effects of Cu forms in *P. tricornutum*,

non-lethal concentrations of Cu were chosen in this study, similar to those found in previous analysis focusing on estuarine systems (Cabrita et al., 2018). Reported concentrations were assumed for both, dissolved and ENP forms, in order to compare effects at similar concentrations.

# MATERIALS AND METHODS

## Experimental Setup

*Phaeodactylum tricornutum* Bohlin (Bacillariophyceae; strain IO 108-01, IPMA) axenic cell cultures (maintained under asexual reproduction conditions) were grown in 250 ml of *f/2* medium (Guillard and Ryther, 1962), under controlled conditions for 6 days (18 ± 1°C, constant aeration and a 12 h light to 12 h dark photoperiod). The growth chamber was programmed with a sinusoidal function simulating sunrise and sunset, with light intensity at noon to simulate a natural light environment [RGB 1:1:1 (molar proportion), maximum photon flux density (PAR) 80 μmol photons $m^{-2}$ $s^{-1}$, 14/10 h day/night rhythm]. Initial cell concentration was approximately $2.7 \times 10^5$ cells $mL^{-1}$, following the Organization for Economic Cooperation and Development (OECD) guidelines for algae bioassays (OECD, 2011). Cultures were exposed to increasing concentrations of copper in either ionic or ENP forms, namely 1 (low), 5 (medium), and 10 (high) μg $L^{-1}$, applied during the exponential growth phase (3 days after inoculation under the described conditions). Exposure trial occurred for an additional 3 days period. The ionic Cu form was $CuSO_4$, whilst Cu ENPs were purchased as CuO nanoparticles with a particle size less than 50 nm and a surface area of 29 $m^2$ $g^{-1}$ (Sigma-Aldrich, Catalog number 544868) These concentrations are in accordance with the observed concentrations in estuarine and coastal systems, considering total metal concentration, and were tested in the past, using the ionic Cu form and the same model diatom species (Duarte et al., 2014; Cabrita et al., 2016, 2018). For every metal concentration, 3 replicates were tested and compared to 3 control experiments without Cu treatment. All glassware were cleaned with $HNO_3$ (20%) for 2 days, rinsed thoroughly with Milli-Q water (18.2 MΩ cm), and autoclaved to avoid contamination. Culture manipulations were performed under laminar airflow in sterile conditions. Samples were collected at the end of the 6th day of the experiment (after 3 days of exposure to the Cu forms), for cell counting, PAM measurements, determination of fresh weight and for biochemical analyses. After centrifuging the samples at 6,000 × *g* for 15 min at 4°C, the supernatant was removed and pellets were immediately frozen in liquid nitrogen and stored at -80°C for biochemical analyses. Three replicates for each analysis were used for all treatments (control, ionic Cu- and CuO ENP -exposed cells).

## Cell Growth Rates

Cell counting of *P. tricornutum* was performed on a Neubauer improved counting chamber, under an Olympus BX50 (Tokyo, Japan) inverted microscope, at 400× magnification. Growth rates, estimated as the mean specific growth rate per day, were calculated from the difference between initial and final logarithmic cell densities divided by the exposure period (Santos-Ballardo et al., 2015).

## Copper Cell Content

All labware for metal analysis were previously decontaminated in a nitric acid bath. Diatom pellets for metal analysis were processed according to Cabrita et al. (2014). Briefly, diatom pellets were double-washed with *f/2* medium to remove externally adsorbed copper ions. After washing, pellets were dried at 60°C until constant weight and mineralized in a Teflon reactor with $HNO_3$:$HClO_4$ acid mixture (7:1) for 3 h at 110°C. After cooling, digestion products were added with ICP-grade Gallium as an internal standard (1 mg $L^{-1}$ final concentration). A 5 μL aliquot of each sample digestion product was then transferred to silicon-coated quartz disks and evaporated to dryness at 80°C. Samples on quartz disks were analyzed by total X-ray fluorescence spectroscopy (TXRF) using a S2 PICOFOX (Bruker, Germany), featuring an air-cooled low power X-ray metal-ceramic tube with a molybdenum target, working at 50 W of max power, and a liquid nitrogen-free Silicon Drift Detector (SSD; Brucker, 2007). Each sample was irradiated for 1,000 s. Possible drift in the spectroscopic amplification was compensated or reset through gain correction (Brucker, 2007). The relative abundance of intensities of the different elements was processed by referring to the Gallium peak (internal standard). The interpretation of the TXRF spectra and Cu concentration calculations was performed using the software program SPECTRA 6.3 (Bruker AXS Microanalysis GmbH). To evaluate the potential release of copper from the nanoparticle form, a set of twin experiments was prepared with f/2 medium and the nanoparticles in the same concentrations and experimental conditions as the exposure trials. Water samples from this trial were collected at the same timepoints as the exposure trial. Samples were centrifuged, to avoid nanoparticle contamination, and Gallium was added to the supernatant as internal standard and the samples analyzed by TXRF, according to the methodology described above for the cell Cu content analysis in this manuscript.

## Copper ENPs Characterization

Cu ENPs, dissolved in distilled water in a final concentration of 40 mg $L^{-1}$, were sonicated for 30 min, prior to dropcasting on 40 nm gold sputtered silicon substrates. Samples were air dried and then mounted on microscope stubs and grounded with Electrodag silver paint and copper tape. A dual-beam focused ion beam scanning electron microscope (SEM; FEI, Oregon, United States) was used to record Cu ENPS. Particle zeta potential was determined in experimental concentrations of Cu ENPS dissolved in *f/2* medium at the Nanophotonics & Bioimaging Facility of the International Iberian Nanotechnology Laboratory (Braga, Portugal), using a Dynamic Light Scattering System (DLSS; model SZ-100Z, Horiba Seisakusho, Japan). Cu ENP size distribution was surveyed using DLSS and through SEM (**Supplementary Figures 1A–D**). Particle elemental compositon and X-ray fluorescence spectra was obtained from the Cu ENPs in *f/2* medium using by TXRF as abovementioned (S2 PICOFOX, Bruker, Germany; **Supplementary Figure 1E**).

## Chlorophyll *a* PAM Fluorometry

Pulse Modulated Amplitude chlorophyll fluorescence measurements were performed using a FluoroPen FP100 (Photo System Instruments, Czech) on samples in a 1 ml cuvette. Cell density was assessed daily using a non-actinic light to induce minimum fluorescence over time (Ft). All fluorometric analyses were carried out in dark-adapted samples. Analysis of chlorophyll transient light curves was carried out with the OJIP test, which can be divided into four main steps. Level O represents all the open reaction centers (RCs) at the onset of illumination without reduction of primary plastoquinone pool (quinone A, $Q_A$; fluorescence intensity lasts for 10 ms). The rise of fluorescence transient from O to J indicates the net photochemical reduction of $Q_A$ (the stable primary electron acceptor of PS II) to $Q_A^-$ (lasts for 2 ms). The transient phase from J to I is due to all reduced states of closed RCs such as $Q_A^-$ $Q_B^-$ (secondary pool), $Q_A$ $Q_B^{2-}$ and $Q_A^-$ $Q_BH_2$ (lasts for 2–30 ms). The level P (300 ms) coincides with the maximum concentration of $Q_A^-$ $Q_B^2$, with the plastoquinone pool reduced. This level also reflects a balance between incident light at the PS II side and the utilization rate of the chemical (potential) energy and the rate of heat dissipation (Zhu et al., 2005). Rapid Light Curves (RLC) were performed using the pre-programmed LC1 protocol, which performs successive measurements of the sample $\phi$PS II under various light intensities (20, 50, 100, 200, 300, and 500 μmol photons $m^{-2}$ $s^{-1}$) of continuous illumination, relating the rate of photosynthesis to PAR. From this analysis, several photochemical parameters were obtained (**Table 1**).

## Pigment Analysis

Pigments were extracted from cell sample pellets with 100% acetone and maintained in a cold ultra-sound bath for 2 min to ensure complete disaggregation of the cell material. Temperature and time of extraction were -20°C and 24 h in the dark, to prevent degradation (Cabrita et al., 2016, 2018; Feijão et al., 2018). Samples were then centrifuged for 15 min at 4,000 × *g* at 4°C. Dual beam spectrophotometer was used to scan supernatants from 350 nm to 750 nm, at 0.5 nm steps. The absorbance spectrum was introduced in the Gauss-Peak Spectra fitting library, using SigmaPlot Software. Pigment analysis was employed using the algorithm developed by Küpper et al. (2007). Thereby, Chlorophyll *a*, its trace element substituted forms, and Pheophytin *a* were detected.

**TABLE 1 |** Summary of fluorometric analysis parameters and their description.

| **OJIP-test** | |
|---|---|
| AOECs | Active oxygen-evolving complexes |
| Area | Corresponds to the oxidized quinone pool size available for reduction and is a function of the area above the Kautsky plot |
| N | Reaction center turnover rate |
| $S_M$ | Corresponds to the energy needed to close all reaction centers |
| $P_G$ | Grouping probability between the two PSII units |
| ABS/CS | Absorbed energy flux per cross-section |
| TR/CS | Trapped energy flux per cross-section |
| ET/CS | Electron transport energy flux per cross-section |
| DI/CS | Dissipated energy flux per cross-section |
| RC/CS | Number of available reaction centers per cross-section |
| $TR_0/DI_0$ | Contribution or partial performance due to the light reactions for primary photochemistry |
| $\delta_{R0}/(1\text{-}\delta_{R0})$ | Contribution of PSI, reducing its end acceptors |
| $\psi_{E0}/(1\text{-}\psi_{E0})$ | Equilibrium constant for the redox reactions between PS II and PS I |
| $RE_0/RC$ | Electron transport from $PQH_2$ to the reduction of PS I end electron acceptors |
| RC/ABS | Reaction center II density within the antenna chlorophyll bed of PS II |

## Fatty Acid Profiles and Lipid Peroxidation Products

Fatty acid analysis was performed by *trans*-esterification of cell pellets in freshly prepared methanol-sulfuric acid (97.5%, v/v) at 70°C for 60 min, as previously described in Feijão et al. (2018). Pentadecanoic acid (C15:0) was used as an internal standard. Fatty acids methyl esters (FAMEs) were recovered using petroleum ether, dried under an $N_2$ flow and re-suspended in an appropriate amount of hexane. One microliter of the FAME solution, obtained from each sample, was analyzed in a gas chromatograph (Varian 430-GC gas chromatograph) equipped with a hydrogen flame ionization detector set at 300°C. The temperature of the injector was set to 270°C, with a split ratio of 50. The fused-silica capillary column (50 m × 0.25 mm; WCOT Fused Silica, CP-Sil 88 for FAME; Varian) was maintained at a constant nitrogen flow of 2.0 mL $min^{-1}$, and the oven temperature was set at 190°C. FAs were identified by comparison of retention times with standards (Sigma-Aldrich), and chromatograms analyzed by the peak surface method using the Galaxy software (from whom?). The double bond index (DBI) and the omega 6/omega 3 ratios were calculated as follows:

$$DBI = \frac{2 \times (\%\ \text{monoenes} + 2 \times\ \%\ \text{dienes} + 3 \times\ \%\ \text{trienes} + 4\ \%\ \text{tetraenes} + 5 \times \text{pentaenes})}{100}$$

antification of lipid peroxidation products was performed by homogenizing cell samples in 10 % (v/v) trichloroacetic acid and brief sonication. Absorbance was recorded at 532 nm and 600 nm wavelengths, and the concentration of thiobarbituric acid reactive substances (TBARS) calculated using the molar extinction coefficient of 155 $mM^{-1}$ $cm^{-1}$ (Heath and Packer, 1968).

## Antioxidant Enzymes Assay

All enzymatic assays were performed at 4°C. Pellets were suspended in 50 mM sodium phosphate buffer (pH 7.6) for extraction. Homogenates were centrifuged at 10,000 × *g* for 20 min (at 4°C), and the supernatant was used for the enzymatic tests. Catalase (CAT) activity was measured by monitoring the consumption of $H_2O_2$ and following the decrease in absorbance at 240 nm ($\varepsilon = 39.4$ $mM^{-1}$ $cm^{-1}$) for two minutes, according to Teranishi et al. (1974). The reaction mixture (1 ml) contained 50 mM of sodium phosphate buffer (pH 7.6) and was started with the addition of 10 μl of $H_2O_2$ (15% v/v). Ascorbate peroxidase (APX) activity was determined by monitoring the decrease in

absorbance at 290 nm and calculating the oxidized ascorbate, over two minutes of reaction time ($\varepsilon = 2.8$ $mM^{-1}$ $cm^{-1}$; Tiryakioglu et al., 2006). The reaction mixture contained 50 mM of sodium phosphate buffer (pH 7.0), 2 mM of $H_2O_2$, 0.1 M L-ascorbate, and 100 μL of pellet extract. The reaction was initiated by addition of ascorbate. Glutathione reductase (GR) activity was tested by measuring for 180 s the decrease in absorbance (at 340 nm) caused by glutathione-dependent NADPH oxidation (Foyer and Halliwell, 1976). The reaction mixture (1 ml) contained 50 mM phosphate buffer (pH 7.6), 1 mM EDTA, 5 mM glutathione oxidized (GSSG), 1.2 mM NADPH and cell extract. The reaction started by adding NADPH and the activity was calculated by using an extinction coefficient of 6.2 $mM^{-1}$ $cm^{-1}$. Superoxide dismutase (SOD) activity was tested by monitoring the reduction of pyrogallol at 325 nm (Marklund and Marklund, 1974). The reaction mixture (1 ml) contained 50 mM of sodium phosphate buffer (pH 7.0), 3 mM of pyrogallol, in order to start the reaction, Milli-Q water (18.2 MΩ cm), and 10 μl extract. To evaluate substrate auto-oxidation, controls were assayed without substrate, as described elsewhere.

## Statistical Analysis

Following normality and homogeneity tests of data, analysis of variance (factorial ANOVA) was applied using the Stat-Soft Inc. STATISTICA version 10 software was used to test for significant differences in effects among control and Cu- and CuO ENP-exposed *P. tricornutum* cells. Fisher's *post-hoc* test was performed in order to investigate significant differences among means. Spearman rank correlation was used to highlight the strength and direction of the relationship between parameters. Significance was set at $p < 0.05$.

# RESULTS

## Cell Growth

Exposure of *P. tricornutum* cells to low (1 μg $L^{-1}$), medium (5 μg $L^{-1}$), and high (10 μg $L^{-1}$) concentrations of Ionic Cu and CuO ENPs during the treatment period resulted in an overall decrease of both biomass (expressed as cell density) and specific growth rate. Cells exposed to CuO ENPs displayed a steeper decrease in cell density with increasing metal concentrations when compared to free Cu-exposed cells (**Figures 1A,B**). This decrease is evaluated throughout the cell growth curves derived parameters. Differences in specific growth rates between Cu-ionic and CuO ENP exposed cells treatments were only significant ($p < 0.05$) at maximum tested concentration levels (10 μg $L^{-1}$; **Figure 1E**). The number of divisions per day (M, **Figure 1D**) and doubling time (d, **Figure 1C**) reflected the decline found in the specific growth rate, and again, significant differences ($p < 0.05$) between the control and the highest level of CuO ENPs (10 μg $L^{-1}$). In sum, CuO ENPs inhibited diatom growth rate.

## Cell Metal Content and Nanoparticle Characterization and Metal Release

Elemental analysis revealed different trends in copper content between the tested groups Cu Ionic form and CuO ENPs (**Figure 2A**). Cell Cu content was higher in cells exposed to Ionic Cu concentrations of 1 and 5 μg $L^{-1}$, and lower following exposure to 10 μg $L^{-1}$. Cu ENPs treatments showed increasing uptake of Cu in the cells with increasing concentrations, albeit more evident in cells exposed to 10 μg $L^{-1}$ of Cu nanoparticles ($p < 0.05$). This suggested that CuO was less bioavailable, except for the higher concentration employed. Cell Cu content was positively correlated with nanoparticle concentration ($r^2 = 0.80$, $p < 0.05$), Cu-substituted chlorophyll *a* ($r^2 = 0.85$, $p < 0.05$), total content of FAs ($r^2 = 0.79$, $p < 0.05$) and with TBARs ($r^2 = 0.87$, $p < 0.05$). This Cu uptake will later be discussed in relation to its physiological implications.

Copper concentrations in the test units exposed to the nanoparticle form were also surveyed along an equivalent exposure period (**Figure 2B**). The Cu content of the collected water samples showed that there were no significant fluctuations of the Cu levels either between concentrations or along with the considered time trial.

The zeta potential of the Cu ENPs determinaed by DLSS was found to be -7.30 ± 3.72 mV. Cu ENP size distribution could not be determined with DLSS due to agglomeration of the particles; however, electron micrograph confirmed size distribution as indicated by the supplier (**Supplementary Figures 1A–D**). Particle elemental compositon and X-ray fluorescence spectra was obtained from the Cu ENPs in *f/2* medium using by TXRF as abovementioned (S2 PICOFOX, Bruker, Germany; **Supplementary Figure 1E**). X-ray fluorescence spectrum analysis revealed high amounts of Cu in Cu ENPs suspension as well as of other minor elements, derived from the *f/2* medium composition.

## Primary Photochemistry

The photochemical processes underlying carbon and light-harvesting and thus biomass production were investigated with non-invasive PAM chlorophyll fluometry. RLC measurements in dark-adapted cells exposed to ionic copper and CuO ENPs evidenced increased relative electron transport rates (rETR) along the thylakoid membrane, observable at 200 μmol photons $m^{-2}$ $s^{-2}$ (**Figures 3A,B**). These results were consistent with the increased photosynthetic efficiency (α, **Figure 3C**) and the maximum electron transport rate ($ETR_{max}$) of Cu exposed cells when compared to control cells (**Figure 3D**). Regarding respiratory efficiency (β, **Figure 3E**), an increase at low concentrations (1 μg $L^{-1}$) and a successive decrease at higher concentrations (5 and 10 μg $L^{-1}$) were observed for both cells exposed to ionic and ENP Cu forms. Photosynthetic efficiency was also found to correlate with increased percentage of tri-unsaturated hexadecatrienoic acid (C16:3; $r^2 = 0.70$, $p < 0.05$) in *P. tricornutum* cells exposed to CuO ENPs. Analysis of strong actinic light induced OJIP fluorescence transients (JIP-test) showed considerable differences in dark-adapted cells. Differences were found in cells exposed to CuO ENPs affecting the shape of the Kautsky curve (**Figures 4A,B**), which gives a general view on the structure, conformation, and function of photosynthetic apparatus, especially focusing on the PS II. Considering these aspects of the photosynthetic process, a further investigation was conducted focusing on the compartments of the photochemical apparatus.

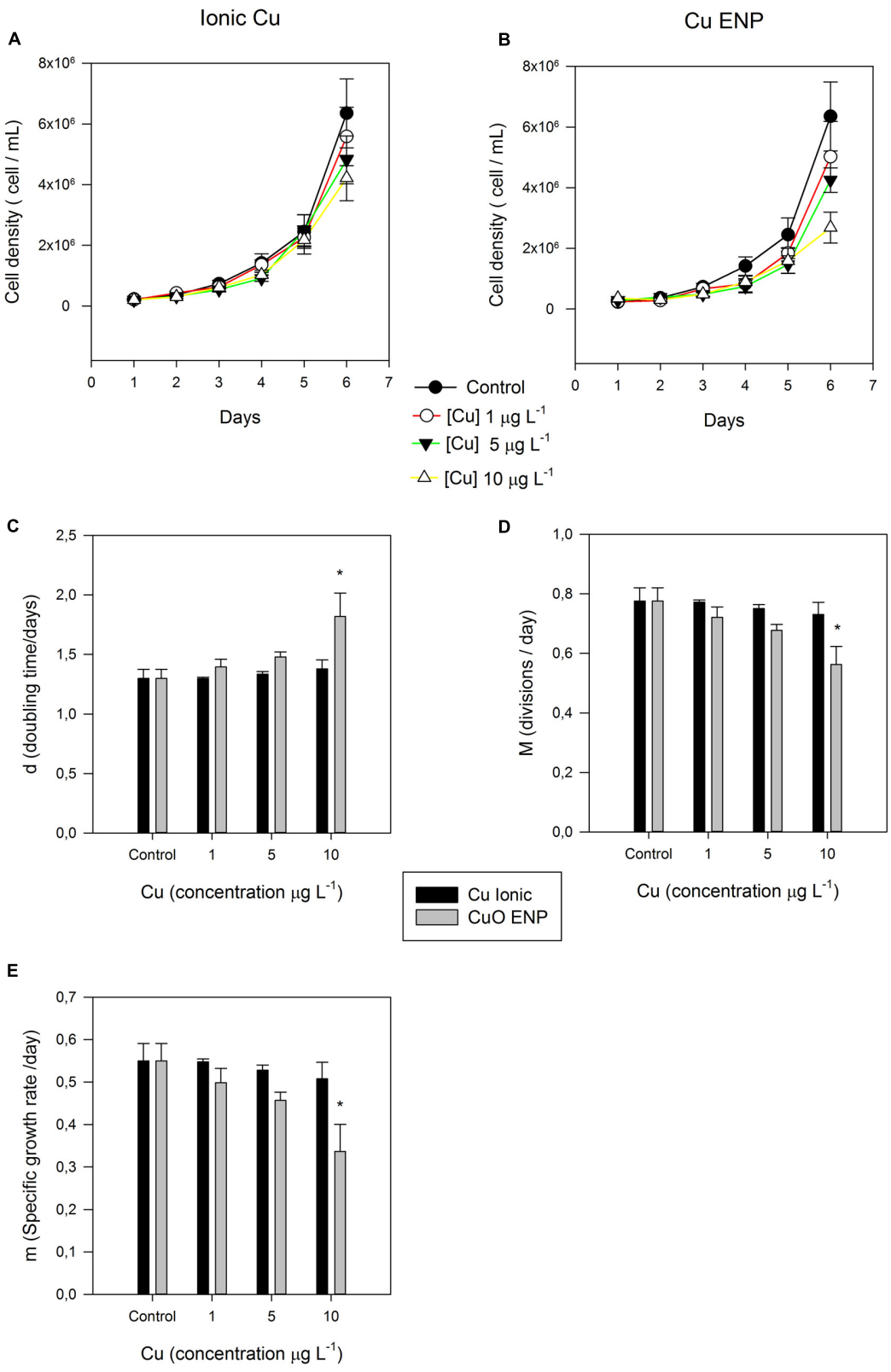


**FIGURE 1 | (A,B)** Cell density (cell $mL^{-1}$) of *P. tricornutum*, during the 6-day experiment. Also shown, **(C)** doubling time (d), **(D)** divisions per day (M), and **(E)** specific growth rate (m), of *P. tricornutum* after 3 days of exposure to increasing ionic Cu (black bars) and CuO ENP (gray bars) concentrations (average ± standard deviation, $N = 3$, *indicate significant differences toward the control at $p < 0.05$).

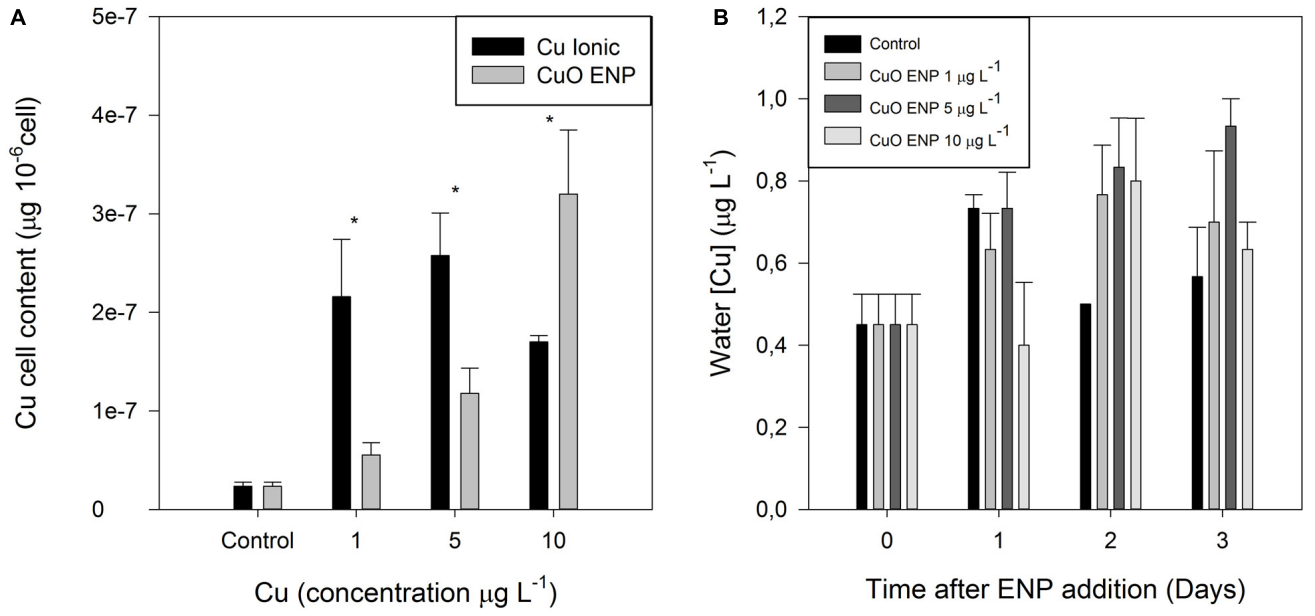


**FIGURE 2 | (A)** Copper cell content in *P. tricornutum* (µg Cu $10^{-6}$ cells) after 3 days of exposure to increasing ionic Cu (black bars) and CuO ENP (gray bars) concentrations and **(B)** Copper release (µg $L^{-1}$) from CuO ENP in f/2 medium under experimental concentrations and conditions (average ± standard deviation, $N = 3$, *above bars indicate significant differences compared with the control at $p < 0.05$).

The size of the oxidized quinone pool (**Figure 4C**) was significantly higher ($p < 0.05$) in cells under low (1 µg $L^{-1}$), medium (5 µg $L^{-1}$), and high concentration (10 µg $L^{-1}$) of CuO ENPs, compared to control treatments. The same was observed at medium and high concentrations of ionic Cu. Regarding the energy necessary to close all RCs (**Figure 4D**), cells exposed to all concentration levels of CuO ENPs showed a significant increase ($p < 0.05$) compared to control cells, as well as for cells treated with medium and high concentrations of ionic Cu. A similar trend was observed for the total number of electrons transferred in the electron transport chain (**Figure 4E**), which significantly increased in cells exposed to medium and high concentrations of ionic Cu, and more markedly to all concentrations of CuO ENPs when compared to control cells. Connectivity between PS II antennae ($P_G$, **Figure 4F**) was found to be significantly lower ($p < 0.05$) in cells exposed to all levels of both Cu forms. Moreover, a positive correlation was found between $P_G$ and the reduction in the long-chain (LC) PUFA EPA (C20:5) content ($r^2 = 0.79$, $p < 0.05$) in the cells subjected to CuO ENPs.

Analyzing OJIP-derived energy transduction fluxes on a cross-section basis in dark-adapted samples (**Figures 5A,B**), differences between ionic Cu and CuO ENPs, and between concentrations were identified. The absorbed (ABS/CS), trapped (TR/CS), transported (ET/CS) energy fluxes and the number of available reaction centers per cross-section (RC/CS) were significantly lower ($p < 0.05$) in cells exposed to increasing concentrations of CuO ENP treatment ($p < 0.05$; **Figure 5B**), compared to either control or ionic- Cu exposed cells. ABS/CS was also found negatively correlated with the content of C16:3 ($r^2 = -0.81$, $p < 0.05$). Regarding the dissipated energy fluxes (DI/CS), only CuO ENP exposure led to an increase in this parameter as a function of concentration, while ionic- Cu exposed cells showed only slight changes with increasing concentrations. All these changes in the several processes and compartments of the photochemical apparatus and in the energy transduction pathway propose possible changes at the biochemical level.

## Pigment Profiles

Considering photochemical changes mentioned before, the composition of light-harvesting pigments was evaluated. Changes in the content of Chlorophyll *a* (MgChl *a*), Pheophytin *a* (Pheo *a*) and Cu-substituted chlorophyll *a* (CuChl *a*) were observed in cells of *P. tricornutum* exposed to CuO ENPs (**Figure 6**). A reduction in total MgChl *a* level with increasing concentrations of CuO ENPs was detected, along with a significant rise ($p < 0.05$) in the Pheo *a* and CuChl *a* content in cells exposed to 10 µg $L^{-1}$ CuO ENPs ($p < 0.05$), suggesting a role of Cu nanoparticles in promoting the $Mg^{2+}$ substitution in the main photosynthetic pigments. In fact, increased Cu-substituted Chl *a* contents correlated with CuO ENP concentrations ($r^2 = 0.73$, $p < 0.05$). In the ionic Cu exposed cells, changes in MgChl *a*, Pheophytin *a* and CuChl *a* content triggered by increasing Cu levels were not significant (**Figure 6**).

## Fatty Acid Profiles

Fatty acid profiles were also conducted. Analysis of the composition and contents of FAs in *P. tricornutum* cells showed significant changes between control and copper exposed cultures (**Figure 7A**). The most relevant differences were found in EPA (20:5) and hexadecatrienoic acid (16:3) relative amounts, for cells subject to CuO ENPs in all tested concentrations. A significant decrease ($p < 0.05$) in EPA (20:5) relative abundance

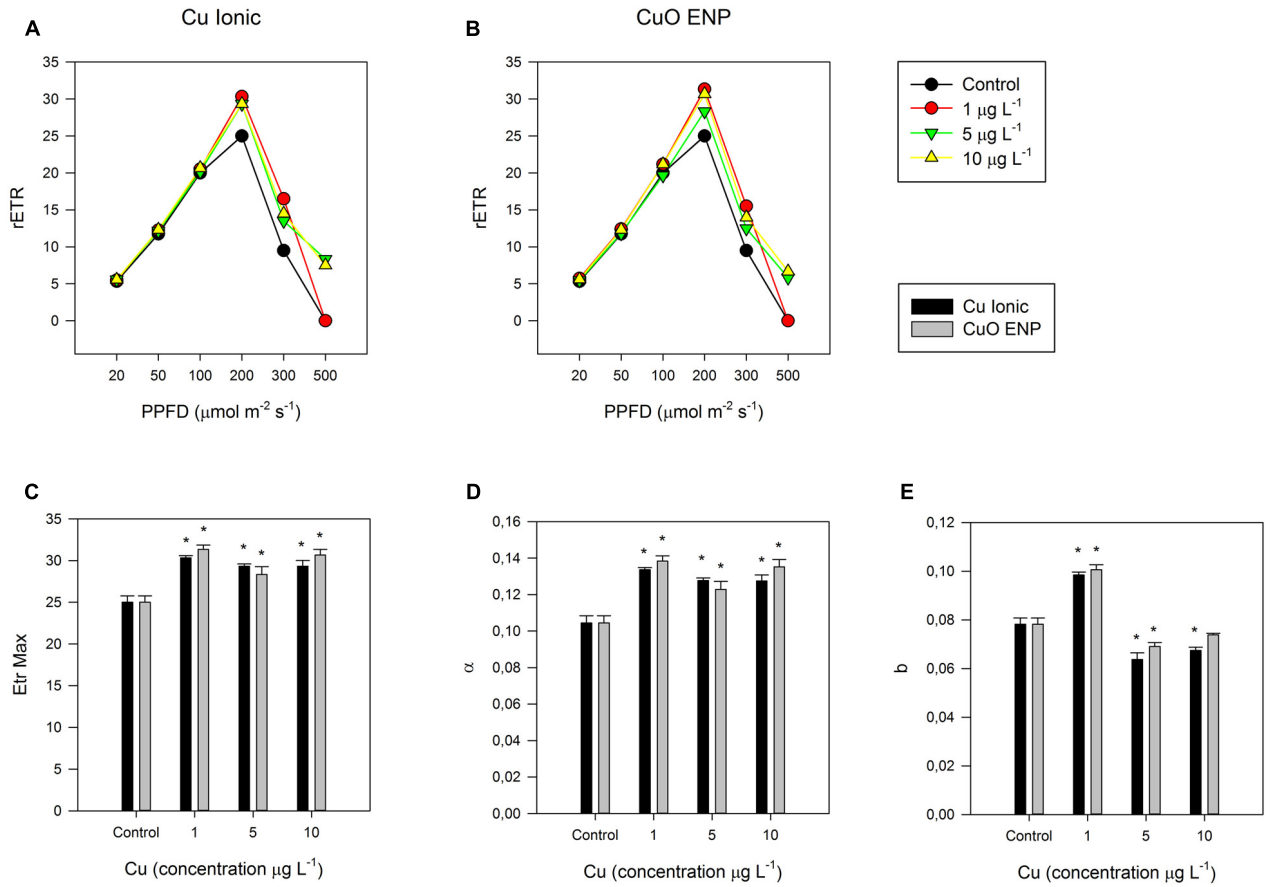


**FIGURE 3 | (A,B)** Rapid light curves and derived parameters: **(C)** maximum electron transport rate ($ETR_{max}$), **(D)** photosynthetic (α), and **(E)** respiratory (β) efficiency in *P. tricornutum*, after 3 days of exposure to increasing ionic Cu (black bars) and CuO ENP (gray bars) concentrations (average ± standard deviation, $N = 3$, *indicate significant differences compared with the control at $p < 0.05$).

was observed combined with a significant rise ($p < 0.05$) in hexadecatrienoic acid (16:3). Palmitic acid (16:0) and the monounsaturated palmitoleic acid (16:1) ratios in cells exposed to medium and high concentrations of ionic Cu and CuO ENPs. Moreover, stearidonic acid (18:4 *n*-3) was reduced for ionic Cu and CuO ENPs at all concentrations, whereas C16:4 content only increased ($p < 0.05$) in cells exposed to CuO ENPs. Exposure to CuO ENPs also caused a decline in the gamma-linolenic acid (18:3 *n*-6) content of the cells. The higher content of C16:3 and C16:4 was correlated with the energy necessary to close all reaction centers (Sm; $r^2 = 0.80$ and 0.81, respectively, $p < 0.05$) and with the total number of electrons transferred in the ETC ($r^2 = 0.81$ in both cases, $p < 0.05$). Modifications in the FA composition resulted in a significant increase ($p < 0.05$) in the DBI (**Figure 7B**), albeit only at the highest concentration of CuO (10 μg $L^{-1}$), and in a higher omega 6/omega 3 ratio (**Figure 7D**) for all CuO ENP concentrations. Regarding total FAs content on a cell number basis, a significant increase ($p < 0.05$) was observed in cells exposed to CuO ENPs at the highest concentration (10 μg $L^{-1}$; **Figure 7C**).

Considering FA saturation classes, the percentage of saturated and monounsaturated FAs was significantly reduced ($p < 0.05$), while a significant rise ($p < 0.05$) in the percentage of polyunsaturated and unsaturated FAs were observable for CuO ENP exposure (**Figure 8A**). Ratios of unsaturation/saturation and polyunsaturation/saturation reflected the abovementioned results on FA composition, with a significant increase of unsaturation and an overall reduction in saturation for CuO ENP exposure (**Figures 8A,B**). Cells exposed to CuO ENPs showed an overall higher stress effect on FA content in comparison with ionic Cu effects.

## Stress Biomarkers

Considering the overall changes in the energetic and biochemical level abovementioned, the cellular oxidative stress levels were tested with enzymatic antioxidant assays. Antioxidant enzymes assays evidenced an overall increase in enzyme activity under nano Cu experimental conditions (**Figures 9A–D**). Specifically, APX and GR, which showed an increase in activity values along the gradient of Cu concentration, with more pronounced responses in cells exposed to CuO ENPs. In contrast, CAT and SOD activity were less evident with increasing Cu concentration, and the highest enzyme activity was measured at medium Cu concentration (5 μg $L^{-1}$). Compared to control cells, the

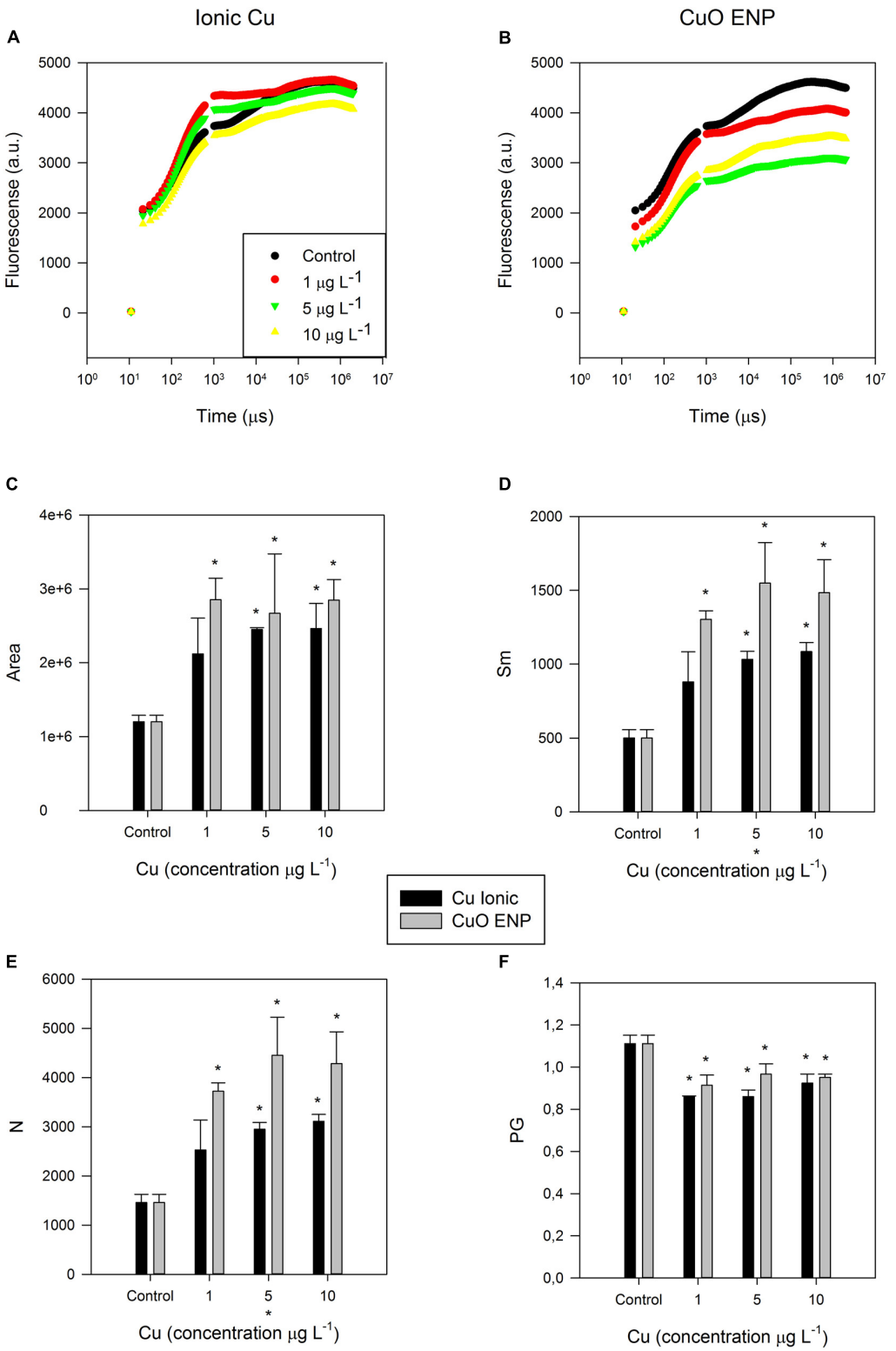


**FIGURE 4 | (A,B)** Kautsky curves obtained from dark-adapted samples; OJIP-derived parameters, namely **(C)** size (Area) of the oxidized quinone pool, **(D)** energy needed to close all Reaction Centers (Sm), **(E)** total number (N) of electrons transferred in the electron transport chain, and **(F)** disconnectivity between PS II antennae ($P_G$), in *P. tricornutum*, after 3 days of exposure to increasing ionic Cu (black bars) and CuO ENP (gray bars) concentrations (average ± standard deviation, $N = 3$, *above bars indicate significant differences compared with the control at $p < 0.05$, whilst *below *x*-axis indicate significant differences between ionic Cu and CuO ENP at a same concentration).

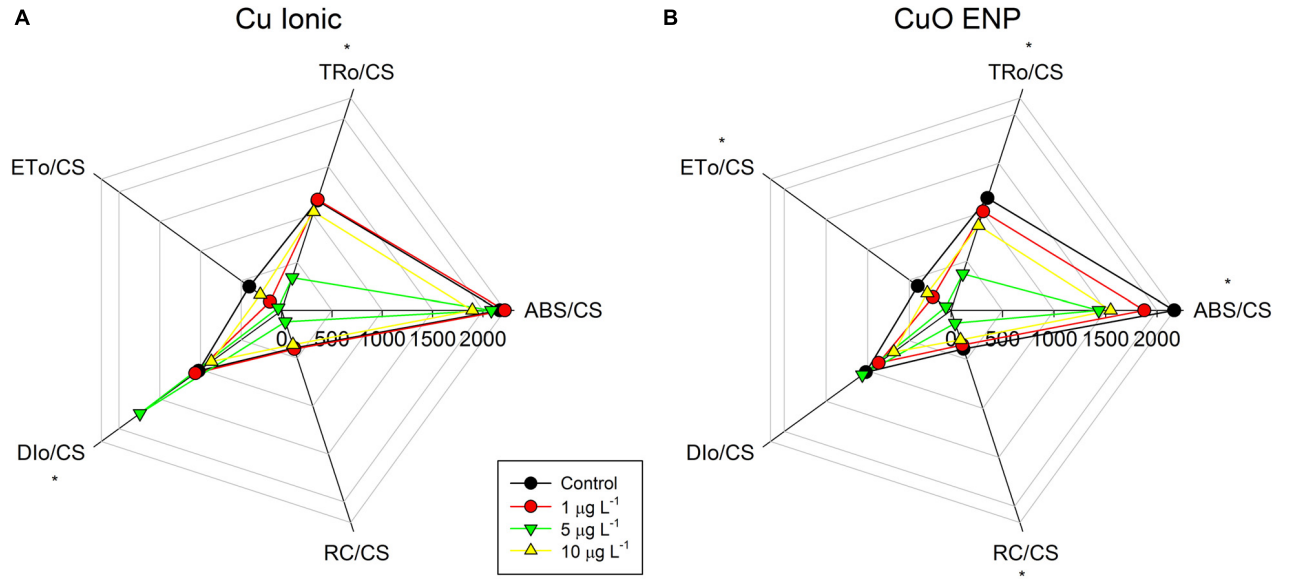


**FIGURE 5 |** Phenomenological energy fluxes per cross-section: absorbed (ABS/CS), trapped (TR/CS), transported (ET/CS), dissipated (DI/CS), and number of available reaction centers per cross section (RC/CS), in *P. tricornutum* after 3 days of exposure to increasing ionic Cu **(A)** and CuO ENP **(B)** (gray bars) concentrations (average ± standard deviation, $N = 3$, *indicate significant differences compared with the control at $p < 0.05$).

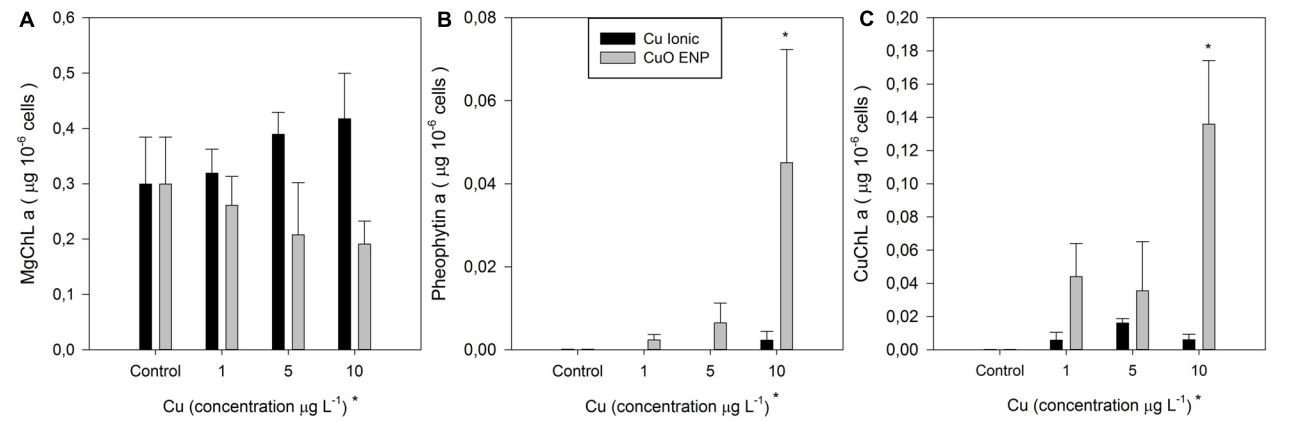


**FIGURE 6 | (A)** Chlorophyll *a*, **(B)** Pheophytin *a*, and **(C)** Cu-chlorophyll *a* concentration (µg $10^{-6}$ cells) in *P. tricornutum* after 3 days of exposure to increasing ionic Cu (black bars) and CuO ENP (gray bars) concentrations (average ± standard deviation, $N = 3$, *above bars indicate significant differences compared with the control at $p < 0.05$, whilst *below *x*-axis indicate significant differences between ionic Cu and CuO ENP at the same concentration).

TBARs total content in exposed cells was significantly enhanced ($p < 0.05$) at the highest CuO ENP concentration (10 µg $L^{-1}$; **Figure 9E**).

## DISCUSSION

Overall results show that exposure to non-lethal concentrations of copper engineered nanoparticles (CuO ENPs) resulted in the reduced fitness of a marine model diatom, *P. tricornutum*, and elicited higher toxicity than its ionic form counterpart. Biomarkers, as specified below, appeared to be sensitive to MeENPs stress in this species. In general, changes in cell growth, photosynthesis, pigment content, FA production, and oxidative stress metabolism, as well as the production of Cu-substituted chlorophylls, were observed for diatoms exposed to all tested Cu concentrations. However, effects were more pronounced for CuO ENPs exposure than for direct ionic Cu, in particular at the highest tested CuO ENP concentration. Although previous studies show that ionic copper can be released from CuO ENPs (Zhang et al., 2018), in our experimental conditions no significant fluctuations could be observed in the dissolved copper levels along with the exposure in reactors containing Cu ENPs. Thus all comparisons discussed here base on the initial form of copper introduced into the culture medium, assuming that there is no Cu transition from nanoparticle to ionic form as observed

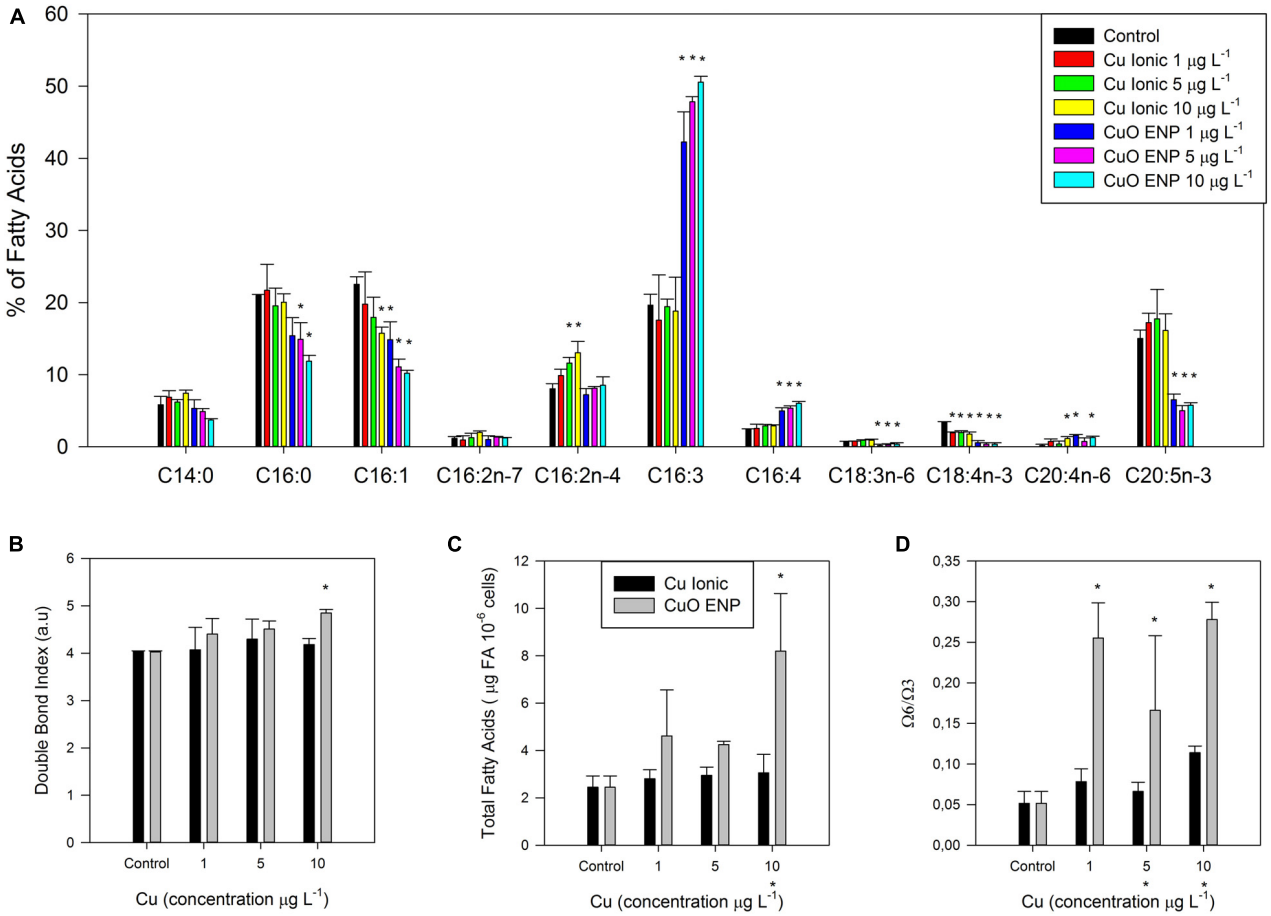


**FIGURE 7 | (A)** Fatty acid composition, **(B)** double-bond index, **(C)** fatty acid content (µg $10^{-6}$ cells), and **(D)** omega-6/omega-3 ratio in *P. tricornutum*, after 3 days of exposure to increasing ionic Cu (black bars) and CuO ENP (gray bars) concentrations (average ± standard deviation, $N = 3$, *above bars indicate significant differences compared with the control at $p < 0.05$, whilst *below *x*-axis indicate significant differences between ionic Cu and CuO ENP at the same concentration).

in the water Cu concentrations results. Cell growth was not significantly reduced in cells exposed to ionic Cu in comparison to the control group, which is in line with previous results reported for *P. tricornutum* at similar metal concentrations (Cabrita et al., 2016, 2018). In contrast, cell growth decreased as a function of exposure to CuO ENP, with significant inhibition at high concentrations (10 µg $L^{-1}$, corresponding to 0.13 µM; add *p* values here). This is in agreement with previous studies that showed that CuO ENPs in antifouling paints could cause severe growth inhibition in different algal species, including *P. tricornutum* (Anyaogu et al., 2008; Zhang et al., 2018). Additionally, Zhang et al. (2018) also observed severe growth inhibition in *Skeletonema costatum* under the exposure to Cu ENPs, pointing out the release of ionic Cu from the ENPs as the principal cause for the verified growth inhibition. On the other hand, Zhu et al. (2017) only found inhibition of *P. tricornutum* growth at both ionic Cu and Cu ENP concentrations of 20 µM and above. The observed impact of CuO ENPs compared to that of ionic Cu on *P. tricornutum* growth can be explained by the fact that CuO ENPs cause cytotoxicity via the release of $Cu^{2+}$ into the culture medium (Horie et al., 2012). This ion release is increased for particles < 50 nm (Anyaogu et al., 2008), which was the size of the CuO ENPs used in this study (here link the SEM image). Furthermore, CuO ENPs can be about 140-fold more bioavailable than its ionic form (Aruoja et al., 2009), which supports the higher inhibitory effect on *P. tricornutum* growth from CuO ENPs compared to the ionic form.

Excess copper is an important inhibitor of photosynthesis (Cid et al., 1995). Copper affects the PS II activity at the Pheo-$Q_A^-$ domain (Küpper et al., 2002), inhibiting the electron transport through damage to the donor and the acceptor sides of PS II (Patsikka et al., 1998). Accordingly, Cid et al. (1995) suggested that $Cu^{2+}$ can be responsible for the inactivation of PS II reactions centers. Mohanty et al. (1989) proposed that $Cu^{2+}$ inhibits PS II photochemistry, primarily affecting the functionality of the secondary quinone electron acceptor, $Q_B$, not only by blocking the electron transport but also by modifying and inactivating the $Q_B$ site. Exposure to either ionic Cu or CuO ENPs leads to an increase in maximum $ETR_{max}$ and photosynthetic efficiency (α), corresponding to a higher amount of oxidized quinones, as well as to a decrease in electron transport energy flux per cross-section ($ET_o$/CS), which suggests

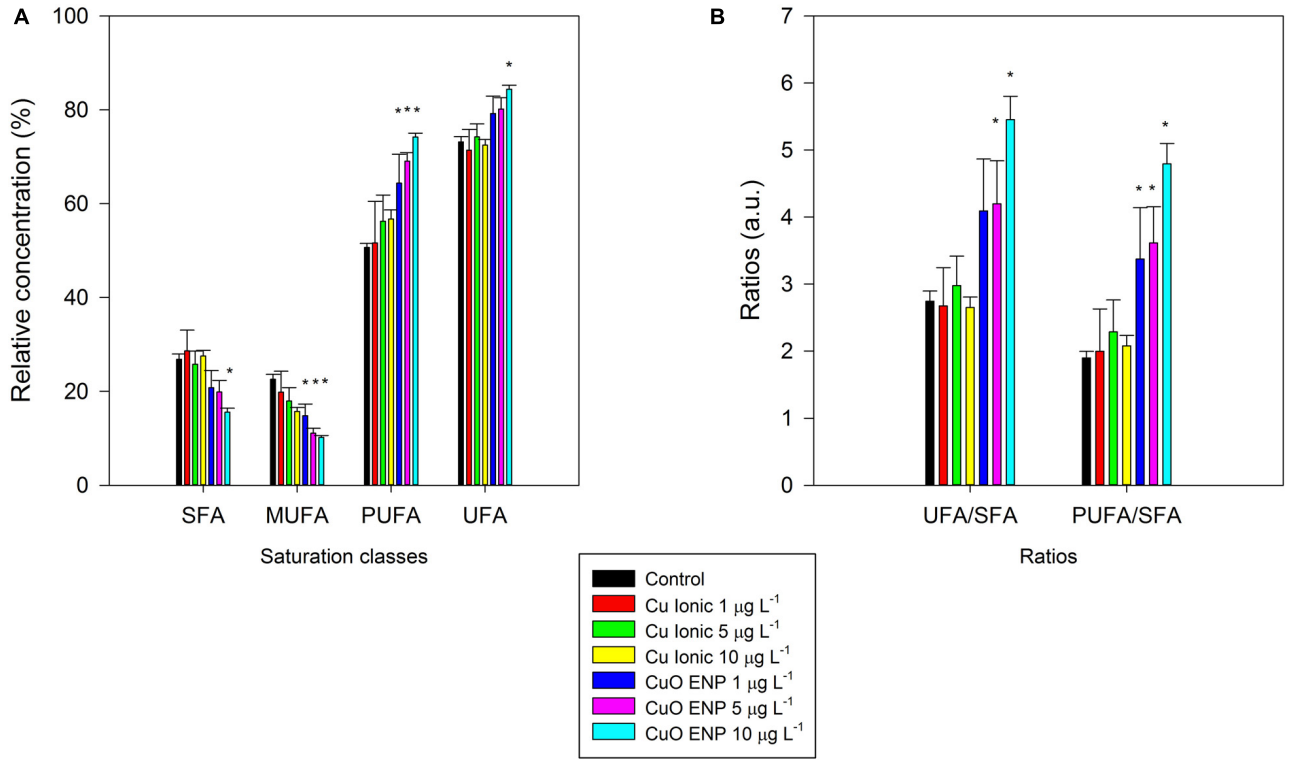


**FIGURE 8 |** Relative concentrations of fatty acid saturation classes (**A**; SFA, Saturated Fatty Acids; MUFA, Monounsaturated Fatty Acids; PUFA, Polyunsaturated Fatty Acids; and UFA, Unsaturated Fatty Acids) and ratios **(B)**, in *P. tricornutum*, after 3 days of exposure to increasing ionic Cu (black bars) and CuO ENP (gray bars) concentrations (average ± standard deviation, $N = 3$, *indicate significant differences compared with the control at $p < 0.05$).

a malfunction between elements of PS II (Duarte et al., 2016). The positive correlation between photosynthetic efficiency and the higher percentage of tri-unsaturated hexadecatrienoic acid (C16:3) in *P. tricornutum* cells exposed to CuO ENP, as observed in this study, suggests a potential mechanism to counteract stress in photosynthesis, as this FA is only found in plastidial lipids, mainly in monogalactosyldiacylglycerol (MGDG), which forms the bulk of thylakoid lipids (Feijão et al., 2018). The larger size of the oxidized quinone pool, and the higher level of energy, needed to close the reaction centers, as evidenced by cells exposed to CuO ENPs, indicate that efficient energy transport is required (Feijão et al., 2018), which if reduced, suggests probable damage in the quinone pool electron transport (Duarte et al., 2017; Cabrita et al., 2018). However, no evidence of enhanced dissipation energy flux was observed. The above-mentioned changes in photosynthetic parameters could thus be due to changes in the grouping probability ($P_G$), which is a direct measure of the connectivity between the PS II antennae. The decrease found for this index in the presence of both ionic Cu and CuO ENPs, indicates a decreased connectivity between the two PS II units and a probable impairment of energetic transport (Duarte et al., 2016). EPA is highly abundant in glycolipids and phospholipids that form the chloroplast membranes lipids, like MGDG and phosphatidylglycerol (PG), and changes in the FAs composition in chloroplast membrane lipids can explain photosynthesis imbalances, through modifications of the redox potential (Kern and Guskov, 2011). Previous studies reported that changes in the FA composition of polar lipids can be one of the causes of dimerization of PS II (Kruse et al., 2000), as suggested also from the correlation between disconnectivity in PS II antennae and the reduction in EPA content found in cells exposed to CuO ENPs. The higher number of electrons transferred in the electron transport chain (turnover number, N) was not reflected in an effective trapping energy flux (TR/CS) in cells exposed to CuO ENPs. Instead, the detected reduction in the density of reaction centers (RC/CS) corresponded to a higher number of inactive reaction centers, and to a lowered ability to reduce the primary electron acceptor $Q_A$. This could be confirmed by the low absorbed photon flux (ABS/CS) and the higher size in the oxidized quinone pool found in CuO ENP exposed *P. tricornutum* cells. Nevertheless, no changes were detected in the net rate of closure of PS II RC ($M_o$) and in the energy needed to close all RCs, which were expected to counteract the inactive RCs (Duarte et al., 2016). Even though trapped energy flux diminished in the ionic Cu exposed cells, little changes were detected in energy dissipation. Overall, changes in photobiology were more evident for *P. tricornutum* subjected to CuO ENPs, suggesting a negative impact of CuO ENPs on PS II functionality or integrity of light harvesting complexes.

This was further promoted by the observation that the content of the light-harvesting pigments and its substituted form also

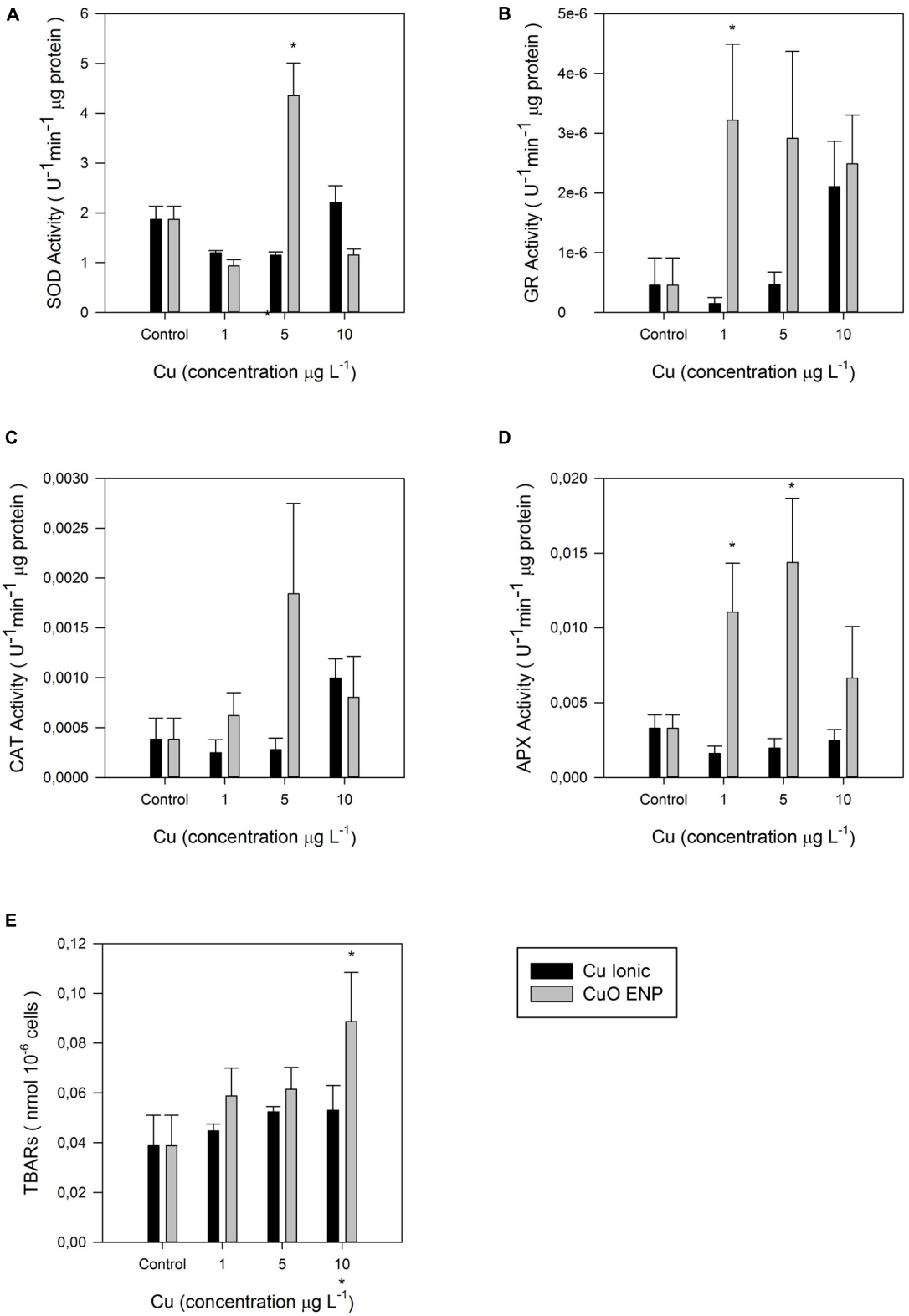


**FIGURE 9 |** Enzymatic activities: **(A)** Superoxide dismutase (SOD), **(B)** glutathione reductase (GR), **(C)** catalase (CAT), **(D)** ascorbate peroxidase (APX) in $U^{-1}$ µg protein, and **(E)** lipid peroxidation measured as concentration of thiobarbituric acid reacting substances (TBARs; nmol $10^{-6}$ cells), in *P. tricornutum* after 3 days of exposure to increasing ionic Cu (black bars) and CuO ENP (gray bars) concentrations (average ± standard deviation, $N = 3$, *above bars indicate significant differences compared with the control at $p < 0.05$, whilst *below *x*-axis indicate significant differences between ionic Cu and CuO ENP at the same concentration).

changed, mostly for *P. tricornutum* exposed to CuO ENPs at the highest concentration (10 $\mu g\ L^{-1}$). The decrease in MgChl *a* along the CuO ENP concentration gradient can be partially explained by direct replacement with CuChl *a*, which was highly significant for *P. tricornutum* exposed to the highest tested level of CuO ENPs. In parallel, a significant enhanced amount of Pheophytin *a*, the main product of degradation of MgChl *a* was observed. This is in agreement with previous findings reported by Zhang et al. (2018), were a similar depletion in Chl-*a* was also detected and attributed to destruction of this molecule promoted by Cu. The formation of CuChl *a* in cells exposed to both ionic Cu and CuO ENPs corroborates previous findings showing the occurrence of this substituted chlorophylls in *P. tricornutum* exposed to ionic Cu (Cabrita et al., 2018). It is already known that the central $Mg^{2+}$ ion of chlorophyll can be substituted by trace metals, such as Cu, and constitutes an important part of the damage occurring in metal-stressed photosynthetic organisms (Küpper and Spiller, 1998; Küpper et al., 2002). As a matter of fact, Cu-substituted Chl *a* was found positively correlated with CuO ENP concentration in this study. Excess levels of this substituted and far less efficient chlorophyll form (CuChl *a*) can partly explain the decrease in efficiency in the absorbing photon flux, and in the ability for trapping and transporting energy, reducing PS II overall capacity.

The FA profiles of lipids from *P. tricornutum,* which are characterized by a high diversity of FAs and distinct signatures for different lipid classes (Abida et al., 2015; Yang et al., 2017; Feijão et al., 2018), was strikingly changed by CuO ENPs, even at the lowest concentration tested (1 $\mu g\ L^{-1}$). Ionic copper had no particular impact on FA profiles neither on total content, most probably because the employed concentrations used were not sufficiently high to cause stress. Given that, the most remarkable changes induced by CuO ENPs involved the LC-PUFAs contained in glyco- and phospholipids, typical of chloroplast membranes of this diatom like mono- and di-galactosyldiacylglycerol (MGDG, DGDG), phosphatidylcholine (PC) and PG. EPA is usually found in high levels in *P. tricornutum* (Dunstan et al., 1993; Feijão et al., 2018), and is part of all membrane lipids but almost absent in triacylglycerol (TAG; Arao et al., 1987), and its significant decrease with exposure suggests probable membrane damage. A reduction in EPA content associated with the membrane lipids has also been found in *P. tricornutum* under other types of stress, such as heat (Feijão et al., 2018) and nitrogen starvation (Remmers et al., 2017). The notable decline in EPA content occurred in parallel with a significant rise in both the percentage of tri-unsaturated hexadecatrienoic acid (C16:3) and tetra-unsaturated hexadecatetraenoic acid (C16:4). These FAs are synthesized by successive desaturations of monounsaturated palmitoleic acid (C16:1) in the inner membrane of the chloroplast (Dolch and Maréchal, 2015), and almost exclusively contained in MGDG (Abida et al., 2015; Popko et al., 2016). The enhancement in C16:3 and C16:4, found positively correlated with the energy necessary to close all reaction centers and with the total number of electrons transferred in the ETC can be a possible way for *P. tricornutum* to counteract changes in photosynthesis associated with Cu stress, by increasing the efficiency in transport along the electron transport chain. Nevertheless, the absorption energy flux was negatively correlated with the content of C16:3; maybe to maintain an efficient energy flow. Alterations in FA composition and the influence of unsaturation on membrane properties connected to photosynthetic performance has already been highlighted in studies over cation-imposed stress in photosynthetic organisms (Allakhverdiev et al., 1999, 2001; Duarte et al., 2017; Cabrita et al., 2018).

The decrease in the content of palmitic acid (C16:0) and palmitoleic acid (C16:1) is likely related to its intensive desaturation to produce C16:3 and C16:4 (Dolch and Maréchal, 2015) to support thylakoid membrane functioning so that cells could cope with CuO ENP stress. However, a decrease in these saturated and mono-unsaturated FA is often associated with a reduction in the content of storage lipids. Although they are present in all lipid classes, C16:0 and C16:1 are quite abundant in diatom triacylglycerols, accounting for nearly 100% of the total FAs at the *sn*-2 position of these storage lipids (Li et al., 2014). This possible decrease in TAG amounts would not be in accordance with other studies, in which storage lipids accumulate under stress conditions (Sharma et al., 2012). However, TAG accumulation in this study cannot be excluded since, under stress conditions such as nitrogen deprivation, FA composition can be altered by the incorporation of FA from membrane lipids (Remmers et al., 2017). Indeed, Shen et al. (2016) found that the content of C16:1 decreases dramatically in phospholipids and remains largely unchanged in glycolipids in *P. tricornutum* under nitrogen starvation, suggesting that C16:1 is not specific to TAGs and cannot serve as a characteristic FA of TAGs. Further investigation on TAG and membrane lipid classes content and FAs compositions in *P. tricornutum* cells exposed to CuO ENPs is necessary to elucidate this question. Further research to understand the mechanisms behind changes in lipids triggered by CuO ENPs in association with their location and function in microalgae cells is therefore suggested. Nevertheless, the alterations on the FAs profiles observed herein imply that they can be used as metal stress biomarkers, as also suggested for other kinds of stress such as heat (Feijão et al., 2018).

Overall, the increase of total FA content, on a cell basis, observed under CuO ENPs was likely a result of higher cell production of C16:3. The presence of the less functional CuChl *a* supports the need for a higher synthesis of FAs composing thylakoid membranes, to store additional MgChl *a*. Previous studies already reported the importance of chloroplast membrane composition in maintaining PS II stability (Kern and Guskov, 2011). The presence of nanoparticles also affected the omega 6/omega 3 ratio, which was significantly increased due to EPA decrease. Double bond Index only increased for the highest concentration of CuO ENPs (10 $\mu g\ L^{-1}$) and is likely a result of the increase in C16:3. The reduction in EPA suggests membrane damage, potentially due to the adhesion of nanoparticles on the plasma membrane or to a higher release of $Cu^{2+}$ ions (Zhao et al., 2016), as mentioned before. It is known that the toxicity of CuO ENPs can result from both the exposure to the metal particles themselves and an increased rate in the release of the metal ions (Anyaogu et al., 2008; Wang et al., 2012; Baker et al., 2014; Zhao et al., 2016). A full analysis of lipid classes composition

and of the eventual presence of internalized nanoparticles should provide further information on the toxicity mechanisms of CuO engineered nanoparticles.

Further impacts of CuO ENPs were associated with the formation of peroxide radicals via Cu-generated free radicals action found at CuO ENP highest concentration (10 $\mu g\ L^{-1}$). Lipid peroxidation is one of the main mechanisms involved in trace metal toxicity through which PUFAs become the main target for free radicals (Rocchetta et al., 2006). The changes in saturated fatty acids (SFA) and PUFA levels caused by copper exposure can be also explained by activation of defense or reparation mechanisms to neutralize cellular damage (Rocchetta et al., 2006). A slightly increasing trend in the activity of some antioxidant enzymes was detected probably due to the relative low Cu concentrations employed in this study, as most studies on antioxidant enzymatic response under copper exposure have been performed using much higher Cu concentrations to evaluate acute stress and lethality (Pinto et al., 2003; Morelli and Scarano, 2004). In the present study, non-lethal concentrations of both Cu in ionic and nanoparticle form were used, allowing cells to maintain viability during the experimental phase, and, at the same time, observe the effects of metal exposure throughout the experiment.

Exposure of *P. tricornutum* cells to both ionic Cu and CuO ENPs resulted in overall increased activity of GR and APX, and a partial increase in CAT, while SOD remained almost unaffected. The more marked increase in GR and APX with CuO ENPs can provide valuable insights on CuO ENP capacity to cause oxidative stress. Copper cations are an important part of the reactive oxygen scavenging system (e.g., CuZnSOD), but they are also able to induce oxidative stress at high concentrations through increased production of ROS (Knauert et al., 2008). Lack of significant induction of CAT and SOD activities suggests minor effects at low Cu concentrations. Studies on *P. tricornutum* already showed that these enzymes play an active role in scavenging of ROS under free copper ions stress (Morelli and Scarano, 2004). Ascorbate is the principal electron donor for APX, and the removal of $H_2O_2$ by APX requires GSH and NADPH (Morelli and Scarano, 2004; Anjum et al., 2016). Fast oxidation of the ascorbate pool can occur under acute stress conditions when high levels of ROS overcome the antioxidant capacity of low molecular weight compounds such as GSH and NADPH (Pinto et al., 2003). It is possible that under Cu exposure conditions, rapid oxidation of the ascorbate pool or depletion of NADPH occurred. The higher activity of GR found in this study also confirms the role of this enzyme in oxidative stress detoxification. Glutathione reductase catalyses the conversion of glutathione disulphide (GSSG) to its reduced form (GSH) in the presence of NADPH (Dringen and Gutterer, 2002; Anjum et al., 2016), and plays a crucial role in maintaining high intracellular [GSH]/[GSSG] ratio. Previous studies already investigated the active detoxification mechanism to avoid trace metal poisoning in plants, algae and fungi (Morelli and Scarano, 2004; Szabó et al., 2008; Anjum et al., 2016), which involves intracellular sequestration of metal ions by GSH and GSH-related peptides named phytochelatins (PCs; Kawakami et al., 2006). Many factors can induce the generation of ROS, and the modulation detoxification capacity of the organisms can be a winning strategy in chronic exposure to contaminants (Pinto et al., 2003). Overall, ROS toxicity in cells exposed to low concentrations of Cu was not clear, especially regarding the lack of activation of CAT and SOD. Nevertheless, the probable higher bioavailability of $Cu^{2+}$ ions associated with CuO ENPs could explain the partial increase in APX and GR activity and clearly differentiated between the effects triggered by ionic Cu and the nanoparticles. Further investigation should clarify the differential activation of the enzymatic pool employed in this study under such non-lethal concentrations.

The alterations found in *P. tricornutum*, particularly those regarding photosynthesis, pigments and FA profiles, triggered by the copper nanoparticles, allow inferring repercussions to the marine food webs and ecosystems. The photosynthetic process was largely compromised by CuO ENPs, which will expectedly have a negative impact on the abundance of phytoplankton assemblages and net primary productivity of marine systems, thereby simultaneously contributing to water deoxygenation. The decline in the omega-3 polyunsaturated FAs, such as EPA, and overall changes in the FA profile at the basis of marine food webs, will expectedly propagate changes to the higher trophic levels. Given that fish natural diet includes high levels of essential LC-PUFA omega-3 (e.g., Ackman, 1989), poor quality phytoplankton in terms of EFAs may reduce the abundance and population dynamics of several species (Gladyshev et al., 2013; Vagner et al., 2015), and, in the long run, compromise humans diet largely relying on fish to obtain these essential compounds. The higher bioavailability of CuO ENPs compared to ionic Cu was demonstrated in our findings and is indicative of higher toxicity risk to marine organisms and ecosystems, even when CuO ENPs are released in relatively low non-lethal concentrations.

## CONCLUSION

The evident changes in photosynthetic performance, the formation of Cu-substituted chlorophyll, the alterations in FA profile observed in the model diatom *P. tricornutum*, suggest that CuO ENPs causes stronger physiological implications compared to their ionic counterparts at similar experimental concentrations. Although our results point toward enhanced $Cu^{2+}$ release from CuO ENPs, rather than the internalization of nanoparticles, further research regarding the mechanisms underlying CuO ENPs toxicity is needed to confirm this assumption. The physiology and biochemistry of *P. tricornutum* were very sensitive to CuO ENPs toxicity and provided further insights into diatom-nanoparticle interactions. Several biomarkers were highlighted to efficiently assess the harmful effects of ENPs, including photosynthetic parameters, CuChl *a*, EPA, omega 3/omega 6 ratio, and, to a lesser degree, enzymatic activity (GR, APX). Hence, the proposed biomarkers could be applied to field assessment of the ecological impacts of nanoparticles in marine environments and as tools to support contamination assessment where these emergent metal contaminants are of major concern.

## DATA AVAILABILITY STATEMENT

The datasets generated for this study are available on request to the corresponding author.

## AUTHOR CONTRIBUTIONS

BD conceived and designed the experiments. MF and EF performed the experiments. MF wrote the manuscript. JG performed the SEM analysis and coordinated sample preparation and measurements with the dynamic light scattering system. CP, AM, MC, IC, CG, JM, and PR-S provided technical and editorial assistance. All authors contributed to the article and approved the submitted version.

## FUNDING

The authors would like to thank Fundação para a Ciência e a Tecnologia (FCT) for funding the research via project grants PTDC/CTA-AMB/30056/2017 (OPTOX), UIDB/04292/2020, and UID/MULTI/04046/2013. BD and VF were supported by investigation contracts (CEECIND/00511/2017 and DL57/2016/CP1479/CT0024). PR-S was supported by FCT through a postdoctoral grant (SFRH/BPD/95784/2013). JG was supported by co-funding through the NanoTRAINforGrowth II Program (project 2000032) by the European Commission through the Horizon 2020 Marie Skłodowska-Curie COFUND Program (2015), and by the International Iberian Nanotechnology Laboratory.

## SUPPLEMENTARY MATERIAL

The Supplementary Material for this article can be found online at: https://www.frontiersin.org/articles/10.3389/fmars.2020.539827/full#supplementary-material

**Supplementary Figure 1 |** Copper ENPs SEM imaging at 35,000x **(A)**, 50,000x **(B)**, 80,000x **(C)**, and 150,000 (d) magnification and X-ray fluorescence spectra elemental composition **(D)**.

## REFERENCES

Abida, H., Dolch, L. J., Meï, C., Villanova, V., Conte, M., Block, M. A., et al. (2015). Membrane glycerolipid remodeling triggered by nitrogen and phosphorus starvation in Phaeodactylum tricornutum. *Plant Physiol.* 167, 118–136. doi: 10.1104/pp.114.252395

Ackman, R. G. (1989). *Marine biogenic lipids, fats and oils*, Florida: CRC Press.

Allakhverdiev, S. I., Kinoshita, M., Inaba, M., Suzuki, I., and Murata, N. (2001). Unsaturated fatty acids in membrane lipids protect the photosynthetic machinery against salt-induced damage in Synechococcus. *Plant Physiol.* 125, 1842–1853. doi: 10.1104/pp.125.4.1842

Allakhverdiev, S. I., Nishiyama, Y., Suzuki, I., Tasaka, Y., and Murata, N. (1999). Genetic engineering of the unsaturation of fatty acids in membrane lipids alters the tolerance of Synechocystis to salt stress. *Proc. Natl. Acad. Sci. U S A.* 96, 5862–5867. doi: 10.1073/pnas.96.10.5862

Anjum, N. A., Duarte, B., Caçador, I., Sleimi, N., Duarte, A. C., and Pereira, E. (2016). Biophysical and Biochemical Markers of Metal/Metalloid-Impacts in Salt Marsh Halophytes and Their Implications. *Front. Environ. Sci.* 4:1–13. doi: 10.3389/fenvs.2016.00024

Ansari, T. M., Marr, I. L., and Tariq, N. (2004). Heavy metals in marine pollution perspective-a mini review. *J. Appl. Sci.* 4, 1–20. doi: 10.3923/jas.2004.1.20

Anyaogu, K. C., Fedorov, A. V., and Neckers, D. C. (2008). Synthesis, characterization, and antifouling potential of functionalized copper nanoparticles. *Langmuir* 24, 4340–4346. doi: 10.1021/la800102f

Arao, T., Kawaguchi, A., and Yamada, M. (1987). Positional distribution of fatty acids in lipids of the marine diatom Phaeodactylum tricornutum. *Phytochemistry* 26, 2573–2576. doi: 10.1016/S0031-9422(00)83880-7

Arts, M. T., Ackman, R. G., and Holub, B. J. (2001). "Essential fatty acids" in aquatic ecosystems: a crucial link between diet and human health and evolution. *Can. J. Fisher. Aqua. Sci.* 58, 122–137. doi: 10.1139/f00-224

Aruoja, V., Dubourguier, H. C., Kasemets, K., and Kahru, A. (2009). Toxicity of nanoparticles of CuO, ZnO and TiO2 to microalgae Pseudokirchneriella subcapitata. *Sci. Total Environ.* 407, 1461–1468. doi: 10.1016/j.scitotenv.2008.10.053

Baker, T. J., Tyler, C. R., and Galloway, T. S. (2014). Impacts of metal and metal oxide nanoparticles on marine organisms. *Environ. Pollut.* 186, 257–271. doi: 10.1016/j.envpol.2013.11.014

Cabrita, M. T., Duarte, B., Gameiro, C., Godinho, R. M., and Caçador, I. (2018). Photochemical features and trace element substituted chlorophylls as early detection biomarkers of metal exposure in the model diatom Phaeodactylum tricornutum. *Ecol. Indicat.* 95, 1038–1052. doi: 10.1016/j.ecolind.2017.07.057

Cabrita, M. T., Gameiro, C., Utkin, A. B., Duarte, B., Caçador, I., and Cartaxana, P. (2016). Photosynthetic pigment laser-induced fluorescence indicators for the detection of changes associated with trace element stress in the diatom model species Phaeodactylum tricornutum. *Environ. Monit. Assess.* 188:285. doi: 10.1007/s10661-016-5293-4

Cabrita, M. T., Raimundo, J., Pereira, P., and Vale, C. (2013). Optimizing alginate beads for the immobilisation of Phaeodactylum tricornutum in estuarine waters. *Mar. Environ. Res.* 8, 37–43. doi: 10.1016/j.marenvres.2013.03.002

Cabrita, M. T., Raimundo, J., Pereira, P., and Vale, C. (2014). Immobilised Phaeodactylum tricornutum as biomonitor of trace element availability in the water column during dredging. *Environ. Sci. Pollut. Res. Int.* 21, 3572–3581. doi: 10.1007/s11356-013-2362-x

Chen, C., Zhang, J., Ma, P., Jin, K., Li, L., and Luan, J. (2012). Spatial-temporal distribution of phytoplankton and safety assessment of water quality in Xikeng reservoir. *Hydroecology* 33, 32–38.

Cid, A., Herrero, C., Torres, E., and Abalde, J. (1995). Copper toxicity on the marine microalga Phaeodactylum tricornutum: effects on photosynthesis and related parameters. *Aquat. Toxicol.* 31, 165–174. doi: 10.1016/0166-445X(94)00071-W

Din, M. I., and Rehan, R. (2017). Synthesis, Characterization, and Applications of Copper Nanoparticles. *Anal. Lett.* 50, 50–62. doi: 10.1080/00032719.2016.1172081

Dolch, L. J., and Maréchal, E. (2015). Inventory of fatty acid desaturases in the pennate diatom Phaeodactylum tricornutum. *Mar. Drugs* 13, 1317–1339. doi: 10.3390/md13031317

Dringen, R., and Gutterer, J. M. (2002). Glutathione reductase from bovine brain. *Methods Enzymol.* 348, 281–288. doi: 10.1016/S0076-6879(02)48646-6

Duarte, B., Cabrita, M. T., Gameiro, C., Matos, A. R., Godinho, R., Marques, J. C., et al. (2017). Disentangling the photochemical salinity tolerance in Aster tripolium L.: connecting biophysical traits with changes in fatty acid composition. *Plant Biol.* 19, 239–248. doi: 10.1111/plb.12517

Duarte, B., Caetano, M., Almeida, P. R. R., Vale, C., and Caçador, I. (2010). Accumulation and biological cycling of heavy metal in four salt marsh species, from Tagus estuary (Portugal). *Environ. Pollut.* 158, 1661–1668. doi: 10.1016/j.envpol.2009.12.004

Duarte, B., Marques, J. C., and Caçador, I. (2016). Ecophysiological response of native and invasive *Spartina species* to extreme temperature events in Mediterranean marshes. *Biol. Invas.* 18, 2189–2205. doi: 10.1007/s10530-015-0958-4

Duarte, B., Prata, D., Matos, A., Rita, Cabrita, M., Teresa, et al. (2019). Ecotoxicity of the lipid-lowering drug bezafibrate on the bioenergetics and lipid metabolism

of the diatom Phaeodactylum tricornutum. *Sci. Total Environ.* 650, 2085–2094. doi: 10.1016/j.scitotenv.2018.09.354

Duarte, B., Silva, G., Costa, J. L., Medeiros, J., Paulo, Azeda, C., et al. (2014). Heavy metal distribution and partitioning in the vicinity of the discharge areas of Lisbon drainage basins (Tagus Estuary, Portugal). *J. Sea Res.* 93, 101–111. doi: 10.1016/j.seares.2014.01.003

Dunstan, G. A., Volkman, J. K., Barrett, S. M., Leroi, J. M., and Jeffrey, S. W. (1993). Essential polyunsaturated fatty acids from 14 species of diatom (Bacillariophyceae). *Phytochemistry* 35, 155–161. doi: 10.1016/S0031-9422(00)90525-9

Fan, K.-W., Jiang, Y., Faan, Y.-W., and Chen, F. (2007). Lipid characterization of mangrove thraustochytrid–Schizochytrium mangrovei. *J. Agric. Food Chem.* 55, 2906–2910. doi: 10.1021/jf070058y

Feijão, E., Gameiro, C., Franzitta, M., Duarte, B., Caçador, I., Cabrita, M., et al. (2018). Heat wave impacts on the model diatom Phaeodactylum tricornutum: Searching for photochemical and fatty acid biomarkers of thermal stress. *Ecol. Indicat.* 95, 1026–1037. doi: 10.1016/j.ecolind.2017.07.058

Fernandes, J. C., and Henriques, F. S. (1991). Biochemical, Physiological, and Structural Effects of Excess Copper in Plants. *Bot. Rev.* 57, 246–273. doi: 10.1007/bf02858564

Filimonova, V., Gonçalves, F., Marques, J. C., De Troch, M., and Gonçalves, A. M. M. (2016). Fatty acid profiling as bioindicator of chemical stress in marine organisms: A review. *Ecol. Indicat.* 67, 657–672. doi: 10.1016/j.ecolind.2016.03.044

Foyer, C. H., and Halliwell, B. (1976). The presence of glutathione and glutathione reductase in chloroplasts: A proposed role in ascorbic acid metabolism. *Planta* 133, 21–25. doi: 10.1007/BF00386001

Gladyshev, M. I., Sushchik, N. N., and Makhutova, O. N. (2013). Production of EPA and DHA in aquatic ecosystems and their transfer to the land. *Prostagl. Other Lipid Mediat.* 107, 117–126. doi: 10.1016/j.prostaglandins.2013.03.002

Guillard, R. R. L., and Ryther, J. H. (1962). Studies of Marine Planktonic Diatoms: I. Cyclotella Nana Hustedt, and Detonula Confervacea (Cleve) Gran. *Can. J. Microbiol.* 8, 229–239. doi: 10.1139/m62-029

Heath, R. L., and Packer, L. (1968). Photoperoxidation in isolated chloroplasts. *Arch. Biochem. Biophys.* 125, 189–198. doi: 10.1016/0003-9861(68)90654-1

Hook, S. E., Osborn, H. L., Gissi, F., Moncuquet, P., Twine, N. A., Wilkins, M. R., et al. (2014). RNA-Seq analysis of the toxicant-induced transcriptome of the marine diatom, Ceratoneis closterium. *Mar. Genom.* 16, 45–53. doi: 10.1016/j.margen.2013.12.004

Horie, M., Fujita, K., Kato, H., Endoh, S., Nishio, K., Komaba, L. K., et al. (2012). Association of the physical and chemical properties and the cytotoxicity of metal oxide nanoparticles: metal ion release, adsorption ability and specific surface area. *Metallomics* 4, 350–360. doi: 10.1039/c2mt20016c

Kawakami, S. K., Gledhill, M., and Achterberg, E. P. (2006). Production of phytochelatins and glutathione by marine phytoplankton in response to metal stress. *J. Phycol.* 42, 975–989. doi: 10.1111/j.1529-8817.2006.00265.x

Kern, J., and Guskov, A. (2011). Lipids in photosystem II: Multifunctional cofactors. *J. Photochem. Photobiol. B Biol.* 104, 19–34. doi: 10.1016/j.jphotobiol.2011.02.025

Klaine, S. J., Alvarez, P. J. J., Batley, G. E., Fernandes, T. F., Handy, R. D., Lyon, D. Y., et al. (2008). Nanomaterials in the Environment: Behavior, Fate, Bioavailability, and Effects. *Environ. Toxicol. Chem.* 27, 1825–1851. doi: 10.1897/08-090.1

Knauert, S., Escher, B., Singer, H., Hollender, J., and Knauer, K. (2008). Mixture toxicity of three photosystem II inhibitors (atrazine, isoproturon, and diuron) toward photosynthesis of freshwater phytoplankton studied in outdoor mesocosms. *Environ. Sci. Technol.* 42, 6424–6430. doi: 10.1021/es072037q

Kruse, O., Hankamer, B., Konczak, C., Gerle, C., Morris, E., Radunz, A., et al. (2000). Phosphatidylglycerol is involved in the dimerization of photosystem II. *J. Biol. Chem.* 275, 6509–6514. doi: 10.1074/jbc.275.9.6509

Kumar, K. S., Dahms, H. U., Lee, J. S., Kim, H. C., Lee, W. C., and Shin, K. H. (2014). Algal photosynthetic responses to toxic metals and herbicides assessed by chlorophyll a fluorescence. *Ecotoxicol. Environ. Saf.* 104, 51–71. doi: 10.1016/j.ecoenv.2014.01.042

Küpper, H., and Spiller, M. (1998). In Situ Detection of Heavy Metal Substituted Chlorophylls in Water Plants. *Photosynth. Res.* 58, 123–133. doi: 10.1023/A:1006132608181

Küpper, H., Seibert, S., and Parameswaran, A. (2007). Fast, sensitive, and inexpensive alternative to analytical pigment HPLC: quantification of chlorophylls and carotenoids in crude extracts by fitting with Gauss peak spectra. *Analyt. Chem.* 79, 7611–7627. doi: 10.1021/ac070236m

Küpper, H., Šetlík, I., Spiller, M., Küpper, F. C., and Prášil, O. (2002). Heavy metal-induced inhibition of photosynthesis: Targets of in vivo heavy metal chlorophyll formation. *J. Phycol.* 38, 429–441. doi: 10.1046/j.1529-8817.2002.t01-1-01148.x

Li, Y.-F., Gao, Y., Chai, Z., and Chen, C. (2014). Nanometallomics: an emerging field studying the biological effects of metal-related nanomaterials. *Metallomics* 6, 220–232. doi: 10.1039/c3mt00316g

Marklund, S., and Marklund, G. (1974). Involvement of the Superoxide Anion Radical in the Autoxidation of Pyrogallol and a Convenient Assay for Superoxide Dismutase. *Eur. J. Biochem.* 47, 469–474. doi: 10.1111/j.1432-1033.1974.tb03714.x

Mohanty, N., Vass, I., and Demeter, S. (1989). Copper Toxicity Affects Photosystem II Electron Transport at the Secondary Quinone Acceptor, Q(B). *Plant Physiol.* 90, 175–179. doi: 10.1104/pp.90.1.175

Morelli, E., and Scarano, G. (2004). Copper-induced changes of non-protein thiols and antioxidant enzymes in the marine microalga Phaeodactylum tricornutum. *Plant Sci.* 167, 289–296. doi: 10.1016/j.plantsci.2004.04.001

Nowack, B., and Bucheli, T. D. (2007). Occurrence, behavior and effects of nanoparticles in the environment. *Environ. Pollut.* 150, 5–22. doi: 10.1016/j.envpol.2007.06.006

Oberdörster, G., Oberdörster, E., and Oberdörster, J. (2005). Nanotoxicology: An emerging discipline evolving from studies of ultrafine particles. *Environ. Health Perspect.* 113, 823–839. doi: 10.1289/ehp.7339

OECD (2011). OECD Guidelines for the testing of Chemicals. Freshwater Alga and Cyanobacteria, Growth Inhibition Test. *Organ. Econ. Coop. Dev* 2011, 1–25. doi: 10.1787/9789264203785-en

Pan, K., and Wang, W.-X. (2012). Trace metal contamination in estuarine and coastal environments in China. *Sci. Total Environ.* 42, 3–16. doi: 10.1016/j.scitotenv.2011.03.013

Parrish, C. C. (2009). *Essential fatty acids in aquatic food webs. In Lipids in aquatic ecosystems*. New York, NY: Springer, 309–326.

Patsikka, E., Aro, E., and Tyystjarvi, E. (1998). Increase in the quantum yield of photoinhibition contributes to copper toxicity in vivo. *Plant Physiol.* 117, 619–627. doi: 10.1104/pp.117.2.619

Pinto, E., Sigaud- Kutner, T. C. S., Leitao, M. A. S., Okamoto, O. K., Morse, D., and Calepicolo, P. (2003). Review - Heavy metal-induced oxidatives stress in algae. *J. Phycol.* 39, 1008–1018. doi: 10.1111/j.0022-3646.2003.02-193.x

Popko, J., Herrfurth, C., Feussner, K., Ischebeck, T., Iven, T., Haslam, R., et al. (2016). Metabolome Analysis Reveals Betaine Lipids as Major Source for Triglyceride Formation, and the Accumulation of Sedoheptulose during Nitrogen-Starvation of Phaeodactylum tricornutum. *PLoS One* 11:e0164673. doi: 10.1371/journal.pone.0164673

Prosi, F. (1981). *Heavy metals in aquatic organisms. In Metal pollution in the aquatic environment*. Berlin: Springer, 271–323.

Remmers, I. M., Martens, D. E., Wijffels, R. H., and Lamers, P. P. (2017). Dynamics of triacylglycerol and EPA production in Phaeodactylum tricornutum under nitrogen starvation at different light intensities. *PLoS One* 12:e0175630. doi: 10.1371/journal.pone.0175630

Research And Markets.com. (2018). *Metal Nanoparticles Market by metal (Platinum, Gold, Silver, Iron, Titanium, Copper, Nickel), End-use industry (Pharmaceutical & healthcare, Electrical & electronics, Catalyst, Personal care & cosmetics), and Region - Global Forecast to 2022*. California: Business Wire.

Rip, A., Misa, T. J., and Schot, J. (eds) (1995). *Managing technology in society*. London: Pinter Publishers.

Rocchetta, I., Mazzuca, M., Conforti, V., Ruiz, L., Balzaretti, V., and De Molina, M. D. C. R. (2006). Effect of chromium on the fatty acid composition of two strains of Euglena gracilis. *Environ. Pollut.* 141, 353–358. doi: 10.1016/j.envpol.2005.08.035

Royal Commission on Environmental Pollution. (2008). *Novel materials in the environment: the case of nanotechnology*, London: The Stationery Office.

Saito, H., and Aono, H. (2014). Characteristics of lipid and fatty acid of marine gastropod Turbo cornutus: High levels of arachidonic and n-3 docosapentaenoic acid. *Food Chem.* 145, 135–144. doi: 10.1016/j.foodchem.2013.08.011

Santos-Ballardo, D. U., Rossi, S., Hernández, V., Gómez, R. V., del Carmen, Rendón-Unceta, M., et al. (2015). A simple spectrophotometric method for biomass measurement of important microalgae species in aquaculture. *Aquaculture* 448, 87–92. doi: 10.1016/j.aquaculture.2015.05.044

Sharma, K. K., Schuhmann, H., and Schenk, P. M. (2012). High lipid induction in microalgae for biodiesel production. *Energies* 5, 1532–1553. doi: 10.3390/en5051532

Shen, P. L., Wang, H. T., Pan, Y. F., Meng, Y. Y., Wu, P. C., and Xue, S. (2016). Identification of Characteristic Fatty Acids to Quantify Triacylglycerols in Microalgae. *Front. Plant Sci.* 7:162. doi: 10.3389/fpls.2016.00162

Sunda, W. G. (1989). Trace metal interactions with marine phytoplankton. *Biol. Oceanogr.* 6, 411–442. doi: 10.1080/01965581.1988.10749543

Szabó, M., Lepetit, B., Goss, R., Wilhelm, C., Mustárdy, L., and Garab, G. (2008). Structurally flexible macro-organization of the pigment-protein complexes of the diatom Phaeodactylum tricornutum. *Photosynth. Res.* 95, 237–245. doi: 10.1007/s11120-007-9252-3

Teranishi, Y., Tanaka, A., Osumi, M., and Fukui, S. (1974). Catalase activities of hydrocarbon-utilizing candida yeasts. *Agric. Biol. Chem.* 38, 1213–1220. doi: 10.1080/00021369.1974.10861301

Tiryakioglu, M., Eker, S., Ozkutlu, F., Husted, S., and Cakmak, I. (2006). Antioxidant defense system and cadmium uptake in barley genotypes differing in cadmium tolerance. *J. Trace Elem. Med. Biol.* 20, 181–189. doi: 10.1016/j.jtemb.2005.12.004

Twining, B. S., and Baines, S. B. (2013). The trace metal composition of marine phytoplankton. *Annu. Rev. Mar. Sci.* 5, 191–215. doi: 10.1146/annurev-marine-121211-172322

UNEP (2006). *Marine and coastal ecosystems and human well- being: A synthesis report based on the findings of the Millennium Ecosystem Assessment*. Kenya: UNEP.

Vagner, M., Lacoue-Labarthe, T., Zambonino Infante, J. L., Mazurais, D., Dubillot, E., Le Delliou, H., et al. (2015). Depletion of Essential Fatty Acids in the Food Source Affects Aerobic Capacities of the Golden Grey Mullet Liza aurata in a Warming Seawater Context. *PLoS One* 10:e0126489. doi: 10.1371/journal.pone.0126489

Wang, Z., Li, N., Zhao, J., White, J. C., Qu, P., and Xing, B. (2012). CuO nanoparticle interaction with human epithelial cells: Cellular uptake, location, export, and genotoxicity. *Chem. Res. Toxicol.* 25, 1512–1521. doi: 10.1021/tx3002093

Wei, Y., Zhu, N., Lavoie, M., Wang, J., Qian, H., and Fu, Z. (2014). Copper toxicity to Phaeodactylum tricornutum: A survey of the sensitivity of various toxicity endpoints at the physiological, biochemical, molecular and structural levels. *BioMetals* 27, 527–537. doi: 10.1007/s10534-014-9727-6

Yang, Y. H., Du, L., Hosokawa, M., Miyashita, K., Kokubun, Y., Arai, H., et al. (2017). Fatty Acid and Lipid Class Composition of the Microalga Phaeodactylum tricornutum. *J. Oleo Sci.* 66, 363–368. doi: 10.5650/jos.ess16205

Zhang, C., Chen, X., Tan, L., and Wang, J. (2018). Combined toxicities of copper nanoparticles with carbon nanotubes on marine microalgae Skeletonema costatum. *Environ. Sci. Pollut. Res.* 25, 13127–13133. doi: 10.1007/s11356-018-1580-7

Zhao, J., Cao, X., Liu, X., Wang, Z., Zhang, C., White, J. C., et al. (2016). Interactions of CuO nanoparticles with the algae Chlorella pyrenoidosa: adhesion, uptake, and toxicity. *Nanotoxicology* 10, 1297–1305. doi: 10.1080/17435390.2016.1206149

Zhu, X. G., Govindjee, Baker, N. R., DeSturler, E., Ort, D. R., and Long, S. P. (2005). Chlorophyll a fluorescence induction kinetics in leaves predicted from a model describing each discrete step of excitation energy and electron transfer associated with Photosystem II. *Planta* 223, 114–133. doi: 10.1007/s00425-005-0064-4

Zhu, Y., Xu, J., Lu, T., Zhang, M., Ke, M., Fu, Z., et al. (2017). A comparison of the effects of copper nanoparticles and copper sulfate on Phaeodactylum tricornutum physiology and transcription. *Environ. Toxicol. Pharmacol.* 56, 43–49. doi: 10.1016/j.etap.2017.08.029

**Conflict of Interest:** The authors declare that the research was conducted in the absence of any commercial or financial relationships that could be construed as a potential conflict of interest.

frontiers in Environmental Science

ORIGINAL RESEARCH
published: 10 May 2021
doi: 10.3389/fenvs.2021.554490

# Ecological Risks of Heavy Metals and Microbiome Taxonomic Profile of a Freshwater Stream Receiving Wastewater of Textile Industry

*Grace Olunike Odubanjo*[1†], *Ganiyu Oladunjoye Oyetibo*[1*] *and Matthew Olusoji Ilori*[1,2]

[1]Department of Microbiology, Faculty of Science, University of Lagos, Lagos, Nigeria, [2]Institute of Maritime Studies, University of Lagos, Lagos, Nigeria

Textile wastewater (TWW) contains toxic metals that are inimical to microbiome, aesthetic quality, and the health of the receiving freshwater. TWW-impacted freshwater (L2) was assessed for metals eco-toxicity and the consequent impact on microbiome taxonomic profile (MTP) compared to a pristine environment (L1). The conductivity (1750 µS/cm), chemical oxygen demand (2,110 mg/L), biochemical oxygen demand (850 mg/L), and salinity (5,250 mg/L) of L2 were far above the permissible limits. Mercury posed very high ecological risks in the water column of L2 as lead, arsenic, and copper exerted high risk in the sediment. The MTP of L2 revealed the dominance of Euryarchaeota (48.6%) and Bathyarchaeota (45.9%) among the Archaea. The relative abundances of Proteobacteria and Bacteroidetes increased from 38.3 to 2.0%, respectively, in the L1 ecosystem to 42.1 and 12.9%, correspondingly, in L2. Unclassified Eukarya_uc_*p* (50.4%) and Fungi_uc (16.0%) were key players among the fungi kingdom in L2. The impact of the TWW on the microbiome was evident with the extinction of 6,249, 32,272, and 10,029 species of archaea, bacteria, and fungi, respectively. Whereas, 35,157, 32,394, and 7,291 species of archaea, bacteria, and fungi, correspondingly, exclusively found in L2 were assumed to be invading resident communities that combined with dominant autochthonous strains in shaping the ecophysiology dynamics in TWW-impacted freshwater. While the sensitive microorganisms in L2 are suggested bio-indicators of TWW ecotoxicity, the emergent and dominant taxa are pivotal to natural attenuation processes in the contaminated ecosystem that could be adopted for biotechnological strategy in decommissioning the TWW-impacted freshwater.

**Keywords: ecotoxicology, textile wastewater, heavy metals, microbiome, freshwater, pollution**

OPEN ACCESS

***Edited by:***
*Senthil Kumar Ponnusamy, SSN College of Engineering, India*

***Reviewed by:***
*Jennifer Mesa-Marín, Sevilla University, Spain*
*Farshid Ghanbari, Abadan University of Medical Sciences, Iran*

****Correspondence:***
*Ganiyu Oladunjoye Oyetibo*
*goyetibo@unilag.edu.ng*

***†Present address:***
*Grace Olunike Odubanjo, Doctoral student at the Department of Microbiology, Faculty of Science, University of Lagos, Lagos, Nigeria*

***Specialty section:***
*This article was submitted to Toxicology, Pollution and the Environment, a section of the journal Frontiers in Environmental Science*

***Received:*** *22 April 2020*
***Accepted:*** *12 April 2021*
***Published:*** *10 May 2021*

***Citation:***
*Odubanjo GO, Oyetibo GO and Ilori MO (2021) Ecological Risks of Heavy Metals and Microbiome Taxonomic Profile of a Freshwater Stream Receiving Wastewater of Textile Industry. Front. Environ. Sci. 9:554490. doi: 10.3389/fenvs.2021.554490*

## INTRODUCTION

The textile industry is one of the most important sectors of the global economy as it contributes mass employment and contributes the gross domestic products (GDP) of many developing countries. Textile operations use a large volume of water and produce a large amount of wastewater that is rich in organic and inorganic pollutants (Dung et al., 2013; Bilinska et al., 2016). Textile dyeing and finishing treatments meted on fabric generate approximately 17–20% of textile wastewater (TWW) (Holkar et al., 2016). Worldwide, dye wastewater remains a major source of severe pollution snag due

to industrialization, the huge demand for textile products, and the proportional humongous volume of production wastewaters discharged to the environment (Ali et al., 2008). Among the pollutants in TWW, are the biodegradables that may sometimes be recalcitrant while others, mainly heavy metals (HMs) and metalloids, are non-biodegradable and exert a toxicological effect on the receiving ecosystem (Dung et al., 2013).

The biodegradables contained in TWW are residues of reactive dyes and chemicals that enrich the chemical oxygen demand (COD) and biochemical oxygen demand (BOD) of the hydrosphere, leading to eutrophication (Bilinska et al., 2016). However, dyes used during the fabric dyeing process introduce, in addition to thick color that increases the turbidity of the water body, a diverse range of chemicals and HMs/metalloids that are hazardous to biota in the environment (Holkar et al., 2016). The commonly reported HMs and metalloids found in TWW include arsenic (As), Mercury (Hg), hexavalent chromium ($Cr^{6+}$), iron (Fe), zinc (Zn), copper (Cu), lead (Pb), cadmium (Cd), and the mixtures of these HMs toxicants. The toxicity and persistence of HMs and metalloids in the receiving environment are of great concern with the resultant effect of biomagnifications along trophic levels (Gao and Chen, 2012). Bioaccumulation of wastewaters' HMs/metalloids in the environmental matrixes has been reported to occur through physical, chemical, and biological processes (Rezaei and Sayadi, 2015).

The ecotoxicity of HMs/metalloids on the microbiome of the receiving environments varies from receptor interaction to membrane toxicity, narcosis, the disturbance of cell homeostasis, and enzyme inhibition (Worms et al., 2006). The degree of HMs/metalloids toxicity at the molecular level depends on the types of HMs/metalloids, dosage/bioavailable concentration at autochthonous microbiome, and other physico-chemical factors prevalent in such ecosystems. Consequently, the observable effects on the receiving biome include lethality, growth reduction, functional impairment, reduced fertility and reproduction, mutagenicity, behavioral disturbances, and eventual adaptation (Worms et al., 2006). Hg, like other HMs/metalloids with no known metabolic function, for example, exerts toxicity to different microbial processes and enzyme activities in impacted environments (Mahbub et al., 2016). The microbial processes impaired by HMs/metalloids toxicity include, but are not limited to, the activities of dehydrogenase (Mahbub et al., 2016), urease (Yang et al., 2007), nitrification (Mahbub et al., 2016), arylsulphatase (Casucci et al., 2003), methane oxidation (Contin et al., 2012), phosphatase and respiration (Tazisong et al., 2012), among others.

Microorganisms are one of the most sensitive bio-indicators for monitoring the influence of HMs toxicants in the polluted hydrosphere. The indiscriminate discharge of effluents from textile industries with disregard for environmental pollution regulations and legislatures, mostly in developing countries, can lead to temporal and spatial shifts of microbial communities in aquatic environments (Zhang et al., 2016). Although microorganisms are key players in the bioremediation of any deteriorating environment (Oyetibo et al., 2017a, Oyetibo et al., 2017b, Egbe et al., 2020; Oyetibo et al., 2021), the ecological response to such continual discharge of TWW is primarily the extinction of sensitive microbial taxa. The microbiome taxonomic profile in the receiving environment is then skewed toward the evolution of: 1) microorganisms that sequester HMs/metalloids; 2) microbes that exhibit resistance to the HMs/metalloids and thus perform their metabolic activities in the presence of the toxicants; and 3) HMs/metalloid-sensitive strains that can tolerate such HMs/metalloids but only become metabolically active once the HMs/metalloid toxicants have been mitigated (Oyetibo et al., 2010; Egbe et al., 2020; Ogwugwa et al., 2020).

To date, studies on the ecological consequences of TWW on the microbiome of the receiving environment are scarce. Therefore, the eventual alteration of ecological balance due to the toxicants (HMs/metalloids) contained in wastewater discharged by a textile industry is worthy of being studied. The present work, therefore, aimed to assess the HMs pollution status and impact of the textile wastewater from the textile industry in Nigeria (Africa) on the receiving freshwater. Therefore, the determination of the ecological impact of TWW was based on profiling the microbiome of the impacted ecosystem in relation to the pristine environment, using a culture independent approach. Consequently, the geochemistry and microbiome taxonomic profile of the TWW-impacted and non-impacted freshwater were integrated to elucidate the ecotoxicity of the TWW toxicants in freshwater. The success of this study would therefore suggest microbial bio-indicators for TWW pollution in freshwater. The outcome of this work provides information on the pivotal microbial taxa required in the circular economy concept for sustainable bioremediation of TWW-impacted freshwater environments.

# MATERIALS AND METHODS

## Study Area and Sampling

Ikorodu is one of the fastest-growing towns in the Lagos metropolis, owing to massive migration from other towns within Lagos State (Nigeria) and industrialization. A textile industry situated on the outskirts of Ikorodu has been operating for decades, discharging its effluents directly to a freshwater stream, forming a tributary that finally empties into Lagos lagoon. The sampling locations were a freshwater stream that daily receives wastewaters from the textile industry (L2: N 6.5719444°, 3.485833° E) and a pristine environment, Nigerian Conservation Foundation (NCF) with no known history of anthropogenic pollution (L1: N 6.43722°, 3.5359° E). Ten composite samples of water filtered through 0.45 µm syringe filters into sterile screw-capped bottles on-site were collected. Similarly, sediments (0–5 cm depth) *via* composite sampling technique were collected using a Ven Veen Grab into a sterile glass beaker and covered with sterile aluminum foil. Sampling in triplicates was between February to March 2017 at 3 weeks intervals. The composite samples were thoroughly mixed to represent each replicate of the triplicate analyses. All samples in triplicate were concealed in Ziploc bags and transported on ice to the laboratory and stored at −20°C for subsequent analyses.

**TABLE 1 |** Physicochemical status of the impacted freshwater receiving textile wastewater and a pristine environment.

| | Wastewater | | Sediment | |
|---|---|---|---|---|
| **Parameter** | **NCF (L1)** | **Impacted freshwater (L2)** | **NCF (L1)** | **Impacted freshwater (L2)** |
| **pH** | 5.33 | 9.85 | 5.75 | 4.47 |
| **Conductivity (μS/cm)** | 210 | 1750 | 260 | 500 |
| **Salinity (mg/L)** | 2,540 | 5,250 | — | — |
| **Turbidity (NTU)** | 50.4 | 82 | — | — |
| **Appearance** | Brownish | Bluish | — | — |
| **Composition** | — | — | Silty | Silty |
| **Chloride** | 141 | 2,910 | — | — |
| **DO (mg/L)** | 8.26 | 8.53 | — | — |
| **COD (mg/L)** | 117 | 2,110 | — | — |
| **BOD (mg/L)** | 80.3 | 850 | — | — |
| **TS (mg/L)** | 2,490 | 930 | — | — |
| **TDS (mg/L)** | 1,330 | 470 | — | — |
| **TSS (mg/L)** | 1,160 | 430 | — | — |
| **Nitrate (mg/L)** | 40.0 | 55.0 | 17.3 | 12.7 |
| **Sulfate (mg/L)** | 6.52 | 0.56 | 9.43 | 10.2 |
| **Phosphate (mg/L)** | 11.7 | 19.2 | 85.9 | 64.1 |
| **Ammonia (mg/L)** | 10.9 | 14.7 | 17.6 | 31.4 |
| **Sulfide (mg/L)** | 2.17 | 0.19 | — | — |
| **MC (%)** | — | — | 14.7 | 6.31 |
| **TOC (%)** | — | — | 1.25 | 1.44 |
| **TOM (%)** | — | — | 2.16 | 2.48 |
| **Hardness (mg/L)** | 100 | 80 | — | — |
| **Alkalinity (mg/L)** | 170 | 310 | — | — |
| **Acidity (mg/L)** | 200 | 160 | — | — |

*DO, Dissolved Oxygen; BOD, Biochemical Oxygen Demand; COD, Chemical Oxygen Demand; TS, Total Solids; TSS, Total Suspended Solids; TDS, Total Dissolved Solids; MC, Moisture Content; TOC, Total Organic Carbon; TOM, Total Organic Matter; BDL, Below Detection Level.*

## Physico-geochemical and Eco-toxicological Analyses

The physicochemical analysis of wastewater and sediments was done as earlier reported (Oyetibo et al., 2019). The parameters including pH, appearance, and temperature were determined *in situ,* while others were determined *ex situ*. Eleven HMs/metalloids were assayed and quantified using Atomic Absorption Spectrophotometry (Perkin-Elmer Analyst 200; Pelkin-Elmer, Canada) after acidic digestion as explained previously (Oyetibo et al., 2010). The normalization, validation, operational conditions, and wavelengths of the analytical lines of the AAS used for the detection of HMs in samples were undertaken as earlier reported (Ogwugwa et al., 2020; Oyetibo et al., 2021). The geochemical indexes of the measured HMs/metalloids were determined to evaluate the degrees of contamination, accumulation, pollution, and eco-toxicity of the HMs/metalloids as previously described (Oyetibo et al., 2019).

## The indexes include:

$$\text{Contamination factor (CF)}, \mathrm{CF} = \frac{Cn}{Bn} \quad (1)$$

where $C_n$ is the concentration of the metal n and $B_n$ is the natural local background concentration of metal n.

$$\text{Geo-accumulation index}\left(\mathrm{I_{geo}}\right) : \mathrm{I_{geo}} = \log_2\left(\frac{C_n}{K \times B_n}\right) \quad (2)$$

where $C_n$ is the concentration of metal n and $B_n$ is as indicated above. The factor K is the background matrix correction factor due to lithospheric effects, which is usually defined as 1.5 according to Muller (1969).

$$\text{Pollution load index (PLI)PLI} = (CF_1 \times CF_2 \times CF_3 \times \ldots \times CF_n)^{\frac{1}{n}} \quad (3)$$

where CF is the contamination factor as described before.

$$\text{Degree of contamination}\ (\mathrm{C_d}), \mathrm{C_d} = \sum_{i=1}^{n} CF \quad (4)$$

$$\text{Potential ecological risk factor (Er)}, \quad E_r^i = T_r^i.CF \quad (5)$$

where $T_r$ is the toxic response factor for a given substance (see **Supplementary Table SA1**)

$$\text{Potential ecological risk index (RI)}, \quad RI = \sum_i^m E_r^i \quad (6)$$

## Community DNA Isolation, Purification, and Quantification

Genomic DNA extraction from 0.5 g (approx.) of sediment sample from each location was achieved with Fast DNA® Spin Kit for Soil (MP Biomedicals) using FastPrep® Cell Distruptor FP120 (Qbiogene, Heidelberg, Germany) at 6.5 speed for 30 s following the manufacturer's instruction. The possible interference of humic substances in the DNA was removed based on the recommendation of Takada and Matsumoto (2005). DNA was purified and visualized in an ethidium

**TABLE 2 |** Heavy metal and metalloid pollution indexes and ecological risks of the textile wastewater impacted freshwater.

| | Water | | | Sediment | | |
|---|---|---|---|---|---|---|
| **Metal/ Metalloid** | **$I_{geo}$** | **PI** | **Er** | **$I_{geo}$** | **PI** | **Er** |
| **Pollution index** | | | | | | |
| **Fe** | 1.8 | 5.2 | 26 | −1.2 | 0.67 | 3.35 |
| **Pb** | −0.59 | 1.0 | 5.0 | 13.0 | 14,000 | 67,500 |
| **Cu** | −0.59 | 1.0 | 5.0 | 13.0 | 14,000 | 70,000 |
| **Ni** | −0.59 | 1.0 | 5.0 | −0.59 | 1.0 | 5 |
| **Cd** | 1.8 | 5.1 | 62 | −0.56 | 1.0 | 12 |
| **Zn** | 2.2 | 7.0 | 16 | −0.75 | 0.89 | 2.0 |
| **Mg** | 2.0 | 6.2 | 31 | −0.41 | 1.1 | 5.6 |
| **Co.** | −0.59 | 1.0 | 5.0 | 0.01 | 1.5 | 7.6 |
| **Hg** | 5.8 | 82 | 410 | 1.3 | 3.7 | 18 |
| **As** | 1.4 | 4.0 | 40 | 5.2 | 54 | 540 |
| **Sb** | −0.59 | 1.0 | 5.0 | −0.59 | 1 | 5 |
| **Ecological risk** | | | | | | |
| **$C_d$ ($16 \leq C_d < 32$** | **Very high ($C_d \geq 32$):** 110 | | | **Very high ($C_d \geq 32$):** 28,000 | | |
| **PLI ($1 < PLI \leq 10$)** | **Polluted system:** 3.2 | | | **Polluted system:** 9.2 | | |
| **RI** | **Very high (RI ≥ 600):** 610 | | | **Very high (RI ≥ 600):** 140,000 | | |
| **CF** | **Low ($C_f^i < 1$):** Non | | | **Low ($C_f^i < 1$):** Zn > Fe | | |
| — | **Moderate ($1 \leq C_f^i < 3$):** Pb = Cu = Ni = Co. = Sb | | | **Moderate ($1 \leq C_f^i < 3$):** Co. > Mg > Ni = Sb | | |
| — | **Considerable ($3 \leq C_f^i < 6$):** Fe > Cd > as | | | **Considerable ($3 \leq C_f^i < 6$):** Hg > Cd | | |
| — | **Very high ($C_f^i \geq 6$):** Hg > Zn > Mg | | | **Very high ($C_f^i \geq 6$):** Cu > Pb > as | | |
| **Er** | **Low ($Er^i < 1$):** Mg > Fe > Zn > Pb = Cu = Ni = Co. = Sb | | | **Low ($Er^i < 1$):** Hg > Cd > Co. > Mg > Ni = Sb > Fe > Zn | | |
| — | **Moderate ($40 \leq Er^i < 80$):** Cd > as | | | **Moderate ($40 \leq Er^i < 80$):** Non | | |
| — | **Very high ($Er^i \geq 320$):** Hg | | | **Very high ($Er^i \geq 320$):** Cu > Pb > as | | |

*$C_d$, Degree of Contamination; PLI, Pollution Load Index; CF, Contamination Factor; Er, Potential Ecological Risk Factor for a given Metal/metalloid; RI, Potential Ecological Risk Index for the Location; $I_{geo}$, Geo-accumulation Index.*

bromide-stained 1% (w/v) agarose gel using UV *trans*-illumination, while quantification was via UV-Vis photo-spectrometry using the Epoch™ Spectrometer system (BioTek, Winooski, VT, United States).

## PCR Amplification, Library Preparation, and Sequencing

The genomic DNA was amplified at the V3-V4 of the 16S rRNA using the primer set 341F and 805R; V4-V5 region of 16S rRNA gene using primer set A519F-Mi and A958R-Mi; and ITS2 region using primer set ITS3-Mi (forward) and ITS4-Mi (reverse) for bacteria, archaea, and eukarya, respectively. The first and second PCR recipes and conditions were presented in the supplementary materials (**Supplementary Table SA2**). The purified amplicons of 1st PCR were tagged with Illumina indices and adapters from a Nextera® XT Index Kit (Illumina, San Diego, CA, United States). Libraries were constructed at ChunLab Inc. Seoul, South Korea using the Illumina MiSeq platform, and the qualities of the constructed libraries were checked with Agilent 2,100 Bioanalyzer System (Agilent Technologies, Palo Alto, CA, United States) using a DNA 7500 chip, and thereafter quantified using Quanti-iT™ PicoGreen™ dsDNA Assay kit (Invitrogen) according to the manufacturer's instructions. A short DNA fragment was removed using CleanPCR™ (CleanNA, Netherlands), and sequencing was performed using Illumina, MiSeq Reagent Kit v2 (500-cycles) of Illumina MiSeq platform at ChunLab Inc. Seoul, Korea.

Metagenome raw reads were processed beginning from the quality check and filtering of low quality (<Q25) reads using Trimmomatic 0.32 software (Bolger et al., 2014). The pair-end sequence of the same strand of PCR amplicon was merged based on overlapping sequence information using PANDAseq software (Masella et al., 2012). ChunLab's pipeline in-house algorithms were used to remove 16S rRNA PCR primer sequences, and UNITE (https://unite.ut.ee) was used to analyze the ITS2 gene. Non-specific amplicons were identified and removed using the HMMER program-based search to exclude Singleton sequences (Eddy, 2011), while sequences denoizing were performed with DUDE-Seq software (Lee et al., 2017), sequences were de-replicated and non-redundant reads were extracted *via* UCLUST-clustering (Edgar, 2010). UCHIME (Edgar et al., 2011) was used for the detection and removal of chimera against BIOiPLUG's chimera-free reference database, while the remaining non-chimeric sequences were clustered into operational taxonomic units (OTUs) using CD-HIT (Fu et al., 2012) and UCLUST (Edgar, 2010) as discussed by Lee et al. (2019). Query sequences that were matched with the reference sequences in the EzBioCloud database (https://www.ezbiocloud.net/) by ≥97% similarity were considered to be at the species level while <97% similarity cut-offs were used for the genus, family, order, class, and phylum. The sequencing metadata obtained and

used in this study have been deposited in the NCBI's sequence read archive (SRA) database under BioProject and SRA accession number **PRJNA545318.**

## Statistical Analyses

Statistical analyses including column/row statistics and regression analyses, unless otherwise stated, and bar charts in this study were performed using the prism 5 software program (GraphPad Software, San Diego, CA, United States). The estimated coverage of the constructed gene libraries was calculated as $C = 1-(\frac{n}{N}) \times 100$ (Kemp and Aller, 2004), where $n$ is the number of Singletons after assembly, and $N$ is the total number of sequences in the initial dataset. Rarefaction curves were obtained by plotting the number of observed OTUs vs. the number of sequences along with calculations of Good's coverage coefficient to determine the level of sequencing depth. Richness and diversity statistics of the bacterial community including the abundance-based coverage estimator ($S_{ACE}$), the bias-correlated Chao1 ($S_{chao1}$), and the Shannon-Weaver diversity index, were estimated using BIOiPLUG and pre-calculated program of CLcommunity™ software package (ChunLab Inc.) to assay taxonomic diversity. Phylogenetic structure diversity was calculated by summing the shortest distance between the nodes of the system diagram to quantify the differences among species. Unweighted pair group method with arithmetic mean (UPGMA) tree was created using the CLcommunity™ software package (ChunLab Inc.).

# RESULTS

## Pollution Status of the Environments

The physico-chemistry of the water and sediment samples from the freshwater receiving textile wastewater (L2) revealed marked degrees of pollution, as shown in **Table 1**. In comparison with the pristine environment, the pH of the water from the impacted environment was alkaline (pH = 9.85) with characteristic high conductivity (1750 μS $cm^{-1}$), COD (2,110 mg $L^{-1}$), BOD (850 mg $L^{-1}$), and salinity (5,250 mg $L^{-1}$). The water of the impacted L2 contained a huge chloride level and appeared deep-bluish unlike that of the pristine environment (L1). It is noteworthy that the physico-chemical values of the water and sediment samples of the impacted L2 exceeded the recommended limits of the local and international regulatory bodies (US EPA, 1998; NESREA, 2010).

The contamination indexes of HMs/metalloids in L2 when the pristine environment was used as the background threshold are shown in **Table 2**. Based on the calculated contamination factor (CF), the very high contamination of Hg was observed in the water while a similar degree of contamination in the sediment was recorded for As and Pb. The water was also considerably contaminated with Cd and As while moderate contamination of the water was associated with Pb, Ni, Co., and Sb. On the contrary, Hg and Cd considerably contaminated the sediment. The potential geological accumulation of the HM/metalloid toxicants revealed moderate to strong pollution of Fe, Cd, Zn, Mg, and As in the water unlike in the sediment where such levels of pollution were found with Hg. However, the water of L2 was extremely polluted with Hg while such pollution in sediment was associated with Pb, Cu, and As. A very high toxic response of Hg ($Er^i$ = 410) was observed with the impacted water, but a lower Hg toxic response was associated with the sediment. Nevertheless, the very high toxic responses of Cu ($Er^i$ = 70,000), Pb ($Er^i$ = 67,500) and As ($Er^i$ = 540) were linked to the sediment in the impacted environment. Overall, the receiving environment is greatly impacted with higher HMs/metalloids pollution occurring at the sediment as exhibited with a higher degree of contamination ($C_d$ = 110, water; 28,000, sediment), pollution load index (PLI = 3.2, water; 9.2, sediment), and potential ecological risk index (RI = 610, water; 140,000, sediment).

## Microbiome Taxonomic Profile

The total valid reads of bacteria, archaea, and fungi after quality filtering, trimming and removing all chimeric reads are presented in **Table 3**. More sequence reads of the bacterial 16S rRNA genes were observed in the sediments of the pristine L1 environment (83,019) unlike fewer sequence reads of archaea 16S rRNA (113,810) and fungal ITS (67,121) genes than the impacted L2 sediment. After the removal of Singletons, more bacterial OTUs (9,950) were found in the impacted sediment than the pristine sediment (8,693). **Figure 1** depicted the microbial composition and the relative abundance of the phyla taxa of the archaea (**Figure 1A**), bacteria (**Figure 1B**), and fungi (**Figure 1C**). A total of seven archaeal phyla were identified in all the sediments, where the impacted L2 ecosystem was mostly composed of Bathyarchaeota (45.9%), Euryarchaeota (48.6%), and not-yet-identified MBGB_p (4.3%) in comparison with the pristine sediments containing Bathyarchaeota (53.5%), Euryarchaeota (34.0%), and Thaumarchaeota (11.2%) as dominant phyla (**Figure 1A**). Proteobacteria (L1, 38.3; L2, 42.1%) and Chloroflex (L1, 16.9; L2, 14.4%) dominated the sediments from both ecosystems in addition to the visible dominance of Bacteroidetes (12.9%) in the textile impacted L2 ecosystem in contrast to the pristine L1 sediment that contained just 2.0% (**Figure 1B**). The relative abundance of Actinobacteria (L1, 5.57; L2, 4.66%) appeared relatively unaffected by the TWW unlike populations of Acidobacteria (11.2%) in the pristine L1 sediment that skewed down to 2.46% in the impacted L2 ecosystem (**Figure 1B**). The fungal community in the two ecosystems were dominantly Eukarya_uc_p, Fungi_uc, Ascomycota, Basidiomycota, and Chtridiomycota. The TWW appeared to have shifted the populations of not-yet-identified Eukarya_uc_p (15.4%), and Fungi_uc (9.6%) in L1 upward to 50.4 and 16.0%, respectively, in the TWW-impacted L2 (**Figure 1C**). Interestingly, Chitridiomycota (28.0%), which was the second-most dominant fungi in the pristine sediments, had become extinct with less than 0.3% relative abundance in the TWW-impacted L2.

## Comparison of the Microbiome in the Ecosystems

Analysis of the sequencing data of the microbial communities in the pristine and textile wastewater impacted ecosystems were revealed by a heat map based on the delineation of OTUs

**TABLE 3 |** Alpha diversity of microbiome evenness, richness, and varieties of species in the sediments.

| | Bacteria | | Archaea | | Eukarya | |
|---|---|---|---|---|---|---|
| | L1 | L2 | L1 | L2 | L1 | L2 |
| Actual | | | | | | |
| Valid reads | 83,019 | 70,104 | 113,810 | 116,132 | 67,121 | 69,612 |
| OTUs | 8,693 | 9,950 | 4,843 | 4,442 | 1,446 | 1,183 |
| **Estimated richness** | | | | | | |
| ACE | 8,851 | 10,078 | 4,846 | 4,456 | 1,460 | 1,189 |
| HCI | 8,882 | 10,105 | 4,851 | 4,465 | 1,469 | 1,195 |
| LCI | 8,821 | 10,052 | 4,842 | 4,447 | 1,451 | 1,183 |
| Chao1 | 8,723 | 9,969 | 4,843 | 4,442 | 1,448 | 1,184 |
| HCI | 8,738 | 9,981 | 4,844 | 4,446 | 1,454 | 1,188 |
| LCI | 8,713 | 9,962 | 4,843 | 4,442 | 1,447 | 1,183 |
| JackKnife | 9,126 | 10,332 | 4,854 | 4,483 | 1,485 | 1,201 |
| HCI | 9,126 | 10,332 | 4,854 | 4,483 | 1,485 | 1,201 |
| LCI | 9,126 | 10,332 | 4,854 | 4,483 | 1,485 | 1,201 |
| **Estimated diversity** | | | | | | |
| NPShannon | 7.96 | 8.25 | 5.70 | 5.82 | 4.52 | 4.32 |
| Shannon | 7.78 | 8.00 | 5.61 | 5.74 | 4.50 | 4.30 |
| HCI | 7.79 | 8.01 | 5.63 | 5.75 | 4.52 | 4.32 |
| LCI | 7.76 | 7.98 | 5.60 | 5.73 | 4.48 | 4.28 |
| Simpson | 0.002 | 0.005 | 0.017 | 0.012 | 0.085 | 0.064 |
| HCI | 0.002 | 0.005 | 0.017 | 0.013 | 0.087 | 0.065 |
| LCI | 0.002 | 0.004 | 0.017 | 0.012 | 0.084 | 0.063 |
| Good's lib. Coverage (%) | 99.5 | 99.4 | 100 | 100 | 99.9 | 100 |

*Clustering of OTUs found was achieved with UCLUST and the open reference method as all taxa were selected for analysis; HCI, High Confidence Interval (95%); LCI, Low Confidence Interval (95%); OTUs, Operational taxonomic units determined at 97%.*

by the OrthoAni scale (**Figure 2**). The most abundant phyla of the three microbial domains in the ecosystems include Bathyarchaeota, Euryarchaeota, Proteobacteria, Eukarya_uc_p, Ascomycota, Chloroflexi, Chytridiomycota, and Fungi_uc, which is in tandem with the earlier discussed taxonomic compositions. Based on the Fast UniFrac metric and the OrthoAni values, the unweighted pair group method and arithmetic mean (UPGMA) dendrogram depicts the expected relatedness of the OTUs in the microbial domains with the highest OTUs richness among the Archaea and the least among the Fungi. Taxon Exclusive Or (XOR) analysis revealed that there was no archaeal phylum exclusively present in L1, except for two Class taxa (Thaumarchaeota_uc, and AF523942_c) that are not yet identified. Rather, 6,249 archaeal species that are mostly not yet identified were present in the sediments of L1 but found missing in those of the impacted L2. Whereas, 35,157 archaeal species were exclusively found in L2 (see **Supplementary Table SA3** for the 20 most abundant taxa exclusively present in the ecosystems). Moreover, 12 bacterial phyla that were mostly yet to be identified, were only found in the pristine sediment contrary to the 30 bacterial phyla found in the impacted sediment but not found in L1. As such, 32,272 bacterial species were solely found in L1, while 32,394 bacterial species found in L2 were missing in L1. Nevertheless, the two fungal phyla (Crytomycota, n = 59; and Kickxellales_p, n = 1) present in L1 were missing in L2, while there was no fungal phylum uniquely found in L2 other than the 11 fungal Class taxa. Intrinsically, 10,029 fungal species were exclusively found in the pristine sediment while 7,291 fungal species were solely found in the TWW-impacted sediment.

## Diversity of Microbiome Based on Alpha Estimates of Diversity Indices

The plot of the correlation between the size of the sediment data and the number of OTUs delineated are depicted in asymptotic rarefaction curves (**Figure 3**). The highest numbers of OTUs were observed with bacteria while the least OTUs were associated with fungi, corresponding to species diversities in the ecosystems. The textile wastewater impacted sediment contained more bacterial OTUs than the pristine sediment. By contrast, less diverse OTUs of Archaea and Fungi domains were associated with the textile impacted sediment. The evenness, richness, and diversity estimations are summarized in **Table 3**.

More than 99% of the sequences in both environments represented the bacteria, archaea, and fungi present in the sediments, signifying the low probability of finding new species, should the number of sequence reads be increased based on Goods library coverage. The values of ACE, Chao 1, and JackKnife were proportional to microbiome richness, whereby the impacted sediment contained richer bacterial

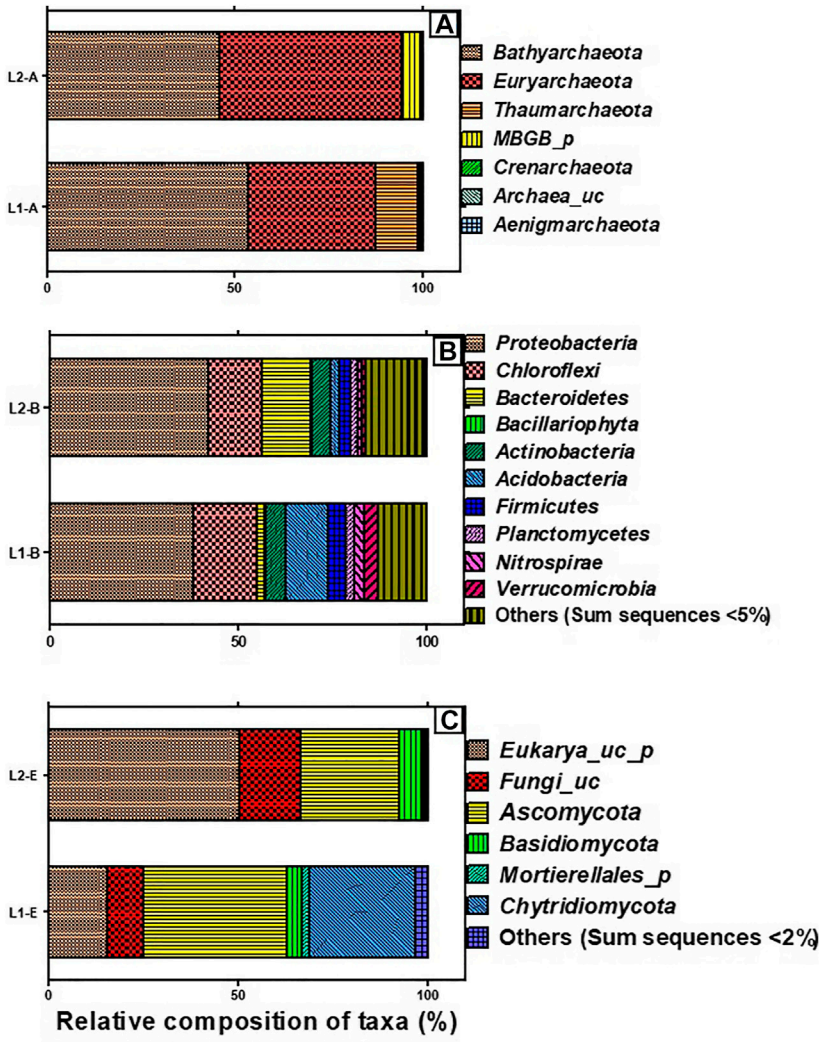


**FIGURE 1 |** Taxonomic composition of microbiome present in the sediments of the pristine environment (L1) and textile wastewater impacted freshwater (L2), showing the archaeal phyla **(A)**, bacterial phyla **(B)**, and fungal phyla **(C)**. Others represent the aggregation of phyla whose sum sequences are less than 5 and 2% in bacteria and fungi, respectively.

OTUs than the pristine sediment. Thus, the TWW-impacted sediment was more diverse, with respect to the sequence reads picked as OTUs by UCLUST and the open reference method. However, the pristine sediments contained higher varieties of Archaea and Fungi than the TWW-impacted sediment. NPShannon, Shannon, and Simpson indexes further revealed the diversity of microbiome in the sediments. While the values of NPShannon and Shannon were proportional to the degree of species diversity, the values of the Simpson index were inversely proportional to species diversity among sediments. It might therefore be adduced that the biodiversity of the microbiome in the textile wastewater impacted sediment and that of the pristine was not marginal. The impacted ecosystem appeared more diverse than the pristine ecosystem but in reality, as revealed by the actual OTUs pick by UCLUST, the pristine sediment was more diverse than the textile wastewater impacted sediment.

## DISCUSSION

Industrialization is a quest of every nation to drive the economic growth of its citizens. The textile industry, unlike other industries, remains one of the major generators of effluent wastewater due to the large volume of water used for its different wet processing operations. The components of textile wastewaters are considered important pollutants that hamper the usability of receiving freshwater and thus damage the environment and public health (Holkar et al., 2016). The nature of pollution that accompanies the textile industry is such that the physico-chemistry of the receiving environment is compromised as evident with parameters of such affected ecosystem fall beyond the recommended limits. As observed in this study, the pH, conductivity, salinity, COD, BOD, and chloride among others of the TWW-impacted system (L2) were unacceptably at variance with the parameters of the pristine environment (L1) and

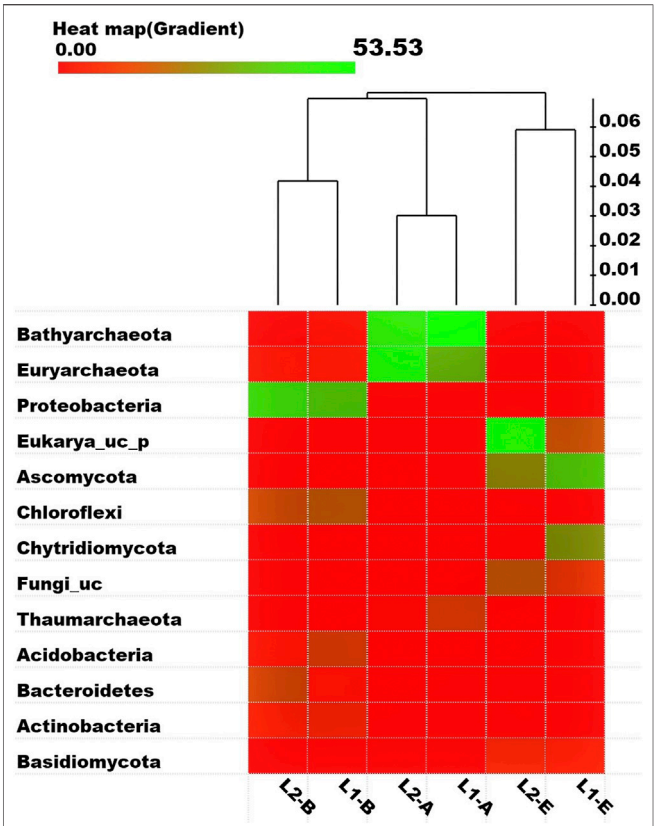


**FIGURE 2 |** Heat map (gradient) representing the abundance of eight bacterial families, above the cut off (phylotypes that are over 5% from an individual sample). Each taxon and its proportion are represented by a square and relativity of samples based on operational taxonomic units (OTUs) delineated by the OrthoAni scale is shown as a dendrogram. The full green square equals 53.53%.

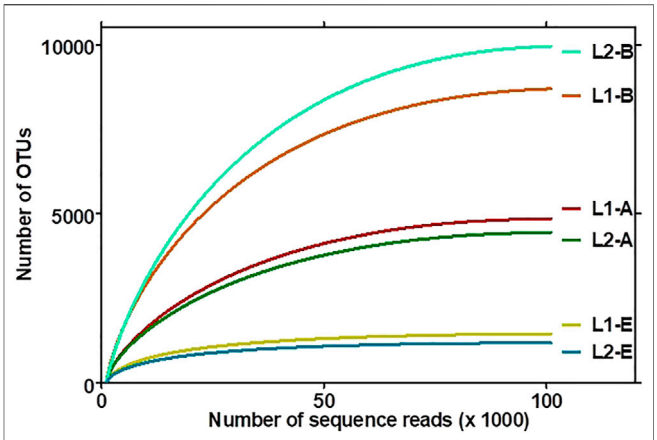


**FIGURE 3 |** Rarefaction curve of the operational taxonomic units (OTUs) of the archaeal (L1-A, L2-A), bacterial (L1-B, L2-B), and fungal (L1-E, L2-E) sequence reads associated with the sediments. Clustering of OTUs in sediments based on taxonomy-dependent clustering and taxonomy-based clustering (TDC-TBC), which first identified sequences at species level using a similarity-based identification method that hits against the EzBioCloud database (https://www.ezbiocloud.net/), and the sequences that cannot be identified (sequences with <97% similarity) were then subjected to a TBC to be assigned OTUs. The confidence intervals of the curves were 95%.

consequently above the recommended limit. The physico-chemical parameters exceeding the recommended limits of regulatory bodies have variously been reported as an indicator of environmental pollution (Gupta et al., 2017; Obijiofor et al., 2018). For example, the Chloride levels in unpolluted waters are often below 10 mg $L^{-1}$ unlike the 2,907 mg $L^{-1}$ recorded for the TWW-impacted L2 that might have been contributed during the textile production step involving bleaching with hypochlorites and chlorites in the wet processing of fabrics. Similarly, the high pH recorded for the TWW-impacted L2 is connected to the alkali treatment of fabrics at a temperature of around 90°C during de-sizing, scouring, and mercerization.

The sources of the high values of COD and BOD in the TWW-impacted L2 must be from impurities in cotton and hemicellulose, and the residual dyes used in textile production. Consequently, the organic compounds in TWW as reflected in the high values of COD and BOD in the water column, and total organic matter of sediments in the impacted ecosystem against the unpolluted ecosystem must have contributed immensely to actual toxicity from the wastewater.

Previous studies have affirmed the relevance of the organic compounds of TWW to the ecotoxicity of the receiving environments (Khan and Malik, 2018). The high conductivity values of both water and the sediment of TWW-impacted L2 suggested that dissolved solids are mostly mineral salts (Ado et al., 2015). Although the microbial degradation of textile dyes is possible (Chen and Yien Ting, 2015; Ajaz et al., 2019), the eco-toxicological impact of textile dyes on autochthonous microorganisms has been reported (Bilinska et al., 2016). The high ecological risk of Hg in the water of the TWW-impacted L2 based on contamination factor (CF), revealed highly mobile Hg in the aqua system driving the bioavailability of toxic Hg in the ecosystem. Other toxic metals of note that variously contaminated the TWW-impacted L2, including Cd, As, Pb, and Ni, do not have any metabolic relevance to microbiota other than toxicity. Hg toxicity along with those of other HMs/metalloids to various ecosystems has been reported (Mahbub et al., 2017; Oyetibo et al., 2019; Ogwugwa et al., 2020; Oyetibo et al., 2021). Interestingly, the higher ecological risk of Hg in the water column (than the sediment) of impacted L2 is evidence that many mercuric ions ($Hg^{2+}$) were bioavailable to the indigenous microbiota of the freshwater. However, the humongous sum of pollution indexes of the TWW-impacted L2 sediment is an indication of overtime accumulation of the HMs/metalloid toxicants from the continuous discharge of wastewaters from the textile industry. The consequences of these eco-toxicants have been variously reported (Ado et al., 2015; Obijiofor et al., 2018).

The high ecological risk indices observed in the TWW-impacted L2 were evident in the taxonomic composition and alpha diversities of the indigenous microbiome. The impact of TWW was more pronounced on the fungal taxa, where most OTUs that were dominant in the pristine ecosystem had gone extinct due to toxicities of HMs/metalloid toxicants present in the

wastewater. Similar observations have been reported from other environments that were either treated with HMs/metalloid toxicants or had been naturally exposed to toxic HMs/metalloids (Catania et al., 2018; Lee et al., 2019). It should also be noted that archaea and bacteria can generally better adapt to extreme environments than eukarya, as represented by fungi in this study. Oyetibo et al., 2015 had earlier reported the low capabilities of fungi, except for a few strains such as *Yarrowia* sp Idd1 and Idd2, to resist/tolerate a toxic dosage of Hg in the environment. Similar eco-toxicity of HMs to the growth or survival of some of the archaea, leading to the observance of a significant reduction in the relative abundance and qualitative difference in the Archaean community (Sandaa et al., 1999; Guo et al., 2019). Moreover, salinity is a key factor in controlling the diversity and composition of the archaeal community in freshwater (Liu et al., 2016) as observed in the TWW-impacted L2 sediment where archaeal richness and evenness were reduced.

The dominance of Bathyarchaeota (53.5%), Euryarchaeota (34.0%), and Thaumarchaeota in the pristine L1 were in tandem with earlier reported archaeal composition in freshwater sediments (Yang et al., 2016; Guo et al., 2019). However, the skewness of archaeal composition in the TWW-impacted L2, as depicted with a lowered relative abundance of Bathyarchaeota (45.9%), increase in abundance of Euryarchaeota (48.6%), and relegation of Thaumarchaeota to <1% sequence reads was due to the influence of the HMs/metalloid toxicants present in the TWW discharged into the ecosystem. It can, therefore, be adduced that members of Thaumarchaeota were sensitive to HMs and chemicals contained in the TWW that were consistently released into L2. This observation agrees with the conclusions of Liu et al. (2018) and Guo et al. (2019) but negates the suggestion of He and colleagues (2018) that there may be HM-resistant Thaumarchaeota organisms in metal polluted freshwater. In agreement with the findings of Guo and colleagues (2019), Bathyarchaeota remained abundant in both pristine L1 and TWW-impacted L2, only that the relative abundance became reduced in the TWW-impacted L2 ecosystem, possibly due to the toxic HMs/metalloids in the TWW, and some members might exhibit resistance to HMs/metalloids. The total organic carbon was reportedly correlated with the abundance of Bathyarchaeota (Pan et al., 2019). Members of Bathyarchaeota might have been active in carbon cycling within the ecosystems despite the impact of HMs toxicants on their diversity and abundance in the TWW-impacted L2 ecosystem. Low abundances of Crenarchaeota (<1% sequence reads) in both pristine L1 and TWW-impacted L2 may be due to the low availability of nitrogen and $CO_2$ in the two ecosystems since members of this archaeal phylum are greatly involved in ammonia oxidation to obtain energy that is used for carbon fixation (Lu et al., 2019). Furthermore, an increase in the relative abundance of Euryarchaeota in the TWW-impacted L2 indicated possible biogeochemical activities that drive the natural attenuation in the polluted hydrosphere as earlier reported by Yang and colleagues (2016).

Bacteria are usually numerically dominant in comparison with Archaea in aquatic environments. Bacterial abundance and diversity are regulated by the physico-chemistry of sediments, playing important roles in the transformation of organic matter and the biogeochemical cycling of primary elements including nitrogen, sulphur, metals, and phosphorus (Cheng et al., 2014). The influence of environmental factors such as salinity, organic matter, and various degrees of pollution on the ecology of the bacterial community has been extensively studied (Oyetibo et al., 2019). Currently, the impact of TWW on the diversity and community of bacteria as found in TWW-impacted L2 is not quite different from previous reports of Oyetibo et al. (2019). Of note, is the increased dominance of Proteobacteria and Bacteroidetes, and lesser relative abundance of Acidobacteria in the TWW-impacted L2, which is not unusual. Members of Proteobacteria are known to be key players in the amelioration of the TWW-impacted aquatic ecosystems. Their dominance in the present study suggested that they must have been actively involved in the functions and processes of the TWW-impacted L2. Furthermore, Bacteroidetes remain pivotal in converting complex molecules into simpler compounds in freshwater sediment. Thus, it is assumed that the increased composition of Bacteroidetes in TWW-impacted L2 could be linked to the increased mineralization of the chemicals contained in the TWW.

The fungal taxonomic profile of the TWW-impacted L2 defied the usual dominance of Ascomycota, Basidiomycota, Cryptomycota, and Chytridiomycota in a freshwater ecosystem (Lepere et al., 2019). On the contrary, the vast majority of ITS sequence reads taxonomy in the TWW-impacted L2 was uncharacterized Eukarya_uc_p (50.4%) and Fungi_uc (16.0%) indicating the plausible toxic consequences of the components of TWW consistently discharged into L2. The dominance of Ascomycota after the uncharacterized phyla in the two ecosystems has been reported in freshwater and is possibly due to the introduction of spores and strands of mycelia during rainwater, runoff, and wind events. As such, it is difficult to categorically conclude that the dominant fungal groups were in-dwellers but rather they might be periodic immigrants in the ecosystems (Grossart et al., 2019). The high sensitivity of Crytomycota to toxic HMs/metalloids may be connected to a lack of chitin in their cell wall, while the posterior whiplash flagella motility of Chytridiomycota due to TWW chemotaxis may explain the low abundance of the phyla in the TWW-impacted L2 (Grossart et al., 2016; Lepere et al., 2019). Moreover, the direct trophic antagonism between fungi and bacteria seemingly explains the low numbers of fungal OTUs in the two ecosystems with fewer OTUs occurring in TWW-impacted L2.

## CONCLUSION

The effects of HMs/metalloid toxicants in textile wastewater on the microbiome of receiving freshwater ecosystems were toward the extinction of some species and emergence of some others. The sensitive microbial taxa in form of 6,028 OTUs present in pristine LI but absent in TWW-impacted L2 are considered efficient bio-indicators of TWW pollution. These efficient bio-indicators are cogent for the early and consistent environmental monitoring of TWW toxicity in the receiving ecosystem in attempts to safely guide the biota in such ecosystems. The gradual decrease and/or eventual loss of the sensitive taxa would indicate the toxic level of the TWW compounds,

thereby signifying the need for mitigating TWW discharges. Nevertheless, the activities of the dominant autochthonous microorganisms present in TWW-impacted freshwater may provide solutions for the effective stimulations required for sustainable bioremediation processes. Hence, the 5,271 OTUs exclusively present in the TWW-impacted L2 are assumed to be functional in the impacted ecosystem and may be crucial to the transformational processes of the HMs/metalloid toxicants. As such, the exclusive dominant OTUs would be prospective biotechnological tools for the circular economy concept to protect environments from the ecotoxicity of TWW discharges and the decommissioning strategies applicable to TWW-impacted freshwater.

## DATA AVAILABILITY STATEMENT

The datasets presented in this study can be found in online repositories. The names of the repository/repositories and accession number(s) can be found below: https://www.ncbi.nlm.nih.gov/, PRJNA545318.

## AUTHOR CONTRIBUTIONS

GOd participated in sample collection, experimentation, data collation and manuscript preparation; GOy participated in experimental design, supervising experimentation, interpretation of data, and manuscript preparation; MI participated in experimental design, and supervising experimentation.

## SUPPLEMENTARY MATERIAL

The Supplementary Material for this article can be found online at: https://www.frontiersin.org/articles/10.3389/fenvs.2021.554490/full#supplementary-material

## REFERENCES


Ado, A., Tukur, A. I., Ladan, M., Gumel, S. M., Muhammad, A. A., Habibu, S., et al. (2015). A Review on Industrial Effluents as Major Sources of Water Pollution in Nigeria. *Chem. J.* 1, 159–164.

Ajaz, M., Rehman, A., Khan, Z., Nisar, M. A., and Hussain, S. (2019). Degradation of Azo Dyes by *Alcaligenes Aquatilis* 3c and its Potential Use in the Wastewater Treatment. *AMB Expr.* 9, 64–75. doi:10.1186/s13568-019-0788-3

Ali, N., Ikramullah, G., Lutfullah, G., Hameed, A., and Ahmed, S. (2008). Decolorization of Acid Red 151 by Aspergillus niger SA1 under Different Physicochemical Conditions. *World J. Microbiol. Biotechnol.* 24, 1099–1105. doi:10.1007/s11274-007-9581-6

Bilinska, L., Gmurek, M., and Ledakowicz, S. (2016). Comparison between Industrial and Simulated Textile Wastewater Treatment by AOPs – Biodegadability, Toxicity and Cost Assessment. *Chem. Eng. J.* 306, 550–559. doi:10.1016/j.cej.2016.07.100

Bolger, A. M., Lohse, M., and Usadel, B. (2014). Trimmomatic: A Flexible Trimmer for Illumina Sequence Data. *Bioinformatics* 30, 2114–2120. doi:10.1093/bioinformatics/btu170

Casucci, C., Okeke, B. C., and Frankenberger, W. T. (2003). Effects of Mercury on Microbial Biomass and Enzyme Activities in Soil. *Bter* 94, 179–192. doi:10.1385/bter:94:2:179

Catania, V., Cappello, S., Di Giorgi, V., Santisi, S., Di Maria, R., Mazzola, A., et al. (2018). Microbial Communities of Polluted Sub-surface Marine Sediments. *Mar. Pollut. Bull.* 131, 396–406. doi:10.1016/j.marpolbul.2018.04.015

Chen, S. H., and Yien Ting, A. S. (2015). Biodecolorization and Biodegradation Potential of Recalcitrant Triphenylmethane Dyes by *Coriolopsis* Sp. Isolated from Compost. *J. Environ. Manage.* 150, 274–280. doi:10.1016/j.jenvman.2014.09.014

Cheng, W., Zhang, J., Wang, Z., Wang, M., and Xie, S. (2014). Bacterial Communities in Sediments of a Drinking Water Reservoir. *Ann. Microbiol.* 64, 875–878. doi:10.1007/s13213-013-0712-z

Contin, M., Rizzardini, C. B., Catalano, L., and De Nobili, M. (2012). Contamination by Mercury Affects Methane Oxidation Capacity of Aerobic Arable Soils. *Geoderma* 189–190, 250–256. doi:10.1016/j.geoderma.2012.06.031

Dung, T. T. T., Cappuyns, V., Swennen, R., and Phung, N. K. (2013). From Geochemical Background Determination to Pollution Assessment of Heavy Metals in Sediments and Soils. *Rev. Environ. Sci. Biotechnol.* 12, 335–353. doi:10.1007/s11157-013-9315-1

Eddy, S. R. (2011). Accelerated Profile HMM Searches. *Plos Comput. Biol.* 7, c1002195. doi:10.1371/journal.pcbi.1002195

Edgar, R. C., Haas, B. J., Clemente, J. C., Quince, C., and Knight, R. (2011). UCHIME Improves Sensitivity and Speed of Chimera Detection. *Bioinformatics* 27, 2194–2200. doi:10.1093/bioinformatics/btr381

Edgar, R. C. (2010). Search and Clustering Orders of Magnitude Faster Than BLAST. *Bioinformatics* 26, 2460–2461. doi:10.1093/bioinformatics/btq461

Egbe, C. C., Oyetibo, G. O., and Ilori, M. O. (2020). Ecological Impact of Organochlorine Pesticides Consortium on Autochthonous Microbial Community in Agricultural Soil. *Ecotoxicol Environ. Saf.* 207, 111319. doi:10.1016/j.ecoenv.2020.111319

Fu, L., Niu, B., Zhu, Z., Wu, S., and Li, W. (2012). CD-HIT: Accelerated for Clustering the Next-Generation Sequencing Data. *Bioinformatics* 28, 3150–3152. doi:10.1093/bioinformatics/bts565

Gao, X., and Chen, C.-T. A. (2012). Heavy Metal Pollution Status in Surface Sediments of the Coastal Bohai Bay. *Water Res.* 46, 1901–1911. doi:10.1016/j.watres.2012.01.007

Grossart, H-P., Van den Wyngaert, S., Kagami, M., Wurzbacher, C., Cunliffe, M., and Rojas-Jimenez, K. (2019). Fungi in Aquatic Ecosystems. *Nat. Rev. Microbiol.* 17(6). 339–354.doi:10.1038/s41579-019-0175-8

Grossart, H.-P., Wurzbacher, C., James, T. Y., and Kagami, M. (2016). Discovery of Dark Matter Fungi in Aquatic Ecosystems Demands a Reappraisal of the Phylogeny and Ecology of Zoosporic Fungi. *Fungal Ecol.* 19, 28–38. doi:10.1016/j.funeco.2015.06.004

Guo, Q., Li, N., Chen, S., Chen, Y., and Xie, S. (2019). Response of Freshwater Sediment Archaeal Community to Metal Spill. *Chemosphere* 217, 584–590. doi:10.1016/j.chemosphere.2018.11.054

Gupta, B. G., Biswas, J. K., and Agrawal, K. M. (2017). Physico-chemical Parameters, Water Quality Index and Statistical Analysis of Surface Water Contamination by Bleaching and Dyeing Effluents at Kalikapur, West Bengal, India. *J. Environ. Sci. Pollut. Res.* 3, 177–180.

Holkar, C. R., Jadhav, A. J., Pinjari, D. V., Mahamuni, N. M., and Pandit, A. B. (2016). A Critical Review on Textile Wastewater Treatments: Possible Approaches. *J. Environ. Manage.* 182, 351–366. doi:10.1016/j.jenvman.2016.07.090

Kemp, P. F., and Aller, J. Y. (2004). Estimating Prokaryotic Diversity: When Are 16S rDNA Libraries Large Enough? *Limnol. Oceanogr. Methods* 2, 114–125. doi:10.4319/lom.2004.2.114

Khan, S., and Malik, A. (2018). Toxicity Evaluation of Textile Effluents and Role of Native Soil Bacterium in Biodegradation of a Textile Dye. *Environ. Sci. Pollut. Res.* 25, 4446–4458. doi:10.1007/s11356-017-0783-7

Lee, B., Moon, T., and Yoon, S. (2017). DUDE-seq: Fast, Flexible, and Robust Denoising for Targeted Amplicon Sequencing. *PLoS One* 12, e0181463. doi:10.1371/journal.pone.0181463

Lee, S. M., Kim, N., Nam, R. H., Park, J. H., Choi, S. I., Park, Y-T., et al. (2019). Gut Microbiota and Butyrate Level Changes Associated with the Long-Term Administration of Proton Pump Inhibitors to Old Rats. *Sci. Rep.* 9, 6626. doi:10.1038/s41598-019-43112-x

Lepere, C., Domaizon, I., Humbert, J-F., Jardillier, L., Hugo, M., and Debroas, D. (2019). Diversity, Spacial Distribution and Activity of Fungi in Freshwater Ecosystems. *PeerJ*. 7, e6247. doi:10.7717/peerj.6247

Liu, J., Cao, W., Jiang, H., Cui, J., Shi, C., Qiao, X., et al. (2018). Impact of Heavy Metal Pollution on Ammonia Oxidizers in Soils in the Vicinity of a Tailings Dam, Baotou, China. *Bull. Environ. Contam. Toxicol.* 101, 110–116. doi:10.1007/s00128-018-2345-1

Liu, Y., Priscu, J. C., Xiong, J., Conrad, R., Vick-Majors, T., Chu, H., et al. (2016). Salinity Drives Archaeal Distribution Patterns in High Altitude Lake Sediments on the Tibetan Plateau. *FEMS Microbiol. Ecol.* 92. doi:10.1093/femsec/fiw033

Lu, S., Liu, X., Liu, C., Wang, X., and Cheng, G. (2019). Review of Ammonia-Oxidizing Bacteria and Archaea in Freshwater Ponds. *Rev. Environ. Sci. Biotechnol.* 18, 1–10. doi:10.1007/s11157-018-9486-x

Mahbub, K. R., Krishnan, K., Megharaj, M., and Naidu, R. (2016). Mercury Inhibits Soil Enzyme Activity in a Lower Concentration Than the Guideline Value. *Bull. Environ. Contam. Toxicol.* 96, 76–82. doi:10.1007/s00128-015-1664-8

Mahbub, K. R., Krishnan, K., Naidu, R., Andrews, S., and Megharaj, M. (2017). Mercury Toxicity to Terrestrial Biota. *Ecol. Indicators* 74, 451–462. doi:10.1016/j.ecolind.2016.12.004

Masella, A. P., Bartram, A. K., Truszkowski, J. M., Brown, D. G., and Neufeld, J. D. (2012). PANDAseq: Paired-End Assembler for Illumina Sequences. *BMC Bioinformatics* 13, 31. doi:10.1186/1471-2105-13-31

Muller, G. (1969). Index of Geoaccumulation in Sediments of the Rhine River. *Geol. J.* 2, 109–118. doi:10.1016/j.envint.2020.106032

NESREA (National Environmental Standards and Regulations Enforcement Agency) (2010). *National Environmental (Surface and Groundwater Quality Control) Regulations*. Abuja, Nigeria: Federal Ministry of Environment, FCT, 32.

Obijiofor, O. C., Okoye, P. A. C., and Ekejiuba, I. O. C. (2018). Assessment of Surface Water Contamination and Effect of Textile Effluents on Ibeshe River, Ikorodu, Lagos State, Nigeria. *J. Chem. Soc. Nigeria* 43, 69–79.

Ogwugwa, V. H., Oyetibo, G. O., and Amund, O. O. (2020). Taxonomic Profiling of Bacteria and Fungi in Freshwater Sewer Receiving Hospital Wastewater. *Environ. Res.* 192, 110319. doi:10.1016/j.envres.2020.110319

Oyetibo, G. O., Chien, M.-F., Ikeda-Ohtsubo, W., Suzuki, H., Obayori, O. S., Adebusoye, S. A., et al. (2017b). Biodegradation of Crude Oil and Phenanthrene by Heavy Metal Resistant Bacillus Subtilis Isolated from a Multi-Polluted Industrial Wastewater Creek. *Int. Biodeterioration Biodegradation* 120, 143–151. doi:10.1016/j.ibiod.2017.02.021

Oyetibo, G. O., Ige, O. O., Obinani, P. K., and Amund, O. O. (2021). Ecological Risk Potentials of Petroleum Hydrocarbons and Heavy Metals Shape the Bacterial Communities of Marine Hydrosphere at Atlantic Ocean, Atlas Cove, Nigeria. *J. Environ. Manag.* 289, 112563. doi:10.1016/j.jenvman.2021.112563

Oyetibo, G. O., Ilori, M. O., Adebusoye, S. A., Obayori, O. S., and Amund, O. O. (2010). Bacteria with Dual Resistance to Elevated Concentrations of Heavy Metals and Antibiotics in Nigerian Contaminated Systems. *Environ. Monit. Assess.* 168, 305–314. doi:10.1007/s10661-009-1114-3

Oyetibo, G. O., Ishola, S. T., Ikeda-Ohtsubo, W., Miyauchi, K., Ilori, M. O., and Endo, G. (2015). Mercury Bioremoval by *Yarrowia* Strains Isolated from Sediments of Mercury-Polluted Estuarine Water. *Appl. Microbiol. Biotechnol.* 99, 3651–3657. doi:10.1007/s00253-014-6279-1

Oyetibo, G. O., Miyauchi, K., Huang, Y., Chien, M.-F., Ilori, M. O., Amund, O. O., et al. (2017a). Biotechnological Remedies for the Estuarine Environment Polluted with Heavy Metals and Persistent Organic Pollutants. *Int. Biodeterioration Biodegradation* 119, 614–625. doi:10.1016/j.ibiod.2016.10.005

Oyetibo, G. O., Miyauchi, K., Huang, Y., Ikeda-Ohtsubo, W., Chien, M.-F., Ilori, M. O., et al. (2019). Comparative Geochemical Evaluation of Toxic Metals Pollution and Bacterial Communities of Industrial Effluent Tributary and a Receiving Estuary in Nigeria. *Chemosphere* 227, 638–646. doi:10.1016/j.chemosphere.2019.04.048

Pan, J., Chen, Y., Wang, Y., Zhou, Z., and Li, M. (2019). Vertical Distribution of Bathyarchaeotal Communities in Mangrove Wetlands Suggests Distinct Niche Preference of Bathyarchaeota Subgroup 6. *Microb. Ecol* 77 (2), 417–428. doi:10.1007/s00248-018-1309-7

Rezaei, A., and Sayadi, M. H. (2015). Long-term Evolution of the Composition of Surface Water from the River Gharasoo, Iran: a Case Study Using Multivariate Statistical Techniques. *Environ. Geochem. Health* 37, 251–261. doi:10.1007/s10653-014-9643-2

Sandaa, R.-A., Enger, Ø., and Torsvik, V. (1999). Abundance and Diversity of Archaea in Heavy-Metal-Contaminated Soils. *Appl. Environ. Microbiol.* 65, 3293–3297. doi:10.1128/aem.65.8.3293-3297.1999

Takada, Y., and Matsumoto, N. (2005). Skim Milk Drastically Improves the Efficacy of DNA Extraction from Andisol, a Volcanic Ash Soil. *Jpn. Agric. Res. Quart.* 39, 247–252. doi:10.6090/jarq.39.247

Tazisong, I. A., Senwo, Z. N., and Williams, M. I. (2012). Mercury Speciation and Effects on Soil Microbial Activities. *J. Environ. Sci. Health A* 47, 854–862. doi:10.1080/10934529.2012.665000

U.S EPA (United States Environmental Protection Agency) (1998). *Guidelines for Ecological Risk Assessment, Risk Assessment Forum*. Washington, DC: U.S Environmental Agency, 114.

Worms, I., Simon, D. F., Hassler, C. S., and Wilkinson, K. J. (2006). Bioavailability of Trace Metals to Aquatic Microorganisms: Importance of Chemical, Biological and Physical Processes on Biouptake. *Biochimie* 88, 1721–1731. doi:10.1016/j.biochi.2006.09.008

Yang, C.-l., Sun, T.-h., He, W.-x., Zhou, Q.-x., and Chen, S. (2007). Single and Joint Effects of Pesticides and Mercury on Soil Urease. *J. Environ. Sci.* 19, 210–216. doi:10.1016/s1001-0742(07)60034-5

Yang, Y. Y., Dai, Y., Wu, Z., Xie, S. G., and Liu, Y. (2016). Temporal and Spatial Dynamics of Archaeal Communities in Two Freshwater Lakes at Different Trophic Status. *Front. Microbiol.* 7, 451. doi:10.3389/fmicb.2016.00451

Zhang, Y., Chen, L., Sun, R., Dai, T., Tian, J., Zheng, W., et al. (2016). Temporal and Spatial Changes of Microbial Community in an Industrial Effluent Receiving Area in Hangzhou Bay. *J. Environ. Sci.* 44, 57–68. doi:10.1016/j.jes.2015.11.023

**Conflict of Interest:** The authors declare that the research was conducted in the absence of any commercial or financial relationships that could be construed as a potential conflict of interest.

# Advantages of publishing in Frontiers

**OPEN ACCESS**
Articles are free to read for greatest visibility and readership

**FAST PUBLICATION**
Around 90 days from submission to decision

**HIGH QUALITY PEER-REVIEW**
Rigorous, collaborative, and constructive peer-review

**TRANSPARENT PEER-REVIEW**
Editors and reviewers acknowledged by name on published articles

**Frontiers**
Avenue du Tribunal-Fédéral 34
1005 Lausanne | Switzerland

**Visit us:** www.frontiersin.org
**Contact us:** frontiersin.org/about/contact

**REPRODUCIBILITY OF RESEARCH**
Support open data and methods to enhance research reproducibility

**DIGITAL PUBLISHING**
Articles designed for optimal readership across devices

**FOLLOW US**
@frontiersin

**IMPACT METRICS**
Advanced article metrics track visibility across digital media

**EXTENSIVE PROMOTION**
Marketing and promotion of impactful research

**LOOP RESEARCH NETWORK**
Our network increases your article's readership